UNIVERSIDAD COMPLUTENSE DE MADRID
FACULTAD DE CIENCIAS QUÍMICAS
DEPARTAMENTO DE QUÍMICA ORGÁNICA I

TESIS DOCTORAL

Fotosensibilización de oxígeno singlete: aplicaciones al estudio de la fotooxidación de tiocetonas y fotoerradicación de *H. pylori*

MEMORIA PARA OPTAR AL GRADO DE DOCTOR

PRESENTADA POR

Antonio José Sánchez Arroyo

DIRECTORES

Nazario Martín León
David García Fresnadillo

Madrid
Ed. electrónica 2019

UNIVERSIDAD COMPLUTENSE DE MADRID

FACULTAD DE CIENCIAS QUÍMICAS

Departamento de Química Orgánica I

Fotosensibilización de oxígeno singlete: aplicaciones al estudio de la fotooxidación de tiocetonas y fotoerradicación de *H. pylori*

MEMORIA PARA OPTAR AL GRADO DE DOCTOR

PRESENTADA POR

Antonio José Sánchez Arroyo

Directores

Nazario Martín León

David García Fresnadillo

UNIVERSIDAD
COMPLUTENSE
MADRID

Fotosensibilización de oxígeno singlete: aplicaciones al estudio de la fotooxidación de tiocetonas y fotoerradicación de *H. pylori*

MEMORIA PARA OPTAR AL GRADO DE DOCTOR

PRESENTADA POR

Antonio José Sánchez Arroyo

Directores

Nazario Martín León

David García Fresnadillo

Madrid, 2019

D. David García Fresnadillo, Profesor Titular del Departamento de Química Orgánica de la Universidad Complutense de Madrid y **D. Nazario Martín León**, Catedrático de Universidad del Departamento de Química Orgánica de la Universidad Complutense de Madrid,

CERTIFICAN

Que la presente Memoria titulada: *Fotosensibilización de oxígeno singlete: aplicaciones al estudio de la fotooxidación de tiocetonas y fotoerradicación de H. pylori* se ha realizado bajo su dirección en el Departamento de Química Orgánica de la Facultad de Ciencias Químicas de la Universidad Complutense de Madrid por el Licenciado en Química D. Antonio José Sánchez Arroyo y autorizan su presentación para ser calificada como Tesis Doctoral.

Y para que así conste firman el presente certificado en Madrid, a 23 de Enero de 2019.

Fdo. Dr. David García Fresnadillo Fdo. Dr. Nazario Martín León

A mi familia: mis padres,
mi hermano y mis abuelos.
La razón de mi ser

Fortunato l'uom che prende
ogni cosa pel buon verso,
e tra i casi e le vicende
da ragion guidar si fa.
Quel che suole altrui far piangere
fia per lui cagion di riso,
e del mondo in mezzo ai turbini
bella calma troverà.

Final Acto II – Così fan tutte
W. A. Mozart / L. Da Ponte

Che goda ogni cor in si bel di
Pietoso amor ci consolò.
Il nuestro duol piacer si fe,
la nostra fe ricompensò

Final Acto II – La festa del villagio
V. Martín y Soler / F. Moretti

Agradecimientos

Quisiera comenzar estos agradecimientos por mis directores, Nazario y David. A Nazario, por haberme abierto las puertas de su grupo de investigación y a David por la confianza en que pudiera poner en marcha estas líneas de trabajo dentro del grupo. Y a ambos, por todo lo que he podido aprender de vosotros durante estos años.

Extiendo mis agradecimientos a la Universidad Complutense de Madrid por el contrato predoctoral CT4/14, que puso fin a los días de *molto honor, e poco contante*.

Agradezco igualmente a todas aquellas personas con las que he colaborado en diferentes partes de este trabajo. Por la parte de RMN, muy especialmente al profesor Antonio Herrera y a la infinita paciencia de Zulay, así como a los miembros del CAI de RMN de la UCM (Lola, Elena y Ángel). También quisiera tener unas palabras cargadas de cariño para el profesor Florencio Moreno, por sus mágicas tiocetonas que tanto juego han dado al enfrentarse al oxígeno singlete. En la parte de la caracterización fotofísica de los derivados, al profesor Santi Nonell y a Roger por aquellos días en el Instituto Químico de Sarriá, así como a la posterior ayuda de Sergio y a la disposición de Cristina Flors en IMDEA-Nanociencia para los ensayos de microscopía de fluorescencia. Igualmente, a todos los integrantes del Hospital de La Princesa (Unidades de Microbiología y Digestivo), que aportaron su saber y su hacer en la parte de las aplicaciones fotodinámicas: Teresa, Javier, David, Adrián, Pedro, Tamara, Alicia y Claudio. Finalmente, a Israel Fernández, M. D. Marazuela, Ramón González, Eduardo Guzmán, Eugenio Vázquez y Jessica Rodríguez por todas sus contribuciones que han permitido redondear lo que esta memoria contiene. Y nada hubiera sido posible sin la presencia día tras día de los técnicos que ponen el Departamento de Química Orgánica en marcha: Laura, Javier (mañana) y Javier (tarde).

Mención especial merecen todos los integrantes del Grupo de Materiales Moleculares Orgánicos. A los "mayores", Mª Ángeles (por estar siempre disponible para aclarar las dudas burocráticas y tener siempre una palabra de apoyo), Beti, Salvatore, Ángel, Andreas, Carmen, Agus, Marta (por todo su cariño y por un futuro en la profesión más bonita del mundo), José y Laura (por sacarme siempre una sonrisa en cualquiera de nuestras conversaciones), Ana y Virginia. Y a todos los que ponen en marcha la maquinaria de los laboratorios cada día, de los que espero no olvidarme de ninguno ahora ni en el futuro: Valentina, Rosa, Mikiko, Alfonso, Andrés, Alicia, Marta, Sara, Marina, Inés, Rafa, Sonia, Silvia, Javi (Ramos), Javi (López), Javi (Urieta), Chus, Paul, Antonio, Juan, Enrique y Andrea.

Tras escribir las páginas de esta memoria he podido recorrer todos y cada uno de los días que han permitido llegar a este momento. Como todo en la vida, ha habido sus días buenos y otros no tan buenos. Estos últimos quizás sean los más importantes, pues es en ellos en donde se pone a prueba la fortaleza de todo: los días en los que *miré los muros de la patria mía, si un tiempo fuertes, ya desmoronados*; los días en los que *soñé que estaba de estas prisiones cargado y soñé que en otro estado más lisonjero me vi*; los días en los *que el mayor bien fue pequeño* y en los que deseé que *toda la vida fuera sueño*. Pero en esos días tuve la inmensa suerte de contar a mi lado con una tripulación de excepción que permitió llevar el navío errante a puerto seguro, *aquél en el que se termina por rendir la más azarosa y difícil de las singladuras*. Quisiera destacar a continuación a algunas personas muy especiales de esa tripulación.

A María Trillo Alcalá, el espejo en el que siempre he procurado encontrar reflejadas las virtudes que me guiasen en este Gran Teatro del Mundo químico, en el que fuiste la maestra responsable de aportarme los cimientos sobre los que se construyó todo lo demás. A ello sumaría las enseñanzas que nunca has dejado de transmitirme y el hecho de abrirme las puertas de "casa" cuando más lo necesitaba, donde continúas siendo el ejemplo que siempre intentaré seguir. Y en esa casa de gloriosos recuerdos e ilusionantes proyectos no podría olvidarme de Rosa, por presentarme hace años a mis queridos y admirados Mozart y Martín y Soler, que tantas horas de felicidad y consuelo me han aportado desde entonces con su música.

A Sandra Jiménez Falcao, quien, haciendo honor a su apellido, ha sido el halcón a cuyas alas me he subido para poder ver más lejos, tanto en los días claros como en aquéllos con niebla. Como nos dice Fausto, *cuando la fantasía se lanza esperanzada en un audaz vuelo, le basta luego un pequeño recodo si, pasada la fortuna, fracasa en el torbellino del tiempo*. Cada segundo compartido contigo ha sido un pequeño recodo que, unidos todos ellos y sumados a los de Héctor, se convirtieron en mi salvación en el pasado y en la rampa de salida hacia un futuro que nos pertenece sólo a nosotros, por derecho natural y por derecho adquirido.

A José Garrido González, mi enantiomérico Duque de Béjar, cuya nobleza tiene por origen un corazón que es la definición misma de bondad. Fuiste el faro que me alumbró en los días de mayor oscuridad, no para *dirigirme poco a poco hacia las rocas*, sino para marcar el punto donde encontrar al alquimista capaz de transmutar los días de "*duelos y quebrantos*" en días de auténticos recuerdos dorados. Y en ese feliz encuentro reservado por el destino, extiendo estas palabras a Sara, pues siempre os veré a los dos, de forma indisoluble, como mi orgullo y mi alegría.

A los integrantes del laboratorio QB404, aislado del centro de poder, mestizo en su composición, pero en el que tantos y tan hondos vínculos se han creado. Entre ellos, a los profesores José Osío (por nuestras conversaciones sobre lo divino y

lo humano), María José Mancheño (por salir del cesto para soltar sus verdades sin filtro) y Paloma Martínez (por ser una fuente de métodos no convencionales para solucionar las cosas, científicas o no). Tras estos años siendo como un árbol perenne en el laboratorio, no podría olvidarme de algunas personas muy especiales a las que he visto pasar: Marta (que trajo la revolución a lo que era un remanso de paz), Nadia (que persistió en la revolución y en el desacato a la autoridad), Laura (la cordura entre tanta locura), Cástor (mi consultorio de dudas experimentales), Sergio (creo que todos estos años en el terremoto de la investigación lo hemos pasado "pos mu" bien), Aitor (por ser la voz de la sensatez y la pasión investigadora), Juanma (por ser un alumno, un investigador y una persona de una categoría y una altura como la suya propia), y tantos otros: Isabel, Marta, Laura, Bea, Elena y Pablo.

Mención especial merecen los escuadrones de la felicidad, los guardianes de la galaxia Analítica en la que tantas estrellas he descubierto: Ana (que ante los nubarrones de la vida siempre podamos decir: ¡*e se chove, que chova*!), Bea (que sigas siendo la voz pensante), Sandrita (sacerdotisa de la gruta de Trofonio, capaz de convertir con su presencia cualquier mal momento en un auténtico deleite), Anabel (la alegría cubana destilada y condensada en una persona), Daniel (flameador *cum laude*, catedrático en el manejo de balas de Argón y diablillo que me inspira ternura sin saber la razón), Jorge (sirva esta frase como una de esas miradas con las que nos lo decimos todo, pues las palabras no son suficientes para expresarte toda mi gratitud por los momentos que hemos pasado y las travesuras que hemos maquinado) e Iñigo (bueno chaval, que me voy yendo).

Quisiera acordarme en este momento de otras personas que me he encontrado en este viaje, pero que han resultado igualmente importantes. En primer lugar, a Bernardo Herradón, mi gratitud más sincera por haber contado siempre conmigo para poner nuestro granito de arena en difundir a la sociedad lo que es la Química, y por nuestra pasión compartida por Mozart, que tanto me ha gustado tratar contigo siempre que hemos tenido ocasión. A la profesora Yolanda Pérez, por toda su ayuda y por haberse acordado siempre de mí en sus proyectos, a los que siempre he acudido encantado. A la profesora Amparo Luna, por toda su comprensión y por sus consejos cargados de sabiduría (*descansar, acaso debas, pero nunca desistir*).

Y así, en este recorrido llego a las personas sin las cuales nada de ésto, y nada en mi vida, hubiera sido posible: mi familia. A mis padres, Adelaida y Miguel Ángel, y a mi hermano Miguel Ángel. Por ser los pilares maestros sobre los que descansa el peso de mi vida. Pilares que emergen firmes gracias a unos ladrillos pegados por el amor más puro. Ellos son las circunstancias necesarias que explican mi yo, sin las cuales no puedo salvarme ni explicarme. Pero llegados a este momento quisiera reconocer mi culpa y pedirles perdón por no haber sabido dejar aparcadas fuera de casa mis frustraciones y tormentos, que han sufrido con

la paciencia del cantero que labra la piedra y con una comprensión que no merezco. Sólo podría decir en mi descargo lo mismo que Vitelia al final de *La clemenza di Tito*: *Chi vedesse il mio dolore, eppur avria di me pietà*. Y en estos momentos, ocupan también un lugar muy especial en mi memoria mis abuelos (Pipa, Lila, Pepe y Titi, nombres que denotan el profundo cariño que brota en mi memoria al recordarles). Hace ya un tiempo que todos ellos partieron y por ello no podrán estar este día presentes en cuerpo. Pero su recuerdo, su honestidad, su ejemplo de superación y su amor estarán bien presentes en espíritu, como todos y cada uno de los días de mi vida. Pero como la vida no es sólo *un río que va a dar a la mar*, sino que también nace y crece, en esta familia y en estos agradecimientos quisiera tener unas palabras muy cariñosas para Sira, Marisol y Ángel, así como a esa pequeña criatura que acaba de llegar, que tanta felicidad y alegría, antes incluso de su nacimiento, nos ha traído y nos traerá.

TABLE OF CONTENTS

Abbreviations and symbols

$^1O_2$: Singlet molecular oxygen (lowest excited state, spectroscopic term $a^1\Delta_g$)

$^3O_2$: Triplet molecular oxygen (ground state, spectroscopic term $X\,^3\Sigma_g^-$)

IC: Internal conversion

ISC: Intersystem crossing

ET: Energy transfer

P(S_1): Excited singlet state for a photosensitizer

P(T_1): Excited triplet state for a photosensitizer

Φ_Δ: Singlet oxygen quantum yield

Φ_T: Triplet state quantum yield (intersystem crossing quantum yield)

Φ_f: Fluorescence quantum yield

τ_Δ: Singlet oxygen lifetime

$\tau_{\Delta 0}$: Singlet oxygen lifetime (in the absence of any quencher)

τ_T: Triplet excited state lifetime

τ_{T0}: Triplet excited state lifetime (in the absence of any quencher)

τ_{fluo}: Fluorescence lifetime

S_t: Instrumental signal for $^1O_2$ phosphorescence emission

k_q: Physical deactivation rate constant

k_q^Δ: $^1O_2$ quenching rate constant

λ_{max}^{abs}: Wavelength for absorption maxima

ε: Absorption coefficient

HOMO: Highest Ocuppied Molecular Orbital

UV-vis: Ultraviolet-visible spectrophotomety

NMR: Nuclear Magnetic Resonance

HMQC: Heteronuclear Multiple Bond Coherence

HMBC: Heteronuclear Multiple Bond Correlation

COSY: Correlated Spectroscopy

GC-MS: Gas Chromatography-Mass Spectrometry

MALDI-TOF: Matrix Assisted Laser Desorption/Ionization – Time of Flight

FTIR: Fourier-Transform Infrared Spectroscopy

TEM: Transmission Electron Microscopy

Θ: Dihedral angle

CuAAC: Copper (I) Azide Alkyne Cycloaddition

γ: Surface tension

D: Difussion coefficient

PDT: Photodynamic Therapy

aPDT: Antimicrobial Photodynamic Therapy

H. pylori: *Helicobacter pylori*

CFU: Colony Forming Unit

COS: Columbia Agar medium supplemented with blood

ABSTRACT

The research presented in this work (**Photosensitization of singlet oxygen: applications to the study of photooxidation of thioketones and photoeradication of *H. pylori***) is focused on the current interest on taking advantage of the energy transported by light and its transfer by photosensitization to the oxygen molecule to generate its excited state of lowest energy, singlet molecular oxygen ($^1O_2$). The production of this reactive oxygen species can be applied in fields as diverse as chemical synthesis in the context of Green Chemistry, in environmental decontamination methods such as Advanced Oxidation Processes, or in new medical treatments such as Photodynamic Therapies against antibiotic-resistant microorganisms or against some types of cancer. In short, this study aims to advance knowledge about the alternative application of light, a potentially inexhaustible resource, in order to achieve some of the fundamental objectives that society sets for the near future: the development of a sustainable chemical industry, the conservation of the environment, as well as new ways to improve health and live better.

$^1O_2$ behaves like an electrophilic species that is capable of transforming a wide variety of organic substrates (*e.g.* alkenes, aromatic rings or functional groups with heteroatoms). Although the structure of the products of these reactions is generally well known, some mechanistic questions about their formation are still open to debate. This is why the fundamental objective of the **first chapter** of this work was to gain insight into the **photooxidation mechanism of thioketones mediated by $^1O_2$**, posing new alternatives to the previous information available. As a consequence of the research carried out in this field, **a new reaction mechanism has been proposed**. The experimental evidence collected has demonstrated that the general scheme of the mechanism evolves through parallel reactions. Moreover, contrary to what was previously stated in the literature, ketones and sulfines are not the only photoproducts, as new compounds have been detected when the starting thioketone has protons in alpha position with respect to thiocarbonyl carbon. Similarly, the distribution of photoproducts is strongly dependent on the type of solvent (protic/aprotic) and the initial concentration of starting thioketone. With respect to this last test, it has been demonstrated that the sulfine group comes from an intermolecular reaction in which two thioketone molecules are involved. This mechanism has been proposed using alicyclic thioketones, although it has also been tested in

other important analogous substrates (thionucleobases used as antitumor drugs). After reaching this mechanistic knowledge, the research was focused on obtaining the sulfine group, a substrate of interest in organic synthesis, under the **principles of Green Chemistry**. For this purpose, a fluidized bed reactor has been developed, where thioketone and photosensitizer are immobilized on silica gel. With this system, photooxidation of thioketones has been achieved on a synthetic scale (50-100 mg), obtaining the sulfine group as the major product (> 85% yield).

In the **second chapter**, taking into account the oxidizing properties of $^1O_2$, **new photosensitizers based on glycodendrimeric derivatives of [60]fullerene** have been developed to be **applied to *H. pylori* photoeradication**. This microorganism, a Gram-negative bacterium that colonizes the gastric mucosa in humans, is considered one of the most widespread pathogens among the world population, and its presence in the gastrointestinal tract is associated with various gastric diseases. However, the development of antibiotic resistance by *H. pylori* has reduced the eradication rates of commonly used therapies to less than 80-90% and, therefore, the search for new treatment alternatives is considered urgent. Among them, Antimicrobial Photodynamic Therapy (aPDT) stands out. Currently, the development of photosensitizers for aPDT focuses on the selective recognition between pathogens and the photosensitizing dye. Therefore, [60]fullerene has been functionalised with peripheral glycodendrimeric structures carrying 6, 12 and 18 L-(–)-fucose units to establish multivalent interactions. This approach takes advantage of the fact that *H. pylori* expresses membrane proteins that act as adhesion molecules in the colonization process (*e.g.*, adhesins that bind to blood group fucosilated antigens (BabA) and adhesins that bind to sialic acid (SabA)). Fluorescent probes have also been synthesized to test the interaction between *H. pylori* and the novel fucosylated glycodendrons, using the flow cytometry technique. All derivatives have been photophysically characterized (photosensitizers: absorption coefficients, Φ_Δ, τ_T, k_q^Δ; fluorescent probes: absorption, emission and excitation spectra, τ_{em}, Φ_{em}). Regarding the $^1O_2$ photosensitizers based on glycofullerenes, the most relevant result is the decrease in the values of Φ_Δ (0.02-0.27) due to its aggregation in water (demonstrated by its surfactant behaviour using the pendant drop method). Despite this fact, the photodynamic activity of these derivatives against *H. pylori* has been tested *in vitro*, proving that the [60]fullerene monoadducts carrying 12

and 18 fucose units reduce the *H. pylori* population by four orders of magnitude after 30 minutes of blue light irradiation.

In **conclusion**, the research carried out in this work has contributed to increasing the mechanistic knowledge about the reactivity of $^1O_2$ with thioketones, opening the door to oxidize these compounds and obtain products of synthetic value under the principles of Green Chemistry, thus contributing to the conservation of the environment. In addition, new and effective photosensitizers based on the chemistry of [60]fullerene for the photoeradication of *H. pylori* have been synthesized, paving the way for future research to prove their viability as candidates in clinical trials.

RESUMEN

La investigación que se ha llevado a cabo en este trabajo (**Fotosensibilización de oxígeno singlete: aplicaciones al estudio de la fotooxidación de tiocetonas y fotoerradicación de *H. pylori***) centra su interés en el aprovechamiento de la energía transportada por la luz y su transferencia mediante fotosensibilización a la molécula de oxígeno para generar su estado excitado de menor energía, el oxígeno molecular singlete ($^1O_2$). La producción de esta especie reactiva del oxígeno puede ser aplicada en campos tan diversos como la síntesis química en el contexto de la Química Verde (*Green Chemistry*), en métodos de descontaminación medioambiental como los procesos avanzados de oxidación (*Advanced Oxidation Processes*), o en nuevos tratamientos médicos como las terapias fotodinámicas (*Photodynamic Therapies*) contra microorganismos resistentes a antibióticos o contra algunos tipos de cáncer. En definitiva, este estudio persigue avanzar en el conocimiento sobre la aplicación alternativa de la luz, un recurso potencialmente inagotable, para conseguir algunos de los objetivos fundamentales que se plantea la sociedad para un futuro cercano: el desarrollo de una industria química sostenible, la conservación del medioambiente, así como nuevos caminos para mejorar la salud y vivir mejor.

El $^1O_2$ se comporta como una especie electrófila que es capaz de transformar gran variedad de sustratos orgánicos (por ejemplo, alquenos, anillos aromáticos o grupos funcionales con heteroátomos). Aunque la estructura de los productos de estas reacciones es, en general, bien conocida, algunas cuestiones mecanísticas sobre la formación de los mismos están todavía abiertas a debate. Esta es la razón por la que el objetivo fundamental del **primer capítulo** de este trabajo fue ahondar en el **mecanismo de fotooxidación de tiocetonas mediado por $^1O_2$**, planteando nuevas alternativas a la información previa disponible. Como consecuencia de las investigaciones llevadas a cabo en este campo se ha planteado un nuevo mecanismo de reacción. Las evidencias experimentales recogidas han permitido demostrar que el esquema general del mecanismo evoluciona a través de reacciones paralelas. Además, al contrario de lo que se afirmaba previamente en la bibliografía, la cetona y el grupo sulfino no son los únicos fotoproductos, ya que se han detectado nuevos compuestos cuando la tiocetona tiene protones en posición alfa respecto al carbono tiocarbonílico. Igualmente, la distribución de fotoproductos es fuertemente dependiente del tipo de disolvente (prótico/aprótico) y de la concentración inicial de tiocetona. Respecto a esta última prueba, se ha demostrado que el grupo sulfino procede de una reacción intermolecular en la que están implicadas dos moléculas de tiocetona. Este mecanismo se ha propuesto usando tiocetonas alicíclicas, aunque se ha probado en otros sustratos análogos de importancia (tionucleobases usadas como medicamentos antitumorales). Tras alcanzar este conocimiento mecanístico, las investigaciones se centraron en obtener el grupo sulfino, un sustrato de interés en síntesis orgánica, bajo los principios de la Química Verde. Para ello se ha desarrollado un reactor de lecho fluidizado, donde la tiocetona y el fotosensibilizador están inmovilizados sobre gel de sílice. Con este sistema se ha conseguido la fotooxidación de tiocetonas a escala sintética (50-100 mg), obteniendo el grupo sulfino como el producto mayoritario (rendimientos mayores al 85%).

En el **segundo capítulo**, teniendo en cuenta las propiedades oxidantes del $^1O_2$, el principal objetivo ha sido desarrollar nuevos **fotosensibilizadores basados en derivados glicodendriméricos de [60]fullereno** para ser aplicados en la **fotoerradicación de *H. pylori***, una bacteria Gram-negativa que coloniza en humanos la mucosa gástrica. Este microorganismo es considerado como uno de los patógenos más extendidos entre la población mundial, cuya presencia está asociada con diversas enfermedades gástricas. Sin embargo, el desarrollo de

resistencia a los antibióticos por parte de *H. pylori* ha reducido las tasas de erradiación de las terapias usadas habitualmente a menos del 80-90%, por lo que se considera urgente encontrar nuevas alternativas de tratamiento. Entre ellas destaca la Terapia Fotodinámica Antimicrobiana (*Antimicrobial Photodynamic Therapy, aPDT*). Actualmente, el desarrollo de fotosensibilizadores para aPDT se focaliza en el reconocimiento selectivo entre los patógenos y el colorante fotosensibilizador. Por ello, el [60]fullereno se ha funcionalizado con estructuras glicodendriméricas periféricas portadoras de 6, 12 y 18 unidades de L-(–)-fucosa para que se establezcan interacciones multivalentes. Esta aproximación aprovecha que *H. pylori* expresa proteínas de membrana que actúan como moléculas de adhesión en el proceso de colonización (entre ellas, las adhesinas que se unen a los antígenos fucosilados de los grupos sanguíneos (BabA) y las adhesinas que se unen al ácido siálico (SabA)). Igualmente, se han sintetizado sondas fluorescentes para probar la interacción entre *H. pylori* y los glicodendrones fucosilados, haciendo uso de la técnica de citometría de flujo. Todos los derivados se han caracterizado fotofísicamente (fotosensibilizadores: coeficientes de absorción, Φ_Δ, τ_T, k_q^Δ; sondas fluorescentes: espectros de absorción, emisión y excitación, τ_{fluo}, Φ_f). Respecto a los fotosensibilizadores de $^1O_2$ basados en glicofullerenos, el resultado más relevante es el descenso en los valores de Φ_Δ (0.02-0.27) debido a su agregación en agua (demostrada por su comportamiento tensioactivo usando el método de gota colgante). A pesar de este hecho, se ha ensayado *in vitro* la actividad fotodinámica de estos derivados contra *H. pylori*, comprobándose que los monoaductos de [60]fullereno portadores de 12 y 18 unidades de fucosa reducen cuatro órdenes de magnitud la población de *H. pylori* tras 30 minutos de irradiación con luz azul.

A modo de **conclusión**, las investigaciones llevadas a cabo en este trabajo han contribuido a aumentar el conocimiento mecanístico sobre la reactividad del $^1O_2$ con tiocetonas, abriendo la puerta para oxidar estos compuestos y obtener productos de valor sintético bajo los principios de la Química Verde, contribuyendo así a la conservación del medioambiente. Además, se han sintetizado nuevos y efectivos fotosensibilizadores basados en la química del [60]fullereno para la fotoerradicación de *H. pylori*, abriendo el camino para futuras investigaciones que prueben su viabilidad como candidatos en ensayos clínicos.

INTRODUCTION

1. INTRODUCTION

From the basic research about its nature to the last technological applications, light has been one of the most challenging and fascinating topics in the History of Science. Among the driving forces which explain the current interest in light based technologies, the need for renewable and clean sources of energy plays a key role. This is a major concern due to the expected increment in the world's population over the next decades, foreseeing 8 billion people in 2025[1] and around 11 billion people at the end of this century.[2] With these numbers in mind and considering that the crude oil reserves are starting to run out after years of massive consumption, the use of fossil fuels does not represent a sustainable way in order to satisfy the expected human and economical requirements of energy in the future. However, most of the current scientific and technological efforts are devoted to take advantage of sunlight as a source of energy, taking into account the solar irradiation that strikes the surface of the Earth (120000 TW of power per year, while human energy consumption will be no more than 30 TW per year by 2050).

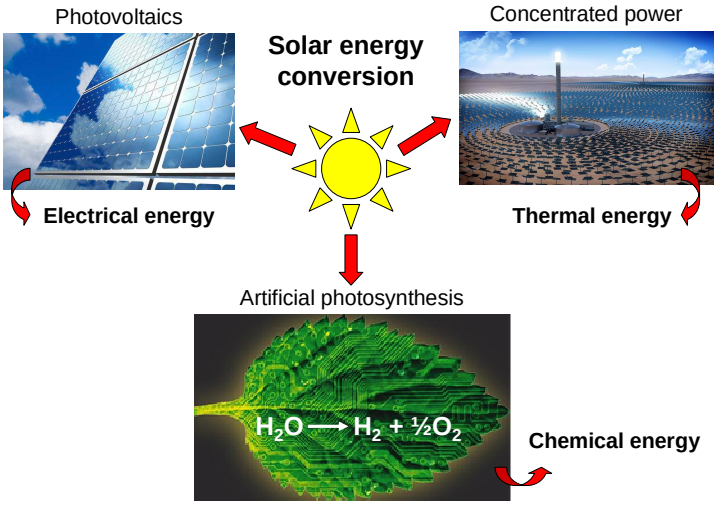

Figure 1. Technologies for solar energy conversion.

[1] J. Toffelson, *Nature*, **2011**, *478*, 300.
[2] P. Gerland, A. E. Raftery, H. Ševčíková, N. Li, D. Gu, T. Spoorenberg, L. Alkema, B. K. Fosdick, J. Chunn, N. Lalic, G. Bay, T. Buettner, G. K. Heilig, J. Wilmoth, *Science*, **2014**, *346*, 234.

In this sense, solar photovoltaics and concentrated solar power have arisen as the most widespread technologies used at industrial scale, although research in solar hydrogen fuel synthesis from photoinduced water splitting has attracted substantial attention as a way for energy storage in the last years (Figure 1).[3]

However, the interest of the energy transported by the photons of light does not lie only in the transformation of solar energy into electrical power, but also in a series of fields such us chemical synthesis or medical therapies, among others. As a result, and trying to emphasize the ability of light-based technologies in order to promote sustainable development and provide solutions to global challenges and social concerns, the United Nations General Assembly proclaimed 2015 as the International Year of Light and Light-based Technologies.[4]

1.1. Light promoted chemical synthesis

Since the seminal works carried out by Giacomo Ciamician at the beginning of the 20th century,[5] the use of light to achieve chemical transformations, at times inconceivable (or even impossible) by alternative means, has lead Photochemistry to be a fundamental part in organic synthesis.[6] In spite of the ability of photochemical reactions to generate compounds of relevant structural complexity, often rapidly through a single photochemical step, one of the reasons why light promoted synthesis is getting attention nowadays is the need of mild, direct and non-polluting synthetic methods. The research that is currently done in this field is driven primarily by the need of avoiding an irreversible damage to the environment and by the economic motivation of avoiding the high cost of using nonrenewable energy resources and recovering polluted air and water. As a consequence, the use of light as an agent of chemical change can be considered as one of the most relevant contributions in Green Chemistry, which can be defined as a synthetic philosophy that tries to minimize the use and generation of hazardous and unwanted substances.[7] Figure

[3] Y. Wang, H. Suzuki, J. Xie, O. Tomita, D. J. Martin, M. Higashi, D. Kong, R. Abe, J. Tang. *Chem. Rev*., **2018**, *118*, 5201.
[4] A. S. Mullin, J. T. Fourkas. *J. Phys. Chem. Lett*., **2015**, *6*, 3882.
[5] G. Ciamician. *Science*, **1912**, *36*, 385.
[6] A. Beeler. *Chem. Rev*., **2016**, *116*, 9629.
[7] A. Albini, M. Fagnoni. *Green Chem*., **2004**, *6*, 1.

2 shows the 12 principles which are the pillars of Green Chemistry,[8] highlighting those which are more related with the goals that can be accomplished using photochemical reactions. Due to the fact that many photochemical processes are initiated by a single photon rather than an extra reagent, the atom economy is good to perfect. Using light as a reagent avoids also the need to resort to other hazardous and toxic compounds, what is especially relevant, for example, in photooxidation reactions. As well, the possibility to carry out photochemical transformations in heterogeneous media is an alternative way to reduce the use of solvents.[9] Related to energy efficiency, most common light sources, such us mercury or halogen lamps, are energetically demanding. However, the progress done in developing cheap and energy-efficient light emitting diodes (LEDs) has made them an alternative to classical light sources in order to overcome these limitations, as they are small, with a wide range of wavelengths available and have the advantage that no cooling is needed because heat generation is minimal. Moreover, the possibility to use sunlight mediated processes opens the door to reach complete nonpolluting and energy efficiency processes, since a renewable source of energy is used in this case. Finally, the use of photocatalysts, especially in photoredox reactions must be considered as an example of efficiency in chemical transformations.[10]

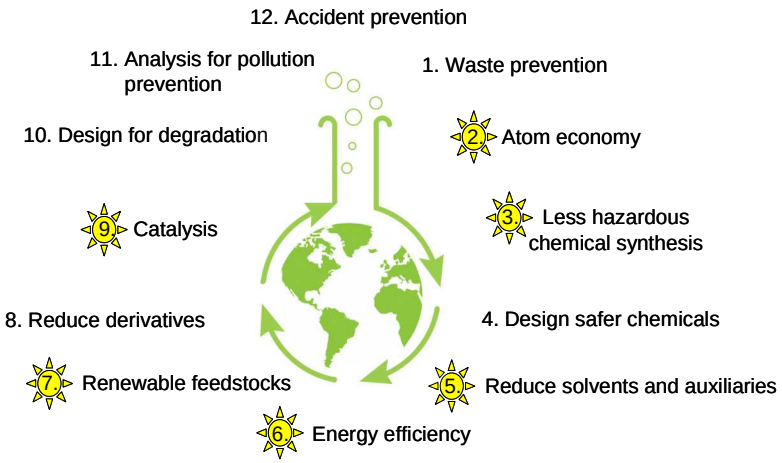

Figure 2. 12 Rules of Green Chemistry. Those most related with photochemical achievements are highlighted.

[8] P. T. Anastas, J. C. Warner. Green Chemistry: Theory and Practice, Oxford University Press: New York, 1998, p.30
[9] C. M. Friend. *Chem. Rec*., **2014**, *14*, 944.
[10] B. König. *Eur. J. Org. Chem*., **2017**, *15*, 1979.

With the aim to show the potential of photochemical synthesis, Figure 3 summarizes at a glance the most common photochemical reactivity, without considering photooxidation reactions mediated by singlet oxygen, which will constitute a specific chapter in this work. For example, the α-cleavage of ketones (Norrish Type I reaction) is a good illustration of dissociation reactions mediated by light. As well, photo-*cis*-*trans* isomerization can be done in order to reach photostationary states where the most thermodynamically unstable isomer can be the major product. In addition, the Fries rearrangement of aryl or acyl esters can also be made using light. Moreover, one of the most interesting fields in synthetic photochemistry are the cycloaddition reactions which cannot be performed by thermal activation. For instance, optimization of the reaction conditions in [2+2] photocycloadditions could be of interest as they can be seen as reactions which fulfil the synthetic philosophy of click Chemistry.[11] As a last example, photoredox catalysis, especially in those processes where Eosin Y is involved, has emerged as an interesting way to carry out, among others, reductive deoxygenations, desulfonylations and dehalogenations, or the oxidation of alkynes or benzylic alcohols.[12]

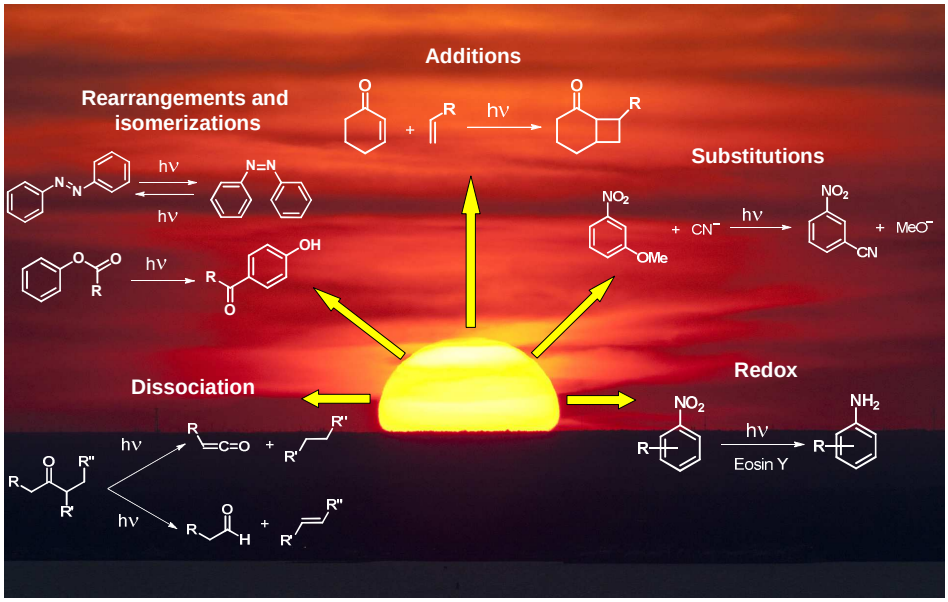

Figure 3. Summary of some of the most general photochemical reactions.

[11] T. Junkers. *Eur. Polym. J.*, **2015**, *62*, 273.
[12] V. Srivastava, P. P. Singh. *RSC. Adv.*, **2017**, *7*, 31377.

1.2. Light as a tool in medicine

In 1903 the Nobel Prize in Physiology and Medicine was awarded to Niels Finsen "*in recognition of his contribution to the treatment of diseases, especially lupus vulgaris, with concentrated light radiation, whereby he has opened a new avenue for medical science*."[13]

Since then, modern medicine has experienced profound changes due to the use of light and optical techniques, where numerous lasers and optical devices are currently being used in clinical practice to improve health and treat disease. The most relevant applications of light in medicine can be organized in three categories: diagnosis, surgery and light-activated therapies.[14] In this sense, Figure 4 lists several illustrative examples among these categories.

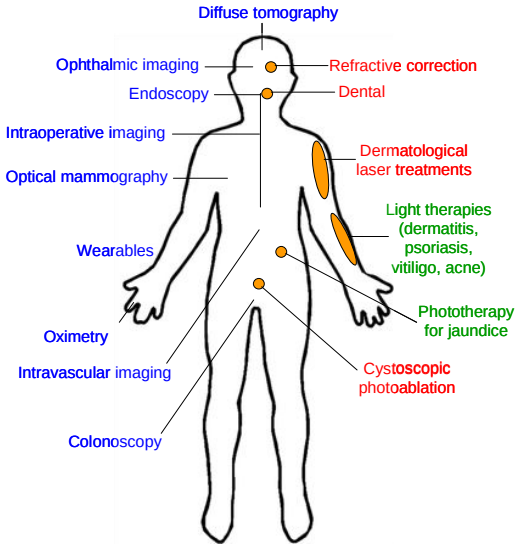

Figure 4. General applications of light in diagnosis (blue), surgery (red) and therapies (green).

In diagnosis, optical technologies enable real-time visualization of tissues and cells at high spatial resolutions, so a wide range of these techniques are used currently in laboratory testing, to screening and diagnostic imaging, treatment monitoring and intraoperative imaging. As a representative example of this application, ocular angiography monitorizes the emission of sodium fluorescein

[13] P. C. Gotzsche. *J. R. Soc. Med.*, **2011**, *104*, 41.
[14] S. H. Yun, S. S. J. Kwok. *Nat. Biomed. Eng.*, **2017**, *1*, 8.

injected intravenously in order to study the vascularization of the retina and choroid in normal and diseased states. On the other hand, the development of lasers has allowed the use of light with high intensities in many applications. First of all, surgeries in ophthalmology, where this energy is able to reshape the cornea, so it is widely used for refractive error corrections as well as to seal retinal tears or small retinal detachments. Lasers are also present in cataract surgeries, where they are used in order to create an incision on the lens and gain access to the cataract. These surgeries can be done also in the treatment of cutaneous disorders, destructing a target within the skin, but minimizing the risk of scarring and damage to normal tissue. Moreover, tissue ablation in internal organs through light delivery via optical fibres can be done, just like the removal and change of soft and hard tissues in the oral cavity. Finally, many more examples may be considered regarding those therapies making direct use of light (those treatments which require concomitant photoactive molecules will be the subject of a specific chapter in this work). One of the best known examples is the blue-light phototherapy, used to treat severe neonatal hyperbilirubinemia. Neonatal jaundice occurs when bilirubine builds up faster than a newborn's liver is able to break it down. This results in the deposition of water-insoluble bilirubine in the skin (giving the skin a yellow colour). The phototherapy is based on the well-known fact that the bilirubine molecule has two isomerisable double bonds, which normally exist as the *cis-cis* isomer, leading to a helical structure which presents intramolecular hydrogen bonds that decrease its solubility in water. In the phototherapy treatment, blue light produces the photoisomerization of these double bonds to the *trans-trans* water-soluble isomer, which is easily excreted from the organism (Scheme 1).[15]

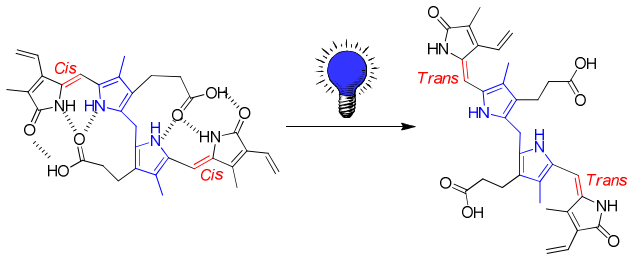

Scheme 1. *Cis-cis* isomer of bilirubine (water–insoluble) isomerized to the *trans-trans* isomer (water–soluble) by blue-light phototherapy in neonatal jaundice treatment.

[15] B. Wardle. Principles and Applications of Photochemistry, Wiley: London, 2009, pp. 148-149.

GENERAL BACKGROUND

2. GENERAL BACKGROUND

2.1. Singlet molecular oxygen: electronic structure

Despite its apparent simplicity, O_2 molecule exhibits a number of rather unusual properties with respect to its magnetic behaviour, spectroscopy, energy transfer processes and chemical reactivity. These peculiarities are a consequence of the open-shell electronic structure of the molecule in its ground state, shown in [1]:

$$(K)(K)(2\sigma_g)^2(2\sigma_u)^2(3\sigma_g)^2(1\pi_u)^4(1\pi_{g,x})^1(1\pi_{g,y})^1 \quad [1]$$

The electron term associated with the presence of two unpaired electrons in $(1\pi_{g,x})$ and $(1\pi_{g,y})$ orbitals (with parallel spins) is $X\ ^3\Sigma_g^-$. However, if these electrons have antiparallel spins, two low-lying singlet excited states, $a^1\Delta_g$ and $b^1\Sigma_g^+$, are produced depending on the π^* orbitals occupied, as it is shown in Figure 5.[16, 17]

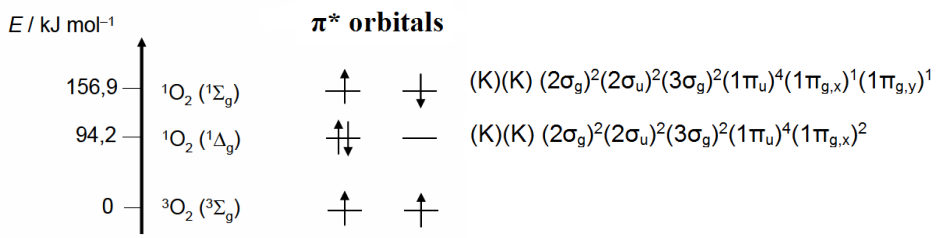

Figure 5. Energy, electron and spin distribution in π^* orbitals for $X\ ^3\Sigma_g^-$, $a^1\Delta_g$ and $b^1\Sigma_g^+$ states and the resulting electron configurations of the excited states.

The transition from ground state $X\ ^3\Sigma_g^-$ to $a^1\Delta_g$ or $b^1\Sigma_g^+$ excited states is forbidden by several selection rules. For instance, the different multiplicity and the same symmetry "g" (with respect to an inversion center in the O–O bond). In addition, $\Delta\Lambda \neq 0, \pm 1$ for $X\ ^3\Sigma_g^- \leftrightarrow a^1\Delta_g$ transition. On the other hand, the main consequence of the spin-allowed transition from $b^1\Sigma_g^+$ to $a^1\Delta_g$ is that $b^1\Sigma_g^+$ state is relatively short-lived in comparison with $a^1\Delta_g$. This difference in stability is confirmed by the radiative lifetimes of $a^1\Delta_g$ and $b^1\Sigma_g^+$, which are 72 min and 11,3 s in the gas phase, respectively. Due to the metastability of $a^1\Delta_g$, this state is commonly referred as "singlet oxygen" ($^1O_2$).[17]

[16] P. R. Ogilby. *Chem. Soc. Rev*., **2010**, *39*, 3181.
[17] C. Schweitzer, R. Schmidt. *Chem. Rev*., **2003**, *103*, 1685.

2.2. Methods for $^1O_2$ production

2.2.1. Thermal generation of $^1O_2$

The production of singlet oxygen by means of chemical reactions is a well stablished topic since several decades ago. Scheme 2 summarises some chemical reactions used for lab-scale singlet oxygen production.[18]

$$H_2O_2 + NaOCl \rightarrow {}^1O_2 + NaCl + H_2O$$

$$Ph_3C{-}P\begin{matrix}O\\ \diagup\ \diagdown\\ O\end{matrix}O \xrightarrow[-78\ ^oC]{} Ph_3PO + {}^1O_2$$

Scheme 2. Chemical reactions for $^1O_2$ production.

However, these procedures involve the use of hazardous reactants and/or harsh experimental conditions, which are relevant limitations for the development of applications. In this sense, several alternatives have been investigated.

For example, reversible molecular carriers of singlet oxygen such us organic endoperoxides release the oxygen molecule as $^1O_2$ upon decomposition. The lifetime of the endoperoxide precursors depends on the temperature and their chemical structure. As a consequence, $^1O_2$ can be stored, ideally, at low temperature for long periods of time and, thereafter, released by heating. Decomposition of the endoperoxide yields the parent organic molecule, which could be bound to a new $^1O_2$ molecule. Derivatives from alkylnaphthalenes and 2-pyridones are among the most studied examples of functional groups which can undergo the reversible formation of endoperoxides for this purpose. For instance, Figure 6 shows a series of 2-pyridones with half-lives ranging from 0.5 to 15 h at 37 ºC and $^1O_2$ yields depending on the stability and recovery of the parent 2-pyridone. It is interesting to highlight some examples of conjugate molecules with a porphyrin core that is able to generate $^1O_2$ using light (see Section 2.2.2) and peripheral 2-pyridone moieties that trap the generated $^1O_2$ and

[18] a) I. Rosenthal. Chemical and Physical Sources of Singlet Oxygen. In Singlet O_2. Vol. I, Physical and Chemical Aspects. A. A. Frimer ed. CRC Press: Boca Raton, FL, 1985, pp. 13-38. b) J. Bland. *J. Chem. Educ*., **1976**, *53*, 274. c) A. M. Braun, M.-T. Maurette, E. Oliveros. Photochemical Technology. Wiley: London, 1991, p. 452.

storage it until it is released by the thermal activation (40 ºC) of the endoperoxide (Scheme 3).[19]

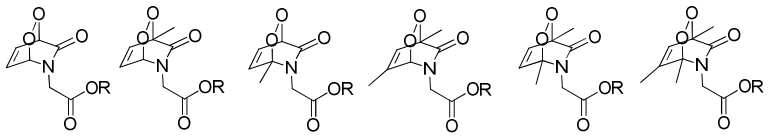

$t_{1/2}$ / h	0.5	8.5	4	13	4	15
$^1O_2$ yield / %	18	78	50	47	50	10

Figure 6. Values for the delivery of $^1O_2$ (half-life and % $^1O_2$ yield) by 2-pyridone endoperoxides in water at 37 °C. R = $CH_2CH_2(OCH_2CH_2O)_2CH_3$.[19a]

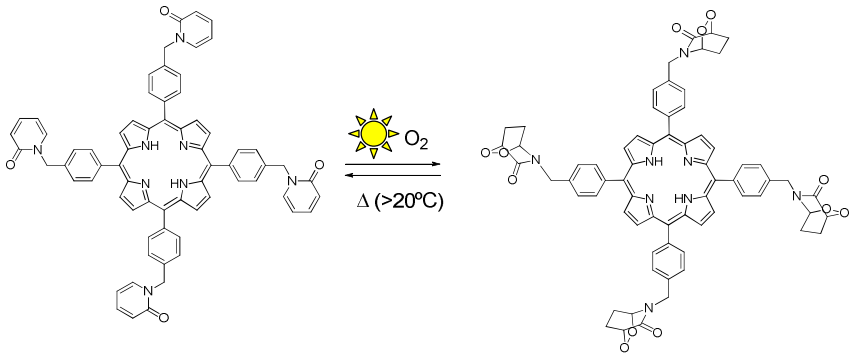

Scheme 3. Example of a conjugate for reversible generation, trapping and release of $^1O_2$.[19c]

Of special interest, mainly in biological applications, are the peroxidation reactions catalyzed with enzimes, which can yield excited triplet carbonyls that photosensitize singlet oxygen production themselves. For example, the aerobic oxidation of 2-methylpropanal catalyzed by horseradish peroxidase (HRP) yields formic acid and acetone in its triplet excited state. By an energy transfer (ET) process from this triplet state, the oxygen molecule can be excited to $^1O_2$ (Scheme 4).[20]

---

[19] a) M. A. Filatov, M. O. Senge. *Mol. Syst. Des. Eng*., **2016**, *1*, 258. b) S. Benz, S. Nötzli, J. S. Siegel, D. Eberli and H. J. Jessen, *J. Med. Chem*., **2013**, *56*, 10171. c) C. Changtong, D. W. Carney, L. Luo, C. A. Zoto, J. L. Lombardi, R. E. Connors. *J. Photochem. Photobiol., A*, **2013**, *260*, 9.

[20] C. M. Mano, F. M. Prado, J. Massari, G. E. Ronsein, G. E. Martínez, S. Miyamoto, J. Cadet, H. Sies, M. H. G. Medeiros, E. J. H. Bechara, P. Di Mascio. *Sci. Rep*., **2014**, *4*, 5938.

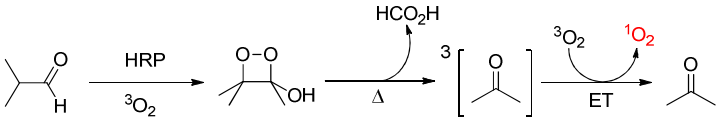

Scheme 4. $^1O_2$ generation induced enzymatically using HRP.

2.2.2. Photosensitized generation of $^1O_2$

In spite of the potential of the previous research, photosensitization represents the most convenient, safe, easy and environmentally-friendly method for $^1O_2$ production. This photocatalytic process requires the presence of light of appropriate wavelength, molecular oxygen and a dye (called photosensitizer) which employs the energy of a photon for the excitation of molecular oxygen. The set of possible competitive processes that can be present in the photosensitized production of $^1O_2$ are shown in the Jablonski diagram depicted in Figure 7 (where radiative pathways are displayed with straight arrows and radiationless pathways with wavy arrows).

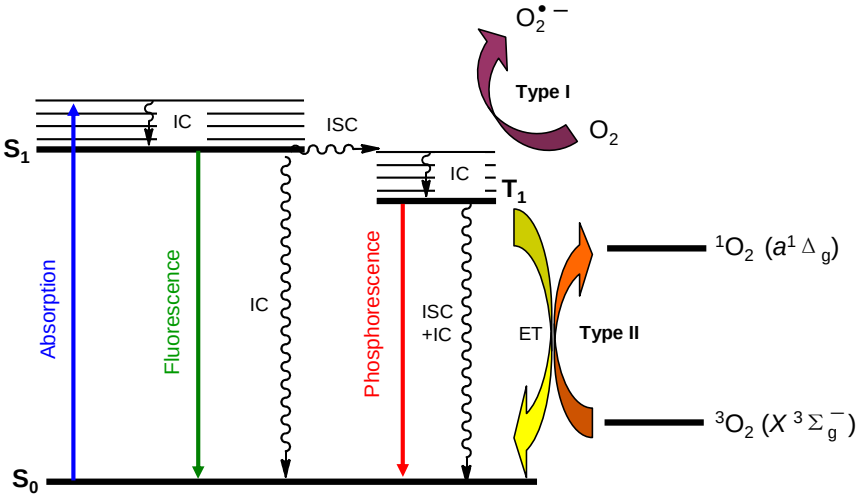

Figure 7. Jablonski diagram for the photosensitized $^1O_2$ production by a photosensitizer.

Upon photon absorption by the photosensitizer (P) in its ground state (S_0), it is excited to a singlet excited state (S_n) with an excess of vibrorotational energy. Subsequently, the excited molecule in S_n relaxes by internal conversion (IC) to the lowest singlet excited state of the photosensitizer (S_1). This state can evolve by different ways: spontaneous emission of energy (fluorescence), thermal

deactivation (internal conversion, IC) or a change in its multiplicity leading to a triplet excited state (T_1) by an intersystem crossing (ISC). T_1 can be deactivated by phosphorescence emission or by an ISC + IC to the ground state. However, the relevance of T_1 lies in its lifetime, which is longer (ms) than that of the S_1 state (ns). In the presence of molecular oxygen, this excited state T_1 is able to react in one of two ways, defined as Type I and II mechanisms:

- **Type I mechanism**: An electron transfer occurs between the excited photosensitizer and molecular oxygen to form active oxygen species such as the superoxide radical anion ($O_2^{\bullet -}$).
- **Type II mechanism**: Singlet oxygen ($a^1\Delta_g$) is generated via an energy transfer process during a collision between the excited photosensitizer (P) in its T_1 state and an oxygen molecule in its ground state ($X\ ^3\Sigma_g^-$).

The efficiency of $^1O_2$ generation can be defined by the $^1O_2$ production quantum yield (Φ_Δ) in [2].

$$\Phi_\Delta = \frac{amount\ of\ ^1O_2\ generated}{amount\ of\ photons\ absorbed} \qquad [2]$$

Type II mechanism is summarized in equations [3] and [4]

$$P(S_0) \xrightarrow{h\nu} P(S_1) \xrightarrow{k_{ISC}} P(T_1) \qquad [3]$$

$$P(T_1) + {}^3O_2 \xrightarrow{k_{en}} P(S_0) + {}^1O_2 \qquad [4]$$

Where P represents the photosensitizer, k_{ISC}, the unimolecular intersystem crossing rate constant, and k_{en} the bimolecular energy transfer rate constant (type II mechanism).

The ability of a photosensitizer for $^1O_2$ production is measured in terms of its singlet oxygen production quantum yield, which takes into account all the photochemical and photophysical processes involving the photosensitizer and molecular oxygen. In addition to path [4], radiative (phosphorescence) [5] and nonradiative pathway [6] (ISC + IC to ground state) must be considered for $P(T_1)$ quenching:

$$P(T_1) \xrightarrow{k_r} P(S_0) + h\nu \qquad [5]$$

$$P(T_1) \xrightarrow{k_{nr}} P(S_0) \qquad [6]$$

In addition, the quenching of $P(T_1)$ is also possible considering bimolecular reactions, such as physical quenching by O_2 [7] and direct electron transfer (type I mechanism) [8].

$$P(T_1) + O_2 \xrightarrow{k_d\,(O_2)} P(S_0) + O_2 \qquad [7]$$

$$P(T_1) + O_2 \xrightarrow{k_{et}} P^{+} + O_2^{\bullet -} \qquad [8]$$

Considering the processes [3-8], the global singlet oxygen production quantum yield, Φ_Δ, is:

$$\Phi_\Delta = \Phi_T \phi_{en} = \Phi_T \left(\frac{k_{en}[O_2]}{k_r + k_{nr} + k_q[O_2]} \right) \qquad [9]$$

Where Φ_T is the quantum yield of $P(T_1)$ formation; ϕ_{en}, the efficiency of energy transfer (between $P(T_1)$ and $^3O_2$) and k_q the sum of rate constants for the quenching of $P(T_1)$ by O_2 ($k_q = k_{en} + k_d(O_2) + k_{el}$), being k_{en} the rate constant of energy transfer and k_{el} the rate constant of electron transfer processes, respectively. As a result, Φ_Δ can also be calculated with [10]:

$$\Phi_\Delta = \Phi_T \; f_\Delta^T \; P_{O_2}^T \qquad [10]$$

Where f_Δ^T represents the fraction of triplet states quenched by oxygen which yields $^1O_2$ (or the efficiency of singlet oxygen formation) and Po_2^T represents the fraction of triplet states quenched by oxygen, yielding or not singlet oxygen.[21]

[21] a) N. J. Turro, J. C. Scaiano, V. Ramamurthy. Principles of Molecular Photochemistry: An Introduction, University Science Books: Sausalito, 2009, p. 383. b) D. García-Fresnadillo, S. Lacombe. Reference Photosensitizers for the Production of Singlet Oxygen. In Singlet Oxygen: Applications in Biosciences and Nanosciences, Volume 1 (Eds.: Nonell, S.; Flors C.), The Royal Society of Chemistry, Cambridge, 2016, pp. 105-143. c) M. C. DeRosa, R. J. Crutchley. *Coord. Chem. Rev*., **2002**, *233-234*, 351.

Regarding the kinetics of $^1O_2$ generation, it can be assumed that at a time close to 0, after the excitation of the photosensitizer to S_1 and the subsequent ISC, there is a population of $P(T_1)$ molecules given by [11]:

$$[P(T_1)]_0 = [P(S_1)]_0 \cdot \Phi_T \quad [11]$$

If the concentration of oxygen is kept constant and much larger than $P(T_1)$, the decay of $[P(T_1)]$ follows first-order kinetics with lifetime τ_T [12]:

$$[P(T_1)]_t = [P(T_1)]_0 \cdot e^{-\frac{t}{\tau_T}} \Rightarrow [P(T_1)]_t = [P(S_1)]_0 \cdot \Phi_T \cdot e^{-\frac{t}{\tau_T}} \quad [12]$$

As a consequence, $^1O_2$ rises (according to $[P(T_1)]$) and decays (according to its deactivation following first-order kinetics with lifetime τ_Δ), and the singlet oxygen decay trace obtained in a time-resolved emission experiment in the near-infrared (NIR) spectral region that can be fitted by a biexponential function [13]:[22]

$$[^1O_2]_t = [P(S_1)]_0 \cdot \Phi_\Delta \cdot \frac{\tau_\Delta}{\tau_\Delta - \tau_T} \cdot \left[e^{-\frac{t}{\tau_\Delta}} - e^{-\frac{t}{\tau_T}} \right] \quad [13]$$

2.3. Methods for $^1O_2$ detection and photophysical characterizations

As it has been shown in the previous section, it is interesting to characterize the ability of a photosensitizer for $^1O_2$ generation, especially in terms of the Φ_Δ value. Due to the fact that $^1O_2$ is a metastable very reactive species, there is only one method for its direct detection: the phosphorescence emission of $^1O_2$ at 1270 nm. However, several indirect methods, based mainly on $^1O_2$ trapping, have been extensively developed. A brief summary of these methods for $^1O_2$ detection will be presented in the following section.

[22] S. Nonell, C. Flors. Steady-State and Time-Resolved Singlet Oxygen Phosphorescence Detection in the Near-IR. In Singlet oxygen. Applications in Biosciences and Nanosciences. Volume 2, The Royal Society of Chemistry, Cambridge, 2016, pp. 10-21.

2.3.1. Time resolved $^1O_2$ phosphorescence

$^1O_2$ shows a characteristic phosphorescence emission in the near-infrared (NIR) region of the spectra, around 1270 nm. Time-resolved $^1O_2$ phosphorescence detection (TRPD) constitutes the most relevant method in order to gain information about the quantification and kinetics of $^1O_2$ production, diffusion, reactivity and decay.

The most widespread $^1O_2$ detection system is based on the scheme shown in Figure 8: a light source, either pulsed or continuous, is used to excite the sample. In the case of time-resolved measurements, diode pumped lasers are the most common sources. It is usual to work with repetition rates around 1–100 kHz and delivering pulses of a few nanoseconds pulsewidth and an energy of a few microjoules. This excitation beam must be cleaned using cut-off filters in order to remove any NIR component. The most common arrangement between excitation and detection beams is the right-angle geometry, so samples can be contained in standard fluorescence cells. In the emission pathway, lenses are inserted to collect and focus as much as possible of the emitted photons onto the detector, cut-on filters to block scattered excitation light and bandpass filters at 1270 nm to isolate $^1O_2$ emission from fluorescence and phosphorescence from the photosensitizer. Regarding the detector, the Hamamatsu H103130A-45 NIR-PMT module in photon-counting mode combined with a multichannel scaler is able to reach a time resolution of a few nanoseconds, which is suitable for most applications.[21, 23]

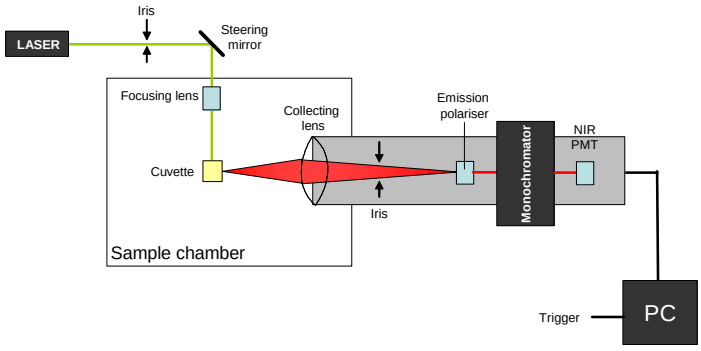

Figure 8. Experimental setup for time resolved $^1O_2$ phosphorescence detection.

[23] a) S. Nonell, S. E. Braslavsky. *Methods in enzymology*, **2000**, *319*, 37. b) A. Jimenez-Banzo, X. Ragas, P. Kapusta, S. Nonell, *Photochem. Photobiol. Sci.*, **2008**, *7*, 1003.

As a result, taking into account the variation of $[^1O_2]$ as a function of time described in [13], the detected phosphorescence signal S_t will be [14].

$$S_t = \kappa \cdot k_{\Delta,R} \cdot [^1O_2]_t = \kappa \cdot k_{\Delta,R} \cdot [P(S_1)]_0 \cdot \Phi_\Delta \cdot \frac{\tau_\Delta}{\tau_\Delta - \tau_T} \cdot \left[e^{-\frac{t}{\tau_\Delta}} - e^{-\frac{t}{\tau_T}} \right] \quad [14]$$

Where κ is a proportionality constant related with instrumental factors and $k_{\Delta,R}$, the $^1O_2$ radiative decay rate constant. Equation [14] can be summarized in [15], where $S_0 = \kappa \cdot k_{\Delta,R} \cdot [P(S_1)]_0 \cdot \Phi_\Delta$.

$$S_t = S_0 \cdot \frac{\tau_\Delta}{\tau_\Delta - \tau_T} \cdot \left[e^{-\frac{t}{\tau_\Delta}} - e^{-\frac{t}{\tau_T}} \right] \quad [15]$$

But the dependence of S_0 on Φ_Δ opens the door to calculate this last value by comparison of S_0 for a sample and a reference photosensitizer measured under the same conditions:[23b]

a) Working with solutions of the same absorbance at the excitacion wavelength and the same light fluence in order to get similar $[P(S_1)]_0$

b) Working with the same solvent for the sample and the reference, due to the dependence between $k_{\Delta,R}$ on the refractive index of the solvent.

Under these conditions, Φ_Δ can be calculated using equation [16]

$$\Phi_{\Delta,Sample} = \Phi_{\Delta,Ref} \cdot \frac{S_{0,Sample}}{S_{0,Ref}} \quad [16]$$

2.3.2. Chemical probes

In spite of the robustness and the specificity of direct $^1O_2$ detection by measuring its phosphorescence, the weak signal and the low signal-to-noise ratios that can be obtained constitute the main drawbacks that may limit the use of this technique, unless suitable experimental conditions and highly sensitive

equipments are used. On the other hand, detection of $^1O_2$ has been explored using different types of chemical probes. These compounds are acceptors which react with $^1O_2$ yielding spectroscopically detectable intermediates or products. This detection can be done by absorption and emission spectroscopy techniques. For example, the specific reaction between 9,10-diphenylanthracene and $^1O_2$ leading to the corresponding endoperoxide can be monitorized by the decrease in absorbance at 355 nm, which is proportional to the amount of $^1O_2$ generated.[24] However, the sensitivity achieved by this method is not good enough for detection in many applications, so most of the efforts have been focused on the development of highly sensitive fluorescent probes, especially those built by the conjugation of a chemical trap and a fluorophore whose emission is quenched by the $^1O_2$ scavenger but is activated only after the reaction of $^1O_2$ with the chemical trap. Such fluorescence quenching enhancement scheme can be developed by means of three main mechanisms. Firstly, a photoinduced electron-transfer (PET) scheme for chemical $^1O_2$ sensing will be presented. As an example, the commercial Singlet Oxygen Sensor Green (SOSG) consists in a covalently bound fluorescein (fluorophore) and an anthracene group (chemical trap), where a PET is responsible for the fluorescence quenching. Only when the anthracene moiety reacts with $^1O_2$ leading to the corresponding endoperoxide, the fluorescein is able to recover its fluorescence (Scheme 5a).[25] The main problem of SOSG is the self-sensitization of $^1O_2$, but other probes based on the same structural design have been synthesized, overcoming this limitation.[26] On the other hand, when the chemical trap is substituted by other moieties like furan derivatives and attached to the fluorophore through extended π systems, the fluorescence is quenched by intramolecular charge transfer processes (CT) (Scheme 5b).[27]

[24] H. Wu, Q. Song, G. Ran, X. Lu, B. Xu. *Trends Anal. Chem.*, **2011**, *30*, 133.
[25] S. Kim, M. Fujitsuka, T. Majima. *J. Phys. Chem. B*, **2013**, *117*, 13985.
[26] S. K. Pedersen, J. Holmehave, F. H. Blaikie, A. Gollmer, T. Breitenbach, H. H. Jensen, P. R. Ogilby. *J. Org. Chem.*, **2014**, 79, 3079.
[27] R. Ruiz-Gonzalez, R. Zanocco, Y. Gidi, A. L. Zanocco, S. Nonell. E. Lemp. *Photochem. Photobiol.*, **2013**, *89*, 1427.

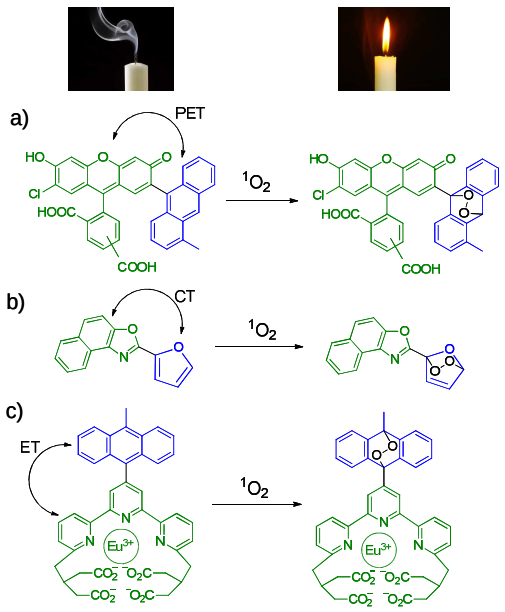

Scheme 5. Examples of photoswitchable $^1O_2$ chemical probes based on: a) photoinduced electron transfer, b) charge transfer and c) energy transfer.

Thirdly, some luminescent rare earths chelates may be conjugated to $^1O_2$ scavengers where the emission spectrum of the fluorophore and the absorption spectrum of the chemical trap overlap, so the quenching is based on an intramolecular energy transfer process (ET). When the chemical trap reacts with $^1O_2$, its absorption spectra is shifted and ET quenching is eliminated (Scheme 5c).[28]

In order to gain even more sensitivity in $^1O_2$ detection, chemiluminescent probes have also been a focus in this field, as they provide luminescence without the need of photoexcitation (eliminating the problem of background fluorescence and light scattering). The most extended approach is the alkene activation in order to generate the corresponding 1,2-dioxetane after the reaction with $^1O_2$. 1,2-Dioxetanes are high-energy moieties which fastly evolve to give a carbonyl compound in its excited-state as product. The radiative deactivation of this excited state is responsible for the emission of light. Scheme 6a shows an example of this sort of probes. However, the main problem dealing with the

[28] B. Song, G. Wang, M. Tan, J. Yuan. *J. Am. Chem. Soc*., **2006**, *128*, 13442.

activation of double bonds is the often common presence of competing reactions. Therefore, other structural designs have also been considered. For instance, a dyad of tetrathiafulvalene (TTF) and anthracene where a photoinduced electron transfer process leads to luminiscence, taking advantage of the electron donor behaviour of the TTF moiety towards $^1O_2$ (Scheme 6b).[29]

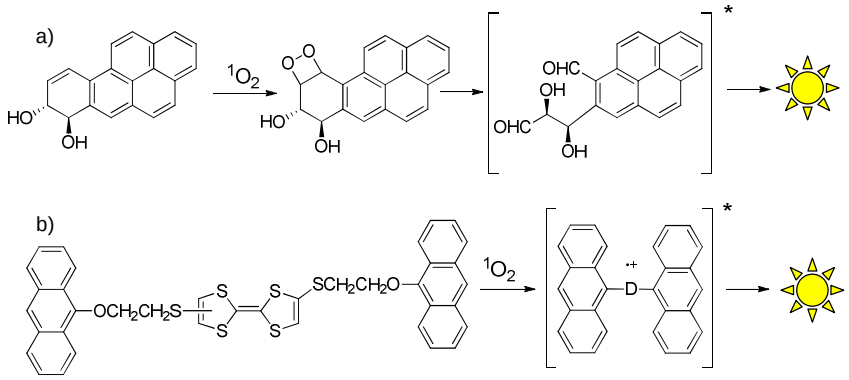

Scheme 6. Examples of chemiluminescent $^1O_2$ probes based on: a) 1,2-dioxetanes generation and b) photoinduced electron transfer.

2.4. Main features of $^1O_2$ photosensitizers

The main requirements that a photosensitizer must fulfil in order to be considered as an ideal singlet oxygen production dye are the following:

- Intense absorption in the UV-vis range (preferentially between 400 and 750 nm in order to develop applications in fields like sunlight-driven Green Chemistry or photodynamic therapy) with molar absorption coefficients larger than 10^4 M^{-1} cm^{-1}.
- High efficiency for intersystem crossing, close to 100%, and $P(T_1)$ energy greater than $^1O_2$ level energy (94,2 KJ mol^{-1}) for an efficient energy transfer.

[29] G. Zhang, X. Li, H. Ma, D. Zhang, J. Li, D. Zhu. *Chem. Commun.*, **2004**, 2072.

- Long $P(T_1)$ lifetimes (around μs) to increase the probability of collision between the excited photosensitizer and $^3O_2$.
- High quantum yields of singlet oxygen production in different organic solvents and in water.
- High thermal and photochemical stability.
- Low rate constant of $^1O_2$ quenching by the photosensitizer itself, avoiding dye-autoxidation processes.
- Ability to be immobilized in polymeric scaffolds in order to develop applications.

The most important drawbacks that can occur in $^1O_2$ production by photosensitizers are:

- Changes in the photophysical properties. This is especially important when the photosensitizer is going to be immobilized in a polymer scaffold, since changes in the absorption bands and lifetimes of $P(T_1)$ can decrease the singlet oxygen production efficiency.
- Quenching of singlet oxygen by solvent and photosensitizer molecules, especially when the concentration of photosensitizer is high.
- Depletion of oxygen. If photogenerated $^1O_2$ reacts with a substrate, oxygen concentration decreases until complete elimination, especially with experiments which involve long irradiations in closed reaction systems.[30]

Although there is no ideal photosensitizer showing all the previous requirements, there are several UV-vis absorbing molecules which are able to efficiently generate $^1O_2$. As a result of the diversity of compounds whose ability to produce $^1O_2$ has been reported, only the main groups of photosensitizers will be presented (Figure 9).

[30] D. García-Fresnadillo. Solarsafewater: Tecnologías solares para la desinfección y descontaminación del agua, UNSAM editorial: Buenos Aires, 2005, pp. 231-232.

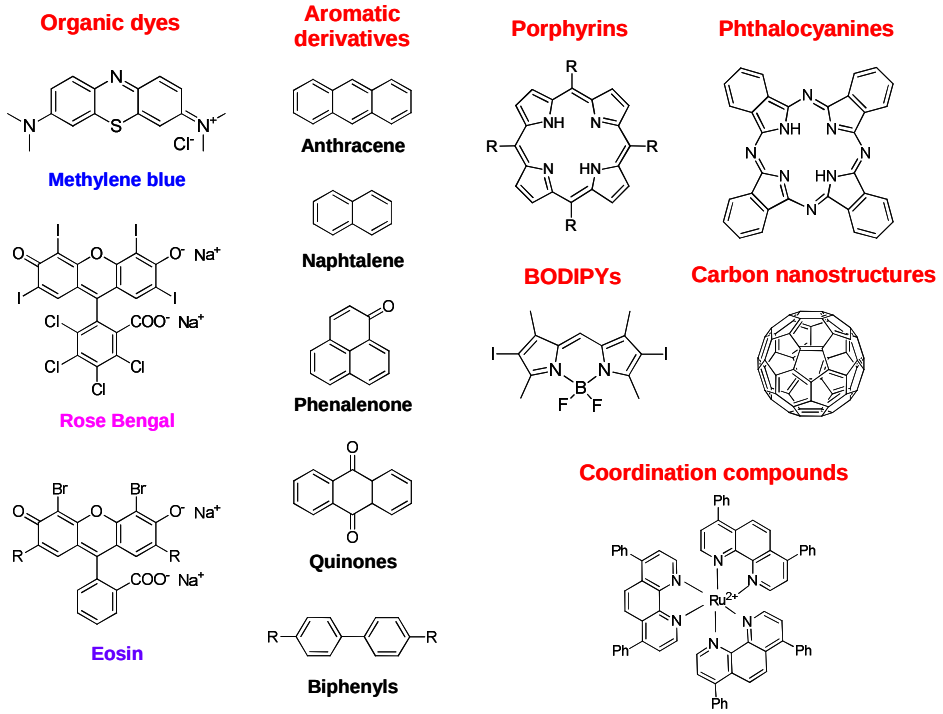

Figure 9. Summary of the main families of compounds used as $^1O_2$ photosensitizers.[21b]

Organic dyes like methylene blue, rose Bengal and eosin are among the most used photosensitizers in $^1O_2$ production. Methylene blue absorbs in the range of 550-700 nm, with a $\Phi_\Delta = 0.52$ in water. On the other hand, rose Bengal and eosin show absorption spectra shifted to the green part of the visible spetrum (480-550 nm), with $\Phi_\Delta = 0.76$ and 0.57, respectively in water.[31] In the latter compounds, the presence of heavy halogen atoms contributes to the increase in Φ_T due to the spin-orbit coupling, which favours ISC. This strategy has been used in other dyes such as BODIPYs for decreasing fluorescence deactivation while producing an enhancement in Φ_Δ values, although the number and kind of halogens, as well as the substitution pattern have been proved to play a key role in this property.[32] Similarly, among the aromatic hydrocarbons (especially for

[31] R. W. Redmond, J. N. Gamlin. *Photochem. Photobiol.*, **1999**, *70*, 391.

[32] a) A. J. Sánchez-Arroyo, E. Palao, A. R. Agarrabeitia, M. J. Ortiz, D. García-Fresnadillo. *Phys. Chem. Chem. Phys.*, **2017**, *19*, 69. b) T. Yogo, Y. Urano, Y. Ishitsuka, F. Maniwa, T. Nagano. *J. Am. Chem. Soc.*, **2005**, *127*, 12162. c) Y. C. Lai, S. Y. Su, C. C. Chang. *Appl. Mater. Interfaces*, **2013**, *5*, 12935.

anthracene, naphthalene and biphenyl derivatives), a strong influence of substituents in $^1O_2$ production has been found depending on the electron donor/withdrawing nature of the groups attached to the dye, since a competition between energy transfer and charge transfer processes arises.[33] However, one of the main interests in the search of new $^1O_2$ photosensitizers is the use of structures which could show good biocompability. In this sense, quinones, porphyrins and phthalocyanines are among the most studied examples. Poprhyrins are characterized by a highly conjugated delocalized π-electron system which is responsible for their absorption and emission features, both in the blue region (Soret band) and the red region (Q-band) of the visible spectrum. However, the peripheral functionalization with halogen groups, the metal ions coordinated in the central core and the use of ligands in axial positions of the metal ion have led to a wide tuning of the photophysical properties of these derivatives. Structurally analogous to porphyrins, phthalocyanines present an extension of the π-system due to the external benzene rings, enhancing the absorption properties. In this case, it has been found that long triplet lifetimes and high Φ_T are obtained in derivatives containing diamagnetic metal ions (Al^{3+} or Zn^{2+}), but the same cannot be said about paramagnetic metal ions (Cu^{2+}) derivatives. In both cases, porphyrins and phthalocyanines, self-degradation mediated by $^1O_2$ can be observed, what, however, can be of interest in medical applications where the fast elimination of the sensitizer could be desired, provided that the photodegradation products are not toxic themselves.[34] The use of inorganic metal complexes has also been considered in $^1O_2$ generation. One of the most widely studied systems are the Ru(II) coordination compounds with general formula $[RuL_3]^{2+}$ (being L= *N*-heteroaromatic ligands such as 1,10-phenanthroline and its derivatives functionalized in positions 4 and 7, 2,2'-bipyridine, 2,2'-bipyrimidine or 2,2'-bipyrazine). The main advantages of this class of compounds are: intense absorption between 400 and 550 nm with molar absorption coefficients between 10^4 and $5\cdot10^4$ M^{-1} cm^{-1}, Φ_T values close to unit efficiency, long lifetimes for $P(T_1)$ ($10^{-7} < \tau < 6\cdot10^{-6}$ s), the possibility of fine tuning of the photophysical properties of the Ru(II) complex via suitable

[33] a) F. Wilkinson, A. A. Abdel-Shafi, *J. Phys. Chem. Sect. A*, **1999**, *103*, 5425. b) D. J. McGarvey, P. G. Szekeres, F. Wilkinson. *Chem. Phys. Lett*., **1992**, *199*, 314.

[34] a) H. G. Jeong, M. S. Choi. *Isr. J. Chem*., **2016**, *56*, 110. b) K. Ishii. *Coord. Chem. Rev*, **2012**, *256*, 1556.

functionalization of the ligands and, finally, the ability to be immobilized in polymeric scaffolds.[35]

Finally, the search for new $^1O_2$ photosensitizers based on two-photon absorption photosensitization instead of the one photon process depicted in Figure 7, is a growing field in the last years. The main difference lies in the excitation of the ground state electrons at the beginning of the process, because in this case two low-energy photons are absorbed and their energies are added in order to reach the excited state of the photosensitizer (the first photon populates a virtual state of the photosensitizer, while the second photon allows the formation of the excited photosensitizer). Biphotonic absorption is an example of a nonlinear process, where the population of the excited state increases quadratically with the intensity of the incident light. Moreover, photons must interact with the photosensitizer in the scale of femtoseconds, so pulsed lasers are the most used sources of light in these cases. The main advantages of using photosensitizers based on the absorption of two photons are: i) sensitization and singlet oxygen generation can be confined in a small volume, ii) the spatial generation of $^1O_2$ can be controlled, and iii) the process can be carried out using near-infrared wavelength, what can be of interest in applications such as photodynamic therapy (see background for Chapter 2). Among the photosentizers investigated for biphotonic processes, aromatic ketones such as pyrene-1,6-dione and benzo[*cd*]pyren-5-one can be highlighted.[36]

[35] a) D. García-Fresnadillo, Y. Georgiadou, G. Orellana, A. M. Braun, E. Oliveros. *Helv. Chem. Acta*, **1996**, *79*, 1222. b) M. E. Jiménez-Hernández, F. Manjón, D. García-Fresnadillo, G. Orellana. *Solar Energy*, **2006**, 80, 1382. c) L. Villén F. Manjón, D. García-Fresnadillo, G. Orellana. *Appl. Catal. B Environ*., **2006**, *69*, 1. d) D. García-Fresnadillo. *ChemPhotoChem*, **2018**, *2*, 512.

[36] a) J. Arnbjerg, M. J. Paterson, C. B. Nielsen, M. Jørgensen, O. Christiansen, P. R. Ogilby. *J. Phys. Chem. A*, **2007**, *111*. b) T. Ishi-i, Y. Taguri, S. Kato, M. Shigeiwa, H. Gorohmaru, S. Maeda, S. Mataka. *J. Mater. Chem*., **2007**, *17*, 3341. c) N. Gandra, P. L. Chiu, W. Li, Y. R. Anderson, S. Mitra, H. He, R. Gao. *J. Phys. Chem. C*, **2009**, *113*, 5182.

2.5. [60]Fullerene as $^1O_2$ photosensitizer

[60]Fullerene is a class of closed-cage nanomaterial made exclusively from carbon atoms, which was discovered by H. W. Kroto, R. F. Curl and R. E. Smalley in 1985.[37]

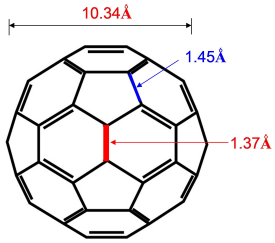

Figure 10. Structure of [60]fullerene with the values of the van der Waals diameter and the lengths of the two different bonds in the molecule.

[60]fullerene presents an icosahedral structure with twelve pentagonal rings isolated by 20 hexagonal rings. The pentagons are responsible for providing the curvature, resulting in two different bonds in the molecule (Figure 10). The unions between two hexagons, [6,6] bonds, are shorter (1.37 Å) than the unions between a hexagon and a pentagon, [5,6] bonds (1.45 Å). As a result, it can be considered that the double bonds are located in the [6,6] bonds, while the pentagonal rings do not present this kind of bonds. Due to the curvature of the molecule, each carbon atom presents a characteristic $sp^{2.3}$ hybridization.[38]

The absorption spectrum of C_{60} is characterized by a strong absorption at 320-350 nm and also a weak sharp absorption peak at 408-410 nm. Although fullerenes present some forbidden transitions in the visible range, these are produced with low absorption coefficients, and are responsible for the purple colour of C_{60} in solution. Related with the emission properties, the fluorescence quantum yield (Φ_f) over the entire emission wavelength region (600-1200 nm) is $3.2 \cdot 10^{-4}$ at room-temperature and toluene as the solvent. However, the lowest-lying triplet state of [60]fullerene plays a key role in its photochemical and photophysical processes. Upon direct photoexcitation, [60]fullerene undergoes

[37] H. W. Kroto, J. R. Heath, S. C. O'Brien, R. F. Curl, R. E. Smalley, *Nature*, **1985**, *318*, 162.
[38] R. C. Haddon, *Acc. Chem. Res.*, **1992**, *25*, 127.

ISC quantitatively (Φ_T = 1) to a long-lived triplet state.[39] As a result, the $^1O_2$ sensitization is a key photochemical feature of this compound, with reported Φ_Δ = 0.96 in toluene.[40]

These properties, in combination with a high stability towards oxidation, has made [60]fullerene an interesting candidate as $^1O_2$ photosensitizer. However, the main limitation which has slowed down its use for this purpose is its low solubility in many solvents, especially in polar ones. In order to overcome this drawback, the functionalization of the carbon central core in [60]fullerene and its inclusion in soluble hosts are the most extended strategies.

[60]Fullerene shows a strong electronwithdrawing behaviour, similar to an electron deficient alkene rather than an aromatic compound. Reactivity in [60]fullerene is driven by the release of strain energy that comes out from the saturation of one or more double bonds located in [6,6] bonds. Precisely, one of the most relevant advantages of [60]fullerene compared to other carbon nanostructures is the possibility to functionalize different positions of the carbon central core in a controlled way. Scheme 7 summarizes the most relevant and well defined reactions of the carbon central core in [60]fullerene.[41]

Nevertheless, the functionalization of [60]fullerene, with the subsequent decrease on the number of π-electrons, has a relevant influence on its photophysical properties. In particular, if the quantum yield and the lifetime of the triplet state are considered, which are key variables in $^1O_2$ production. In this sense, several systematic studies have been carried out in order to characterize these modifications taking into account not only the degree of functionalization, but also the influence of the addition pattern. Figure 11 shows a series of mono-, bis- and tris-adducts of epoxy and bis(ethoxycarbonyl) regioisomers of C_{60} with the correspondent $^1O_2$ generation efficiency considered as the $^1O_2$ emission intensity at 1270 nm divided by the absorption coefficient at 514.5 nm, the excitation wavelength (relative values to [60]fullerene).

---

[39] a) H. Ajie, M. M. Alvarez, S. J. Anz, R. D. Beck, F. Diederich, K. Fostiropoulos, D. R. Huffman, W. Krätschmer, Y. Rubin, K. E. Shriver, D. Sensharma, R. L. Whetten, *J. Phys. Chem.*, **1990**, *94*, 8630. b) Y. P. Sun. Molecular and Supramolecular Photochemisty. Organic Photochemistry. CRC Press: Boca Raton, 1997, p. 329.

[40] a) J. W. Arbogast, A. P. Darmanyan, C. S. Foote, F. N. Diederich, R. L. Whetten, Y. Rubin, M. M. Alvarez, S. J. Anz. *J. Phys. Chem.* **1991**, *95*, 11. b) F. Wilkinson, W. P. Helman, A. B. Ross. *J. Phys. Chem. Ref. Data*, **1993**, *22*, 113

[41] A. Montellano-López, A. Mateo-Alonso, M. Prato. *J. Mater. Chem.*, **2011**, *21*, 1305.

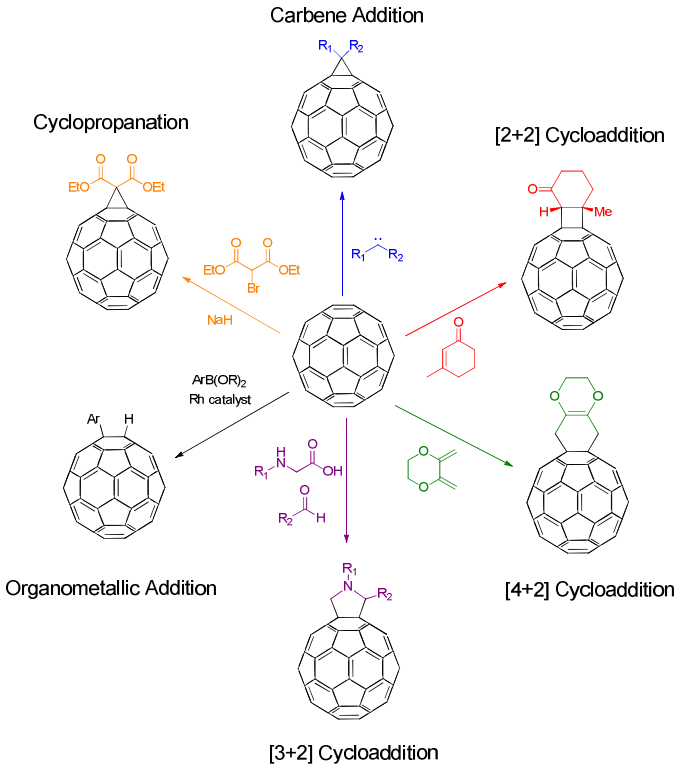

Scheme 7. Examples of well-established C_{60} functionalization protocols.[41]

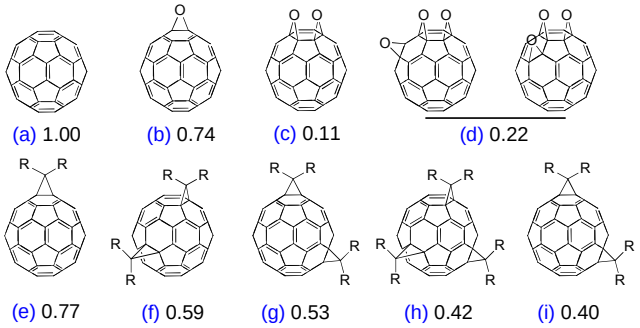

Figure 11. Relative $^1O_2$ efficiency for several epoxy and bis(ethoxycarbonyl) regioisomers of C_{60}.[42]

Considering these values, it is possible to conclude that the larger is the functionalization, the greater is the decrease in the ability for $^1O_2$ production. However, it is true that the introduction of a second addend at an adjacent position to the existing one has a higher impact on the electronic structure, so the

generation of $^1O_2$ decreases considerably (especially for (c) and (d) in Figure 11).[42] This trend has also been observed in the series of [60]fullerene-*o*-quinodimethane bisadducts shown in Figure 19, where both Φ_T and Φ_Δ are reported, in toluene as solvent.[43] In this case, the most remarkable fact is the low Φ_Δ in regiosomer b (Figure 12), in spite of its similar Φ_T in comparison with other bisadducts.

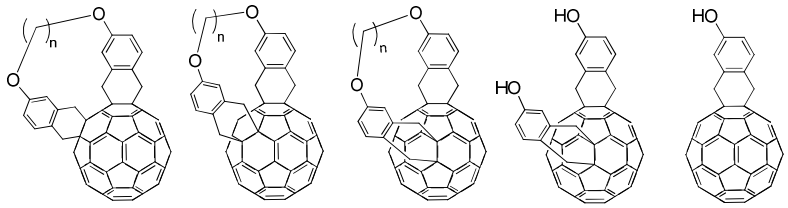

	(a)	(b)	(c)	(d)	(e)
Φ_Δ	0.54	0.35	0.56	0.53	0.79
Φ_T	0.55	0.54	0.57	0.54	0.80

Figure 12. Φ_Δ and Φ_T for several *o*-quinodimethane bisadducts of C_{60}.[43]

Regarding the influence of the degree of functionalization, a more extended analysis is summarized in Table 1 for a series of dialkylmalonates, with one to six addends attached to the carbon central core.[44]

Finally, the Φ_Δ changes were also explored in non-homoconjugated [60]Fullerene derivatives where one, two or three C=C bonds of a single six member ring were functionalized.[45] Interestingly, these derivatives exhibited higher singlet oxygen quantum yields than analogous homoconjugated Bingel adducts with the same number of saturated double bonds.

---

[42] Y. Nakamura, M. Taki, S. Tobita, H. Shizuka, H. Yokoi, K. Ishiguro, Y. Sawaki, J. Nishimura. *J. Chem. Soc. Perkin Trans. 2*, **1999**, 127.

[43] T. Hamano, K. Okuda, T. Mashino, M. Hirobe, K. Arakane, A. Ryu, S. Mashiko, T. Nagano. *Chem. Commun.*, **1997**, 21.

[44] F. Prat, R. Stackow, R. Bernstein, W. Qian, Y. Rubin, C. S. Foote. *J. Phys. Chem. A*, **1999**, *103*, 7230.

[45] K. K. Chin, S.-C. Chuang, B. Hernández, L. M. Campos, M. Selke, C. S. Foote, M. A. García-Garibay. *Photochem. Photobiol. Sci*. **2008**, *7*, 49.

Table 1. Φ_T and Φ_Δ values for a series of [60]fullerene mono- to hexaadducts.[43]

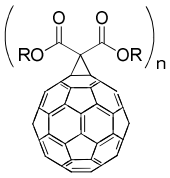

Compound	Φ_T	Φ_Δ
$C_{60}[C(COOEt)_2]$ **(a)**	0.95	0.93
e-$C_{60}[C(COOMe)_2]_2$ **(b)**	0.79	0.79
e-face, *e*-edge, *trans*-1-C_{60}- $[C(COOMe)_2]_3$ **(c)**	0.69	0.60
D_{2h}-all-*e*-$C_{60}[C(COOEt)_2]_4$ **(d)**	0.42	0.44
C_s-all-*e*-$C_{60}[C(COOMe)_2]_4$ **(e)**	0.20	0.30
all-*e*-$C_{60}[C(COOMe)_2]_5$ **(f)**	0.07	0.11
T_h-all-*e*-$C_{60}[C(COOEt)_2]_6$ **(g)**	0.11	0.16

From these results, it is interesting to highlight the correlation depicted in Figure 13 between Φ_Δ and the conjugated fused area in the fullerene core through [6,6] bonds.

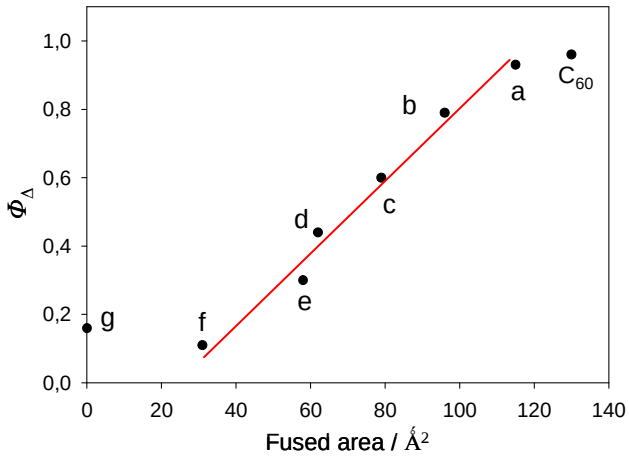

Figure 13. Correlation of Φ_Δ with the fused area of the fullerene core. Φ_Δ values from Table 1.[43]

CHAPTER 1

CHAPTER 1

BACKGROUND

3. CHAPTER 1 BACKGROUND

Singlet oxygen has a sufficiently long lifetime to allow it to play a role in chemical reactions in solution. The presence of an empty π^* molecular orbital (see Figure 5) is the reason why $^1O_2$ behaves as an electrophilic species and reacts with electron rich substrates such as alkenes, aromatic rings or sulfur containing compounds. In addition, as the electrons are paired in the HOMO, most reactions of $^1O_2$ are two-electron reactions, analogous to those of *ethylene*.[46] A summary of the most important reactions of singlet molecular oxygen is shown in Scheme 8. Each reaction will be presented in detail in subsequent sections, and the most relevant mechanistic aspects and some synthetic applications will be considered as well.

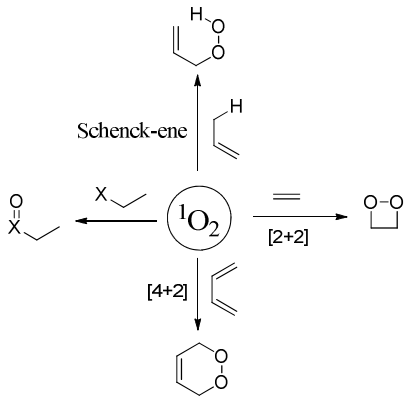

Scheme 8. General reactivity of $^1O_2$ (X = S, P)

3.1. Schenck-ene reaction

Since the first report of this reaction by Schenck,[47] the synthesis of allylic hydroperoxides mediated by $^1O_2$ has shown to be a valuable synthetic tool due to its controllable stereo- and regiochemistry. Moreover, it has to be taken into account the possibility to get valuable allylic alcohols from the reduction of the

[46] a) M. Zamadar, A. Greer. Handbook of Syntehtic Photochemistry. Wiley-VCH: Weinheim, 2010, pp. 353-354. b) A. M. Braun, M.-T. Maurette, E. Oliveros. Photochemical Technology. Wiley: London, 1991, p. 452.

[47] G. O. Schenck, *Naturwissenschaften*, **1948**, *35*, 28.

hydroperoxide moiety. Globally, the reaction can be described as the addition of $^1O_2$ to a sp^2 carbon of the alkene substrate and the abstraction of hydrogen from a distal allylic carbon leading to a double bond migration.

The stereochemistry in this reaction is dictated by the mechanism, which is depicted in Scheme 9. The first step is the approximation of the $^1O_2$ molecule to the double bond forming the exciplex A, which afterwards evolves to perepoxide B, where the oxygen atom with negative electron density can abstract either H_a or H_b (located on the same face of the alkene as the oxygen molecule). This mechanism is generally accepted, although the consideration of B in Scheme 9 as a transition state or as a reaction intermediate is still open to debate.

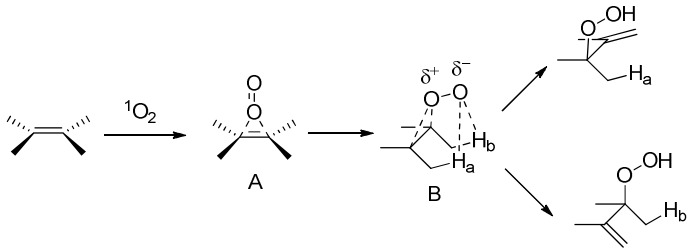

Scheme 9. Mechanism proposed for the Schenck-ene reaction.

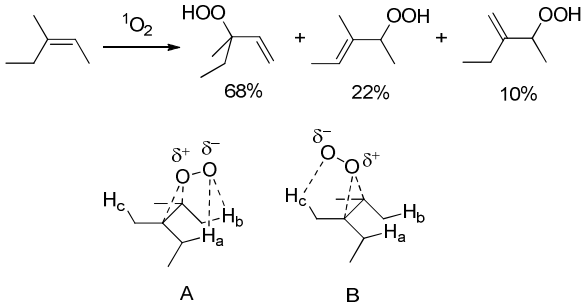

Scheme 10. *Cis* effect in the Schenck-ene reaction attending to the greater electronic stabilization of A compared to B.

From this mechanism it is easy to conclude that ene reactions can lead to a mixture of products when there are several allylic hydrogens in the substrate structure. However, in these cases it is interesting to point out the *cis* effect, where those hydrogen atoms from the most substituted side are expected to be preferentially abstracted *vs*. those in the less substituted one. An example is shown in Scheme 10 for perepoxide A, which is more electronically stabilized

than B. However, this effect does not rule when sterically demanding groups are present in the most substituted side.[48]

One of the most interesting examples of the synthetic potential of this reaction is the synthesis shown in Figure 14 for Artemisinin (Art), a compound with outstanding antimalarial properties. Starting from the intermediate dihydroartemisinin (DHA), its ene reaction mediated by $^1O_2$ affords a hydroperoxide, whose acid catalyzed ring closure yields Artemisinin. Due to the pharmacological interest of the target compound, several proposals have been done in order to develop procedures which could be applied at industrial scale. The key step in this process is the system used as source of $^1O_2$, and disproportionation of H_2O_2 in the presence of Na_2MoO_4 has been proposed as an accessible way.[49] Moreover, an approach based on flow chemistry has also been reported. In this case, $^1O_2$ is produced by photosensitization using tetraphenylporphyrin (TPP). The reported overall yield for this setup was 39%, what could be translated into 200 g of artemisinin per day.[50]

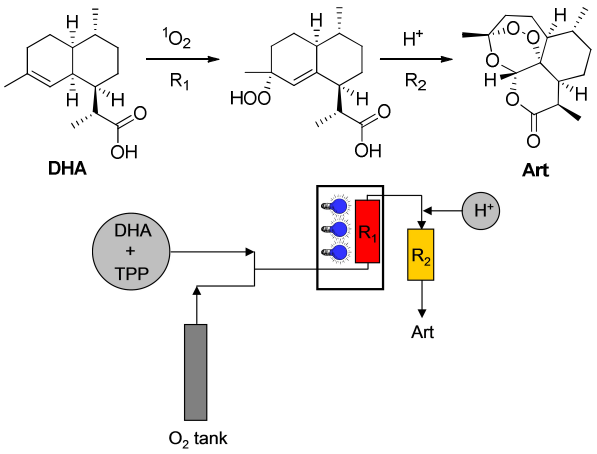

Figure 14. $^1O_2$ semitotal syntheis of artemisinin (Art) starting from dihydroartemisinin (DHA). Flow diagram for the synthetical setup based on a flow chemistry approach.

[48] a) M. Prein, W. Adam. *Angew. Chem. Int. Ed*., **1996**, *35*, 477. b) E. L. Clennan *Tetrahedron*, **2000**, *56*, 9151. c) D. A. Singleton, C. Hang; M. J. Szymanski, M. P. Meyer, A. G. Leach, K. T. Kuwata, J. S. Chen, A. Greer, C. S. Foote, K. N. Houk. *J. Am. Chem. Soc*., **2003**, *125*, 1319.

[49] H.-J. Chen, W.-B. Han, H.-D. Hao and Y. Wu, *Tetrahedron*, **2013**, *69*, 1112.

[50] F. Lévesque, P. H. Seeberger. *Angew. Chem. Int. Ed*., **2012**, *51*, 1706.

3.2. [2+2] cycloadditions

The reaction of singlet oxygen with olefins where the double bond is found in a small ring or is activated by an electron donor substituent (generally, an heteroatom, as in enamines, enamides, enolethers, ketene aminals, ketene ketals, vinylsulfides, thioketenes and thiones), is a [2+2] cycloaddition leading to the formation of 1,2-dioxetanes. This type of reaction is mechanistically close to the Schenck-ene reaction, so a competition with the formation of dioxetane can be observed if the alkene has a hydrogen atom in the allylic position. The most accepted mechanism for these reactions involves formation of a perepoxide (similarly to the Schenck-ene reaction) followed by a zwitterionic intermediate,[51] although proposals based on biradical intermediates can be also found (Scheme 11).[52]

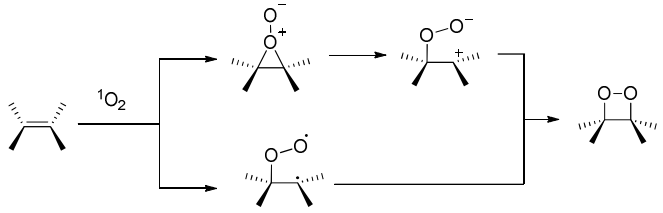

Scheme 11. Mechanisms proposed for $^1O_2$ [2+2] cycloaddition to a double bond.

The application of the $^1O_2$ [2+2] cycloaddition as a tool in chemical synthesis is less widespread than Schenk-ene reaction. The main reaction that can undergo 1,2-dioxetanes is their decomposition to carbonyl products, a way to achieve the rupture of C–C bonds. But the valuable point of this process is that one of these carbonyl products can be obtained in an excited state which is deactivated with the emission of light. This is precisely the basis of chemiluminescent $^1O_2$ probes shown in Section 2.3.2 (Scheme 6), where this cycloaddtion reaction is considered in the molecular design of new and efficient $^1O_2$ probes.[53]

[51] G. Vassilikogiannakis, M. Stratakis and M. Orfanopoulos. *J. Org. Chem.*, **1998**, *63*, 6390.

[52] G. Mazzone, M. E. Alberto, N. Russo, E. Sicilia. *Phys. Chem. Chem. Phys.*, **2014**, *16*, 12773.

[53] N. Hananya, O. Green, R. Blau, R. Satchi-Fainaro, D. Shabat. *Angew. Chem. Int. Ed.*, **2017**, *56*, 11793.

3.3. [4+2] cycloadditions

The 1,4-addition of $^1O_2$ to a π-conjugated system leads to the formation of endoperoxides. Generally, this reaction can be observed with 1,3-dienes in acyclic hydrocarbons, aromatics and heterocycles. Again, there are several proposals about the mechanism, ranging from concerted to stepwise reaction pathways (Scheme 12),[54] although the most accepted mechanism is a Diels-Alder-type cycloaddition where $^1O_2$ plays the role of a dienophile, forming a six-membered ring in a concerted process. The utility of endoperoxides obtained by this reaction has been shown in Section 2.2.1 as $^1O_2$ molecular carriers. However, many other useful synthetic transformations can be addressed (Scheme 12).[55]

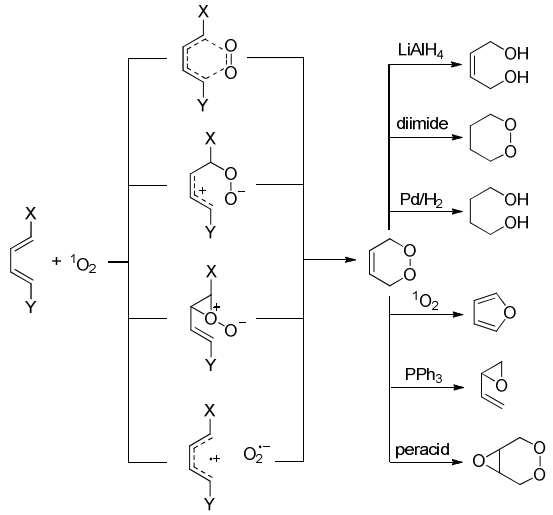

Scheme 12. Mechanisms proposed for $^1O_2$ [4+2] cycloaddition to a diene moiety, and potential subsequent transformations of the resulting endoperoxide.

3.4. Photooxidation on heteroatom centres

The oxidation reactions mediated by singlet oxygen have been explored with a variety of organic molecules containing heteroatoms, as in the case of organosulfur, phosphines or nitrogen compounds.

---

[54] W. Adam, M. Prein. *Acc. Chem. Res.* **1996,** *29*, 275.
[55] R. Ozen, F. Kormal, M. Balci, B. Atasoy. *Tetrahedron*, **2001**, *57*, 7529.

3.4.1. Photooxidation of organic sulfides

The oxidation of organic sulfides is of interest from a mechanistic point of view but also because of its implication in several biological processes. This is due to the fact that a large number of different natural products contain the sulfide functional group. For instance, it has been reported that the oxidation of a single methionine residue in amyloid β-peptide plays a key role in the neurotoxicity responsible for Alzheimer's disease.[56]

However, the mechanism of this singlet oxygen reaction has proven to be surprisingly complex. The gross features of this mechanism were delineated in a paper published by Foote and co-workers in the 1980s decade.[57] These authors postulated the general "two intermediates" mechanism shown in Scheme 13.

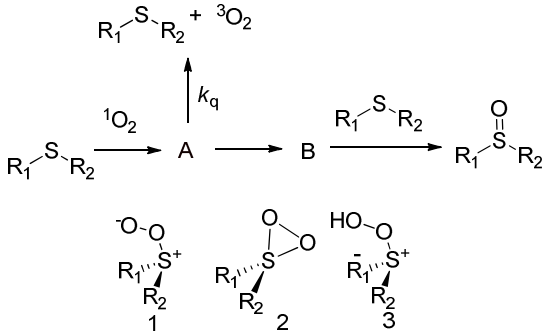

Scheme 13. Two intermediates mechanism proposed for the oxidation of organic sulfides by $^1O_2$ in aprotic solvents.

The first intermediate (A) was characterized as a nucleophilic oxidant capable of transferring an oxygen atom to an electrophilic acceptor. The structure of this intermediate was assigned to the persulfoxide structure **1** (Scheme 13). It is a weakly bound species that, nevertheless, has a sufficient lifetime to undergo several inter- and intramolecular reactions. Its behaviour suggests that it can be considered as a resonance hybrid of zwitterionic and diradical canonical structures ($R_2S^+–OO^-$ ↔ $R_2S^\bullet–OO^\bullet$). However, the chemistry of this intermediate is consistent with dominance of the dipolar form according to the calculated wave function (the MP2/6-31G* natural occupation numbers for the

[56] a) D. A. Butterfield, J. Kanski. *Peptides*, **2002**, *23*, 1299. b) C. Schöneich. *Arch. Biochem. Biophys.*, **2002**, *397*, 370.
[57] J. J. Liang, C. L. Gu, M. L. Kacher, C. S. Foote. *J. Am. Chem. Soc*., **1983**, *105*, 4717.

HOMO-LUMO orbitals are 1.94 and 0.05, respectively).[58] The weak bond between S and O in persulfoxide intermediate is responsible for the physical quenching, where molecular oxygen in its ground state is released and sulfide is recovered without any chemical modification (path with k_q rate constant in Scheme 13). As a result, the inability to spectroscopically detect persulfoxides under typical photooxidative conditions has hindered the progress in examining their reactivity. For this reason, several attempts have been made in order to trap this intermediate.[59] For example, transfer of an oxygen atom to diphenyl sulfoxide (Ph_2SO) has been used to explore the mechanism of diethyl sulfide photooxidation. These studies took advantage of the fact that Ph_2SO is unreactive toward $^1O_2$ but efficiently reacts with diethyl persulfoxide to give diethylsulfoxide and diphenylsulfone.[60] Nevertheless, there is no agreement about the identity and structure of intermediate B (Scheme 13) and it is possible to find several proposals. The most important intermediates are the thiadioxirane (represented as **2** in Scheme 13) and the hydroperoxysulfonium ylide (**3** in Scheme 13). However, theoretical calculations showed that the activation energy for a direct formation of thiadioxirane from persulfoxide is 20 Kcal mol^{-1}, while this barrier is 6 Kcal mol^{-1} for the formation of hydroperoxysulfonium ylide. Several experimental results supported the formation of this last intermediate, *e.g.*: in the reaction of singlet oxygen with 2-chlorethyl ethyl sulfide, elimination of HCl and production of α,β-unsaturated sulfoxides were observed, according to the process depicted in Scheme 14.[61]

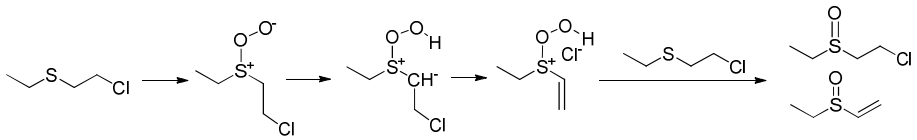

Scheme 14. Mechanism for α,β-unsaturated sulfoxides production from reaction between 2-chlorethyl ethyl sulfide and $^1O_2$.

Nevertheless, all this information is only valid for reactions in aprotic solvents. In protic solvents like MeOH, the nature of the second intermediate is different

[58] F. Jensen, A. Greer, E. L. Clennan. *J. Am. Chem. Soc*., **1998**, *120*, 4439.
[59] E. L. Clennan. *Acc. Chem. Res*., **2001**, *34*, 875.
[60] E. L. Clennan, A. Greer. *J. Org. Chem*., **1996**, *61*, 4793.
[61] E. L. Clennan. *Tetrahedron Lett*., **1999**, *40*, 6519.

and structures C (hydrogen bonding between solvent and persulfoxide) and D (nucleophilic addition to persulfoxide to form hydroperoxyalkoxysulfurane) shown in Scheme 15 have been proposed.

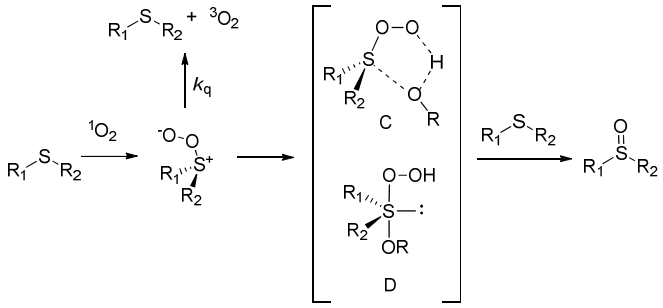

Scheme 15. Mechanism proposed for the oxidation of organic sulfides by $^1O_2$ in protic solvents.

However, it was observed that the ability of alcohols to suppress physical quenching was a function of their pK_a's. On this basis and, taking into account the results of computational calculations, a "concerted" addition of the alcohol to sulfide via an activated complex (D in Scheme 15) was proposed, excluding a hydrogen bonding between solvent and persulfoxide.[62]

3.4.2. Photooxidation of thioketones

The interaction between singlet oxygen and thioketones was mainly studied by Ramamurthy and co-workers in the 1980s, in order to develop clean oxidation methods and to reveal the mechanism of thiocarbonyl transformation into other functional groups of interest in organic synthesis.[63]

In all the cases the reported photoproducts were the corresponding ketone and sulfine (*S*-oxide), according to the mechanism depicted in Scheme 16.

---

[62] S. M. Bonesi, A. Albini. *J. Org. Chem*., **2000**, *65*, 4532.

[63] a) R. Rajee, V. Ramamurthy. Tetrahedron Lett., **1978**, *19*, 5127. b) V. Jayathirtha Rao, V. Ramamurthy. *Indian J. Chem. Sect. B*, **1980**, *19B*, 143. c) N. Ramnath, V. Ramesh, V. Ramamurthy. *J. Chem. Soc., Chem. Commun*., **1981**, 112. d) V. J. Rao, K. Muthuramu, V. Ramamurthy. *J. Org. Chem*., **1982**, *47*, 127. e) N. Ramnath, V. Ramesh, V. Ramamurthy. *J. Org. Chem.* **1983**, *48*, 214. f) P. Arjunan, V. Ramamurthy, K. Venkatesan. *J. Org. Chem.* **1984**, *49*, 1765. g) V. P. Rao, V. Ramamurthy. *Tetrahedron* 1985, *41*, 2169.

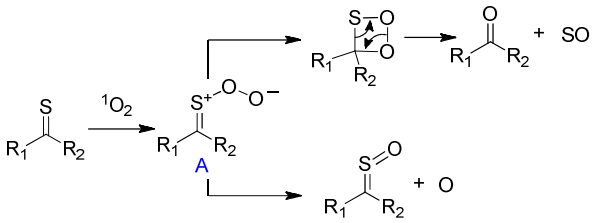

Scheme 16. Reaction mechanism proposed for the oxidation of thioketones mediated by $^1O_2$.

The proposed mechanism considers a common zwitterionic/diradical intermediate (A in Scheme 16) arising out of the primary interaction of singlet oxygen with the thiocarbonyl group, which evolves intramolecularly to the ketone and sulfine (the closure of A affords 1,2,3-dioxathiethane which decomposes to ketone, while the competing atomic oxygen elimination leads to sulfine). This scheme has been accepted for decades and described in several reviews and photochemistry books.[64]

Nevertheless, several controversial aspects about this mechanism and the experimental results which support it must be pointed out. Firstly, direct elimination of atomic oxygen from intermediate A (Scheme 16) is an unlikely possibility, especially because atomic oxygen is an extremely reactive species and a possible evolution for this product in the reaction crude mixture was not described. Secondly, the reported product distribution (ketone and sulfine) does not add up to 100% (in several cases only 42%). Trying to explain this fact, the authors comment that yields less than 100%, in spite of total photooxidation of the thioketone, could be due to the volatility of the ketones formed and would not be related to any other side products. This explanation, however, hinders any quantitative mechanistic study (*e.g.*: these authors did not observe any modification in the ratio of products by changing the initial concentration of the starting thioketone)

In general, carbonyl compounds corresponding to desulfurization were reported as the main photoproducts. However, from a synthetic point of view, the most valuable photoproduct obtained in this reaction is the sulfine moiety. Sulfines

[64] a) A. Maciejewski, R. P. Steer. *Chem. Rev.*, **1993**, *93*, 67. b) A. Corsaro, V. Pistarà. *Tetrahedron*, **1998**, *54*, 15027. c) A. Gilbert, J. Baggott, Essentials of Molecular Photochemistry, Blackwell Scientific Publications: Oxford, 1991, pp 518−520.

are a unique class of sulfur-centred heterocumulenes with *Z/E* isomerism (Scheme 17). Magnetic properties, vibrational frequencies and ionization energies of several sulfines were determined by spectroscopic methods. These results suggested that in S–O bond there is a polarization and that the zwitterion depicted in Scheme 17 is the predominant form.[65] In general, sulfines with aromatic substituents are more stable than those with aliphatic substituents. Electron-withdrawing substituents decrease the stability of their sulfines, whereas electron-donating substituents have a stabilizing effect.[66]

In general, sulfines can take part in a variety of reactions summarized in Scheme 17.

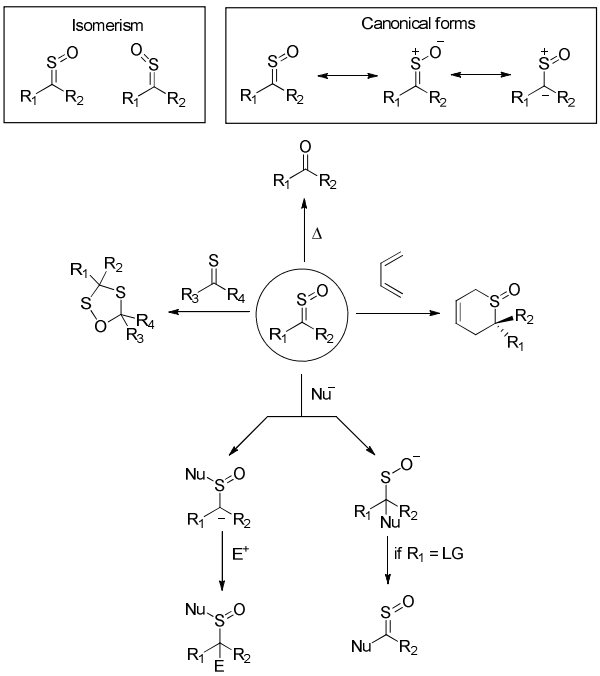

Scheme 17. Isomerism, structure and reactivity of the sulfine functional group.

Of special interest, the stereospecific [4 + 2] cycloaddition of thiocarbonyl *S*-oxides with 1,3-butadienes, where the geometry of the sulfine is retained in the

[65] R. Huisgen, G. Mloston, K. Polborn. *J. Org. Chem.*, **1996**, 61, 6570.
[66] A. C. B. Lucassen. Sulfine-based Synthesis of Four-, Five- and Six-Membered Heterocycles. Ph.D. Thesis, Radboud University Nijmegen, Netherlands. 2003.

cycloadduct, might be a shorter alternative route for the preparation of new dihydrothiopyran *S*-oxides and related heterocyclic compounds such as Aprikalim, a potassium channel activator with antihypertensive and antianginal activity.[67]

Regarding the thioketone group, its properties have been a focus of attention in the last years due to the relevance of nucleothiobases (Figure 15)

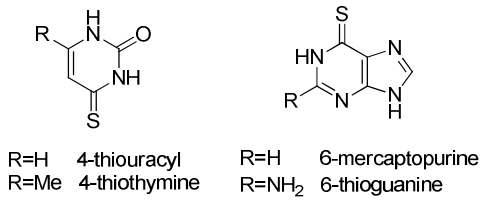

Figure 15. Most relevant nucleothiobases.

These compounds, where the oxygen atom of a carbonyl group is replaced by a sulfur atom, are of interest as a consequence of their natural ocurrence in transfer-RNA[68] and the disorders whose absence can modify the mitochondrial metabolism.[69] However, some nucleothiobases are being developed as drugs for clinical applications against cancer or leukemia (for instance, 6-thioguanine is commercially available as Tabloid^{TM}). [70] In addition, the photophysical properties [71] shown by these derivatives can be exploited also in photocrosslinking experiments[72] and therapies using light, as they are able to generate $^1O_2$.[73]

[67] R. Bastin, H. Albadri, A. C. Gaumont, M. Gulea. *Org. Lett*., **2006**, *8*, 1033.
[68] J. Carbon, H. David, M. H. Studier, *Science*, **1986**, *161*, 1146
[69] F.-Y. Wei, T. Suzuki, S. Watanabe, S. Kimura, T. Kaitsuka, A. Fujimura, H. Matsui, M. Atta, H. Michiue, M. Fontecave, K. Yamagata, T. Suzuki, K. Tomizawa. *J. Clin. Invest.*, **2011**, *121*, 3598.
[70] M. Presta, M. Belleri, A. Vacca, D. Ribatti. *Leukemia*, **2002**, *16*, 1490.
[71] S. Mai, M. Pollum, L. Martínez-Fernández, N. Dunn, P. Marquetand, I. Corral, C. E. Crespo-Hernández, L. González. *Nat. Commun*., **2016**, *7*, 13077.
[72] A. Favre, C. Saintomé, J. L. Fourrey, P. Clivio, P. Laugâa. *J. Photochem. Photobiol. B*, **1998**, *42*, 109.
[73] E. Gemenetzidis, O. Shavorskaya, Y.-Z. Xu, G. Trigiante. *J. Dermatol. Treat*., **2013**, *24*, 209.

Precisely, the effectivity of these compounds in such phototherapies can be modified as a consequence of the reactivity between $^1O_2$ and the thioketone group. In this sense, several computational studies have been carried out in order to gain insight into the mechanism which operates in this process. Scheme 18 shows the postulated mechanism for the oxidation of 4-thiouracil mediated by $^1O_2$ at the B3LYP/6-311+G(d,p) level. However, no structural confirmation of the products was reported in the literature.[74]

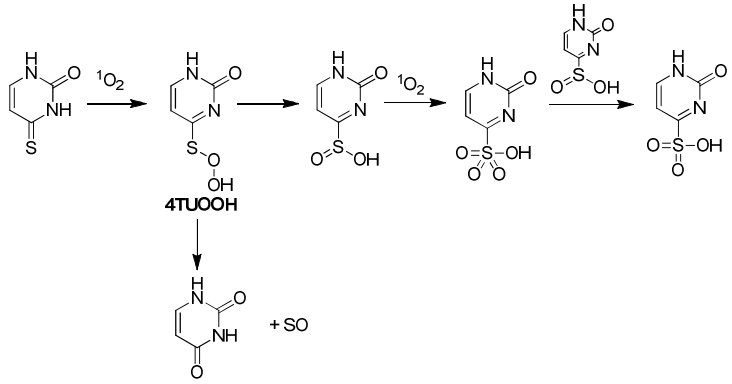

Scheme 18. Computational proposed mechanism for 4-thiouracil oxidation by $^1O_2$.

[74] a) X. Zou, X. Dai, K. Liu, H. Zhao, D. Song, H. Su. *J. Phys. Chem. B*, **2014**, *118*, 5864. b) P. Mehta, S. C. Mehta. *Asian J. Chem*., **1999**, 11, 528.

CHAPTER 1

OBJECTIVES

4. CHAPTER 1 OBJECTIVES

The main objective in this chapter is to gain insight into the photooxidation mechanism of thioketones mediated by $^1O_2$. The main topics that will be considered are the following:

- Detection of photoproducts which have not been mentioned before in the bibliography.
- Contributing with new experimental findings to improve the general mechanistic proposal (parallel or consecutive reactions).
- To study the influence of solvents (protic/aprotic) to the distribution of photoproducts, as well as the presence of H^+.
- Investigating the influence on sulfine formation of the initial concentration of thioketone, in order to postulate an alternative to the pathway involving atomic oxygen production.
- To study the diastereoisomeric excess in the sulfine formation and to rationalize the results in terms of steric control, with support of computational modelization.
- To measure the rate constant of $^1O_2$ quenching by each thioketone.

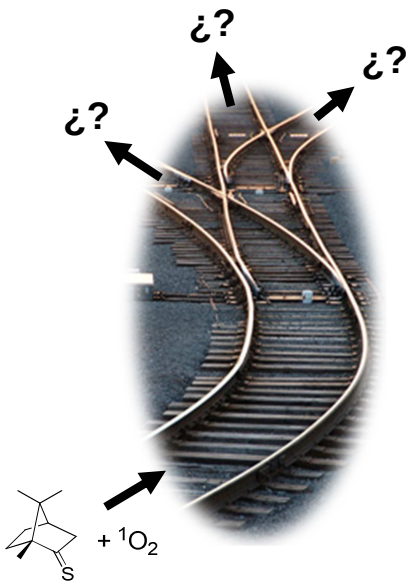

Once stablished the new reaction scheme, advantage can be taken from the acquired mechanistic knowledge in order to find a suitable way to get sulfine group as the major photoproduct in synthetic scale procedures for the preparation of fine chemicals.

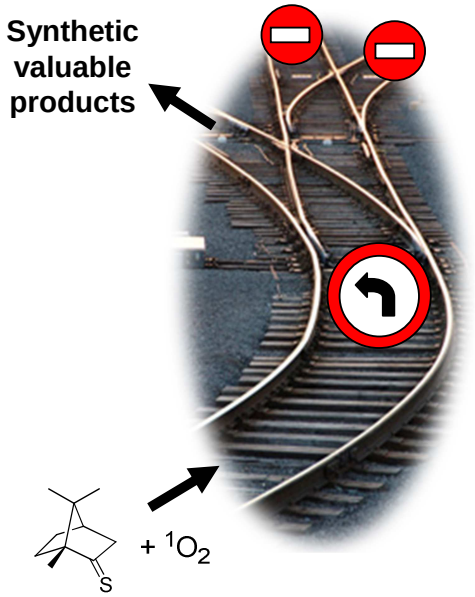

In addition, an effort to extend the validity of the new mechanistic proposal to new substrates (nucleothiobases such as 4-thiouracyl) will be made, especially in those cases where there is a lack of experimental work regarding the reaction mechanism.

CHAPTER 1

RESULTS AND DISCUSSION

5. CHAPTER 1 RESULTS AND DISCUSSION

5.1. Thermal synthesis of thioketones and their sulfines

Mechanistic studies were carried out using alicyclic thioketones (1*R*)-thiocamphor (**2a**) and (1*R*)-thiofenchone (**2b**) as reactants. Both compounds were synthesized using the Lawesson's reagent and the corresponding ketones, (1*R*)-camphor (**1a**) and (1*R*)-fenchone (**1b**). According to the bibliography shown in the background section, the sulfine group arises from the reaction between the thioketone group and $^1O_2$, so (1*R*)-thiocamphor sulfine (**3a**) and (1*R*)-thiofenchone sulfine (**3b**) were obtained via oxidation of the corresponding thioketone with *m*-chloroperbenzoic acid, in order to elucidate those diagnostic signals that should be looked for when the analysis of reaction crudes and photoproducts identification by spectroscopic techniques was performed. Figure 16a shows the UV-vis spectra for **1a** (inset), **2a** and **3a** in methanol, while Figure 16b depicts the equivalent UV-vis spectra for **1b** (inset), **2b** and **3b**.

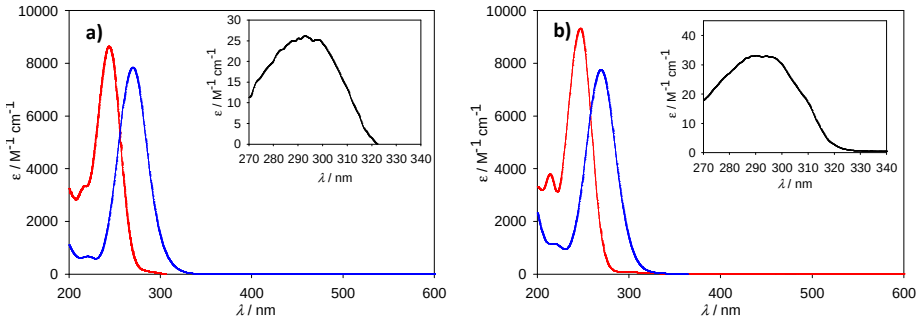

Figure 16. a) UV-Vis spectra for **1a** (inset), **2a** (red solid line) and **3a** (blue solid line). b) UV-Vis spectra for **1b** (inset), **2b** (red solid line) and **3b** (blue solid line).

From Figure 16, it is interesting to point out a remarkable increment of the absorption coefficient from the ketone to the thioketone. Sulfine group retains similar ε values compared to the thioketone, although a bathochromic shift was observed in both cases.

Moreover, the structural characterization of sulfine **3b** showed that a mixture of *Z* and *E* diastereoisomers was obtained in 4:1 ratio. The analysis of the HMQC and HMBC spectra (Figures 17 and 18, respectively) allowed the structural elucidation of both diastereoisomers.

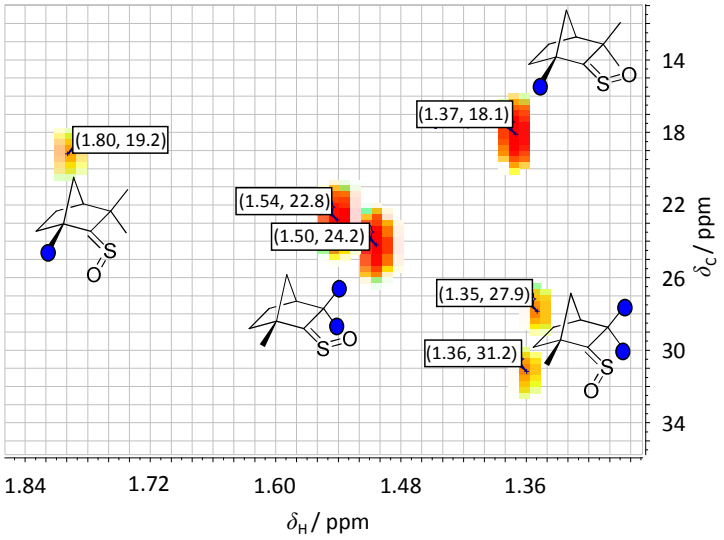

Figure 17. HMQC spectrum obtained for the *Z*/*E* mixture of **3b**.

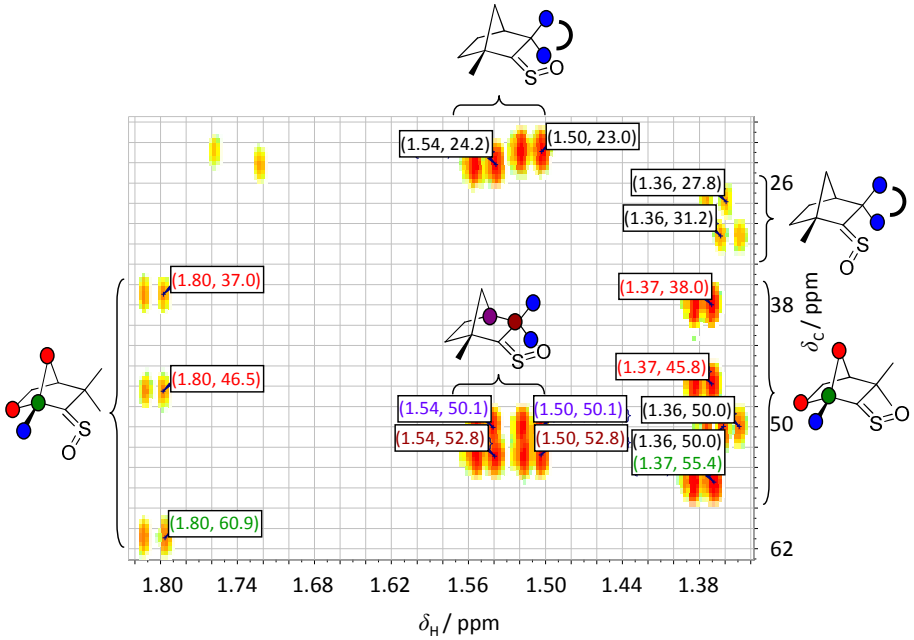

Figure 18. HMBC spectrum obtained for the *Z*/*E* mixture of **3b**.

From these figures it is possible to conclude that the closer is the spatial position of the oxygen atom to the methyl groups in alpha position respect to thiocarbonyl carbon, the greater is the induced magnetic deshielding. The same

behaviour was observed in the case of **3a**, where only the *E* diastereoisomer was detected. In this case, the protons for the CH_2 in alpha position to sulfine group were deshielded from 2.81 to 2.95 ppm (comparing the chemical shift of these protons with respect to **2a**).

5.2. Determination of $P(T_1)$ and $^1O_2$ quenching rate constant by (1*R*)-thiocamphor and (1*R*)-thiofenchone

As it was stated in equation [7] in the General Background section, $P(T_1)$ can be physically quenched by O_2 molecules, but also by other substrate molecules if they are present in the reaction medium. In order to know the physical deactivation rate constant (k_q) induced by the thioketones used as substrates, $\tau(P(T_1))$ values were measured at different [thioketone]. In all the cases, $[Ru(dip)_3]Cl_2$ (dip = 4,7-diphenyl-1,10-phenanthroline) was used as the $^1O_2$ photosensitizer (see experimental section). Figure 19 shows, as a representative example, the time-resolved $P(T_1)$ emission at 620 nm for different [**2a**] air equilibrated solutions using methanol as solvent. The higher is [**2a**], the shorter is $\tau(P(T_1))$ due to a more efficient physical quenching. These decays were fitted to single-exponential kinetics in order to get $\tau(P(T_1))$. The inset in Figure 19 represents an example of the fitting residues (for line 4)

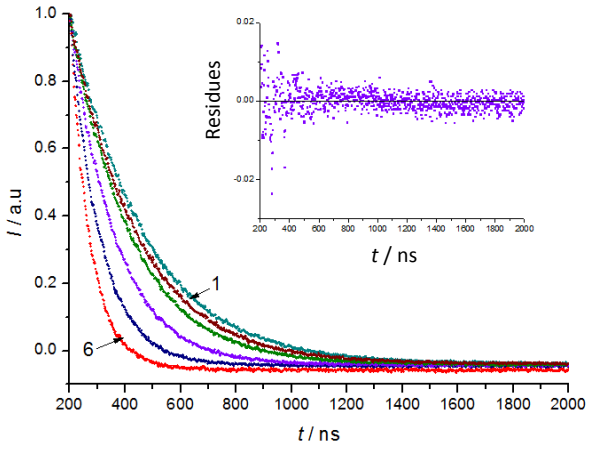

Figure 19. Changes in $P(T_1)$ emission at 620 nm as [**2a**] increases in air-equilibrated methanol. **1**: 0 M; **2**: 0.005 M; **3**: 0.01 M; **4**: 0.03 M; **5**: 0.06 M; **6**: 0.1 M. **Inset:** residuals of the single-exponential fitting in line 4.

τ_0/τ values (where τ_0 represents $\tau(P(T_1))$ when [thioketone] = 0) as a function of [**2a**] and [**2b**] are shown in Figures 20 and 21, respectively. In all the cases, the linear fitting to the Stern-Volmer equation [17] allowed k_q determination.

$$\frac{\tau_0}{\tau} = 1 + k_q \cdot \tau_0 \cdot [Thioketone] \quad [17]$$

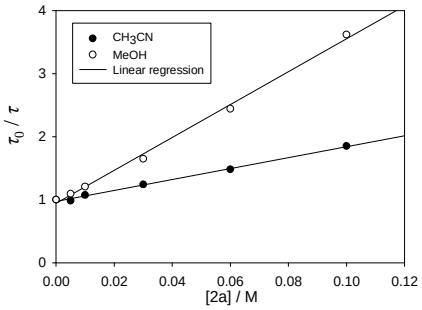

Figure 20. Linear fitting to Stern-Volmer equation for $P(T_1)$ quenching by **2a** in CH_3CN and MeOH.

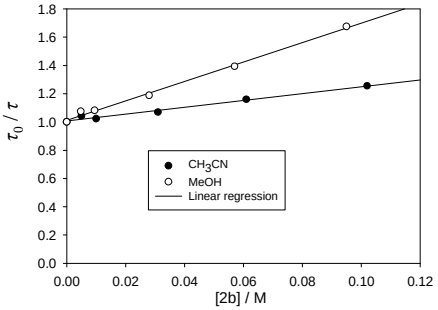

Figure 21. Linear fitting to Stern-Volmer equation for $P(T_1)$ quenching by **2b** in CH_3CN and MeOH.

Table 2 summarizes the experimental k_q values obtained from the previous fittings.

Table 2. k_q for $P(T_1)$ quenching by **2a** and **2b** in air equilibrated CH_3CN and MeOH.

Compound	Solvent	$k_q \cdot 10^{-7}$ / M^{-1} s^{-1}
2a	CH_3CN	4.1 ± 0.1
	MeOH	9.7 ± 0.3
2b	CH_3CN	1.27 ± 0.04
	MeOH	2.49 ± 0.08

Similarly, $^1O_2$ quenching rate constant by **2a** and **2b**, k_q^{Δ}, (considering both contributions, physical and chemical quenching) was also determined. In this case, Figure 22 shows the time-resolved $^1O_2$ phosphorescence emission decay at 1270 nm for different [**2a**] in air-equilibrated acetonitrile solutions. Again, an increment in [**2a**] is related to a more efficient $^1O_2$ quenching, so τ_{Δ} decreases. However it has to be pointed out that, in these decays, a residual contribution due to the emission of $P(T_1)$ was detected, so the decays were fitted to a biexponential function in order to separate both contributions in the acquired signal ($P(T_1)$ and $^1O_2$). In addition, deuterated methanol was used in order to

take advantage of longer τ_Δ values in comparison to nondeuterated methanol. The inset in Figure 22 represents an example of the fitting residuals (for line 4).

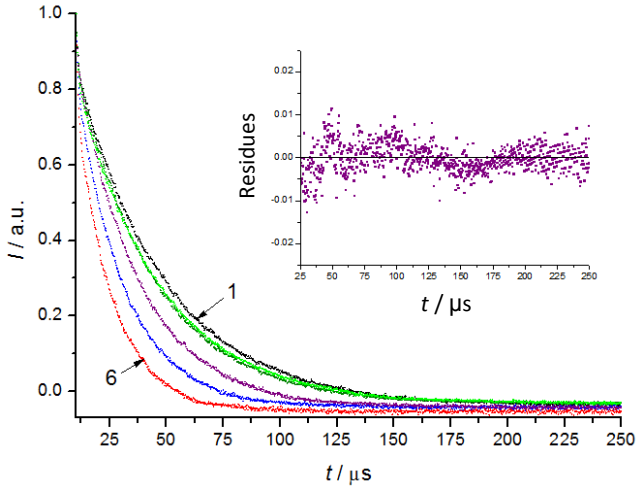

Figure 22. Changes in $^1O_2$ emission at 1270 nm as [**2a**] is modified in air equilibrated acetonitrile. **1**: 0 M; **2**: 0.005 M; **3**: 0.01 M; **4**: 0.03 M; **5**: 0.06 M; **6**: 0.1 M. **Inset:** residues for the biexponential fitting in line 4.

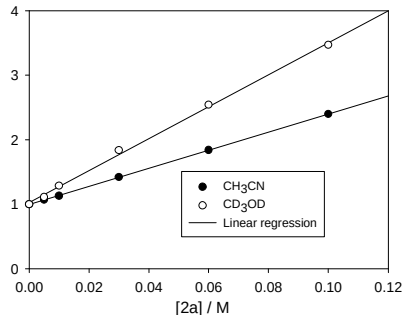

Figure 23. Linear fitting to Stern-Volmer equation for $^1O_2$ quenching by **2a** in CH_3CN and CD_3OD.

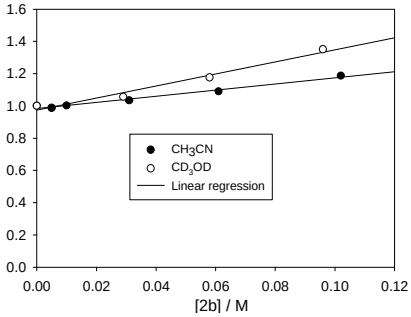

Figure 24. Linear fitting to Stern-Volmer equation for $^1O_2$ quenching by **2b** in CH_3CN and CD_3OD.

Figures 23 and 24 illustrate how $\tau_{\Delta 0}/\tau_\Delta$ values (where $\tau_{\Delta 0}$ represents τ_Δ when [thioketone] = 0) are modified as a function of [**2a**] and [**2b**], respectively. Linear fitting to the Stern-Volmer equation [17] allowed k_q^Δ determination.

Table 3 summarizes the experimental k_q^Δ values obtained from the previous fittings

Table 3. k_q^{Δ} for $^1O_2$ quenching by **2a** and **2b** in air equilibrated CH_3CN and CD_3OD.

Compound	Solvent	$k_q^{\Delta} \cdot 10^{-5}$ / M^{-1} s^{-1}
2a	CH_3CN	1.81 ± 0.09
	CD_3OD	1.0 ± 0.2
2b	CH_3CN	0.24 ± 0.01
	CD_3OD	0.14 ± 0.02

5.3. Monitorization of thioketones photooxidation in the search for new mechanistic evidences

Evidences supporting the new proposal of reaction mechanism were collected from photosensitized oxidation experiments of thioketones **2a** and **2b** in (deuterated) acetonitrile or methanol, in the presence of $[Ru(dip)_3]Cl_2$ dye (Φ_{Δ} = 0.97 ± 0.08 in methanol, 0.75 ± 0.06 in acetonitrile), irradiated with an experimental setup comprising a blue LED lamp described in the Experimental Section. The reaction crudes were analysed by UV-vis spectroscopy at low thioketone concentrations (ca. 0.07 mM) or NMR spectroscopy and GC-MS spectrometry when irradiations were carried out at higher thioketone concentrations (1−80 mM).

5.3.1. Evidences from UV-vis spectrophotometry

UV spectral changes showed a decrease of the absorption band of thioketones **2a** and **2b** in acetonitrile or methanol with the irradiation time. Figure 25 shows, as a representative example, the spectral evolution for the photooxidation of **2a** in acetonitrile, while Figures 26 and 27 show the corresponding changes registered for **2a** and **2b** in methanol, respectively. In the case of Figure 25, only a slight increment in absorbance was observed in the region above 270 nm. However, for the reactions carried out in methanol, the appearance of a new band was clearly seen, matching its maxima with that of the sulfine group characterized and showed in Figure 16. In addition, taking into account the low absorption coefficient of the ketone group, this aforementioned new band can be attributed to sulfine generation. Considering the absorption of **3a** and **3b** above 283 nm in methanol, where the absorption of **2a** and **2b** is negligible, the changes of [**3a**]

and [**3b**] over time could be determined. As well, after considering the contribution of **3a** to the absorption at 247 nm, and the contribution of **3b** to the absorption at 244 nm, the changes in [**2a**] and [**2b**] as a function of the irradiation time were also measured. These changes are depicted in Figure 28a (thiocamphor monitorization) and Figure 28b (thiofenchone monitorization). In both cases, a single-exponential decay and growth for thioketone disappearance and sulfine generation, respectively, were observed. These trends were fitted to first-order kinetics with R^2 values higher than 0.992 (Table 4). The asymptotic behaviour at long irradiation times revealed that quasi-quantitative phototransformation of the thioketones (>96%) was achieved.

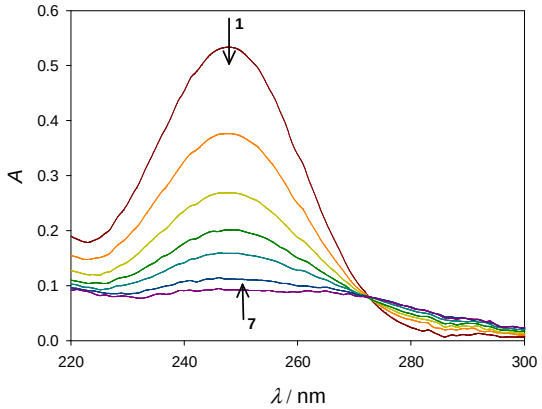

Figure 25. UV-vis monitorization of the photosensitized oxidation of **2a** in acetonitrile at different reaction times (**1**: 0 min, **2**: 30 min, **3**: 1 h, **4**: 1 h 30 min, **5**: 2 h, **6**: 3 h, **7**: 4 h).

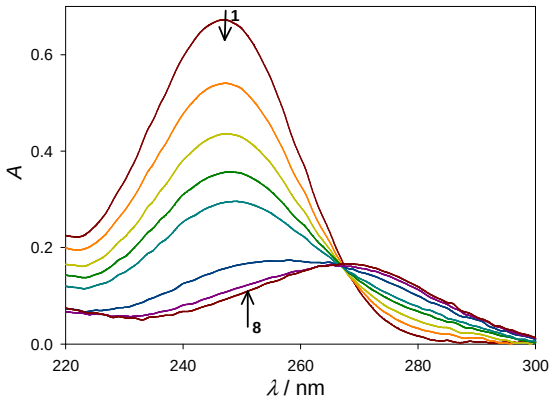

Figure 26. UV-vis monitorization of the photosensitized oxidation of **2a** in methanol at different reaction times (**1**: 0 min, **2**: 30 min, **3**: 1 h, **4**: 1 h 30 min, **5**: 2 h, **6**: 4 h, **7**: 5 h 45 min, **8**: 7 h).

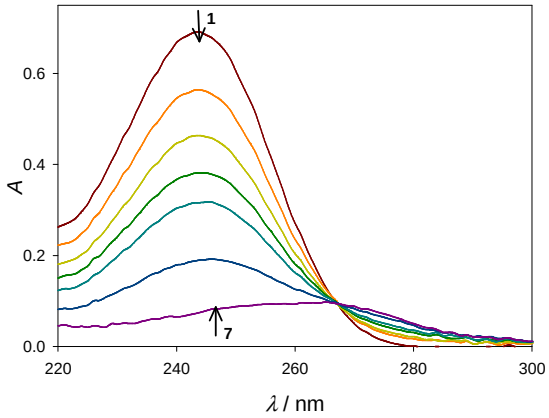

Figure 27. UV-vis monitorization of the photosensitized oxidation of **2b** in methanol at different reaction times (**1**: 0 min, **2**: 30 min, **3**: 1 h, **4**: 1 h 30 min, **5**: 2 h, **6**: 4 h, **7**: 7 h).

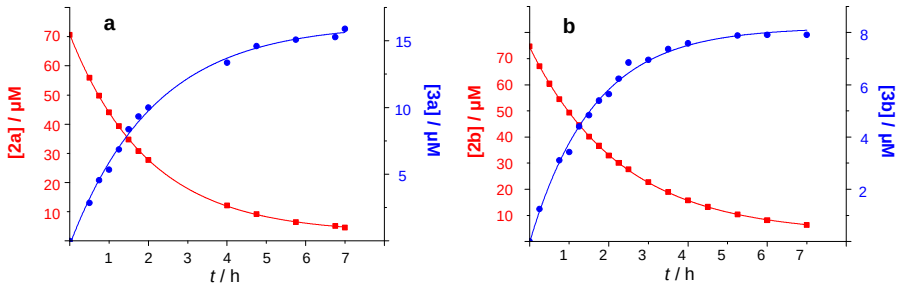

Figure 28. Kinetics for thioketone disappearance (red) and sulfine formation (blue). a) Values for **2a** and **3a**. b) Values for **2b** and **3b**.

Table 4 also summarizes the rate constants obtained from the first-order fittings for thioketone oxidation and sulfine generation, as well as the quantum yields for these processes, taking into account the amount of photons absorbed by the photosensitizer and the initial and final concentrations of the involved compounds ($[\mathbf{2a}]_0 = (7.07 \pm 0.02) \times 10^{-5}$ M; $[\mathbf{3a}]_{t\to\infty} = (1.72 \pm 0.04) \times 10^{-5}$ M; $[\mathbf{2b}]_0 = (7.44 \pm 0.02) \times 10^{-5}$ M; $[\mathbf{2b}]_{t\to\infty} = (8.2 \pm 0.2) \times 10^{-6}$ M); $(1.6 \pm 0.2) \times 10^{-3}$ mol of photons absorbed during an irradiation time of 7 h).

Interestingly, from the spectra shown in Figures 25-27, the presence of isosbestic points must be highlighted (272 nm in acetonitrile and 268 nm in methanol).

Table 4. Kinetic results for the photooxidation of **2a** and **2b** in methanol.

Compound	Conversion	Yield	k / h^{-1}	R^2	$\Phi_{photooxidation}$	$\Phi_{photoproduction}$
2a	96.2	-	0.499	0.999	$1.24 \cdot 10^{-4}$	-
3a	-	24.0	0.47	0.996	-	$0.30 \cdot 10^{-4}$
2b	96.1	-	0.431	0.999	$1.28 \cdot 10^{-4}$	-
3b	-	11.0	0.61	0.992	-	$0.15 \cdot 10^{-4}$

Occurrence of isosbestic points (IP) during the transformation of a substrate can give relevant information about the reaction mechanism, although several key aspects must be considered concerning the nature of these points. Starting from the general reaction [18]

$$A \xrightarrow{k_1} B \quad [18]$$

If the UV-vis spectra from reactant A and product B are different but overlap, the conversion of A into B will show the presence of an isosbestic point. It is commonly accepted that the wavelength of an isosbestic point corresponds to the wavelength where the molar absorption coefficients of A and B are the same. Implicitly, this statement implies that all the transformed A molecules are converted into B molecules, so at the isosbestic point, equation [19] rules:

$$\left(\varepsilon_A[A]_t + \varepsilon_B[B]_t\right) l = \left(\varepsilon_A[A]_t + \varepsilon_B[A]_{transformed}\right) l = A_{IP} = \text{Constant} \quad [19]$$

However, a non-quantitative transformation of A in B can also induce the presence of an isosbestic point.[75] In this case, a new product C must be generated in order to reduce the yield of B production. Nevertheless, production of both products, B and C, can be assumed under two main general reaction schemes: consecutive and parallel pathways (Scheme 19).

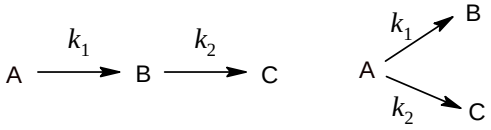

Scheme 19. Consecutive and parallel reaction mechanisms for B and C generation from a reactant A.

Figures 29a and 29b show the changes of [A], [B] and [C] over the time (normalized to $[A]_0$) considering a consecutive and parallel reactions mechanism, respectively (assuming that $k_1 = 0.02\ s^{-1}$ and $k_2 = 0.01\ s^{-1}$)

[75] S. E. Braslavsky. *Pure Appl. Chem.*, **2007**, *79*, 293.

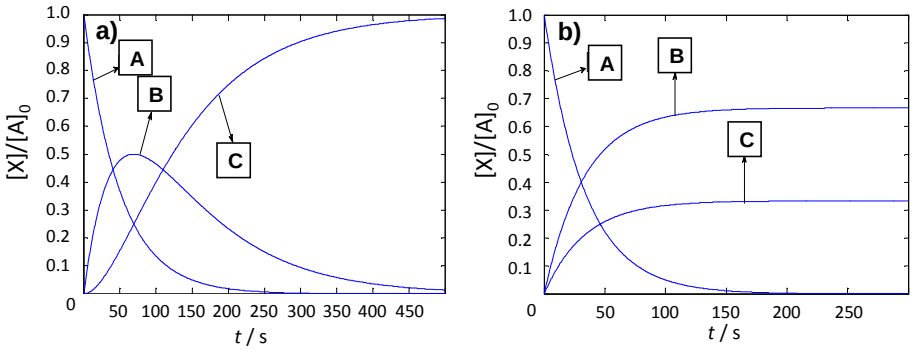

Figure 29. Changes of [A], [B] and [C] over time assuming consecutive (a) and parallel (b) reactions for B and C production starting from A.

Both mechanisms illustrated in Scheme 19 could be compatible with the generation of sulfine and ketone products, as the sulfine group can decompose to the corresponding ketone (see Scheme 17). However, it has been demonstrated[76] that the presence of isosbestic points is compatible only when A, B, and C spectra overlap and, in addition, the conversion of the reaction substrate in different products occurs via parallel reactions. Taking the photooxidation of **2b** in methanol as example, if the absorption spectra of **2b** and **3b** are considered, as well as [**2b**] and [**3b**] values calculated for different times using the general kinetic equations for consecutive and parallel reactions (k_1 = 0.02 s^{-1} and k_2 = 0.01 s^{-1}), the evolution of the spectra over time can be plotted. As it was previously anticipated, the isosbestic point only appears in the case of parallel reactions (Figure 30b) while is absent if consecutive reaction pathways operate (Figure 30a).

[76] A. E. Croce. *Can. J. Chem.*, **2008**, *86*, 918.

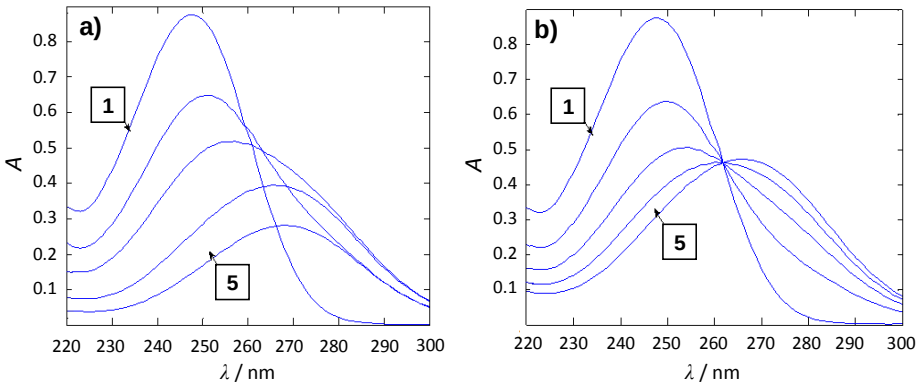

Figure 30. a) Evolution of the UV-vis spectra for the transformation of **2b** into **1b** and **3b**, considering consecutive reactions (**1**: 0 s, **2**: 25 s, **3**: 50 s, **4**: 100 s, **5**: 150 s). b) Evolution of the UV-vis spectra for the transformation of **2b** into **1b** and **3b**, considering parallel reactions (**1**: 0 s, **2**: 15 s, **3**: 30 s, **4**: 45 s, **5**: 60 s).

Moreover, from the wavelength of the isosbestic point (λ_{IP}) it is possible to know the yield (f) of products, considering the molar absorption coefficients for the product and the reactant, as it is stated in [20].[77]

$$f = \frac{\varepsilon_{IP}^{B}}{\varepsilon_{IP}^{A}} \quad [20]$$

As a consequence, λ_{IP} depends on the conversion factor f. Figure 31 shows this dependence in the case of **2a** and **2b** transformation into **3a** and **3b** in methanol, respectively.

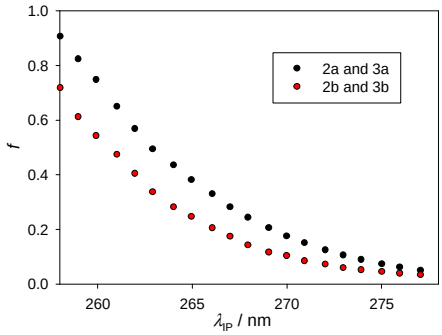

Figure 31. f factors for the conversion of **2a** into **3a** (black) and **2b** into **3b** (red) as a function of λ_{IP}.

[77] B. S. Berlett, R. L. Levine, E. R. Stadtman. *Anal. Biochem.*, **2000**, *287*, 329.

According to these values of *f* and taking into account that, for example, λ_{IP} = 268 nm in methanol for **2a** and **2b** photooxidation, the sulfine yields using this approach are 28 ± 4 % and 14 ± 2 %, respectively. These values are in good agreement with those obtained from the kinetic analysis (Table 4).

As a consequence, the detection of isosbestic points in the monitorization of thioketone photooxidation can be considered as the first experimental evidence in favour of a reaction scheme with parallel reaction pathways.

5.3.2. Evidences from NMR spectroscopy

Although UV-vis spectrophotometry proved to be a suitable way to get valuable information about the kinetics and the general reaction scheme, detailed structural information about the photoproducts obtained was accomplished using other spectroscopic techniques.

Ketone and sulfine are not the only photoproducts

A 50 mM solution of **2a** in CD_3CN was irradiated in the presence of $[Ru(dip)_3]Cl_2$ dye as photosensitizer.

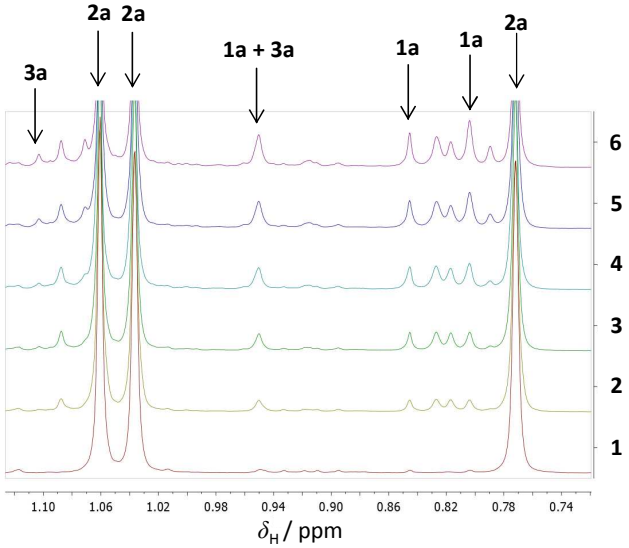

Figure 32. Evolution of ^{1}H-NMR signals in the methyls region by irradiation of **1a** in CD_3CN. **1**: 0 h, **2**: 0.5 h, **3**: 1 h, **4**: 1.5 h, **5**: 2 h, **6**: 3h.

Figure 32 represents a series of spectra acquired at different irradiation times. It is possible to see how the characteristic signals for the methyl groups of **2a** and **3a** can be assigned. However, contrary to previous reports about the photooxidation of thioketones,[63] more signals than those belonging only to ketone and sulfine derivatives were detected in the methyl region and, what is more interesting, in the alkene region (Figure 33). From this Figure it is possible to observe at short irradiation times (up to 5 h) the appearance of doublets at 6.30 ppm (J = 3.2 Hz) and 6.05 ppm (J = 3.2 Hz). At long irradiation times (22 h), a new evident signal at 6.45 ppm and other incipient ones at 6.26, 6.39, 6.50, 6.58 and 6.85 ppm were also detected. It is interesting to highlight the relative evolution in the intensity of these signals, especially for those at 6.30 and 6.05 ppm. The signal at 6.30 ppm grows faster at the beginning of the irradiation, being surpassed after 3 h of irradiation by the signal at 6.05 ppm, whose growth is slower at the beginning of the reaction. This trend could be tentatively explained if the compound showing the ^{1}H signal at 6.30 ppm is a reaction intermediate which evolves by a consecutive reaction pathway to a new compound with an alkene proton at 6.05 ppm (similar to the graph depicted in Figure 29a).

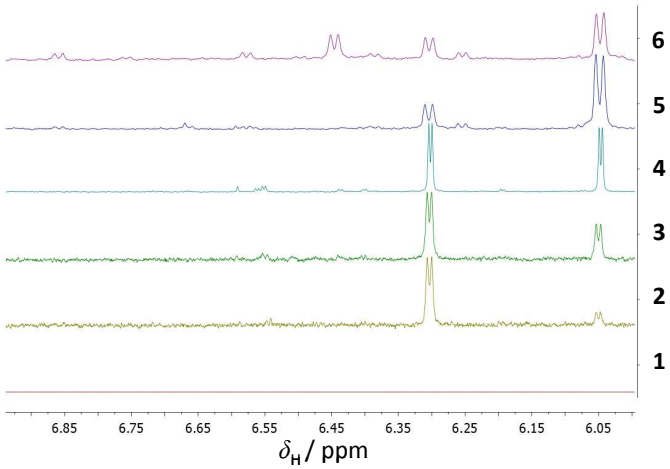

Figure 33. Evolution of ^{1}H-NMR signals in the alkene region by irradiation of **1a** in CD_3CN. **1**: 0 h, **2**: 1 h, **3**: 2 h, **4**: 3 h, **5**: 5 h, **6**: 22h.

Moreover, the COSY spectrum of the reaction crude (Figure 34) showed the correlations of these signals. In particular, the signal at 6.30 ppm correlates with a triplet at 2.45 ppm (J = 3.3 Hz) and the signal at 6.05 ppm correlates with

another one which could not be characterized because it overlapped with a signal belonging to **2a** (inset Figure 32).

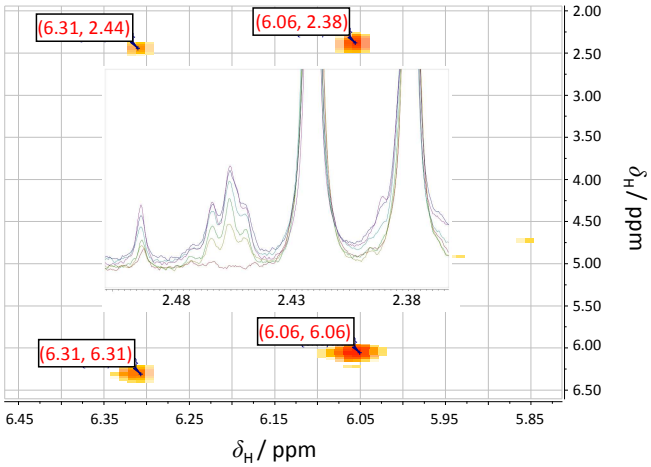

Figure 34. COSY correlations of the new signals in the alkene region after 3 h of **1a** irradiation in CD_3CN. Inset: aliphatic region showing the growth of some signals which correlate with the alkene signals.

Figure 35 summarizes a series of (1*R*)-thiocamphor alkene derivatives found in the bibliography,[78] with the reported chemical shifts and the coupling constants for the olefinic proton and the proton in position 4 (which could be the responsible for the ^3J correlation observed in COSY spectrum).

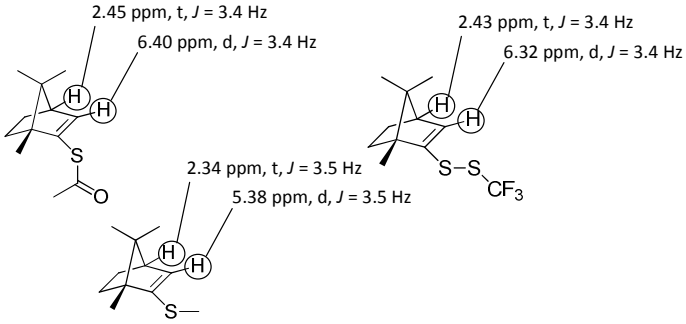

Figure 35. Characteristic ^{1}H-NMR signals of some alkene derivatives of thiocamphor found in the bibliography.

[78] a) A. M. Álvarez-García. Síntesis estereoselectiva y aplicaciones de nuevos tioderivados con esqueleto norbornánico. Ph.D. Thesis, Complutense University of Madrid, 2008. b) R. Huisgen, G. Mloston, A. Pröbstl. *Hetereoatom Chem.*, **200**1, *12*, 136.

Due to the similarities in the multiplicity, coupling constant values and, to a lesser extent, the chemical shift of these signals, some chemical transformations involving the protons in alpha position with respect to the thiocarbonyl carbon must be taking place. This idea was supported by two new experimental findings: no olefinic signals were observed in the photooxidation of **2b** (where the alpha position with respect to the thiocarbonyl carbon is substituted by methyl groups and not with protons) and, in addition, the growth of these signals was minimal when the photooxidation of **2a** was carried out in methanol.

These findings could be explained considering the peroxythiocarbonyl intermediate **A** postulated in Scheme 20: the terminal oxygen in this intermediate could tend to stabilize its negative charge via an intramolecular proton transfer when there are hydrogen atoms available in alpha position to the thiocarbonyl carbon. This behaviour could be compared with the mechanism depicted in Scheme 9 for the Schenck-ene reaction (hydrogen removal and double bond migration), and also with the typical reactivity of persulfoxide intermediate in the photooxidation of organic sulfides leading to the hydroperoxysulfonium ylide (Scheme 14). As a result, a vinylpersulfenic acid derivative **4a** could be produced (Scheme 20), which could subsequently evolve to other derivatives bearing olefinic protons. However, formation of **4a** would be promoted in acetonitrile but minimized in methanol due to the stabilization of **A** by protic solvents like methanol, in a similar way to the persulfoxide intermediate (Scheme 15)

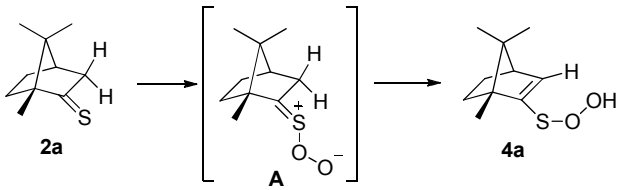

Scheme 20. Proposed evolution for intermediate A in order to explain the generation of signals in the ^{1}H NMR alkene region.

Photoproducts distribution is strongly dependent on the reaction solvent

The reaction solvent played a key role influencing the photoproducts distribution, what proved to be a valuable information from a mechanistic point of view.

Some experiments were carried out in CD_3CN as aprotic solvent, MeOD-d_4 as protic one, and in a mixture of CD_3CN and CF_3COOH 50 mM, in order to study the influence of protons in the reaction pathways. Thioketone conversion and its corresponding $\Phi_{photooxidation}$, as well as photoproduct yields and $\Phi_{photoproduction}$ are summarized in Table 5 for each experimental condition. Integration of the signals from the spectra of the reaction crudes afforded the conversion and the reported yield values.

Table 5. Experimental results of the photooxidation of thioketones **2a** and **2b** in CD_3CN, $CD_3CN + H^+$ and CD_3OD. [a]: $[\mathbf{2a}]_0 = 50$ mM, 3 h of irradiation. [b]: $[\mathbf{2a}]_0 = 50$ mM, $[H^+] = 50$ mM, 3 h of irradiation. [c]: $[\mathbf{2a}] = 55$ mM, 3 h of irradiation. [d]: $[\mathbf{2b}] = 68$ mM, 3 h of irradiation. [e]: $[\mathbf{2b}]_0 = 50$ mM, $[H^+] = 50$ mM, 3 h of irradiation. [f]: $[\mathbf{2b}]_0 = 70$ mM, 4 h of irradiation.

Compound	Solvent	Conversion	Yield	$\Phi_{photooxidation}$	$\Phi_{photoproduction}$
2a	CD_3CN [a]	34%	-	$8.5\cdot10^{-3}$	-
	$CD_3CN + H^+$ [b]	35%	-	$8.8\cdot10^{-3}$	-
	CD_3OD [c]	36%	-	$9.9\cdot10^{-3}$	-
1a	CD_3CN [a]	-	14.6%	-	$3.6\cdot10^{-3}$
	$CD_3CN + H^+$ [b]	-	9.0%	-	$2.2\cdot10^{-3}$
	CD_3OD [c]	-	4.5%	-	$1.3\cdot10^{-3}$
3a	CD_3CN [a]	-	4.6%	-	$1.2\cdot10^{-3}$
	$CD_3CN + H^+$ [b]	-	13.6%	-	$3.4\cdot10^{-3}$
	CD_3OD [c]	-	25.6%	-	$7.1\cdot10^{-3}$
Alkene-a1 6.30 ppm	CD_3CN [a]	-	6.6%	-	$1.7\cdot10^{-3}$
	$CD_3CN + H^+$ [b]	-	6.2%	-	$1.5\cdot10^{-3}$
	CD_3OD [c]	-	2.0%	-	$0.6\cdot10^{-3}$
Alkene-a2 6.05 ppm	CD_3CN [a]	-	6.0%	-	$1.5\cdot10^{-3}$
	$CD_3CN + H^+$ [b]	-	6.0%	-	$1.5\cdot10^{-3}$
	CD_3OD [c]	-	2.0%	-	$0.6\cdot10^{-3}$
2b	CD_3CN [d]	8%	-	$2.7\cdot10^{-3}$	-
	$CD_3CN + H^+$ [e]	11%	-	$2.8\cdot10^{-3}$	-
	CD_3OD [f]	29%	-	$10.1\cdot10^{-3}$	-
1b	CD_3CN [d]	-	8.0%	-	$2.7\cdot10^{-3}$
	$CD_3CN + H^+$ [e]	-	3.6%	-	$0.9\cdot10^{-3}$
	CD_3OD [f]	-	3.3%	-	$1.1\cdot10^{-3}$
3b	CD_3CN [d]	-	0.0%	-	-
	$CD_3CN + H^+$ [e]	-	7.2%	-	$1.8\cdot10^{-3}$
	CD_3OD [f]	-	25.7%	-	$8.9\cdot10^{-3}$

Figure 36 illustrates the methyls region for **2a** photooxidation depending on the media used, making clear the influence of the experimental conditions in the distribution of photoproducts. In the same manner, for the sake of clarity, Figure 35 represents the yields of each photoproduct. In CD_3CN the major photoproduct was the ketone **1a**, although small amounts of the alkenes **a1** and **a2**, as well as the sulfine **3a** were detected. Conversely, when the reaction was carried out in methanol, the reverse distribution was obtained, as the sulfine **3a** was by far the major photoproduct, while ketone generation was drastically decreased. Interestingly, sulfine generation was partially improved when an equimolar amount of CF_3COOH to **2a** was used, in comparison to results with aprotic CD_3CN.

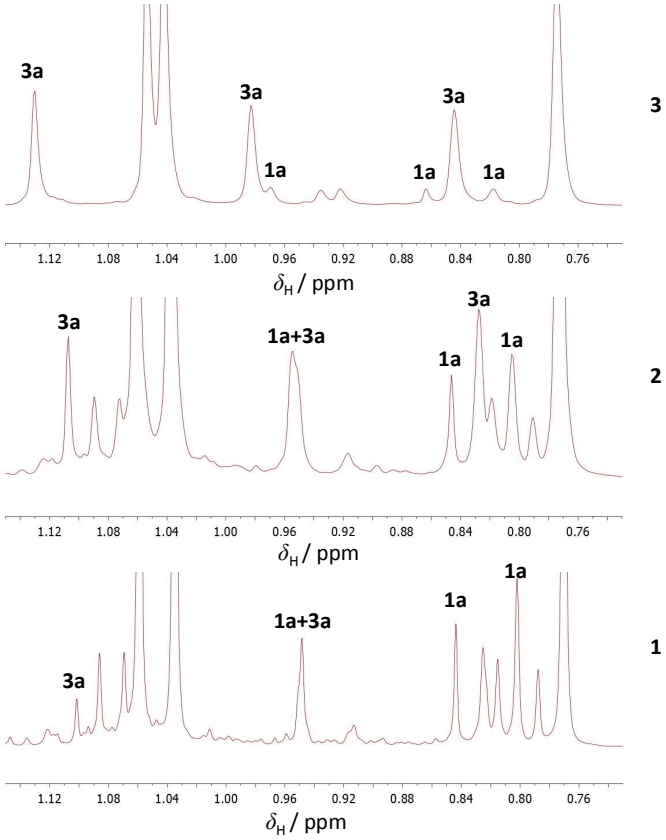

Figure 36. ^{1}H-NMR signals in the methyls region by irradiation of **2a** in CD_3CN (1), $CD_3CN + H^+$ (2) and MeOD-d_4 (3).

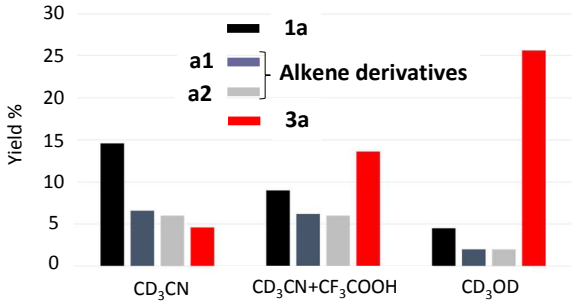

Figure 37. Distribution of the photooxidation products of **2a** under different reaction conditions. (Alkene derivatives – **a1**, – **a2**). Conversions summarized in Table 5.

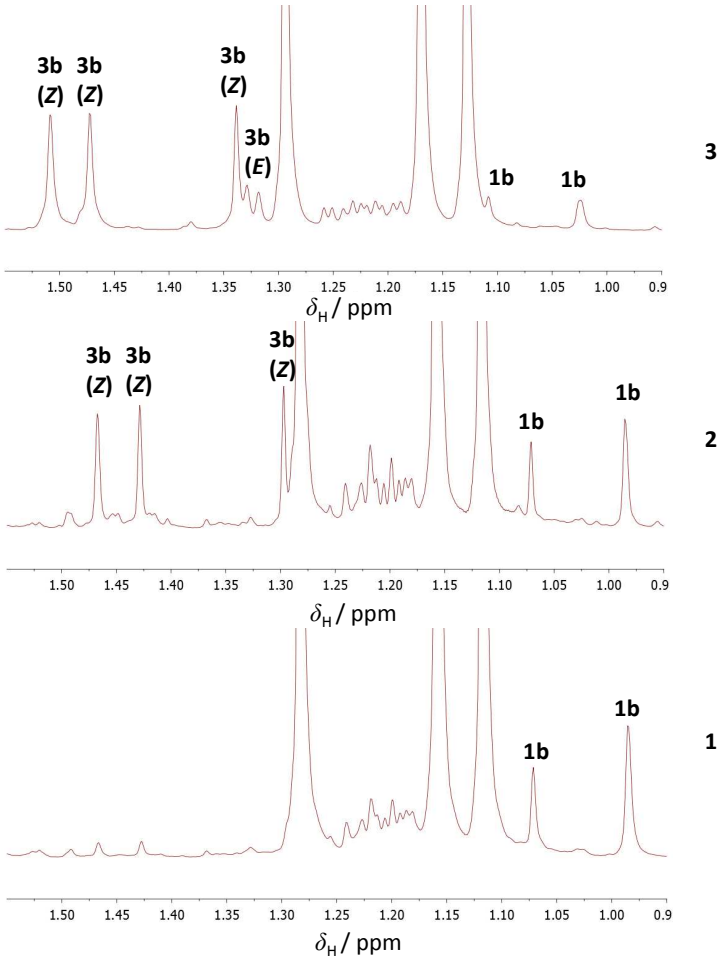

Figure 38. ^{1}H-NMR signals in the methyls region by irradiation of **2b** in CD_3CN (1), CD_3CN+H^+ (2) and MeOD-d_4 (3).

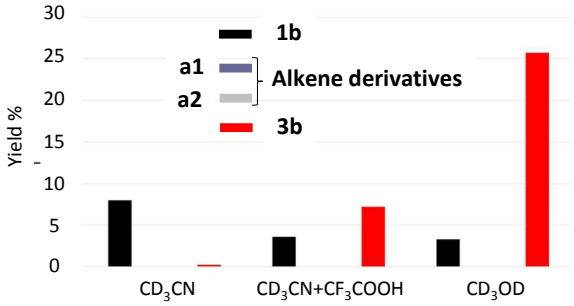

Figure 39. Distribution of the photooxidation products of **2b** under different reaction conditions. Alkene derivatives **a1** and **a2** were not detected. Conversions summarized in Table 5.

Similar trends were observed in the photooxidation experiments of **2b** (Figure 38). However, several aspects must be pointed out. Firstly, it was not possible to undoubtedly detect the methyl signals corresponding to **3b** when the reaction was carried out in CD_3CN. For this reason, the improvement in sulfine generation observed when the reaction is performed in CD_3OD or CD_3CN in the presence of CF_3COOH is even more remarkable. Secondly, the *Z* and *E* diastereoisomers of **3b** were detected for the first time in this kind of reactions, and the diastereomeric ratio was the same for the photooxidation and for the thermal synthesis using *m*-chloroperbenzoic acid (values for **3b** yields in Table 5 and Figure 37 are the added values of the yields of *Z* and *E* diastereoisomers).

Nevertheless, it has to be highlighted that overall kinetics were slowed down in NMR experiments in comparison with the experiments with UV-vis monitorization. This fact can be explained considering the k_q for $P(T_1)$ quenching by **2a** or **2b** (Table 2). For example, in the experiments followed by UV-vis spectrophotometry, where [Thioketone] ~ 70 μM, the portion of $P(T_1)$ states physically quenched ($P = 1-(\tau/\tau_0)$) by **2a** in acetonitrile is 0.06%. On the other hand, in NMR experiments, where [Thioketone] ~ 50 mM, this portion is increased to 42%. This means that there is a lower population of $P(T_1)$ states which can produce $^1O_2$. Moreover, it is possible to see that conversion values of **2b** photooxidation are also lower than those obtained for **2a**. In this case, this fact could be explained by taking into account k_q^{Δ} values for $^1O_2$ quenching by **2a** or **2b** (Table 3). The higher k_q^{Δ} values observed for **2a** could be related to a higher chemical interaction in comparison with **2b**.

Sulfine / Ketone ratio depends on $[Thioketone]_0$

Since sulfine production was clearly improved in CD_3OD, several experiments were carried out in order to study the influence of the initial concentration of thioketone in the sulfine/ketone ratio. Results are summarized in Table 6, while a sample of the changes observed in the ^{1}H-NMR spectra for **2a** and **2b** photooxidation are depicted in Figures 40 and 41, respectively, clearly showing a dependence on $[thioketone]_0$.

Table 6. Influence of $[Thioketone]_0$ in the sulfine/ketone ratio in CD_3OD.

[**2a**]/mM	1	10	25	50	80
3a/**1a**	0.31	2.22	3.84	3.57	4.17
[**2b**]/mM	1	10	40	70	80
3b/**1b**	1.61	3.33	5.88	6.25	6.66

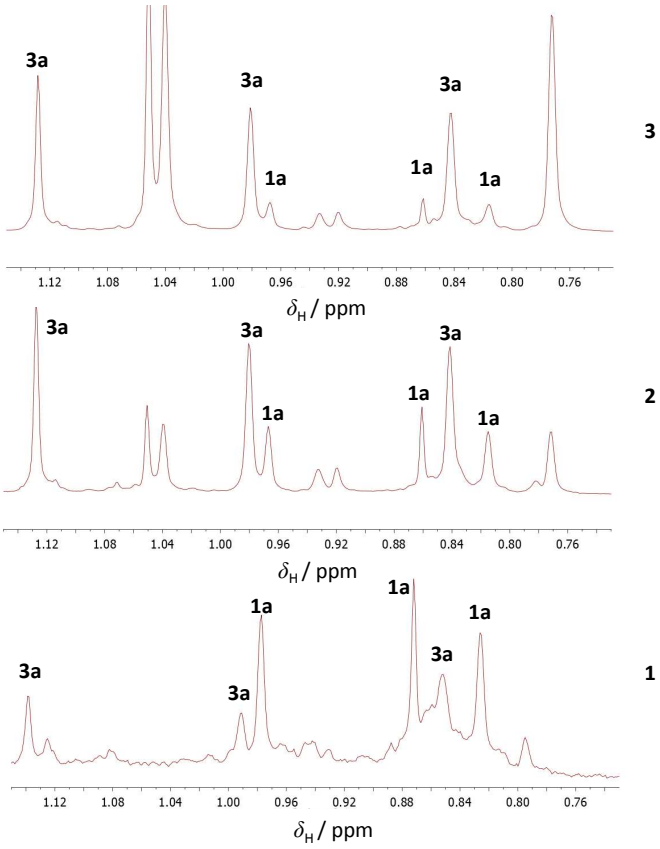

Figure 40. ^{1}H-NMR signals in the methyls region by irradiation of **2a** in CD_3OD. (1) $[\mathbf{2a}]_0$ = 1 mM, (2) $[\mathbf{2a}]_0$ = 10 mM and (3) $[\mathbf{2a}]_0$ = 50 mM.

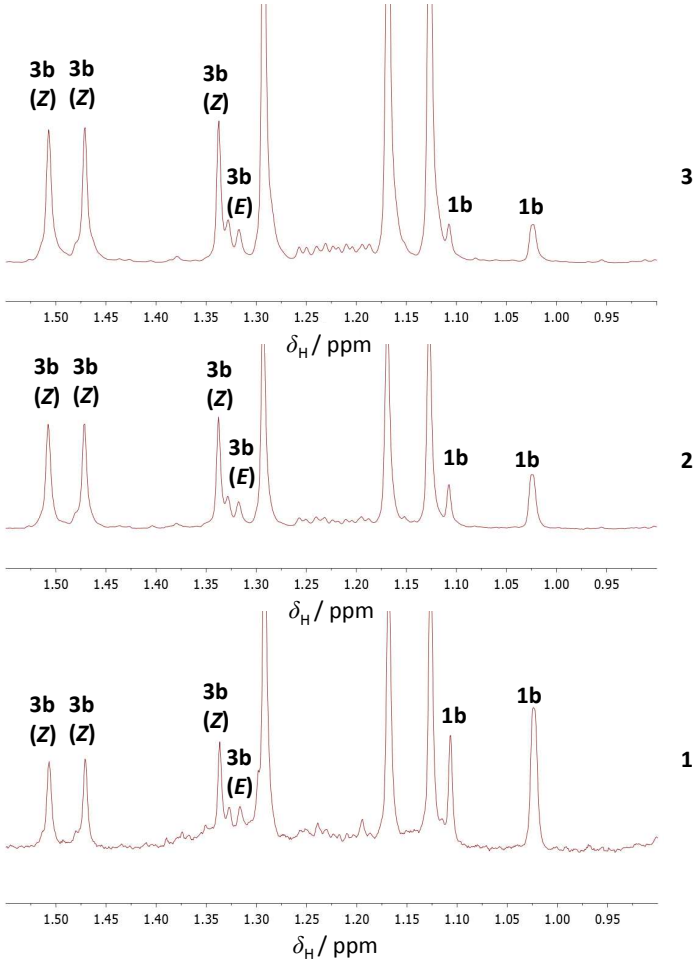

Figure 41. ^{1}H-NMR signals in the methyls region by irradiation of **2b** in CD_3OD. (1) $[\mathbf{2b}]_0$ = 1 mM, (2) $[\mathbf{2b}]_0$ = 10 mM and (3) $[\mathbf{2b}]_0$ = 70 mM.

In all the cases it is possible to conclude that $[\text{thioketone}]_0$ has an influence in the sulfine/ketone ratio since, at higher $[\text{thioketone}]_0$, more sulfine is produced at the expense of ketone product. Moreover, in the case of **2a**, it was possible to reverse the sulfine/ketone ratio from $[\mathbf{2a}]_0$ = 1 mM to $[\mathbf{2a}]_0$ > 10 mM. For the sake of clarity, it is informative to represent the changes observed in these ratios as a function of $[\text{thioketone}]_0$ (Figure 42).

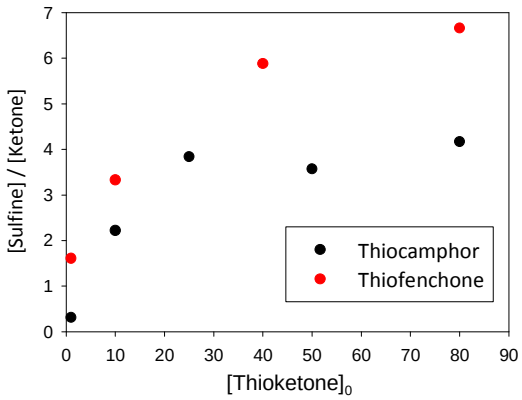

Figure 42. Sulfine/ketone ratio dependence on $[thioketone]_0$ for **2a** (black points) and **2b** (red points).

At this point, it is possible to consider some new mechanistic conclusions from the experimental data obtained by NMR analysis. For this aim, it must be taken into account the peroxythiocarbonyl intermediate **A** shown in Scheme 20 (previously considered in Scheme 16), whose evolution by parallel reactions had been postulated from the experimental results obtained by UV-vis spectrophotometry. It has been proved in this section that protic conditions (methanol as solvent or the presence of an acid in aprotic solvents) are related to an increment in sulfine production. It could be expected that protic conditions are suitable for the stabilization of the negative charge located on the terminal oxygen of **A** via hydrogen bonding (protic solvent) or direct protonation (acidic conditions). As a consequence, this stabilization could prevent the ring closure to the intermediate **B** (Scheme 21) and the subsequent evolution to the ketone. By analogy, a similar behaviour was presented in Scheme 15 for the photooxidation of organic sulfides in protic solvents. On the contrary, in aprotic solvents such as acetonitrile, this stabilization is not possible and the intermediate **A** evolves mainly via the intermediate **B** (Scheme 21).

Moreover, the dependence of sulfine/ketone ratio on $[thioketone]_0$ proved to be a key factor in order to propose an alternative to the release of atomic oxygen from intermediate **A** for the generation of sulfine group. If this atomic oxygen release were taking place, no dependence on $[thioketone]_0$ should be observed since both processes, ketone and sulfine generation, would be intramolecular pathways arising from intermediate **A** (Scheme 21). However, the experimental

results could be better explained if an intermolecular oxygen transfer step from intermediate **A** to a second thioketone molecule is considered. In this sense, in protic solvents, the aforementioned stabilization of intermediate **A** could increase its lifetime and the probability of interaction with a second thioketone molecule, what explains the improved generation of sulfine group in comparison with aprotic solvents where the intramolecular evolution of **A** prevails. The proposed oxygen transfer from intermediate **A** could make sense due to the similarity between its reactive group ($–S^+–O–O^-$) and the peracid moiety of *m*-chloroperbenzoic acid (–C(O)–O–O–H).

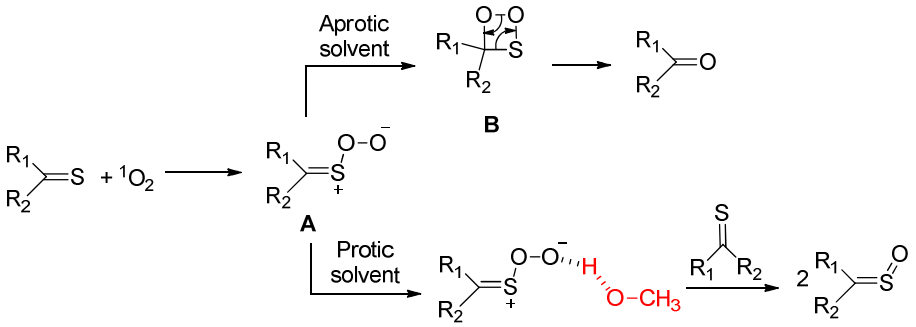

Scheme 21. Reaction scheme explaining the sulfine/ketone ratio dependence on the type of solvent and $[thioketone]_0$.

The kinetics of the sulfine/ketone ratio dependence on $[thioketone]_0$ could be modelized. For this aim, the general and simplified reaction pathways shown in Scheme 22 will be considered as representative of the processes leading to ketone and sulfine (starting from thioketone A with an unimolecular evolution to ketone B and a bimolecular reaction to sulfine C. $[^1O_2]$ may be assumed to be constant if continuous supply of $^1O_2$ is considered (photostationary $^1O_2$ generation). Although the pathways leading to alkene derivatives should be considered in the kinetic model of **2a** photooxidation, for the sake of clarity they will not be taken into account since their reaction yields are low (< 7%, see Table 5).

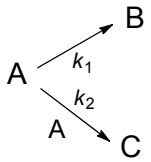

Scheme 22. General reaction scheme considered for kinetic modelization.

From this scheme, the first step is to calculate the dependence of [A] as a function of time. For this purpose, the differential equation [21] is solved to get [22]

$$\frac{d[\mathrm{A}]}{dt} = -k_1[A] - k_2[A]^2 \Rightarrow \int_{[\mathrm{A}]_0}^{[\mathrm{A}]} \frac{d[\mathrm{A}]}{k_1[A] + k_2[A]^2} = -\int_0^t dt \quad [21]$$

$$[A] = \frac{k_1[A]_0}{e^{k_1 t}\left(k_1 + k_2[A]_0\right) - k_2[A]_0} \quad [22]$$

Equation [22] can be simplified assuming two limiting cases:

a) k_1 >> $k_2[A]_0$: Unimolecular pathway prevailing over the bimolecular pathway (low thioketone concentration)

In this case, [*A*] dependence on time is defined by [23].

$$[A] = [A]_0 e^{-k_1 t} \quad [23]$$

As a result, in order to get [*B*] and [*C*] dependence on time, differential equations [24] and [26] were proposed and solved to get [25] and [27], respectively.

$$\frac{d[B]}{dt} = k_1[A] = k_1[A]_0 e^{-k_1 t} \Rightarrow \int_{[B]_0}^{[B]} d[B] = k_1[A]_0 \int_0^t e^{-k_1 t} dt \quad [24]$$

$$[B] = [A]_0\left(1 - e^{-k_1 t}\right) \quad [25]$$

$$\frac{d[C]}{dt} = k_2[A]^2 = k_2[A]_0^2 e^{-2k_1 t} \Rightarrow \int_{[C]_0}^{[C]} d[\mathrm{C}] = k_2[A]_0^2 \int_0^t e^{-2k_1 t} dt \quad [26]$$

$$[C] = \frac{k_2[A]_0^2}{2k_1}\left(1 - e^{-2k_1 t}\right) \quad [27]$$

Under this approximation it is possible to demonstrate that [C]/[B] shows a linear dependence on $[\mathrm{A}]_0$ (equation [28])

$$\frac{[C]}{[B]} = \frac{k_2[A]_0}{2k_1} \frac{\left(1 - e^{-2k_1 t}\right)}{\left(1 - e^{-k_1 t}\right)} \quad [28]$$

b) $k_1 << k_2[A]_0$: Bimolecular pathway prevailing over the unimolecular pathway (high thioketone concentration)

In this case, [A] dependence on time is defined by [29]

$$\frac{1}{[A]} = \frac{1}{[A]_0} + k_2 t \Rightarrow [A] = \frac{[A]_0}{1+[A]_0 k_2 t} \quad [29]$$

In order to get [*B*] and [*C*] dependence on time, differential equations [30] and [32] were proposed and solved to get [31] and [33], respectively.

$$\frac{d[B]}{dt} = \frac{k_1[A]_0}{1+[A]_0 k_2 t} \Rightarrow \int_{[B]_0}^{[B]} d[B] = k_1[A]_0 \int_0^t \frac{1}{1+[A]_0 k_2 t} dt \quad [30]$$

$$[B] = \frac{k_1}{k_2} ln\left(1+[A]_0 k_2 t\right) \quad [31]$$

$$\frac{d[C]}{dt} = \frac{k_2[A]_0^2}{\left(1+[A]_0 k_2 t\right)^2} \Rightarrow \int_{[C]_0}^{[C]} d[C] = k_2[A]_0^2 \int_0^t \frac{1}{\left(1+[A]_0 k_2 t\right)^2} dt \quad [32]$$

$$[C] = \frac{k_2[A]_0^2\, t}{1+[A]_0 k_2 t} \quad [33]$$

Under this approximation it is possible to demonstrate that [C]/[B] also shows a dependence on $[A]_0$, [34], although more complex than that of [28]

$$\frac{[C]}{[B]} = \frac{k_2^2}{k_1} \frac{[A]_0^2\, t}{\left(1+[A]_0 k_2 t\right)\left(ln\left(1+[A]_0 k_2 t\right)\right)} \quad [34]$$

Taking into account the experimental data shown in Figure 42, it is evident that after an initial increment at low substrate concentration, a plateau is reached at high $[\text{thioketone}]_0$. This trend is not predicted by the previous kinetic modelization, although it should be borne in mind that, due to its lack of sensitivity, NMR spectroscopy could not be the most suitable technique in order to detect the slight variations in ketone production at high $[\text{thioketone}]_0$ (where signals are close to the background noise an their integration could be affected by a relevant experimental error).

Finally, NMR spectroscopy was also used to demonstrate that photooxidation of thioketones **2a** and **2b** was mediated by $^1O_2$. For this aim, experiments were carried out in presence of DABCO (1,4-diazabicyclo[2.2.2]octane), a well-known $^1O_2$ quencher.[79] In its presence, the formation of products was slowed down and, in the case of **2a** in CD_3CN, alkene signals were completely suppressed (Figure 43. Spectrum 2), demonstrating that the evolution of alkene by-products is linked to $^1O_2$ production in the reaction system.

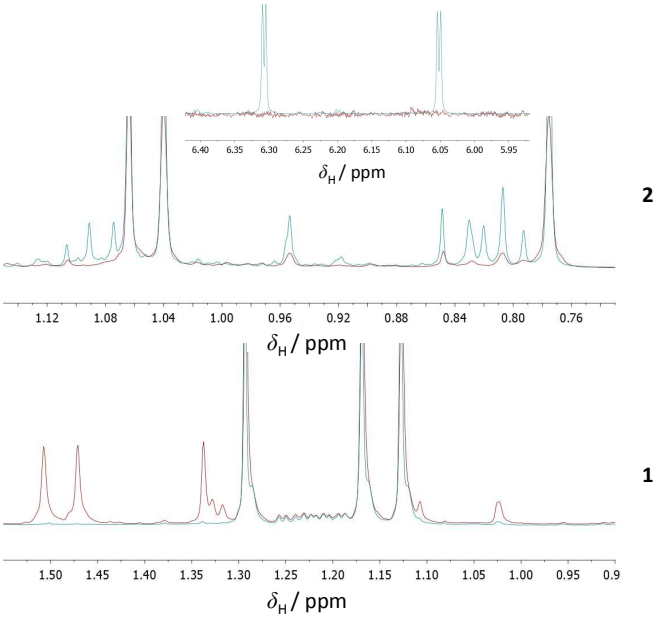

Figure 43. (1) ^{1}H-NMR signals in the methyls region by irradiation of **2b** in the presence (red) and absence (blue) of DABCO. Solvent: MeOD-d_4. (2) ^{1}H-NMR signals in the methyls region (inset: alkene region) by irradiation of **2a** in the presence (blue) and absence (red) of DABCO. Solvent: CD_3CN.

[79] F. Wilkinson, W. P. Herman, A. B. Ross. *J. Phys. Chem. Ref. Data*, **1995**, *24*, 663.

5.3.3. Evidences from GC-MS spectrometry

GC-MS was used to analyse the reaction crude of photooxidized **2a** in CD_3CN, in the search for the new secondary products whose structure could not be elucidated by NMR. The chromatogram obtained between 22 and 70 min is shown in Figure 44.

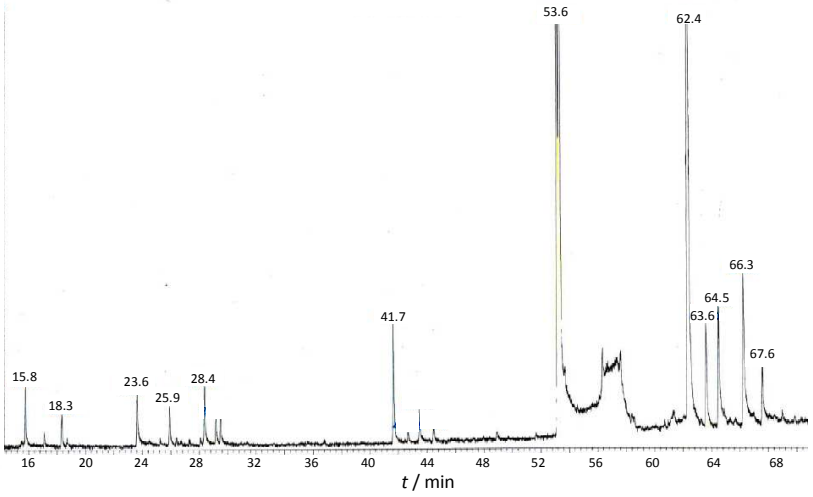

Figure 44. Gas chromatogram between 23 and 70 min of the reaction crude after irradiation of **1a** in CD_3CN.

Only the peaks where the molecular ion was undoubtedly detected will be considered for the mechanistic analysis. The retention times and the experimental masses are summarized in Table 7. This table contains also the calculated masses for the most probable structures (Figure 45). Although not shown in Figure 42, ketone **1a** was detected as the major photoproduct. However, it is very important to keep in mind that the relative abundance for the products found after GC-MS analysis could be altered as a consequence of the high temperatures used in the gas chromatograph (for example, the thermal decomposition of sulfine group to the corresponding ketone). However, the generation of these products can be explained only by the presence of some functional groups, especially those related to the vinylpersulfenic acid derivative **4a** (Scheme 20).

Table 7. Summary of peaks detected by GC-MS for **2a** photooxidation after 22 h of irradiation. Found masses have been tentatively assigned to compounds represented in Figure 45.

Compound	Retention time / min	Calculated mass	Found mass
M1	23.6	182.08	182.1
M2	28.4	184.09	184.1
M3	41.7	300.21	300.3
M4	53.6	332.18	332.2
M5 or M6	62.4 / 64.5 66.3 / 67.6	364.15	364.2
M7	63.5	350.17	350.2

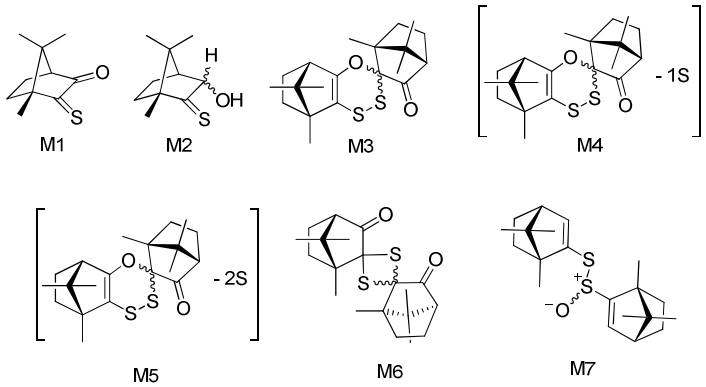

Figure 45. Tentative structures assigned to the detected peaks in GC-MS analysis

First of all, generation of α-oxothioketone **M1** and α-hydroxythiocamphor **M2** could be rationalized considering a rearrangement of the hydroperoxyl group to the α position of the thiocarbonyl carbon (Scheme 23). By analogy, this kind of migrations (Pummerer rearrangement) have been proposed in the photooxidation of organic sulfides, yielding α-hydroperoxysulfides from hydroperoxysulfonium ylides (Scheme 14).[80] The α-hydroperoxythiocamphor intermediate could evolve by two reaction pathways: intramolecular dehydration leading to **M1**, or an intermolecular oxygen transfer to a second thioketone molecule affording more sulfine and **M2**. By analogy, α-hydroperoxysulfides proved to be able to oxidize a second sulfide molecule yielding the corresponding sulfoxide by oxygen

[80] a) A. Toutchkine, D. Aebisher, E. L. Clennan. *J. Am. Chem. Soc*. **2001**, *123*, 4966. b) A. Toutchkine, E. L. Clennan. *J. Am. Chem. Soc*. **2000**, *122*, 1834.

transfer. It has to be noticed that the formation of derivatives bearing a thiocarbonyl carbon have been observed through ^{13}C-NMR analysis of the reaction crude after 3 h of irradiation in CD_3CN (Figure 44), where a signal was detected at 277.5 ppm.

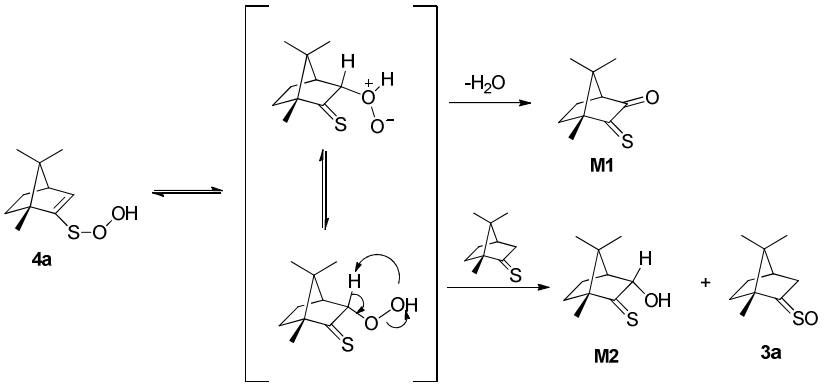

Scheme 23. Proposal of reaction mechanism for the generation of α-oxothioketone **M1** and α-hydroxythioketone **M2** from vinylpersulfenic acid intermediate **4a**.

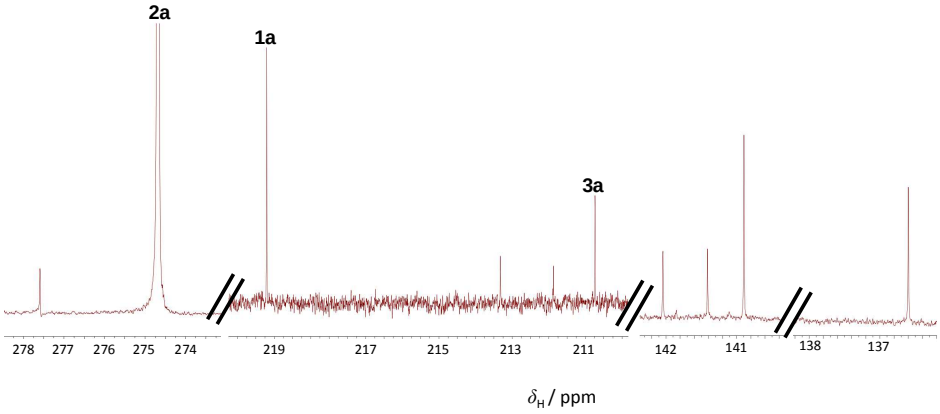

Figure 46. ^{13}C-NMR spectrum of the new signals detected in the thiocarbonyl, carbonyl and alkene regions after irradiation of **2a** in CD_3CN for 3 h.

In addition, four intense peaks related to intermolecular reactions of **M1** were observed. They can be attributed to the different diastereoisomers of adducts **M3** and **M6** formed via the [4 + 2] and [2 + 2] self-cycloadditions of **M1**, respectively (Scheme 24). Three also intense chromatographic peaks

corresponding to decomposition by-products of these adducts by loss of one (**M4**) or two (**M5**) sulfur atoms were also detected, as could be expected for the two possible by-products related to the loss of one sulfur atom, and one by-product when two sulfur atoms are extruded from **M3**. The two carbonyl peaks observed by ^{13}C-NMR at 211.1 and 212.6 ppm could therefore be assigned to the most abundant diastereoisomers of these adducts (Figure 46). Although several carbonyl signals could be expected from **M1**, **M3** and **M6** products (C_2 symmetry group), it is likely that the observed carbonyl peaks correspond to the most stable diastereoisomers among the four possible structures of adducts **M3** and **M6**, as fast *in situ* [2+2] and hetero-Diels-Alder [4+2] self-cycloaddition reactions of α-oxothioketones have previously been described in the bibliography.[81]

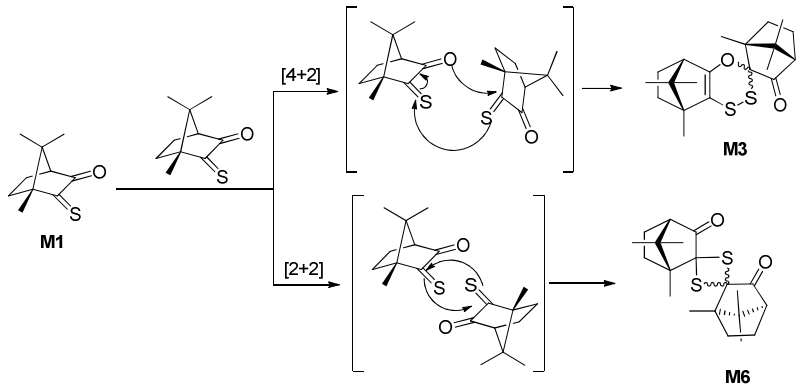

Scheme 24. Proposal of reaction mechanism for the generation of [4+2] (**M3**) and [2+2] (**M5**) cycloadducts from self-cycloaddition of α-oxo thioketone **M1**.

In order to explain the different signals observed by ^{1}H- and ^{13}C-NMR in the alkene region, and their evolution with time, the GC-MS peak assigned to one of the two possible diastereoisomers of thiosulfinate, **M7**, would support the formation of vinylpersulfenic acid **4a** (Scheme 25). As it has been previously stated in Scheme 23, it could be expected that the hydroperoxyl moiety in vinylpersulfenic acid **4a** reacts with a second thioketone molecule, yielding more

[81] a) T. J. Back, B. P. Dyck, M. Parvez. *J. Org. Chem*., **1995**, *60*, 703. b) I. Crossland. *Acta Chem. Scand*., **1977**, *31b*, 890. c) F. A. G. El-Essawy, S. M. Yassin, I. A. El-Sakka, A. F. Khattab, I. Sotofte, J. O. Madsen, A. Senning, *J. Org. Chem*., **1998**, *63*, 9840. d) M. I. Hegab, A. A. Abd El-Galil, F. M. E. Abdel-Megeid, *Z. Naturforsch. (B)*, **2002**, *57*, 922.

sulfine and the corresponding vinylsulfenic acid. The subsequent dehydration, in agreement with the typical chemistry of sulfenic acids, would lead to **M7**.

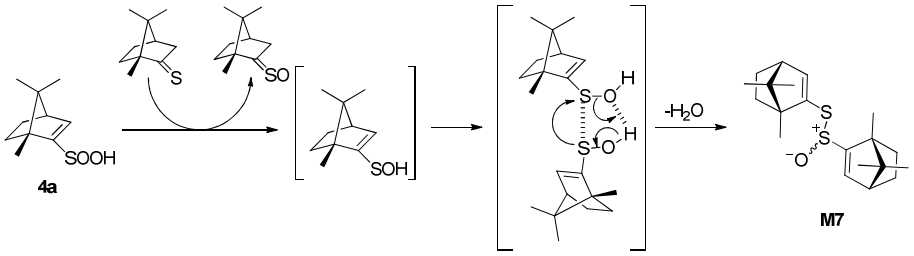

Scheme 25. Proposal of reaction mechanism for the intermolecular formation of thiosulfinate **M7** from vinylpersulfenic acid **4a**.

5.3.4. Evidences from computational calculations

Although the photoproducts generated from thioketone photooxidation have been described, modelization of the interaction between the $^1O_2$ molecule and the thioketone moiety can be of interest in order to explain several experimental facts previously shown, which are valuable data from a mechanistic point of view. First of all, as it was discussed after Figure 33, the occurrence of alkene derivatives through the proposed **4a** intermediate could be compared to a Schenck-ene reaction. For this aim, Scheme 26 shows the vinylpersulfenic acid generation in the same manner as hydroperoxide production depicted in Scheme 9.

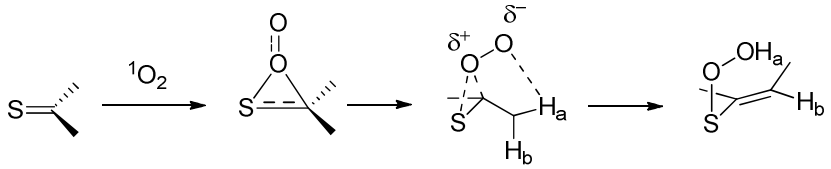

Scheme 26. Schenck-ene reaction between $^1O_2$ and thioketone group.

However, in spite of the overall similarities between both processes (hydrogen abstraction and double bond migration), there are some differences that must be considered. Figures 47 and 48 represent the shape of HOMO and HOMO-1 orbitals for **2a** and **2b**, respectively. Computational calculations were made

using GAMESS at B3LYP/6-31G* level. Taking into account the frontier molecular orbitals theory, it is expected that the thioketone group would act as a nucleophile with its HOMO and $^1O_2$ would act as an electrophile. As a result, from the spatial distribution shown in Figures 47 and 48, it is evidenced that the HOMO orbital is located on the sulfur atom and in the same plane as the C=S bond. So $^1O_2$ molecule would not interact preferentially in the fashion expected in a Schenck-ene reaction (Scheme 26). As a result, it is possible to consider peroxythiocarbonyl A (Scheme 21) as a common intermediate for all photoproducts.

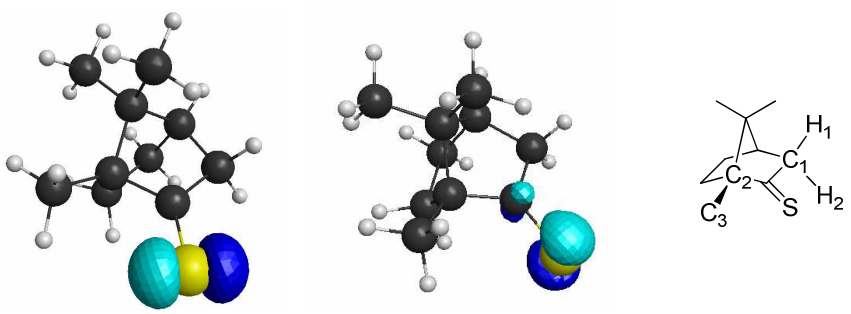

Figure 47. HOMO (left) and HOMO-1 (centre) orbitals for **2a**.

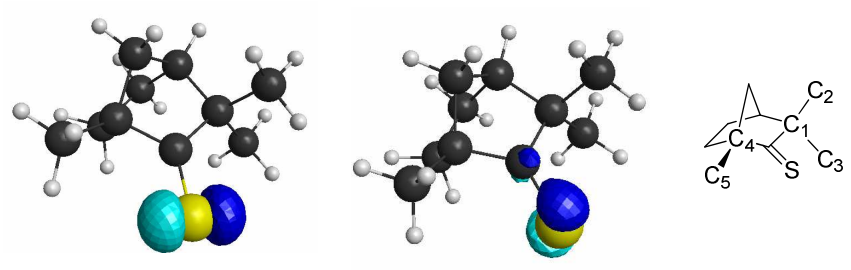

Figure 48. HOMO (left) and HOMO-1 (centre) orbitals for **2b**.

Moreover, this proposed interaction between $^1O_2$ molecule and the HOMO orbital in the thioketone could explain two more experimental findings, taking into account the dihedral angles (Θ) for C=S bond and the groups in alpha position to thiocarbonyl carbon. Using the nomenclature showed in Figure 47, for **2a**: Θ (C=S/C_2–C_3) = 9º, Θ (C=S/C_1–H_1) = 56º and Θ (C=S/C_1–H_2) = 51º. On the other hand, using the nomenclature showed in Figure 48, for **2b**: Θ (C=S/C_4–C_5) = 5º, Θ (C=S/C_1–C_2) = 51º and Θ (C=S/C_1–C_3) = 57º. As it was previously discussed considering the results summarized in Table 5, conversion values for

2b photooxidation were lower than those obtained for **2a**. In addition, the kinetic constant for **2b** photooxidation calculated in methanol from UV-vis monitorization was slightly lower than that for **2a** (Table 4). From a quantitative point of view, it could be explained taking into account the greater k_q^{Δ} values for **2a** than **2b**. From a qualitative point of view, depicted in Figure 49, steric hindrance in **2b** by the methyl groups in alpha position to thiocarbonyl carbon could explain why $^1O_2$ interacts more easily with **2a** than with **2b**.

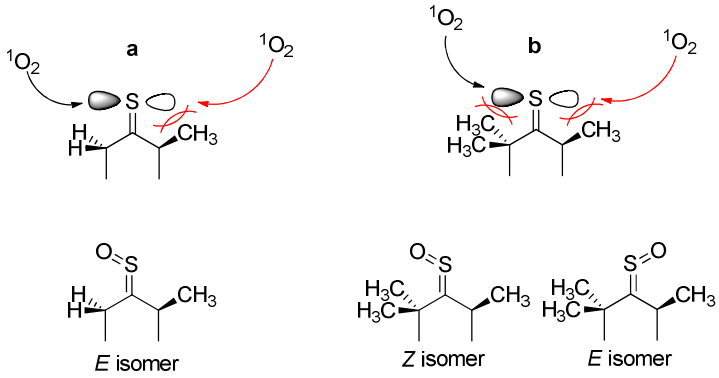

Figure 49. Interaction between $^1O_2$ and HOMO orbital from (1*R*)-thiocamphor (**a**) and (1*R*)-thiofenchone (**b**) considering steric factors.

In addition, the steric factors may influence the diastereoisomeric excess found in sulfine production from **2a** and **2b**. In the case of **3a**, the *E* isomer is expected to be the most thermodynamically stable, coming from the side where $^1O_2$ interacts with S, so this is the only diastereoisomer detected. On the other hand, considering **3b**, both sides are sterically hindered, although C=S bond is almost eclipsed to C_4–C_5 bond (Figure 48) and in gauche conformation respect to C_1–C_2 and C_1–C_3 bonds, so *Z* isomer is expected to be more stabilized than *E* isomer.

5.4. New mechanistic proposal

Taking into consideration all these experimental facts, a new mechanistic proposal for the photooxidation of alicyclic thioketones with sensitized singlet oxygen has been proposed (Scheme 27). Evidences collected from UV-vis spectrophotometry demonstrated that a mechanism based on parallel reactions rules this transformation. Ketone and sulfine are the major photoproducts but not

the only ones. Regarding the formation of the keto group (pathway (i), Scheme 27), no modifications have been introduced over the previous works. However, sulfine formation (pathway (ii), Scheme 27) can now be explained considering an intermolecular oxygen transfer to a second thioketone molecule from the firstly formed peroxythiocarbonyl zwitterionic intermediate A. Moreover, in the case of thiones bearing a hydrogen atom at the α-position, experimental evidences of proton transfer to the peroxythiocarbonyl group have been found in an aprotic solvent such as acetonitrile (pathway (iii), Scheme 27), producing a vinylpersulfenic acid intermediate **4a**. This intermediate can evolve through different pathways. Upon 1,3-migration of the hydroperoxyl moiety in **4a** to the α carbon, the reaction with another thiocamphor molecule and subsequent dehydration promotes the formation of **M1** (pathway (iv), Scheme 27), while the direct oxidation of thiocamphor yields the α-hydroxy thioketone **M2** (pathway (vi), Scheme 27). Self-cycloaddition reaction of **M1** yields cycloadducts **M3** (pathway (v), Scheme 27) and **M4** (pathway (vi), Scheme 27). Finally, the reaction of **4a** with another thiocamphor molecule can produce the intermediate **C** (pathway (viii), Scheme 27), which dimerizes to the corresponding thiosulfinate **M7** (pathway ix, Scheme 27).

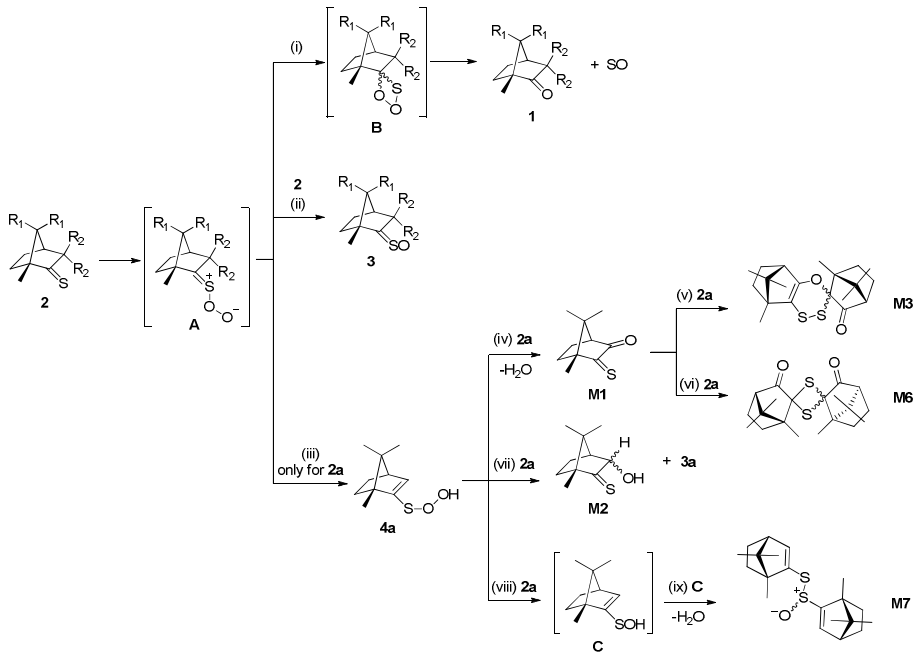

Scheme 27. New proposal of reaction pathways.

5.5. Photooxidative synthesis of sulfines under the principles of Green Chemistry

Once the new mechanism proposal for the photooxidation of thioketones has been described, a logical next step could be to get the sulfine group at synthetic scale as the major photoproduct. Taking into account the aforementioned experimental evidences collected from the previous mechanistic study, the most suitable experimental conditions were protic solvents (methanol) and high substrate concentration. However, both conditions can be considered a drawback in $^1O_2$ chemistry, as $^1O_2$ lifetime in methanol drastically decreases in comparison with other organic solvents, and high thioketone concentration, as it was demonstrated by NMR analysis, due to the slowing down of the kinetics because of the physical quenching of $P(T_1)$. Therefore, the system used in the mechanistic study proved to be not a realistic approach in order to get the sulfine group at synthetic scale with good efficiency.

In order to find a solution to overcome these limitations, it was considered that $^1O_2$ lifetime in gas phase is much longer than in solution, as it was commented in 2.1 section. Moreover, it was known from the proposed mechanism that the stabilization of the charges in peroxythiocarbonyl intermediate **A** (Scheme 27) prevents the evolution to the ketone group and favours high yields of sulfine production. Therefore, the use of an heterogeneous solid/gas system was explored, where the substrate and the photosensitizer were immobilized in a polar solid phase, swirled in a fluidized bed reactor (see Experimental Section), and irradiated with a blue LED lamp (starting from 40 mg of thioketone).

Table 8. Distribution of photoproducts and conversion values for **2b** photooxidation using different solid phases, after 5.5 h of irradiation time.

Solid phase	**3b** / %	**1b** / %	**2b** conversion
Silica	93	7	85
Neutral alumina	70	30	42
Basic alumina	60	40	19

The first tested substrate was **2b**, as the expected photoproducts distribution was simpler to be analysed. Table 8 summarizes **2b** conversion and **3b** and **1b** yields obtained after 5.5 h of irradiation. The solid phases explored were silica, neutral alumina and basic alumina.

From these results, the good selectivity achieved towards **3b** generation using silica, as well as the high conversion rates must be highlighted.

Regarding **2a** photooxidation, the most relevant difference observed in comparison to **2b** was the improved conversion at shorter irradiation times. Although these experiments are not being carried out in solution, the interaction between $^1O_2$ and thioketone moiety seems to behave in the same manner discussed in Figure 49. As it is shown in Table 9, after 5.5 h of irradiation, total conversion was achieved, but worse **3a**/**1a** selectivity than that obtained in **2b** photooxidation was observed. However, trying to optimize the reaction time, it was detected that sulfine **3a** tended to decompose to ketone **1a**, what was evident from NMR analysis of the reaction crudes at different irradiation times (Figure 50).

Table 9. Photoproducts distribution and conversion values for **2a** photooxidation at different times using silica as solid phase.

t / h	**3a** / %	**1a** / %	Conversion / %
0.75	88	12	25
2.5	81	19	100
5.5	70	30	100

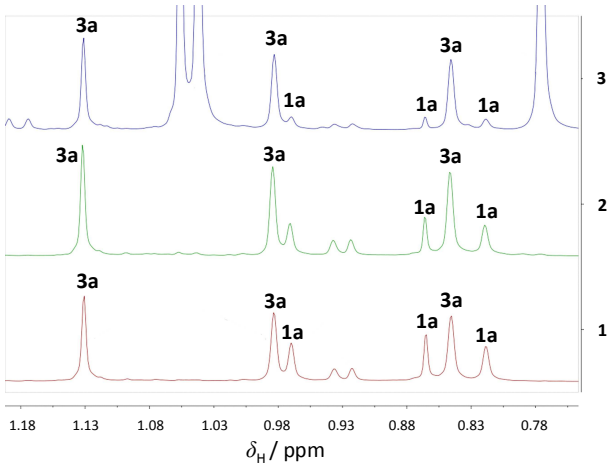

Figure 50. ^{1}H-NMR signals in the methyls region by irradiation of **2a** using silica as the solid phase at different irradiation times. (1) 5.5 h, (2) 2.5 h and (3) 0.75 h.

Photooxidation experiments were performed using different solid phases. The results are summarized in Table 10. Again, the best selectivity for sulfine

generation was observed in silica as the solid phase. Moreover, no signals of other by-products different from ketone and sulfine were detected.

Table 10. Photoproducts distribution and conversion values for **2a** photooxidation using different solid phases and irradiation times.

Solid phase	**3a** / %	**1a** / %	Conversion / % (t / h)
Silica	88	12	25 (0.75)
Neutral alumina	23	77	28 (2)
Basic alumina	40	60	9 (1)

Considering these results, a synthetic alternative for sulfine generation using $^1O_2$ as a reagent in the gas phase has been found. Moreover, it can be considered that this proposal fulfils several of the precepts of Green Chemistry, especially if other synthetic methods described for sulfine synthesis based on thioketone oxidation with less amenable reagents are taken into account (Table 11).[82]

Table 11. Yields of sulfines prepared by different methods of thioketone oxidation.[82]

Oxidizing reagent	Conditions	Sulfine yield
CH_3ReO_3 (cat) / H_2O_2	Room temperature, < 5min	> 90
Perbenzoic acid	Room temperature	80-90
m-chloroperbenzoic acid	0ºC, 30-40 min	50-90
Monoperoxyphthalic acid	0ºC, 30-45 min	38-89
Ozone	-70 to -78 ºC, N_2	0-71
N-sulfonyloxaziridines	0 ºC, N_2, 0.5-1.5 h	70-90

- **Atom economy**. For example, in the synthesis of sulfine group using *m*-chloroperbenzoic acid as oxidant, only one oxygen atom coming from the peracid moiety becomes part of the final product. The remaining structure is a secondary product with no synthetic interest. On the other hand, both oxygen atoms in $^1O_2$ are present in the sulfine molecules generated, which is an example of perfect atom economy (Scheme 28)

[82] R. Huang, J. H. Espenson. *J. Org. Chem.*, **1999**, *64*, 6935.

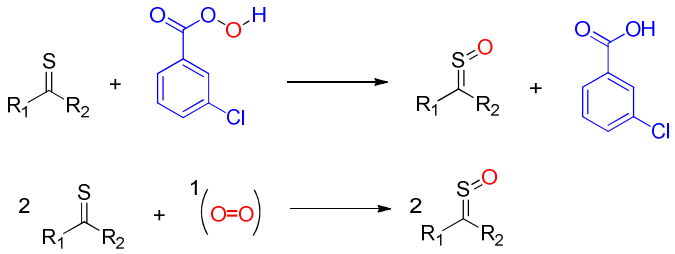

Scheme 28. Comparison of atom economy in sulfine synthesis using *m*-chloroperbenzoic acid and $^1O_2$.

- **Less hazardous chemical synthesis**. Using this approach, hazardous reagents such as H_2O_2 or ozone, and harsh conditions are avoided.
- **Reduced use of solvents**. No reaction solvent is used, and only a small amount is needed for the final workup. Moreover, no waste solutions are generated in L-L extractions.
- **(Photo)Catalysis**. As it was stated in 2.2.2 section, photosensitized production of $^1O_2$ is a photocatalytic process, using, in this case, an efficient source of energy such as blue-LED lamps. Moreover, the photosensitizer remains fixed to the solid phase, so it can be reused in several photooxidation cycles.
- **Improved yields**. Sulfine yields using silica as the solid phase are among the highest when compared with those reported in Table 11.

5.6. Photooxidation of 4-thiouracil

As it was stated in the background section (3.4.2 section), photooxidation of thionucleobases by $^1O_2$ are of interest in biomedical applications. From the mechanism postulated in Scheme 18, based on computational calculations, it is interesting to point out the intramolecular proton transfer from the N atom in α position respect to the thiocarbonyl carbon leading to **4TUOOH**, just in the same manner as intermediate **A** to yield vinylpersulfenic acid **4a** (Scheme 27). In the case of 4-thiouracyl, this process could be thermally favoured by the conjugation of two double bonds in **4TUOOH**. However, in these computational

proposals, sulfine is never considered as a likely photoproduct. In order to prove if the postulated mechanism in Scheme 27 could be applied to the photooxidation of 4-thiouracil (**6**) by $^1O_2$, preliminary experiments were done in order to elucidate the structure of the photoproducts. For this aim, **6** was synthesized from the correspondent ketone **5** (uracil). Irradiation of **6** in presence of $Ru(dip)_3Cl_2$ in CD_3OD afforded ketone **5** as the only photoproduct. However, when this irradiation was done in CD_3OD as solvent, it was clearly seen the generation of two products: ketone **5** as the minor product, and a second compound as the major one. Interestingly, when the irradiated solution was kept in the dark and analysed after several days, it was found that this second compound decomposed thermally to the ketone **5** (Figure 51), while **6** remained constant.

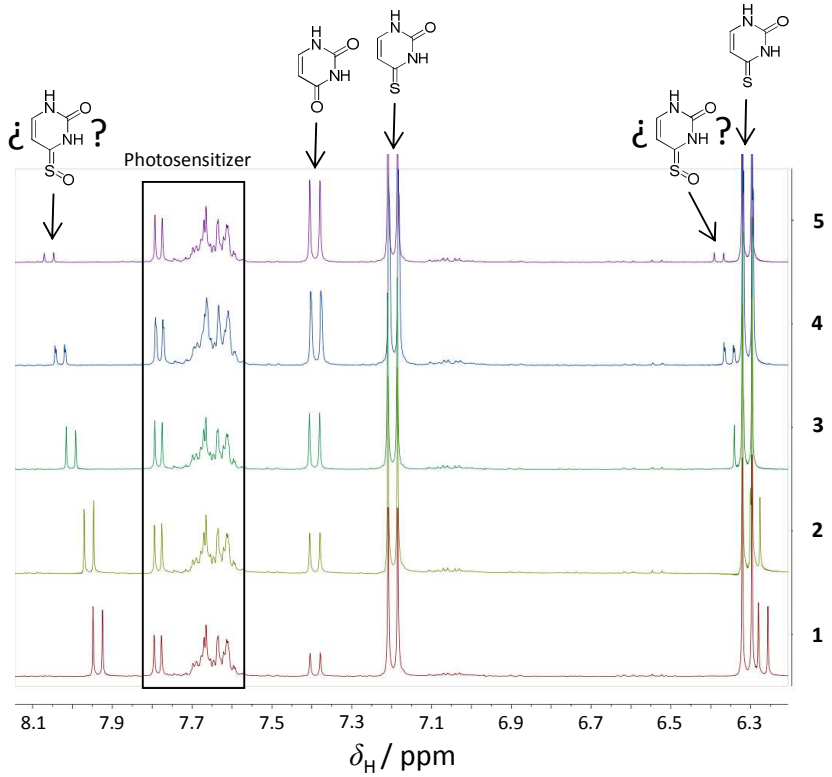

Figure 51. Temporal evolution in the dark for the reaction crude of 4-thiouracil photooxidation after 5 h of irradiation (1: 0 days, 2: 2 days, 3: 5 days, 4: 8 days, 5: 12 days).

This second compound could be tentatively assigned to the sulfine group based on three evidences. Firstly, from a mechanistic point of view, it is quite remarkable that formation of products can be compared to that observed in the photooxidation experiments with **2a** and **2b**, where aprotic solvents yield the ketone as the major photoproduct and protic solvents enhance the generation of sulfine group. Secondly, it is well known that sulfines can decompose to the corresponding ketone (for instance, it was observed in Figure 50). Thirdly, the proton at 8.0 ppm is structurally equivalent to that at 7.4 ppm in **5** and 7.2 ppm in **6**. The reason for this strong deshielding effect could be found in the resonant forms for the sulfine derivative (Scheme 29), particularly in the one shown in red, where the positive charge is delocalized in the carbon adjacent to the alkenic proton.

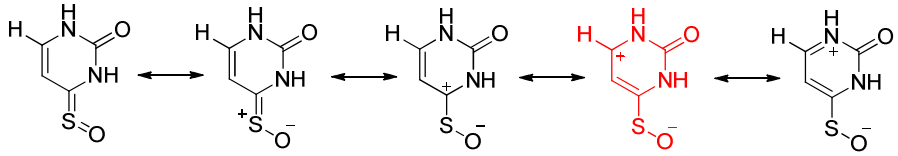

Scheme 29. Resonant forms for the sulfine derivative of 4-thiouracil.

Nevertheless, the complexity of the mechanism computationally postulated in Scheme 18 was not observed in this experimental assay. Certainly, **4TUOOH** could be assigned to this second compound produced in methanol, as it evolves to the ketone according to the mechanism depicted in Scheme 18. But the same should be observed in CD_3CN, where only the ketone is detected. Moreover, the decomposition of the second compound only yields the keto group, and not a second product, as it could be expected from the mechanism postulated in Scheme18.

CHAPTER 1

EXPERIMENTAL SECTION

6. CHAPTER 1 EXPERIMENTAL SECTION

6.1. General Methods

-Thin layer chromatography: Reactions were monitored by thin-layer chromatography carried out on 0.2 mm TLC-aluminum sheets of silica gel (Merck, TLC Silica gel 60 F_{254}).

-Purification of Reaction Mixtures: Flash column chromatography was performed using silica gel (Merck, 230-400 mesh).

-Photooxidation experiments: Photosensitized oxidation of thioketones was carried out in quartz cells (10 mm optical path length) and standard NMR tubes (5 mm outer diameter) in the presence of $[Ru(dip)_3]Cl_2$ photosensitizer. The photooxidation process was monitored at different time intervals by UV–vis spectrophotometry, ^{1}H- and ^{13}C-Nuclear Magnetic Resonance spectroscopy, and Gas Chromatography-Mass Spectrometry, using the experimental setup shown in 5.2 section. The volumes of the irradiated solutions (containing thioketone substrate, photosensitizer, and the corresponding solvent) were 3 and 0.6 mL for the quartz cells and NMR tubes, respectively.

For the photooxidation experiments carried out with the substrate immobilized in solid phases, 40 mg of thioketone, 3.5 mg of $Ru(dip)_3Cl_2$ and 250 mg of solid phase (silica, neutral and basic alumina. Panreac) where dissolved in CH_2Cl_2. After evaporation of the solvent, the solid mixture was irradiated using the experimental setup shown in 5.2 section.

-UV-Vis Spectrophotometry: Spectra were recorded using quartz cells (Hellma 114-QS 10 mm optical path length and Hellma 110-QS 1 mm optical path length) and a Cary 50 Conc UV-Vis spectrophotometer.

-Nuclear Magnetic Resonance Spectroscopy: ^{1}H-NMR and ^{13}C-NMR spectra were recorded on a BRUKER DPV-300MHz, BRUKER AV-500MHz or BRUKER AVIII-700MHz using deuterated solvents as reference. Coupling constants (J) are reported in Hz and the chemical shifts (δ) in ppm. Spectra were referenced to solvent signals at $\delta_{H/C}$ 1.94/1.39 and 118.3 ppm (acetonitrile-d_3) or 3.31/49.15 ppm (methanol-d_4) relative to tetramethylsilane as the internal standard at room temperature. Spin multiplicities are reported as a singlet (s), broad singlet (br s), doublet (d), triplet (t) quartet (q) and multiplet (m).

-Gas Chromatography-Mass Spectrometry analysis of reaction crudes*:* Gas chromatograms were recorded using an Agilent 6890N Network GC System chromatograph coupled to an Agilent 5973 MSD mass detector, and a DB5-MS (30 m × 0.25 mm × 0.25 μm) column. In general, 1 μL of the irradiated reaction crude was injected using helium as carrier gas (injector temperature: 220 ºC; oven temperature: 70 ºC, 2.5 ºC min^{-1}, 300 ºC; interface temperature: 150 ºC; ion source: 230 ºC; electron energy: 70 eV)

-Solvents: The solvents used were dried following the usual methods.[83] Otherwise, HPLC grade solvents were used.

[83] D. D. Perrin, I. F. Armarego, D. R. Perrin, *Purification of Laboratory Chemicals*, Pergamon Press, Oxford, **1980**.

6.2. Experimental setup for the photooxidation experiments

A LED lamp (GU10 blue LED 240 V, 1.8 W T/C; λ_{em}^{max} = 463.5 nm, FWHM = 22 nm, emission spectrum shown in Figure 52) was used to illuminate either a quartz cell (10.00 mm optical length) or a standard NMR tube placed 5 cm away from the LED lamp. Homogenization of the illuminated solutions and equilibration with air was achieved with a 3 mm × 1 mm magnetic bar and a magnetic stirrer placed below the irradiated vessels (Figure 53). Air equilibration was assured during the experiments by periodically removing the caps of the quartz cells and NMR tubes. Reproducibility of the illumination geometry was possible with a piece of graph paper on top of the magnetic stirrer and an appropriate holder for the NMR tube (Figure 54). The illumination system was mounted inside a rigid box equipped with a sliding cover. The interior of the setup was lined with pieces of black card. Temperature during the irradiation experiments was 21 ± 2 °C.

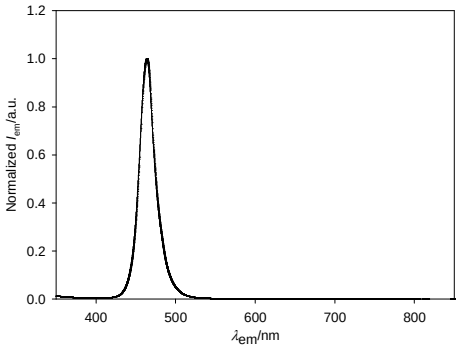

Figure 52. Normalized emission spectrum for blue LED lamp.

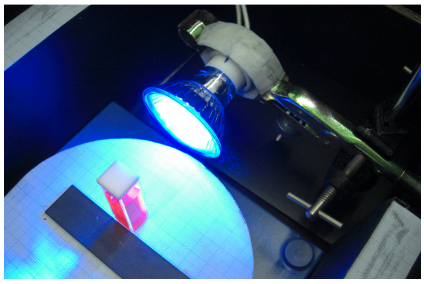

Figure 53. Spatial distribution of lamp and quartz cell for monitorization.

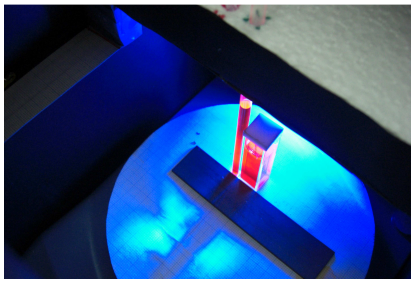

Figure 54. Combined irradiation of quartz cell and NMR tube using the holder

Regarding the experimental setup for the experiments carried out using solid phases, two sintered glass filters (Pore 3, 2 cm ∅) were coupled. The stem corresponding to the lower filter was introduced in a vortex in order to shake the solid phase. The LED lamp was placed in the external wall of the filter (Figure 53).

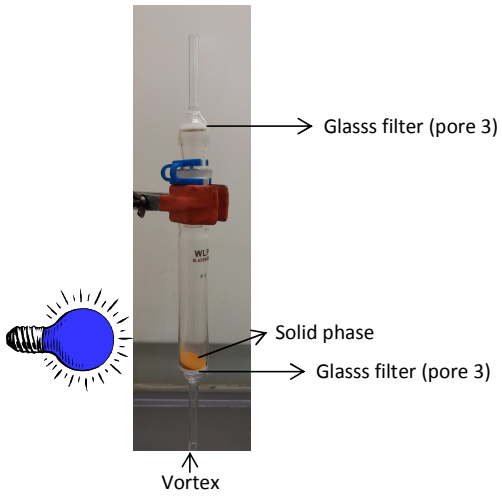

Figure 55. Experimental setup for the solid state irradiations.

6.3. Chemical actinometry

In order to determine the amount of photons absorbed by the specific geometries of the irradiated systems, the following procedure was carried out:[84] Six samples of 3 mL (V_1) each were prepared, under red light, from a 0.15 M stock solution of potassium ferrioxalate in H_2SO_4 0.05 M. Each sample was added, under red light, to a 10 mm quartz cell containing a 3 mm × 1 mm magnetic bar. The quartz cell was placed, under red light, inside the box used for the irradiation experiments and care was taken to ensure reproducibility of the relative geometry with respect to the blue LED lamp. The samples were exposed to blue light for 5, 10, 30, 60, 90, and 120 s, respectively. Conversions of Fe(III) to Fe(II) were always below 5% for all the irradiation times used. A blank sample was also prepared under red light with 0.1 mL of the aforementioned stock solution in a glass vial, which was kept in the dark. A buffered solution of 1,10-phenanthroline 0.1% (w/v) was prepared in a 25 mL volumetric flask with 0.0250 g of 1,10-phenanthroline, 3.3944 g of sodium acetate, and H_2SO_4 0.5 M. 0.1 mL (V_2) of each irradiated solution were added to a vial. One mL of distilled and deionized water and 0.5 mL of 1,10-phenanthroline buffered solution were added to the vials containing each irradiated sample and also to the vial with the blank sample, for a total volume of 1.6 mL (V_3) in each vial. These solutions were stirred and kept in the dark for 1 h to allow quantitative formation of the tris(1,10-phenanthroline)iron(II) complex. Absorbance of each solution (irradiated and dark control) at 510 nm was measured (triplicates) in quartz cells of 1 mm optical path length in order to determine the amount of Fe(II) formed as a result of the radiation absorbed by the illuminated system. The same procedure was used for the standard NMR tube geometry, except V_1 = 0.6 mL and the irradiation times were 30, 45, 60, 75 and 90 s.

Calibration graphs corresponding to the NMR experiments and the UV-vis experiments are shown in Figures 54 and 55, respectively. *S* represents the slope of the calibration plot.

[84] a) H. J. Kuhn, S. E. Braslavsky, R. Schmidt. *Pure Appl. Chem.*, **2004**, *76*, 2105. b) M. Montalti, A. Credi, L. Prodi, M. T. Gandolfi. Handbook of Photochemistry, 3rd ed.; CRC Press: Boca Raton, FL, pp. 601−616, **2006**.

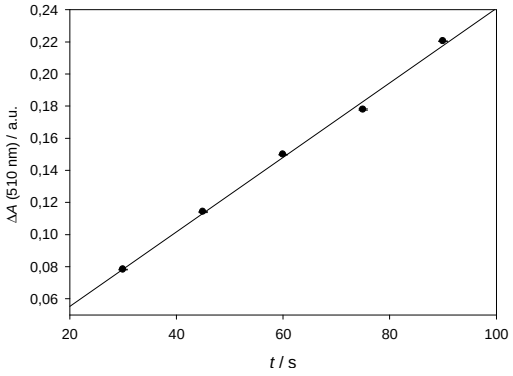

$S = (1.65 \pm 0.03) \cdot 10^{-3}\ s^{-1}$
intercept = $(0.2 \pm 0.2) \cdot 10^{-2}$
r = 0.999

Figure 56. Calibration graph of the chemical actinometry experiment (NMR tube).

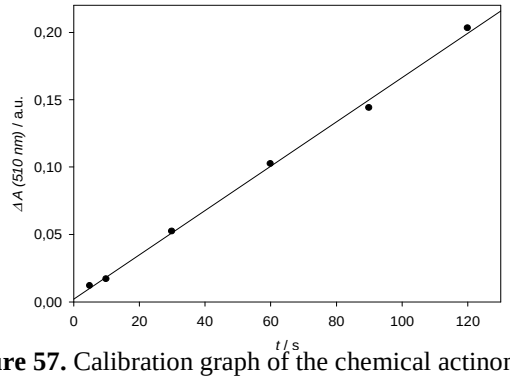

$S = (2.32 \pm 0.07) \cdot 10^{-3}\ s^{-1}$
intercept = $(0.9 \pm 0.4) \cdot 10^{-2}$
r = 0.999

Figure 57. Calibration graph of the chemical actinometry experiment (Quartz cell).

Taking into account the amount of iron(II) liberated from potassium ferrioxalate photodegradation, [35], the amount of incident photons, q_p, is calculated with equation [36].

$$mol\ Fe^{2+} = \frac{V_1 V_3\, \Delta A(510nm)}{10^3 V_2\, l\, \varepsilon(510nm)} \quad [35]$$

$$q_P = \frac{N\, h\nu}{t} = \frac{mol\ Fe^{2+}}{\Phi_\lambda\, t\, F} = \frac{V_1 V_3\, S}{10^3 V_2\, l\, \varepsilon(510nm)\, \Phi_\lambda\ F} \quad [36]$$

In equation [36], S represents the slope from the calibration plot shown in Figures 54 and 55, Φ_λ, the quantum yield of Fe(II) release. The reported quantum yield of this process is 1.2 for wavelengths shorter than 410 nm,

progressively decreasing for longer wavelengths. As the blue LED lamp emits between 420 and 530 nm, a series of Φ_λ has been considered for wavelength intervals in this range, according to the values shown in Table 12. *F* factor represents the portion of photons absorbed by the irradiated potassium ferrioxalate solution, as it is stated in [37].

$$F = 1 - 10^{-A} \quad [37]$$

Where *A* is the absorbance for each wavelength. As a result, equation [36] can be expressed as [38].

$$q_P = \sum_{\lambda=420}^{530} \frac{V_1 V_3 S}{10^3 V_2 l \varepsilon(510nm) \Phi_\lambda F_\lambda} \quad [38]$$

Table 12. Φ_λ values for the blue LED emission range.

λ / nm	Φ_λ
420-440	1.11
440-460	1.00
460-500	0.92
500-510	0.86
510-520	0.65
520-530	0.53

Table 13, summarizes the amount of incident photons (q_p), the amount of incident photons per unit of area ($q_p(A)$) and the incident power (*P*)

Table 13. q_p, $q_p(A)$ and *P* values for the quartz cell and the NMR tube.

Geometry	q_p / einstein s^{-1}	q_p(A) / einstein s^{-1} cm^{-2}	*P* / mW
Quartz cell	$(1.34 \pm 0.04) \cdot 10^{-7}$	$(0.45 \pm 0.02) \cdot 10^{-8}$	34 ± 1
NMR tube	$(1.11 \pm 0.04) \cdot 10^{-7}$	$(0.38 \pm 0.01) \cdot 10^{-8}$	28 ± 1

6.4. Synthesis

General procedure for the synthesis of thioketones

Commercial ketones (20 mmol) were dissolved in 15 mL of dry toluene. Lawesson's reagent (4.04 g, 10 mmol) was added and the mixture was refluxed for 7 h. Thereafter, solvents were removed under reduced pressure and the reaction crude was purified by column chromatography using hexane as eluent.

(1*R*)-Thiocamphor (2a)

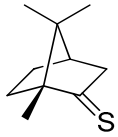

2a

Following the general procedure, compound **2a** was obtained as an orange solid (75% yield).

^{1}H-NMR (CD_3CN, 300 MHz) δ / ppm: 2.81 (dm, *J* = 21 Hz, 1H), 2.44 (d, *J* = 21 Hz, 1H), 2.22 (t, *J* = 4.2 Hz, 1H), 2.10-2.00 (m, 1H), 1.89-1.79 (m, 1H), 1.47-1.38 (m, 1H), 1.30-1.21 (m, 1H), 1.10 (s, 3H), 1.08 (s, 3H), 0.72 (s, 3H).

^{13}C-NMR (CD_3CN, 75 MHz) δ / ppm: 274.1, 69.6, 55.7, 49.1, 45.4, 34.2, 27.1, 19.4, 19.3, 13.0.

UV-vis (CH_3CN) λ_{abs}^{max} / nm (ε/ $M^{-1}cm^{-1}$ (±7%)): 479 (12), 247 (8750), 214 (3030).

UV-vis (MeOH) λ_{abs}^{max} / nm (ε/ $M^{-1}cm^{-1}$ (±7%)): 480 (11), 247 (9320), 214 (3960).

(1*R*)-Thiofenchone (2b)

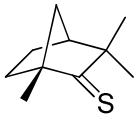

2b

Following the general procedure, compound **2b** was obtained as an orange oil (80% yield).

^{1}H-NMR (CD_3CN, 300 MHz) δ / ppm: 2.33 (s, 1H), 1.87 (d, J = 9.9 Hz), 1.80-1.63 (m, 4H), 1.28 (s, 3H), 1.24-1.18 (m, 1H), 1.16 (s, 3H), 1.12 (s, 3H).

^{13}C-NMR (CD_3CN 75 MHz) δ / ppm: 280.3, 67.3, 58.7, 47.8, 44.2, 36.3, 29.0, 26.8, 25.6, 19.5.

UV-vis (CH_3CN) λ_{abs}^{max} / nm (ε/ $M^{-1}cm^{-1}$ (±7%)): 477 (12), 244 (8915), 218 (sh, 4160).

UV-vis (MeOH) λ_{abs}^{max} / nm (ε/ $M^{-1}cm^{-1}$ (±7%)): 477 (11), 244 (8640), 218 (sh, 3380).

General procedure for the synthesis of thioketone sulfines

To a solution of the thioketone (1.90 mmol) in 15 mL of CH_2Cl_2 at 0 ºC, 1.55 mmol of *m*-chloroperbenzoic acid dissolved in 15 mL of CH_2Cl_2 were added dropwise. The reaction mixture was vigorously stirred for 60 minutes. Thereafter, the reaction mixture was allowed to reach room temperature and the reaction crude was washed with Na_2SO_3 10% (w/v) (2 × 30 mL), saturated Na_2CO_3 (2 × 30 mL) and water (2 × 20 mL). The organic layer was dried over anhydrous $MgSO_4$ and filtered. The solvent was removed at low pressure and the reaction crude was purified by column chromatography using hexane:AcOEt (9:1, v/v) as eluent.

(1*R*)-Thiocamphor sulfine (3a)

Following the general procedure, compound **3a** was obtained as a pale yellow solid (72% yield).

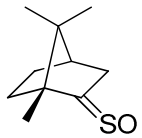

3a

^{1}H-NMR (CD_3CN 300 MHz) δ / ppm: 2.95 (dm, *J* = 21 Hz, 1H), 2.46 (d, *J* = 21 Hz, 1H), 2.04 (t, *J* = 4.2 Hz, 1H), 1.92-1.82 (m, 2H), 1.54-1.39 (m, 2H), 1.10 (s, 3H), 0.95 (s, 3H), 0.83 (s, 3H).

^{13}C-NMR (CD_3CN 300 MHz) δ / ppm: 210.2, 56.1, 50.1, 44.3, 38.1, 35.5, 26.9, 19.2, 18.2, 12.0.

UV-vis (MeOH) λ_{abs}^{max} / nm (ε/ $M^{-1}cm^{-1}$ (±7%)): 269 (7750).

(1*R*)-Thiofenchone sulfine (3b)

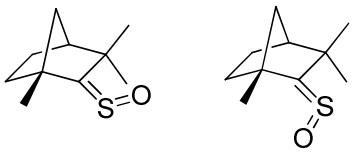

Z isomer *E* isomer

3b

Following the general procedure, compound **3b** (a 4:1 mixture of *Z* and *E* diastereoisomers) was obtained as an oil (46% yield).

^{1}H-NMR (CD_3CN 300 MHz) δ / ppm: (*Z* diastereoisomer) 1.54 (s, 3H), 1.51 (s, 3H), 1.37 (s, 3H). (*E* diastereoisomer) 1.80 (s, 3H), 1.36 (s, 3H), 1.35 (s, 3H).

^{13}C-NMR (CD_3CN 75 MHz) δ / ppm: (*Z* diastereoisomer) 218.0 (C, C=S=O), 55.4 (C), 52.8 (C), 50.1 (CH), 45.3 (CH_2), 38.0 (CH_2), 26.0 (CH_2), 24.2 (CH_3), 23.0 (CH_3), 18.1 (CH_3). (*E* diastereoisomer) 215.1 (C, C=S=O), 60.9 (C), 50.3 (CH), 49.7 (C), 46.5 (CH_2), 37.0 (CH_2), 31.2 (CH_3), 27.8 (CH_3), 25.5 (CH_2), 19.2 (CH_3).

UV-vis (MeOH) λ_{abs}^{max} / nm (ε/ $M^{-1}cm^{-1}$ (±7%)): 270 (7800).

4-Thiouracil (6)

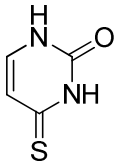

6

To a suspension of 1.12 g (10 mmol) of uracil in 10 mL of hexamethylphosphoramide, 2.22 g (5.5 mmol) of Lawesson's reagent were added. The mixture was heated to 120 ºC for 1 h under Ar atmosphere. After reaching room temperature, 100 mL of hot water and 200 mg of charcoal were added and boiled to remove soluble impurities. The reaction crude was filtered, and the filtrate was cooled in order to favour precipitation of **6**. The product was collected by filtration and washed with water. **6** was obtained as a yellow solid (yield 60%).

^{1}H-NMR (DMSO-d_6 300 MHz) δ / ppm: 11.9 (br s, 2H), 7.33 (d, *J* = 7.2 Hz, 1H), 6.16 (d, *J* = 7.2 Hz, 1H).

^{13}C-NMR (DMSO-d_6 300 MHz) δ / ppm: 191.4, 148.7, 138.6, 111.6.

CHAPTER 2

CHAPTER 2

BACKGROUND

7. CHAPTER 2 BACKGROUND

7.1. Introduction to Photodynamic Therapy

Photodynamic therapy (PDT) is a therapeutic modality where the photosensitized generation of $^1O_2$ using UV, visible or infrared irradiation serves to induce a photooxidative damage on cells or microorganisms in the surroundings of the photosensitizer.[85] Since 1904, when this concept was first established,[86] the potential of this therapy has been explored mainly for cancer treatments and, to a minor extent, to fight infections due to pathogenic agents. In both cases, the overall process could by described as follows (Figure 58).

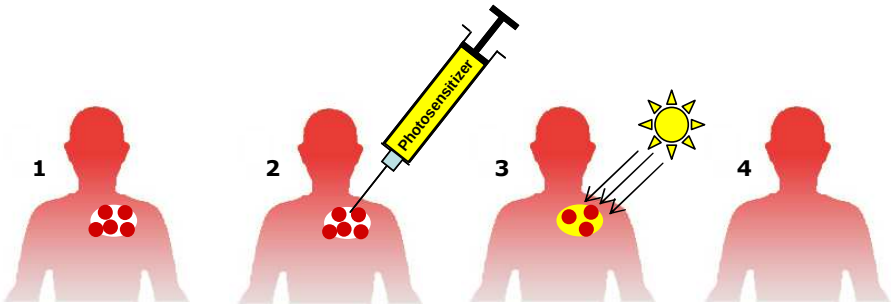

Figure 58. Steps of a typical PDT assay.

Firstly, to a patient showing a particular disease (**1** in Figure 58), the photosensitizer is administered (orally, topically, or intravenously, **2** in Figure 58). Thereafter, there is a delay time to allow the selective binding of the photosensitizer to the tumour cells or the microorganisms. Subsequently, the tumour or the region infected by the microorganism is irradiated directly by a light source with the desired wavelength (**3** in Figure 58). The generation of $^1O_2$ leads to irreparable photooxidative damage of malignant cells/microorganisms and, ideally, to the recovery of the patient (**4** in Figure 58).[87]

[85] S. E. Braslavsky. *Pure Appl. Chem.*, **2007**, *79*, 293.
[86] H. von Tappeiner, A. Jodlbauer. *Dtsch. Arch. Klin. Med.*, **1904**, *80*, 427.
[87] P. Agostinis, K. Berg, K. A. Cengel,T. H. Foster, A. W. Girotti, S. O. Gollnick, S. M. Hahn, M. R. Hamblin, A. Juzeniene, D. Kessel, M. Korbelik, J. Moan, P. Mroz, D. Nowis, J. Piette, B. C. Wilson, J. Golab. *CA-Cancer J. Clin.*, **2011**, *61*, 250.

7.2. Photodynamic Therapy and Chemical reactivity

The $^1O_2$ reactivity outlined in the background of Chapter 1 constitutes the basis for understanding how $^1O_2$ is able to induce a photooxidative damage on cells or bacteria. This damage depends on the especific location of the photosensitizer within particular cellular compartments, as a consequence of the lower lifetimes of $^1O_2$ in biological media and the limited diffusion of $^1O_2$ from the place where it is generated.[88] The most relevant molecular targets of $^1O_2$ are proteins, followed by ascorbate and nucleic acids and, to a considerable less extent, lipids[88] (taking into account the reported rate constants for reaction of $^1O_2$ with such substrates and their relative abundance in cells). All these biological structures present functional groups which can be oxidized by $^1O_2$.

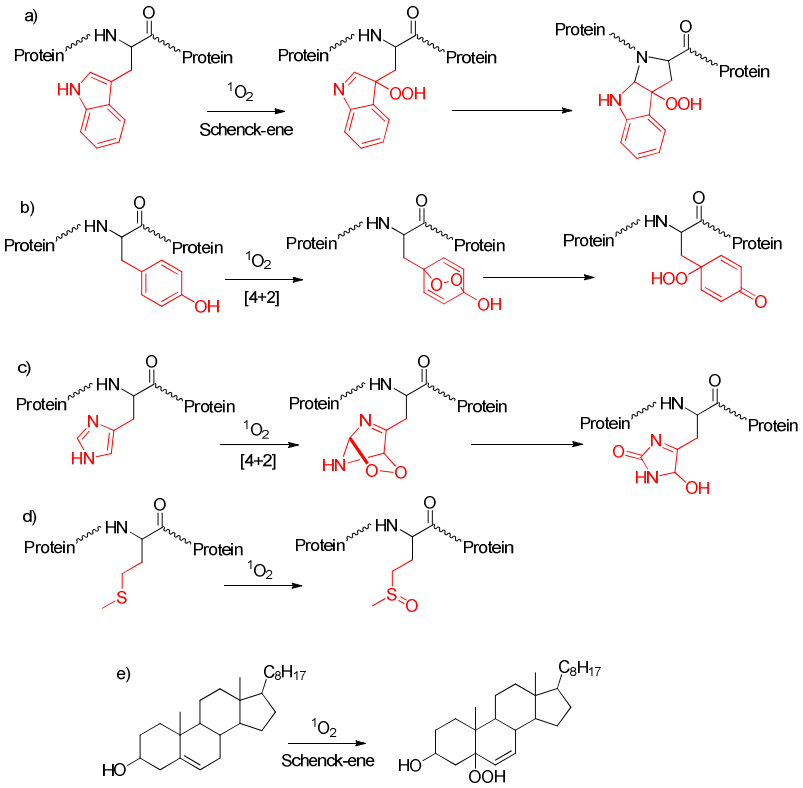

Figure 59. Reactivity of $^1O_2$ with aminoacids: tryptophan (a), tyrosine (b), histidine (c) and methionine (d), as well as membrane lipid derivatives such as cholesterol (e).

[88] M. J. Davies. *Biochem. Biophys. Res. Commun*., **2003**, *305*, 761.

Figure 59 summarizes the known reactions of $^1O_2$ with the membrane cell components: proteins and lipids.[89] Among the aminoacids, the most reactive are tryptophan, tyrosine, histidine and methionine. The rate constants for chemical reaction of $^1O_2$ with the side-chains of other amino acids vary dramatically, resulting in selective damage to particular residues. Although it has not been depicted in Figure 59, cysteine reacts rapidly with $^1O_2$, leading to the corresponding disulfide (cystine) and other photoproducts whose structure is still unknown (but cysteic acid, RSO_3H, and RSS(=O)R are likely products).[90]

Regarding nucleic acids, $^1O_2$ can lead to DNA damage by oxidation of any of the four nucleobases. However, the interaction with guanosine residues in DNA or oligonucleotides (*dGuo* in Figure 60) is especially favoured, due to its lower redox potential. The [4+2] cycloadduct produced can evolve by two parallel pathways leading to *4-OH-8-oxodGuo* or *8-oxodGuo*, which can be oxidized by singlet oxygen to the *5-OH-8-oxodGuo* derivative (the oxidation of *8-oxodGuo* is reported to be even easier than that corresponding to *dGuo*).[91]

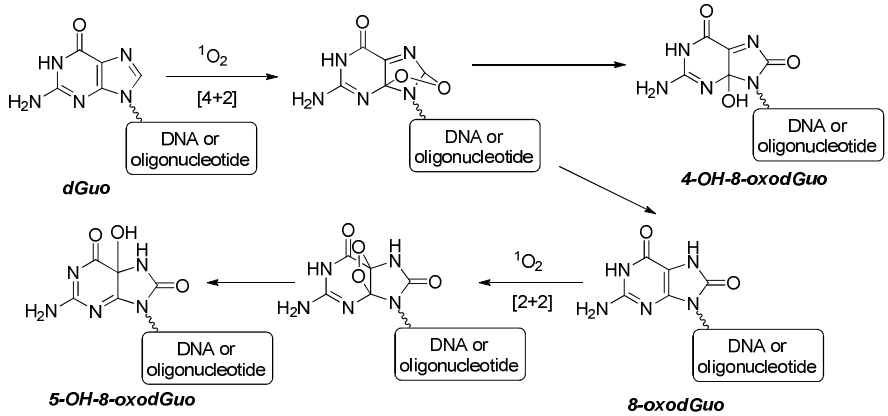

Figure 60. Reactivity of $^1O_2$ with guanosine derivative (*dGuo*).

[89] K. Suwa, T. Kimura, P. Schaap. *Photochem. Photobiol*., **1978**, *28*, 469.
[90] M. Rougee, R. V. Bensasson, E. J. Land, R. Pariente. *Photochem. Photobiol*., **1988**, *47*, 485.
[91] a) J. Cadet, R. Teoule. *Photochem. Photobiol*., **1978**, 28, 661. b) S. Steenken, S.V. Jovanovic. *J. Am. Chem. Soc*., **1997**, *119*, 617. c) J. L. Ravanat, G. Remaud, J. Cadet. *Arch. Biochem. Biophys*., **2000**, *374*, 118.

7.3. Photodynamic Therapy and Biological response

One of the key points for PDT effectiveness is the intracellular distribution of the photosensitizer. This distribution depends on its structural characteristics: net ionic charge, the presence of hydrophobic groups and the degree of asymmetry of the molecule. In general, photosensitizers which are hydrophobic and have two negative charges or less can diffuse across the plasma membrane, and then relocate to other intracellular membranes (mitochondria, lysosomes, Golgi apparatus and nucleus). On the contrary, those photosensitizers which are less hydrophobic and have >2 negative charges tend to be too polar to diffuse across the plasma membrane, and could be internalized by endocytosis.[92]

Cells can response to photooxidative damage by initiating a rescue or a mechanism leading to cell death. The mechanisms for cell killing are generally classified as apoptosis or necrosis. Mitochondrial localized photosensitizers are able to induce apoptosis very rapidly. Regarding lysosomal localized photosensitizers, they can cause either a necrotic or an apoptotic response. Finally, in the plasma membrane, a target for various photosensitizers, rescue responses, apoptosis and necrosis can be initiated.[93]

Rescue response of cells to sublethal physical or chemical stress generally involve changes in gene and protein expression. These changes allow the cells to endure the damage induced by the stress.

Apoptosis is a normal physiological process which is used by the organism for tissue homeostasis and that can be controlled or induced by both intracellular and extracellular signals.[94] In the case of PDT, after photooxidative damage, signalling pathways from the place where the damage has been induced are initiated, leading to a series of common pathways where hydrolytic enzymes (mainly proteases and nucleases) are activated for the final cell killing (Figure 61). Concretely, in the case of photosensitizers located on the mitochondria, a decrease in the membrane potential leads to an increment in the permeability of the membrane,[95] so pro-apoptotic factors such as cytochrome c are released,[96]

---

[92] A. P. Castano, T. N. Demidova, M. R. Hamblin. *Photodiagnosis Photodyn. Ther.*, **2004**, 1, 279.
[93] A. C. E. Moor. *J. Photochem. Photobiol. B*, **2000**, 57, 1.
[94] N. L. Oleinick, R. L. Morris, I. Belichenko. *Photochem. Photobiol. Sci.*, **2002**, *1*, 1.
[95] C. Salet, G. Moreno, F. Ricchelli, P. Bernardi. *J. Biol. Chem.*, **1997**, *272*, 21938.

activating a series of caspases (caspase-9, -3, -6, -7 y 8. Caspase 3 is the most relevant one, as it is related with the activation of other caspases).[97] Effector caspases are responsible for cleaving and inactivating proteins that protect cells from apoptosis (for instance, nuclear lamins leading to nuclear breakdown).[98] In the case of photosensitizers located on the plasma membrane, PDT stress can activate surface death receptors FAS and TNFR, and a subsequent activation of caspases-8 and -3, joining the route coming from the mitochondria. However, caspase-8 is able to cleave Bcl-2,[99] a protein found in the outer membrane of mitochondria, as well as in the endoplasmic reticulum and the nuclear envelope, leading to cytochrome c release. Finally, photoactivation of photosensitizers bound to the lysosome can cause the release of cathepsins, which can activate again caspase-3.

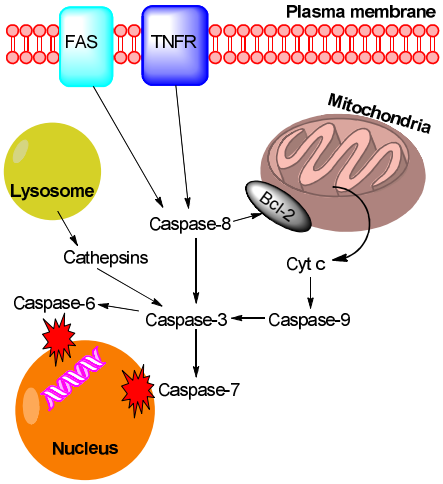

Figure 61. Signalling pathways leading to apoptosis activated during PDT assays by photosensitizers located on different intra and extracellular compartments.

---

[96] a) D. J. Granville, C. M. Carthy, H. Jiang, G. C. Shore, B. M. McManus, D. W. Hunt. *FEBS Lett.*, 1998, *437*, 5. b) M. E. Varnes, S. M. Chiu, L. Y. Xue, N. L. Oleinick. *Biochem. Biophys. Res. Commun.*, **1999**, *255*, 673. c) D. Kessel, Y. Luo. *Cell Death Differ.*, **1999**, *6*, 28.

[97] a) N. A. Thornberry, Y. Lazebnik. *Science*. **1998**, *281*, 1312. b) G. Nunez, M. A. Benedict, Y. Hu, N. Inohara. *Oncogene*, **1998**, 17, 3237.

[98] A. G. Porter, R. U. Janicke. *Cell Death Differ.*, **1999**, *6*, 99.

[99] S. Krajewski, S. Tanaka, S. Takayama, M. J. Schibler, W. Fenton, J.C. Reed. *Cancer Res.*, **1993**, *53*, 4701.

7.4. Photodynamic Therapy against cancer

The first photosensitizer approved by the Food and Drug Administration (FDA) in the United States for PDT treatment had to wait to 1990s, and it is possible to say that, even now, PDT remains underutilized clinically. One of the reasons which could explain this situation is the number of variables that must be optimized: type and dose of photosensitizer, delay time between the administration of the photosensitizer and light exposure, total light dose, fluence rate and, what is more important, the selective binding of the photosensitizer to the tumour cells. Most of the efforts done in PDT research have been focused on the synthesis of new photosensitizers with optimal characteristics for its use in biological media.[100] This is a challenging topic, as biological photosensitizers must show several characteristics in addition to those presented in section 2.4:

- Low or none dark toxicity in order to minimize side effects.
- Selective accumulation in tumour tissue, in order to minimize skin sensitivity to sunlight exposure and avoid damage to normal tissues during irradiation.
- *In vivo* stability depending on the length of the clinical procedure. Fast accumulation and release is desired for treatments in the same day, but a long residence should be achieved in prolonged therapies with several sessions, without the need of multiple infusions of the photosensitizer.
- High absorption in the red and infrared region of the spectrum, in order to take advantage of the higher penetration in tissues of light with longer wavelengths.

[100] R. R. Alison, C. H. Sibata. *Photodiagnosis Photodyn. Ther*., **2010**, *7*, 61.

Table 14. Approved photosensitizers for anticancer PDT, divided by structural families and specifying their clinical applications.

Structural family	Common use name	Trade name	Potential indication	λ_{abs}
Hematoporphyrin	Porfimer sodium	Photofrin Photogem	Cervical, gastric, lung cancer	630
Protoporphyrin prodrugs	δ-aminolevulinic acid HCl	Levulan	AK, BCC, oesopagheal dysplasia	417
	5-aminolevulinate	Metvixia	BCC, AK and Bowen's disease	630
	Hexamino-levulinate HCl	Cysviex or Hexvix	Colon and bladder diagnosis Cervical intraepithelial neoplasia (Phase II)	360-450
Chlorins	Meta-tetra(hydroxyphenyl) chlorin	Foscan	Head an neck cancer SCC Prostate and pancreatic cancer	652
	Talaporfin sodium, *N*-aspartyl chlorin e6	Aptocine, Laserphyrin or Litx	Lung cancer Glioma	660-664
	Chlorin e6	Photolon	BCC and SCC Oesophagus, vulva, breast, cervix and oral cancers	660-670
Porphycenes	9-Acetoxy-2,7,12,17-tetrakis-(β-methoxyethyl)	ATMPn	Psoriasis, Non melanoma skin cancer Head and neck cancers	610-650
Phthalocyanines	Mixture of chloroaluminium sulphonic phthalocyanines	Photosens	Stomach, lung, skin, lips, oesophagus, oral cavity, tongue and breast cancers, AMD	675
Psoralens	8-Methoxypsoralen,	Uvadex	Cutaneous T-cell lymphoma	320-400

Approved photosensitizers for clinical applications are reported in Table 14 (where AK means Actinic Keratosis, BCC, Basal Cell Carcinoma, SCC,

Squamous Cell Carcinoma and AMD, Age-related Macular Degeneration).[101] These compounds have been classified in this Table attending to structural characteristics of the chromophore, although it is interesting to consider the different chronological generations[102] depending on their selectivity towards tumour cells and absorption properties.

Photofrin™, the first approved photosensitizer (first generation) is characterized by its low ability to be excreted (inducing prolonged patient photosensitivity) and low long wavelength absorption. In addition, the initial selectivity between tumour tissue and healthy one can be also low, as well as long delay times of 48-72 h between administration and irradiation.[103] These drawbacks encouraged the researchers to find a new generation of photosensitizers with improved properties, especially in longer wavelength absorption regions. Most of the second generation photosensitizers are based on modified tetrapyrrolic (porphyrin) structure, such as chlorins (Foscan™), porphycenes (ATMPn), phthalocyanines (Photosens™), benzoporphyrin (Visudyne™ and Verteporfin™), naphthalocyanines, protoporphyrin IX and δ-aminolevulinic acid (Levulan™, which is a precursor in the heme biosynthetic pathway).[104] However, some of these photosensitizers, as Foscan™, are still associated with pronounced skin photosensitivity and can show little initial selectivity. Foscan™ also needs to be administered 96 h before irradiation. On the contrary, in spite of being designed for ophthalmological purposes in the treatment of macular degeneration and not for cancer, Verteporfin™ represents a good example of photosensitizer which is effective, cleared rapidly, without inducing skin photosensitivity beyond 24 h and delay times no longer than 15 min. In this sense, targeting strategies in order to increase the affinity of the photosensitizer for tumour tissue is currently the most important topic in the new design of photosensitizers (third generation).

For this aim, it has to be taken into account that tumours can be differentiated from healthy tissue in different ways as a result of disease progression and/or

[101] B. Rodríguez-Amigo, O. Planas, R. Bresolí-Obach, J. Torra, R. Ruíz-González, S. Nonell. Photodynamic Medicine. From Bench to Clinic. RSC: Cambridge. p. 27, 2016.
[102] L. B. Josefsen, R. W. Boyle. *Br. J. Pharmacol*., **2008**, *154*, 1.
[103] S. B. Brown, E. A. Brown, I. Walker. *Lancet Oncol*., **2004**, *5*, 497.
[104] Q. Peng, K. Berg, J. Moan, M. Konqshauq, J. M. Nesland. *Photochem. Photobiol*., **1997**, *65*, 235.

tumour cells survival mechanisms. For example, enhanced permeability and retention effect in tumours is an accessory consequence of angiogenesis (a fast and an irregular vascular growth), leading to an improved extravasation from these vessels for larger-molecular-weight molecules or nanosized carriers. Consequently several approaches have been studied in order to take advantage of this fact, using delivery vehicles, such as gold nanoparticles, [105] silica nanoparticles, [106] polymeric nanoparticles, [107] liposomes [108] and dendrimers,[109]although the efficacy of such systems can be variable due to the heterogeneous cellular internalization processes. In addition, some of these photosensitizer nanocarriers have been functionalized with antibodies and lectins for tumour associated receptors.[110]

In addition, regarding direct targeted delivery of photosensitizers, it has been dominated by functionalization of photosensitizers with antibodies, antibody derivatives, antibody mimetics and peptides in order to stablish a direct

[105] a) D. C. Hone, P. I. Walker, R. Evans-Gowing, S. FitzGerald, A. Beeby, I. Chambrier, M. J. Cook, D. A. Russell. *Langmuir*, **2002**, *18*, 2985. b) M. E. Wieder, D. C. Hone, M. J. Cook, M. M. Handsley, J. Gavrilovic, D. A. Russell. *Photochem. Photobiol. Sci.*, **2006**, *5*, 727.

[106] a) P. Couleaud, V. Morosini, C. Frochot, S. Richeter, L. Raehm, J. O. Durand. *Nanoscale*, **2010**, *2*, 1083. b) J. Zhou, L. Zhou, C. Dong, Y. Feng, S. Wei, J. Shen, X. Wang, *Mater. Lett.*, **2008**, *62*, 2910.

[107] A. Labib, V. Lenaerts, F. Chouinard, J. C. Leroux, R. Ouellet, J. E. van Lier. *Pharm. Res.*, **1991**, *8*, 1027.

[108] C. S. Jin, G. Zheng. *Lasers Surg. Med*., **2011**, *43*, 734.

[109] N. Nishiyama, H. R. Stapert, G. D. Zhang, D. Takasu, D. L. Jiang, T. Nagano, T. Aida, K. Kataoka. *Bioconjugate Chem.*, **2003**, *14*, 58.

[110] a) T. Stuchinskaya, M. Moreno, M. J. Cook, D. R. Edwards, D. A. Russell. *Photochem. Photobiol. Sci.*, **2011**, *10*, 822. b) G. Obaid, I. Chambrier, M. J. Cook, D. A. Russell. *Angew. Chem., Int. Ed.*, **2012**, *51*, 6158. c) H. Benachour, A. Seve, T. Bastogne, C. Frochot, R. Vanderesse, J. Jasniewski, I. Miladi, C. Billotey, O. Tillement, F. Lux, M. Barberi-Heyob. *Theranostics*, **2012**, *2*, 889. d) M. Gary-Bobo, Y. Mir, C. Rouxel, D. Brevet, I. Basile, M. Maynadier, O. Vaillant, O. Mongin, M. Blanchard-Desce, A. Morere, M. Garcia, J. O. Durand, L. Raehm. *Angew. Chem., Int. Ed.*, **2011**, *50*, 11425. e) G. R. Reddy, M. S. Bhojani, P. McConville, J. Moody, B. A. Moffat, D. E. Hall, G. Kim, Y. E. Koo, M. J. Woolliscroft, J. V. Sugai, T. D. Johnson, M. A. Philbert, R. Kopelman, A. Rehemtulla, B. D. Ross. *Clin. Cancer Res.*, **2006**, *12*, 6677. f) Y. Mir, S. A. Elrington, T. Hasan. *Nanomedicine*, **2013**, *9*, 1114.

interaction with tumour cells that are overexpressing target receptors or biomolecules.[111]

7.5. Antimicrobial Photodynamic Therapy

The second half of the 20th century could be described as "the antibiotic era".[112] However, the inappropriate prescription and use of antibiotics has led to the appearance of bacterial resistant strains, so new therapies are desired, especially those to which bacteria could not be able to develop resistance. Among them, due to the high diversity of killing pathways caused by Reactive Oxygen Species such as $^1O_2$, the research in antimicrobial Photodynamic Therapy (aPDT)[113] has risen interest in the last years as development of resistance could be minimal.[114] Most of the dyes used in aPDT were originally designed for other applications and they belong to a wide variety of structural families: Rose Bengal, Methylene Blue, Toluidine Blue, Indocyanine Green, among others. However, reported results in aPDT are focused mainly on *in vitro* assays, while *in vivo* experiments using animal models or clinical applications have only been described in a few reports, focused on dental practice.[115]

One of the key points in aPDT is related with the different structure of the outer membrane between Gram-(+) and Gram-(–) bacteria. It has been found that, in general, neutral or anionic photosensitizers are more efficiently bound to Gram-(+) bacteria than Gram-(–) bacteria. As a consequence, the photodynamic efficiency is greater against Gram-(+) bacteria.

This susceptibility can be explained by the cytoplasmic membrane structure, which can be easily crossed by the photosensitizer through the porous layer of peptidoglycan and lipoteichoic acid. However, the cell envelope of Gram-(–)

---

[111] P. M. R. Pereira, B. Korsak, B. Sarmento, R. J. Schneider, R. Fernandes, J. P. C. Tomé. *Org. Biomol. Chem*., **2015**, *13*, 2518.
[112] R. I. Aminov. *Front. Microbiol*., **2010**, *1*, 134.
[113] M. R. Hamblin, T. Hasan. *Photochem. Photobiol. Sci.*, **2004**, *3*, 436.
[114] a) A. Tavares, C. M. B. Carvalho, M. A. Faustino, M. G. P. M. S. Neves, J. P. C. Tomé, A. C. Tomé, J. A. S. Cavaleiro, A. Cunha, N. C. M. Gomes, E. Alves, A. Almeida. *Mar. Drugs*, **2010**, *8*, 91. b) O. E. Akilov, K. O'Riordan, S. Kosaka, T. Hasan. *Med. Laser Appl*., **2006**, *21*, 251.
[115] F. Javed, L. P. Samaranayake, G. E. Romanos. *Photochem. Photobiol. Sci*., **2014**, *13*, 726.

bacteria consists of an inner cytoplasmic membrane and an outer membrane, that are separated by the peptidoglycan layer. The outer membrane forms a physical and functional barrier between the cell and its environment (Figure 62).

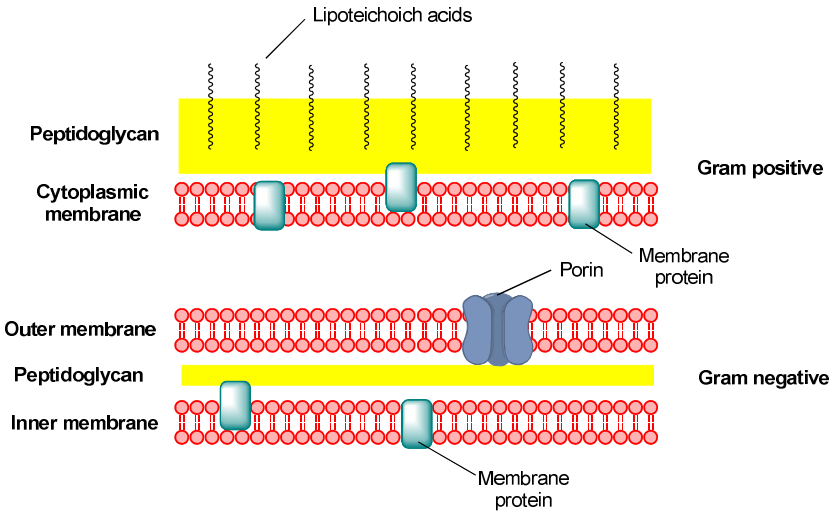

Figure 62. Membrane wall structure for Gram-(+) and Gram-(–) bacteria.

Contrary to eukaryotic cells, two main mechanisms for lethal damage caused to bacteria can be considered using aPDT: damage to the cytoplasmic membrane and DNA damage.

Regarding the morphological alterations induced to the bacteria wall, several modifications have been described using TEM, SEM and AFM: bubble formation, vesiculations after release of outer membrane vesicles, pores, gaps, increased roughness and leakage of cellular content in *E. coli*[116] and *Yersinia pseudotuberculosis*,[117] among others. Moreover, localized photosensitizers on the bacteria wall can alter the functionalities of some membrane systems. For example, modifications on membrane potential can produce the inactivation of membrane transport systems and enzymes such as NADH dehydrogenase and

[116] a) B. Pudziuvyte, E. Bakiene, R. Bonnett, P. A. Shatunov, M. Magaraggia, G. Jori. *Photochem. Photobiol. Sci.*, **2011**, *10*, 1046. b) M. B. Spesia, D. A. Caminos, P. Pons, E. N. Durantini. *Photodiagn. Photodyn. Ther.*, **2009**, *6*, 52.

[117] a) W. Du, C. Sun, Z. Liang, Y. Han, J. Yu. *World J. Microbiol. Biotechnol.*, **2012**, *28*, 3151. b) K. Sahu, H. Bansal, C. Mukherjee, M. Sharma, P. K. Gupta. *J. Photochem. Photobiol. B*, **2009**, *96*, 9.

ATPase, leading to the lethal disruption of the respiratory chain.[118] The impairing of the K^+ pump is also a consequence observed in some aPDT assays performed.[119] Direct modification of membrane proteins has also been described by proteomic analysis in *S. aureus*, supporting that oxidative damage is selective, modifying several functional proteins involved in metabolic activities, cell division and sugar uptake.[120] In spite of the fact that bacterial lipids are mostly monounsaturated and, consequently, not so susceptible to oxidation as polyunsaturated lipids, a decrease in the amount of unsaturated fatty acids in *E. coli* proves that lipids can be also oxidized leading to hydroxy and hydroperoxy derivatives.[121]

Furthermore, although considered a mechanism for lethal damage, modifications induced to DNA do not seem to be the main pathway in aPDT inactivation. This statement has been proposed by several authors taking into account that *Deinococcus radiodurans*, an extremophile known to have a very efficient DNA repair mechanism, is easily killed in aPDT experiments.[122] However photocleavage of bacterial DNA can be observed when bacteria are already not viable.

[118] a) G. Valduga, B. Breda, G. M. Giacometti, G. Jori, E. Reddi. *Biochem. Biophys. Res. Commun.*, **1999**, *256*, 84. b) K. Komagoe, H. Kato, T. Inoue, T. Katsu. *Photochem. Photobiol. Sci*., **2011**, *10*, 1181.

[119] H. Kato, K. Komagoe, T. Inoue, T. Katsu. *Anal. Sci.,* **2010**, 26, 1019.

[120] R. Dosselli, R. Millioni, L. Puricelli, P. Tessari, G. Arrigoni, C. Franchin, A. Segalla, E. Teardo, E. Reddi. *Proteomics*, **2012**, *77*, 329.

[121] E. Alves, N. Santos, T. Melo, E. Maciel, M. L. Dória, M. A. Faustino, J. P. Tomé, M. G. Neves, J. A. Cavaleiro, A. Cunha, L. A. Helguero, P. Domingues, A. Almeida, M. R. Domingues. *Rapid Commun. Mass Spectrom.,* **2013**, *27*, 2717.

[122] M. Schäfer, C. Schmitz, G. Horneck. *Int. J. Radiat. Biol.*, **1998**, *74*, 249.

7.6. *Helicobacter pylori*

Helicobacter pylori is a Gram-negative bacterium that colonizes human gastric mucosa. It is considered one of the most widespread pathogens among the world's population. The global rate of infection reaches around 50% of the population, although in some less developed countries this rate can be increased to 80%.[123]

Once *H. pylori* colonizes the stomach, it can persist for life if left untreated, although only 30% of those infected are clinically symptomatic.[124] In order to fully understand the success of *H. pylori* in its colonizing strategies, this pathogen has been even detected in the stomach of a 5300 years old European Copper Age glacier mummy (whose genomic analysis has been a useful tool to understand the migration flows from Africa and Asia and the colonization of Europe).[125] This prevalence shows that *H. pylori* has developed a wide repertory of strategies in order to survive in such acidic and hostile environment. Precisely, the adverse conditions found in the stomach decrease the competition from other bacteria for its survival. Among these strategies, the most relevant are the following:

- Excretion of surface-associated urease, a nickel enzyme formed by two subunits (UreA and UreB. Figure 63), for the hydrolysis of urea. As a result, large amounts of ammonia are produced, neutralizing the acidic media and creating a neutral localized niche around the bacteria.[126]

[123] A. O'Connor, C. A. O'Morain, A. C. Ford. *Nat. Rev. Gastroenterol. Hepatol.*, **2017**, *14*, 230.
[124] A. P. Moran. *Carbohydr. Res*., **2008**, *343*, 1952.
[125] F. Maixner, B. Krause-Kyora, D. Turaev, A. Herbig, M. R. Hoopmann, J. L. Hallows, U. Kusebauch, E. E. Vigl, P. Malfertheiner, F. Megraud, N. O'Sullivan, G. Cipollini, V. Coia, M. Samadelli, L. Engstrand, B. Linz, R. L. Moritz, R. Grimm, J. Krause, A. Nebel, Y. Moodley, T. Rattei, A. Zink. *Science*, **2016**, *351*, 162.
[126] H. L. Mobley. *Aliment. Pharmacol. Ther*., **1996**, *10*, 57.

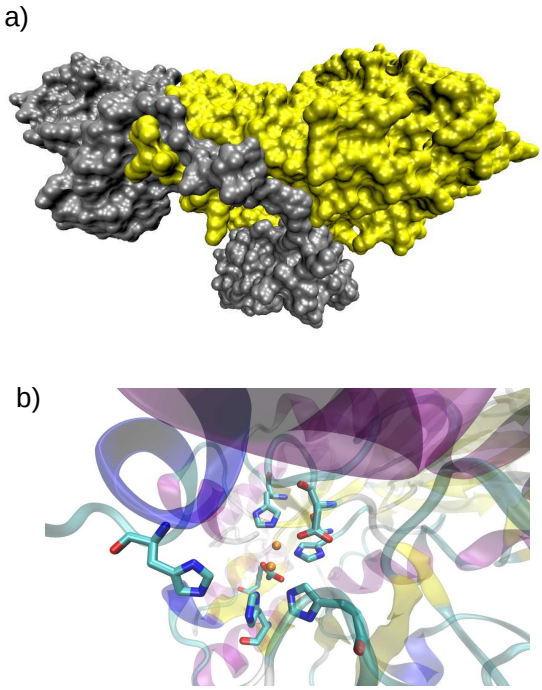

Figure 63. Dimeric domains (a) and catalytic centre (b) of urease in *H. pylori*.

- Evasion of the human immune system. The O-antigen of lipopolysaccharides in *H. pylori* expresses the Lewis blood group antigens Lewis X (Le^x), sialyl Le^x, Le^y Le^a, Le^b and blood group A (Figure 64). Lewis antigens are also expressed by the gastric epithelium, so it has been hypothesized that showing a molecular mimicry of its host, *H. pylori* prevents the formation of antibodies directed against the antigens shared by the bacteria and the microorganism,[127] although it has been found some controversy about this point.[128]

[127] a) M. A. Monteiro, P.Y. Zheng, B. J. Appelmelk, M. B. Perry. *FEMS Microbiol. Lett.*, **1997**, *154*, 103. b) T. O. Croinin, M. Clyne, B. Drumm. *Gastroenterology*, **1998**, *114*, 690. c) H. P. Wirth, M. Yang, E. Sanabria-Valentín, D. E. Berg, A. Dubois, M. J. Blaser. *FASEB J*., **2006**, *20*, 1534.

[128] B. J. Appelmelk, M. A. Monteiro, S. L. Martin, A. P. Moran, C. M. J. E. Vandenbroucke-Grauls. *Trends Microbiol*., **2000**, *8*, 565.

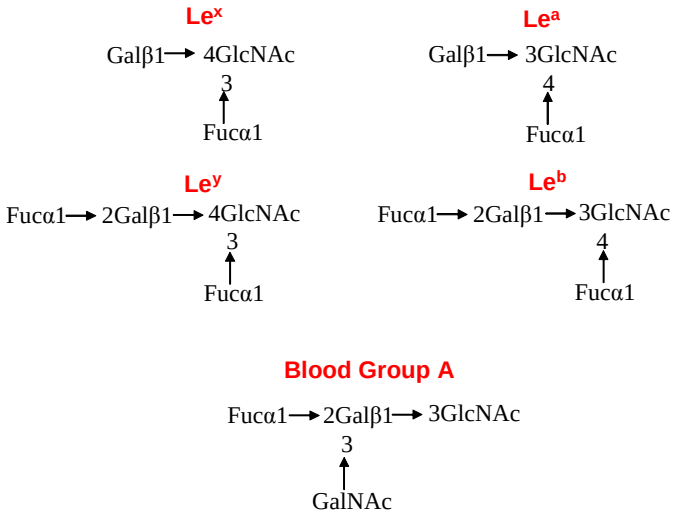

Figure 64. Series of Lewis antigens expressed by *H. pylori*.

- Binding to epithelial cells. The expression of Lewis antigens by the gastric epithelial cells is a key factor for their interaction with *H. pylori*. This bacteria has several outer membrane proteins which act as adhesion molecules. Among them, the blood group antigen binding adhesin (BabA) and sialic acid binding adhesin (SabA). Le^b antigen and related fucosylated blood group antigens are recognized by BabA,[129] whereas sialyl Le^x is recognized by SabA.[130]
- Elevated mutation rate and frequent intraspecific recombination, leading to a wide genetic variability.[131]
- Morphological properties. *H. pylori* is a flagellar and helical bacterium, a shape which can provide a mechanical advantage for penetrating, using a screw-like movement, into the mucus layer in the stomach. In addition,

[129] D. Ilver, A. Arnqvist, J. Ogren, I. M. Frick, D. Kersulyte, E. T. Incecik, D. E. Berg, A. Covacci, L. Engstrand, T. Boren. *Science*, **1998**, *279*, 373.
[130] J. Mahdavi, B. Sonden, M. Hurtig, F. O. Olfat, L. Forsberg, N. Roche, J. Angstrom, T. Larsson, S. Teneberg, K. A. Karlsson, S. Altraja, T. Wadström, D. Kersulyte, D. E. Berg, A. Dubois, C. Petersson, K. E. Magnusson, T. Norberg, F. Lindh, B. B. Lundskog, A. Arnqvist, L. Hammarström, T. Borén. *Science*, **2002**, *297*, 573.
[131] S. Suerbaum, C. Josenhans. *Nat. Rev. Microbiol.*, **2007**, *5*, 441.

the mobility given by the flagella increases the potential for penetration and attaining a robust infection (Figure 65).[132]

H. pylori infection is associated with inflammation of the gastric mucosa, which can evolve to the development of gastritis, gastric and duodenal ulcers, gastric adenocarcinoma and mucosa-associated lymphoid tissue (MALT) lymphoma.[133] Precisely, the discovery of *H. pylori* in 1980s and its role in gastritis and peptic ulcer disease was the reason why Robin Warren and Barry Marshall were awarded with the Nobel Prize in Medicine in 2005.[134]

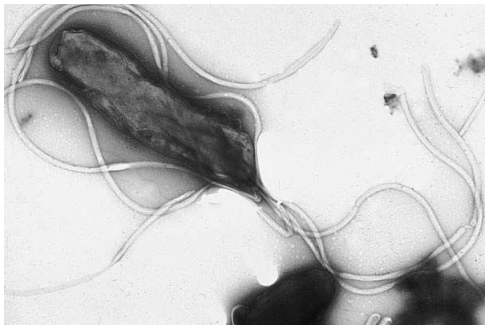

Figure 65. Electron micrograph of *H. pylori*.

In clinical practice, a triple therapy administered over a 7- to 14-day period using a proton pump inhibitor (PPI, such as omeprazole, lansoprazole, pantoprazole, rabeprazole or esomeprazole), clarithromycin and amoxicillin was stablished as standard therapy for the treatment of *H. pylori* infection.[135] However, currently, the efficacy of this therapy has proven to be not enough in many parts of the world (with eradication rates less than 80-90% of success), due to the development of resistance by *H. pylori* to clarithromycin.[136] Various strategies have been designed in order to minimize the impact of this situation: optimizing the standard therapy (increasing the duration and PPI drug dose,

[132] K. M. Ottemann, A. C. Lowenthal. *Infect Immun*. **2002**, *70*, 1984.
[133] a) P. Ruggiero. *Curr. Pharm. Des*., **2010**, *16*, 4225. b) P. B. Ernst, B. D. Gold. *Annu. Rev. Microbiol*., **2000**, *54*, 615.
[134] J. G. Kusters, A. H. M. van Vliet, E. J. Kuipers. *Clin. Microbiol. Rev*., **2006**, *19*, 449.
[135] F. Bazzoli, R. M. Zagari, S. Fossi, P. Pozzato, A. Roda, E. Roda. *Gastroenterology*, **1993**, *104*, 40.
[136] J. Y. Park, K. B. Dunbar, M. Mitui, C. A. Arnold, D. M, Lam-Himlin, M. A. Valasek, I. Thung, C. Okwara, E. Coss, B. Cryer, C. D. Doern. *Dig. Dis. Sci.*, **2016**, *61*, 2373.

among others)[137] and using new therapies as bismuth quadruple therapy (bismuth subcitrate potassium, metronidazole, tetracycline and a PPI).[138]

In this context, it is easy to understand the need for new and effective therapies for *H. pylori* treatment. In this sense the aforementioned properties of aPDT can be a valuable way to be explored. Several experiments have been performed successfully *in vitro* and *ex vivo*, using phthalocyanines,[139] methylene blue,[140,129] toluidine blue O, haematoporphyrin derivatives, 5-aminolevulinic acid, [141] porphyrins, [142] glass microparticles functionalized with Ru complex [143] and chlorins[144] as photosensitizers. Interestingly, several pilot clinical trials have been done using blue[145] and violet[146] light guided with optical fibres. In these last cases, no external photosensitizer is added, as the self-accumulation of significant quantities of protoporphyrin IX by *H. pylori* induces the self-sensitization of $^1O_2$.

7.7. Multivalent interactions for 3rd generation photosensitizers

As it can be concluded from Sections 7.4 and 7.6, the development of third generation photosensitizers with improved selectivity towards the tumour cells

[137] J. Molina-Infante, J. P. Gisbert. *World J. Gastroenterol*., **2014**, *20*, 10338.
[138] V, Papastergiou, S. D. Georgopoulos, S. Karatapanis. *World J. Gastrointest. Pathophysiol*., **2014**, *5*, 392.
[139] J. Bedwell, J. Holton, D. Vaira, A. J. MacRobert, S. G. Bown. *Lancet*, **1990**, *335*, 1287.
[140] S. S. Choi, H. K. Lee, H. S. Chae. *J. Photochem. Photobiol. B: Biology*, **2010**, *101*, 206.
[141] E. Millson, M. Wilson, A. J. MacRobert, S. G. Bown. *J. Photochem. Photobiol. B: Biology*, **1996**, *32*, 59.
[142] M. R. Hamblin, J. Viveiros, C. Yang, A. Ahmadi, R. A. Ganz, M. J. Tolkoff. *Antimicrobial Agents Chemother*., **2005**, *49*, 2822.
[143] M. Calvino-Fernández, D. García-Fresnadillo, S. Benito-Martínez, A. McNicholl, X. Calvet, J. P. Gisbert, T. Parra-Cid. *Eur. J. Med. Chem*., **2013**, *68*, 284.
[144] D. Hüttenberger, C. Simon, C. Mohrbacher, N. Betz, I. Bauer-Marschall, A. Stachon, T. Giesen, H.-J. Foth. *Photodiagn. Photodyn*., **2017**, *17*, 12.
[145] R. A. Ganz, J. Viveiros, A. Ahmad, A. Ahmadi, A. Khalil, M. J. Tolkoff, N. S. Nishioka, M. R. Hamblin. *Lasers Surg. Med*., **2005**, *36*, 260.
[146] A. J. Lembo, R. A. Ganz, S. Sheth, D. Cave, C. Kelly, P. Levin, P. T. Kazlas, P. C. Baldwin III, W. R. Lindmark, J. R. McGrath, M. R. Hamblin. *Lasers Surg. Med*., **2009**, *41*, 337.

(in PDT) or the pathogenic microorganism (in aPDT) has emerged as a key factor to be achieved.

In the particular case of *H. pylori*, it has to be kept in mind that the recognition and bacterial adhesion to the gastric epithelial cells is accomplished through protein (adhesins)-carbohydrate (Lewis antigens) interactions. This kind of interactions are characterized by its high selectivity, but also for its weakness. *In vivo* processes mediated by protein-carbohydrate interactions need greater affinity, so biological systems in nature have overcome this limitation creating proteins aggregated in oligomeric structures which show multivalent binding sites, as well as a multivalent presentation of the ligands (Figure 66).[147]

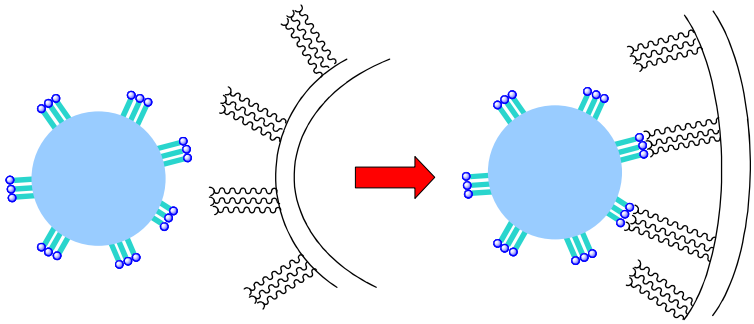

Figure 66. Example of microorganism-cell recognition mediated by multivalent trimeric ligand-receptor interaction.

In order to attain a multivalent presentation of ligands, chemists have emulated several natural entities with spherical shapes like viruses, whose surface is decorated with these receptors. In this sense, the carbon central core in [60]fullerene has proven to be a very convenient scaffold for its spherical functionalization with carbohydrates in hexakis adducts.[148] As a result, tridecafullerene derivatives decorated in their periphery with a total number of

[147] a) Y. C. Lee, R. T. Lee. *Acc. Chem. Res*., **1995**, 28, 321. b) M. Mammen, S.-K. Choi, G. M. Whitesides. *Angew. Chem. Int. Ed*., **1998**, *37*, 2754. c) J. J. Lundquist, E. J. Toone. *Chem. Rev.*, **2002**, *102*, 555. d) J. C. Sacchettini, L. G. Baum, C. F. Brewer. *Biochemistry*, **2001**, *40*, 3009.

[148] a) M. Sánchez-Navarro, A. Muñoz, B. M. Illescas, J. Rojo, N. Martín. *Chem. Eur. J*., **2011**, *17*, 766. b) J. F. Nierengarten, J. Iehl, V. Oerthel, M. Holler, B. M. Illescas, A. Muñoz, N. Martín, J. Rojo, M. Sánchez-Navarro, S. Cecioni, S. Vidal K. Buffet, M. Durka, S. P. Vincent. *Chem. Commun*., **2010**, *46*, 3860.

120 carbohydrates units via click Chemistry have been applied to study the successful multivalent blockade of DC-SIGN receptors, which are related with Ebola virus infection.[149]

[149] a) A. Muñoz, D. Sigwalt, B. M. Illescas, J. Luczkowiak, L. Rodríguez-Pérez, I. Nierengarten, M. Holler, J. S. Remy, K. Buffet, S. P. Vincent, J. Rojo, R. Delgado, J. F. Nierengarten, N. Martín. *Nat. Chem.*, **2016**, *8*, 50. b) B. M. Illescas, J. Rojo, R. Delgado, N. Martín. *J. Am. Chem. Soc*., **2017**, *139*, 6018.

CHAPTER 2

OBJECTIVES

8. CHAPTER 2 OBJECTIVES

The main objective in this chapter is the synthesis of fucosylated [60]fullerene monoadducts for their use as third generation $^1O_2$ photosensitizers in aPDT assays against *H. pylori*. This general aim will be accomplished by the following specific objectives:

- To carry out the synthesis of glycodendrons functionalized with α-L-fucose for the selective recognition by *H. pylori*.
- To achieve the synthesis of [60]fullerene monoadducts decorated with fucosylated glycodendrons via click Chemistry, as $^1O_2$ photosensitizers.
- To accomplish the synthesis of fluorescent probes based on the fluorescein core and their functionalization with glycodendrons or chains with terminal cationic charges to prove their recognition by *H. pylori*.

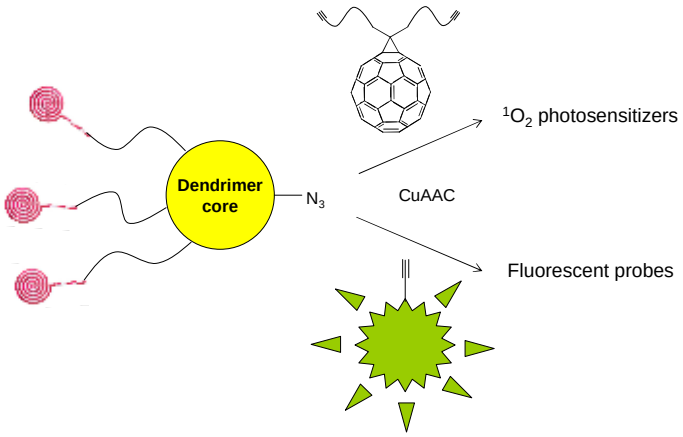

- To implement the synthesis of clickable silica nanoparticles as heterogeneous $^1O_2$ photosensitizers.
- To perform the photophysical characterization (absorption coefficients, Φ_Δ, τ_T, k_q^Δ) of parent [60]fullerene monoadducts in toluene and their correspondent glycofullerenes in D_2O. The photophysical characterization (absorption coefficients, emission spectra, excitation spectra, τ_{fluo}, Φ_f) of the fluorescent probes will be also carried out.

- To explore the interaction and recognition of fluorescent probes by *H. pylori*.
- To optimize the protocols and evaluate the photodynamic activity of the synthesized glycofullerenes against *H. pylori*.

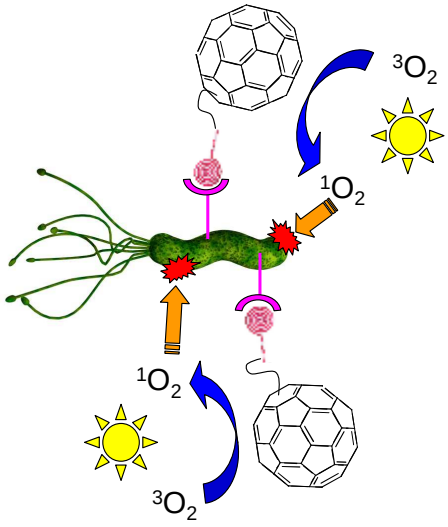

CHAPTER 2

RESULTS AND DISCUSSION

9. CHAPTER 2 RESULTS AND DISCCUSION

9.1. Synthesis

9.1.1. Synthesis of glycodendrons functionalized with α-L-fucose

The synthesis of dendrimers bearing peripheral sugar units was carried out taking advantage of good yields and the synthetic versatility shown by click chemistry reactions, especially the Copper (I) Azide Alkyne Cycloaddition (CuAAC).[150]

For this aim, the first step was the synthesis of the acetyl protected 2-azidoethyl α-L-fucopyranoside **9**.[151] As it is shown in Scheme 30, OH groups in L-(–)-fucose were protected with acetyl groups by esterification. 4-Dimethylaminopyridine was used as the base in order to activate OH groups and to facilitate their nucleophilic attack to acetic anhydride. Moreover, pyridine maintained a basic media for neutralizing the acetic acid which was formed during the reaction. Preparation of **7** was confirmed by ^{1}H-NMR and ^{13}C-NMR, as four methyl signals adding up 12 protons and four carbonyl carbons were observed, respectively, as well as a strong band located at 1748 cm^{-1} in FTIR spectrum due to the C=O stretching.

Thereafter, glycosylation of **7** with 2-bromoethanol was performed using $BF_3 \cdot OEt_2$ as the catalyst. Subsequently, the anomeric carbon of **7** was functionalized with a 2-bromoethyl chain. The analysis by ^{1}H-NMR confirmed the loss of one singlet corresponding to the methyl of an acetyl group, as well as the appearance of signals corresponding to the 2-bromoethyl group. It is interesting to remark the diastereotopic behaviour of *h* protons (nomenclature used in the Experimental Section), as they are close to a chiral carbon. Finally, the substitution of Br by an azide group was achieved using a large excess of NaN_3. The presence of the azide moiety was confirmed by the FTIR spectrum, since a band centred at 2106 cm^{-1}, corresponding to the –N=N=N stretching mode was observed.

---

[150] a) X. P. He, Y. L. Zeng, Y. Zang, J. Li, R. A. Field, G. R. Chen. *Carbohydr. Res*., **2016**, *429*, 1. b) V. K. Tiwari, B. B. Mishra, K. B. Mishra, N. Mishra, A. S. Singh, X. Chen. *Chem. Rev*., **2016**, *116*, 3086.

[151] E. Arce, P. M. Nieto, V. Díaz, R. García-Castro, A. Bernad, J. Rojo. *Bioconjugate Chem*. **2003**, *14*, 817.

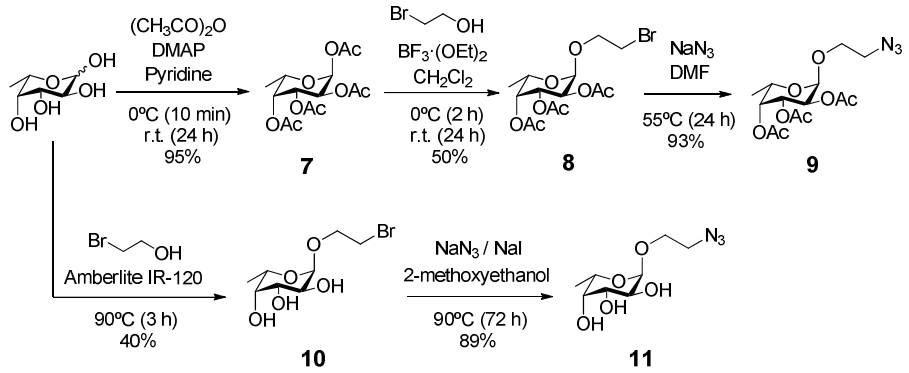

Scheme 30. Synthesis of protected and unprotected 2-azidoethyl-α-L-fucopyranoside.

In order to get directly the unprotected 2-azidoethyl α-L-fucopyranoside **11**, L-(–)-fucose was treated with Amberlite-IR-120^{TM}, an acidic cation exchange resin, and 2-bromoethanol. In the same manner as **8**, compound **10** reacted in the presence of an excess of NaN_3 affording **11**, which in the FTIR spectrum also showed the –N=N=N stretching band at 2094 cm^{-1}.

The next step was to get the dendrimer core. For this purpose, methyl 3,5-dihydroxybenzoate and methyl 3,4,5-trihydroxibenzoate (gallic acid methyl ester) were used as the starting materials (Scheme 31).[152]

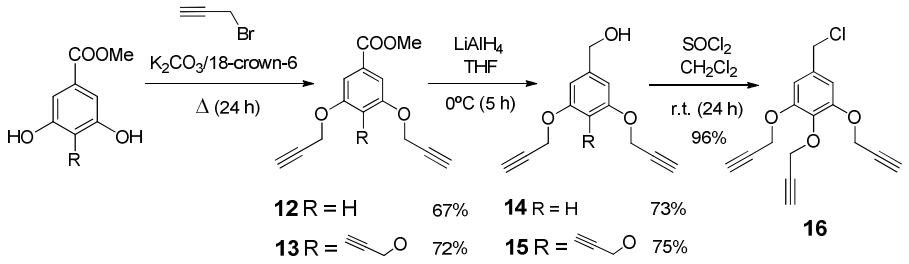

Scheme 31. Synthesis of propargylated dendrimer core based on gallic acid derivatives.

Firstly, potassium carbonate was used as the base to deprotonate the phenol groups and favour the nucleophilic substitution of Br in propargyl bromide, yielding the bis- and tripropargylated derivatives **12** and **13**, respectively. Propargyl groups showed the characteristic signals in ^{1}H-NMR: a doublet for –OC**H**$_2$C≡CH and a triplet for –OCH$_2$C≡C**H**, with a low ^3J constant of 2.4 Hz. Moreover, the typical C≡**C–H** and **C≡C** stretching vibrations around 3270 cm^{-1}

[152] D. Kushwaha, V. K. Tiwari. *J. Org. Chem.*, **2013**, *78*, 8184.

and 2125 cm^{-1}, respectively, confirmed the presence of the carbon-carbon triple bonds.

Afterwards, both esters were reduced using $LiAlH_4$ to the corresponding benzyl alcohols **14** and **15**. In spite of all the experimental cautions, the reaction yields were far from quantitative. Nevertheless, the transformation of the methyl ester group was confirmed by the disappearance of the **C=O** stretching band at 1720 cm^{-1} in the FTIR spectrum, showing up instead of a broad band at 3300 cm^{-1} due to the **O–H** stretching. The dendrimer core was finally obtained substituting the alcohol group by a Cl in the case of **15**, as it could yield more branched structures. For this aim, reaction of **15** with thionyl chloride afforded the benzyl chloride **16**, where the alcohol proton signal (1.75 ppm) and the **O–H** stretching in FTIR were supressed. Likewise, the benzyl carbon was shielded from 65.3 to 46.2 ppm in comparison to that in **15**.

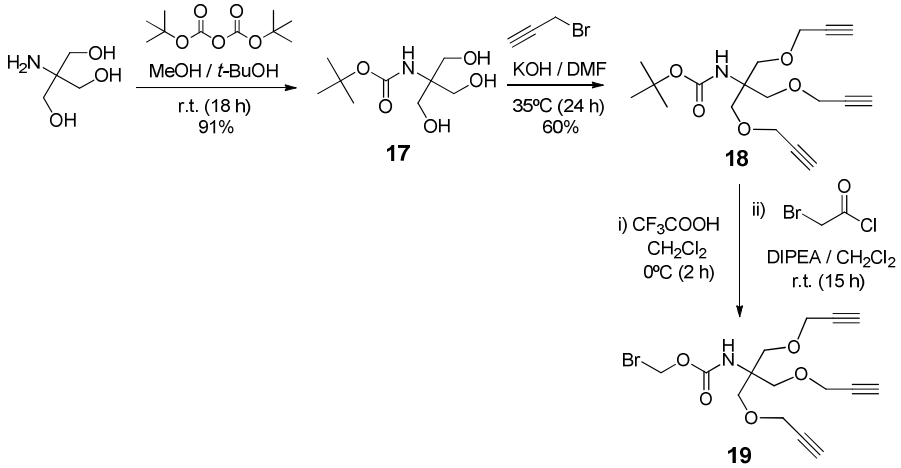

Scheme 32. Synthesis of propargylated dendrimer core.

The synthesis of a second class of dendrimer core was explored (Scheme 32).[153] Similarly to **16**, three alkyne groups were introduced in the Boc protected derivative **17**, which had been previously synthesized starting from commercial tris(hydroxymethyl)aminomethane. In this case, a stronger base such as potassium hydroxide was used in order to deprotonate the alcohol groups. Similar spectroscopic characteristics to those mentioned for **12** and **13** were

[153] Y. M. Chabre, D. Giguère, B. Blanchard, J. Rodrigue, S. Rocheleau, M. Neault, S. Rauthu, A. Papadopoulos, A. A. Arnold, A. Imberty, R. Roy. *Chem. Eur. J.*, **2011**, *17*, 6545.

observed in the characterization of **18**. Thereafter, derivative **18** was deprotected using trifluoroacetic acid, yielding the corresponding amine, which, without further purification, was treated with bromoacetyl chloride in order to get **19**. In this last reaction, *N*,*N*-diisopropylethylamine (DIPEA) was used for the amine activation. It is interesting to point out that in the ^{1}H-NMR spectrum, the protons corresponding to the amide group and the CH_2 bound to Br were split in two singlet signals, due to the presence of *Z* and *E* amide conformers.

Once both azide and alkyne moieties had been obtained, click reactions via CuAAC were used in order to get a trivalent fucose glycodendrimer. One of the reasons why CuAAC reactions are of interest is the triazole ring which emerges from the interaction between the azide and the alkyne, as it is essentially chemically inert to reactive conditions, *e.g.* oxidation, reduction and hydrolysis.

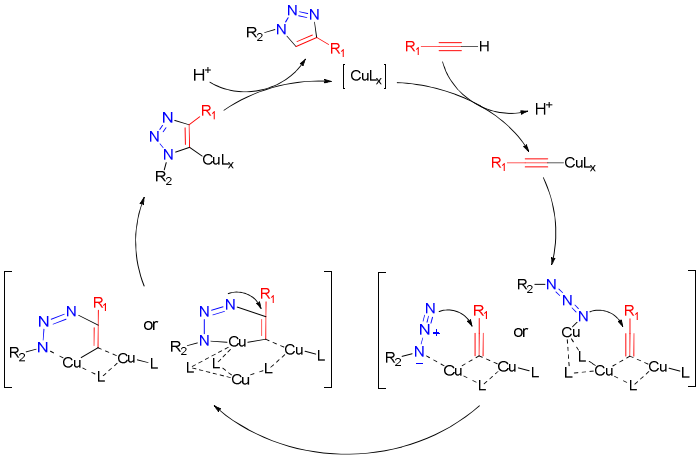

Scheme 33. Proposed catalytic cycle for Cu (I) promoted cycloaddition of alkynes and azides.

The most accepted mechanism for CuAAC reaction is depicted in Scheme 33. CuAAC can be considered as a robust reaction since it can be performed under a wide variety of conditions and with almost any source of solvated Cu(I) species. As Cu(I) shows an influence on the regiochemistry of the reaction (yielding only 1,4-disubstituted 1,2,3-triazoles over the corresponding 1,5-triazole analogues), the most important factor is maintaining the Cu(I) concentration at a high level during all the process. This is why the use of a Cu(II) source with addition of a reducing agent has been one of the preferred methods. The presence of reducing

agents renders the reaction less susceptible to oxygen, and such reactions have often been carried out under open-air conditions.[154]

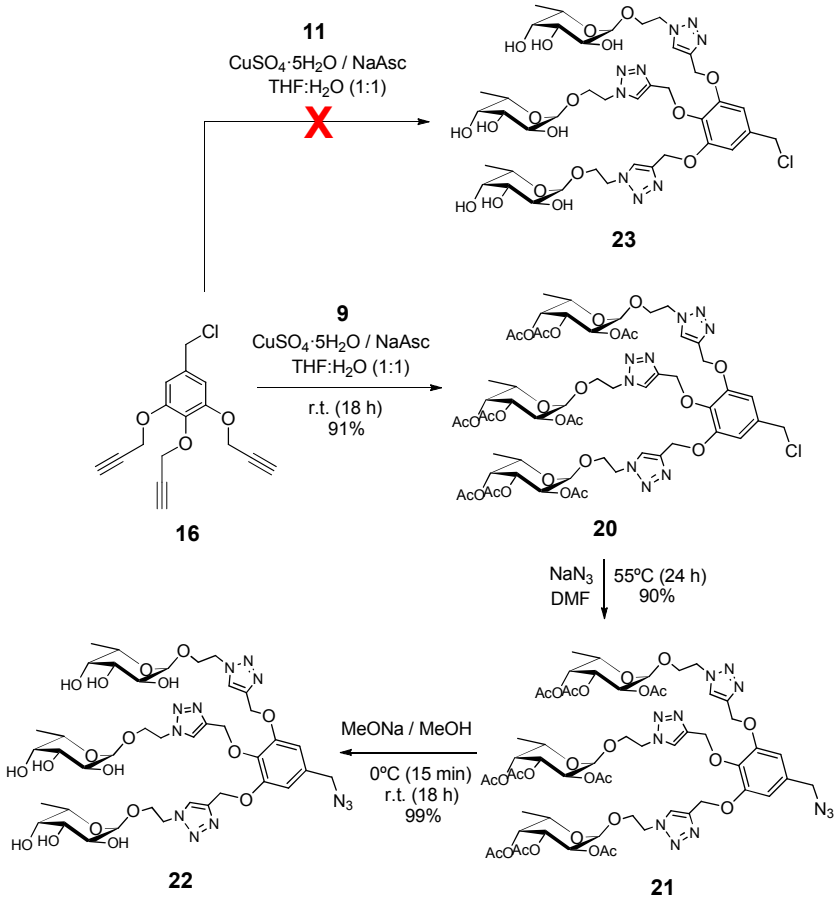

Scheme 34. Synthesis of glycodendrimers decorated with fucose units via CuAAC.

Taking into account all this information, the synthesis of the glycodendrimer was done starting from the reaction between **16** and **9**, yielding the protected dendrimer **20** (Scheme 34). In order to assure the complete functionalization of the propargyl groups in **16**, an excess of **9** was used. The mixture of THF:H_2O (1:1, v/v) was found to be the most suitable for dissolving all the species involved in the reaction. Moreover, as Cu(I) source, a mixture of $CuSO_4 \cdot 5H_2O$ and sodium ascorbate as reducing agent, allowed to carry out the reaction with

[154] M. Medal, C. W. Tornøe. *Chem. Rev*., **2008**, *108*, 2952.

an excellent yield. Nevertheless, the solvents were previously deoxygenated by bubbling argon and keeping the reaction under inert atmosphere. After the reaction, copper was removed by successive washings of the reaction crude using a saturated ammonium chloride solution. One of the most important spectroscopic evidences which allowed to confirm the generation of **20** were the proton signals corresponding to the triazole rings in the region of 8.0 ppm, as well as the total disappearance of the alkyne signals. Regarding the ^{13}C-NMR, it is interesting to show (Figure 67) how the spectrum of **20** is approximately, equal to the addition of the spectra corresponding to **16** and **9**. In the region depicted in Figure 67, carbons of the triazole ring are shown in the section 120-145 ppm. It is possible to differentiate two signals showing a 1:2 ratio, one corresponding to substituents in positions 3 and 5, and the other one corresponding to the substituent in position 4.

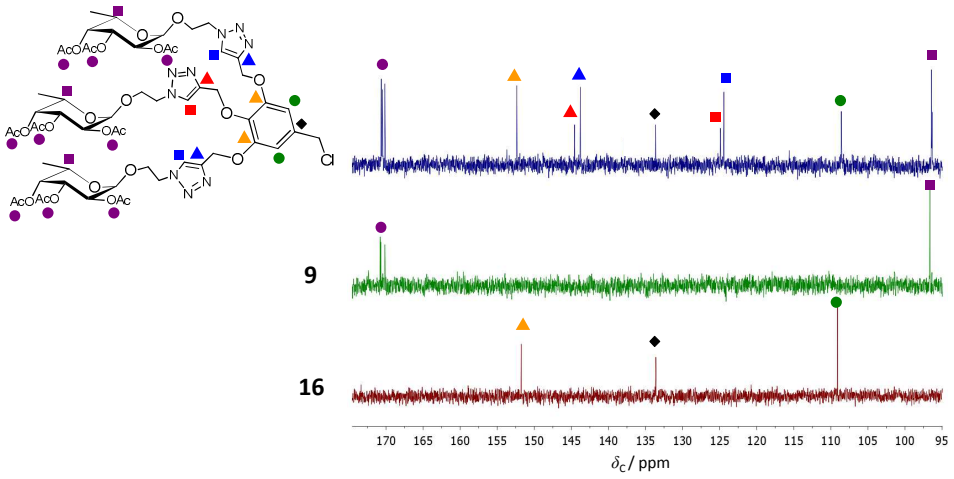

Figure 67. Comparison between ^{13}C-NMR (75 MHz) spectra for **16**, **9** and **20**.

Thereafter, benzyl chloride **20** was transformed in the corresponding benzyl azide **21**, where the protons for the CH_2 bound to the azide group were shielded from 4.51 to 4.26 ppm in comparison to those in **20**, and the azide stretching band appeared at 2102 cm^{-1}. Finally, the glycodendron **22** was obtained after deprotecting the fucose units, by treating **21** with sodium methoxide in methanol and keeping the reaction at pH 9. Figure 68 shows several characteristic signals in the ^{1}H-NMR spectrum of **22**. For instance, the diagnostic signals for the

triazole rings at 8.27 and 8.09 ppm, integrating two and one proton, respectively, as it could be expected for the equivalent protons of substituents in positions 3 and 5, and the substituent in position 4. This difference was also observed for the CH_2 group between the phenoxy and the triazole ring. Although the signal at 5.22 ppm integrating four protons appeared as a singlet, as it could be expected, that corresponding to the substituent in position 4 was split as an AB spin system. It can be said in advance that this kind of protons lose their magnetic and chemical equivalence in sterically hindered environments, as it will be shown afterwards in more detail for other compounds with related structure, which will display a similar behaviour.

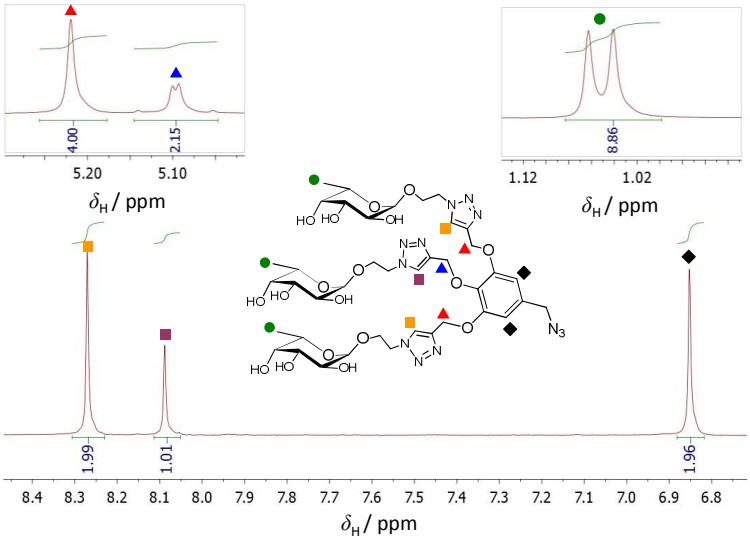

Figure 68. ^{1}H-NMR (300 MHz) spectrum of **22** showing several diagnostic signals.

Direct synthesis of glycodendron **23** was tried in order to avoid the protection/deprotection protocols carried out in the previous synthesis. The experimental conditions were the same regarding the mixture of solvents, reaction times and source of copper. The only difference was the workup, as the solubility in water of **23** prevented the removal of copper by liquid-liquid extractions, so Quadrasil Mercaptopropyl™, a silica gel functionalized exchanger with thiolated groups, was used for this purpose. However, the desired product was not obtained, as it was confirmed by mass spectrometry.

Figure 69 shows the MALDI-TOF spectra recorded for **20** (spectrum a), **21** (spectrum b), **22** (spectrum c) and **23** (spectrum d).

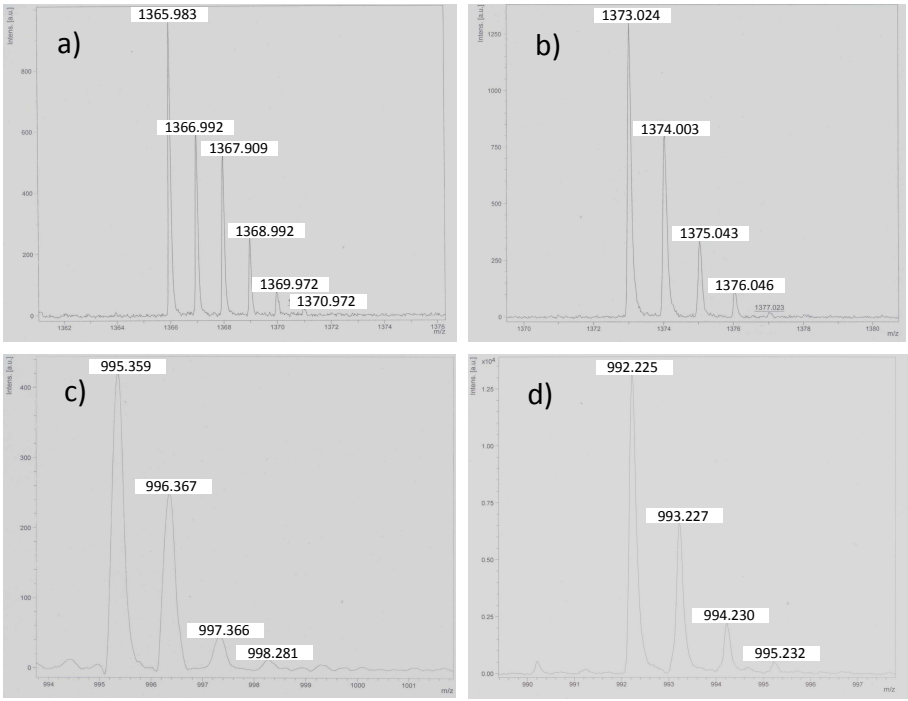

Figure 69. MALDI-TOF spectra for **20** (a), **21** (b), **22** (c) and the attempted compound **23** (d). Of special relevance is the change in isotopic distribution for the M+2 peak in spectra a and b, proving the presence or absence of Cl.

From the spectrum shown in Figure 69d, an experimental mass of 992.23 was obtained. However for compound **23** ($C_{40}H_{58}O_{18}N_9Cl$), the calculated mass for $[M]^+$ is 987.35, with a characteristic isotopic pattern for M+2, as a consequence of the presence of Cl. Both aspects, the found mass and the isotopic pattern did not confirm the presence of **23**. At this point it is interesting to compare this result with those for **20** and **21**. The spectrum of **20** (Figure 69a) showed a more intense M+2 peak due to the presence of Cl (*m/z* 1365.41 calculated for $[M]^+$ $C_{58}H_{76}ClN_9O_{27}$, found: 1365.98), but this was not observed when the Cl was substituted by the azide group in **21** (*m/z* 1372.49 calculated for $[M]^+$ $C_{58}H_{76}N_{12}O_{27}$, found: 1373.02. Figure 69b). The compound which could explain the found mass in Figure 69d is not the benzyl chloride, but the benzyl alcohol, as the calculated $[M+Na]^+$ mass for $C_{40}H_{59}O_{19}N_9$ was 992.38.

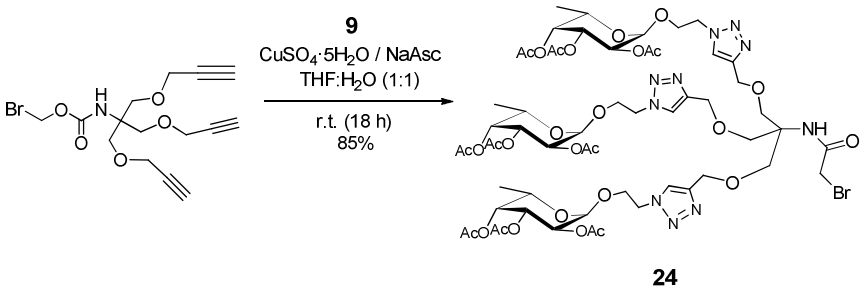

Scheme 35. Synthesis of protected glycodendron **24** using the dendrimeric unit **19**.

Dendrimeric unit **19** was also functionalized with the protected fucose **9** in order to get te protected glycodendron **24** and prove the versatility of this approach (Scheme 35), although this structure was not used in subsequent functionalizations.

9.1.2. Synthesis of [60]fullerene monoadducts with peripheral terminal alkynes

After the synthesis of fucosylated glycodendrons bearing a terminal azide group, a series of [60]fullerene monoadducts were prepared showing peripheral terminal alkynes which could be functionalized via CuAAC. According to the reactions showed in Scheme 36, benzyl alcohols **14** and **15**, and the commercial 4-pentyn-1-ol were used to get the symmetric malonates **25**, **26** and **27**, respectively. In this reaction, 4-dimethylaminopyridine activated the alcohol group of the reactant and triethylamine base neutralized the HCl formed as by-product. The singlet at 3.50 ppm in ^{1}H-NMR spectrum corresponding to the malonic methylene, carbonyl carbons at 166 ppm in ^{13}C-NMR spectrum, as well as the **C=O** stretching band at 1720 cm^{-1} were the most relevant spectroscopic evidences found to confirm the synthesis of these products.

These malonates were employed in the synthesis of the corresponding [60]fullerene monoadducts through the Bingel-Hirsch cyclopropanation.[155] In this reaction, 1,8-diazabicyclo[5.4.0]undec-7-ene (DBU) was used as a non-

[155] a) C. Bingel. *Chem. Ber*., **1993**, *126*, 1957. b) A. Hirsch, I. Lamparth, H. R. Karkunfel. *Angew. Chem*.,**1994**, *106*, 453.

nucleophilic base which is able to capture one of the protons in α position with respect to the carbonyl carbons in the malonate (Scheme 37). In the presence of molecular iodine, the deprotonated malonate yields the corresponding α-iododerivative. Another DBU molecule captures the second proton in α with respect to the carbonyl carbons leading to a α-iodocarbanion, which is added to a double bond from [60]fullerene. The subsequent attack by the remaining electron pair on [60]fullerene replace the iodine and a cyclopropane ring is formed.

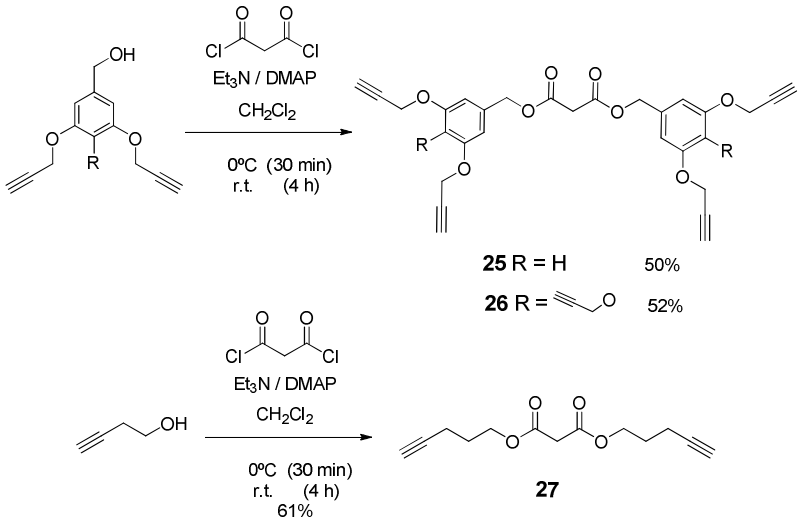

Scheme 36. Synthesis of symmetric malonates for subsequent [60]fullerene functionalization.

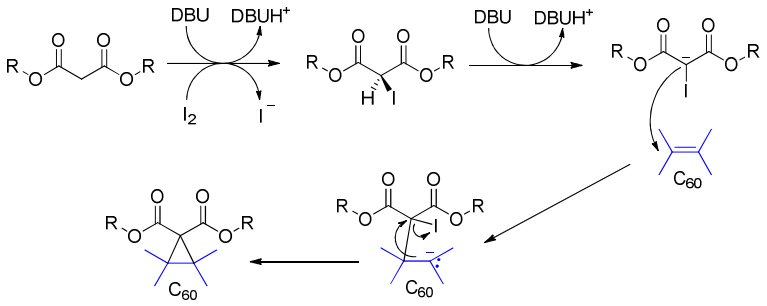

Scheme 37. Proposed mechanism for Bingel-Hirsch cyclopropanation of [60]fullerene.

Experimental conditions used for Bingel reaction are a consequence of the trend shown by [60]fullerene to easily yield polyadducts through this reaction. For this reason, in order to get the monoadduct as the major product, the reaction was done with a large excess of [60]fullerene with respect to the malonates, at low temperature (0 ºC) and stopping the reaction when appearance of polyadducts was confirmed by thin layer chromatography analysis. In spite of these cautions, reaction yields were no greater than 40% (Scheme 38).[156]

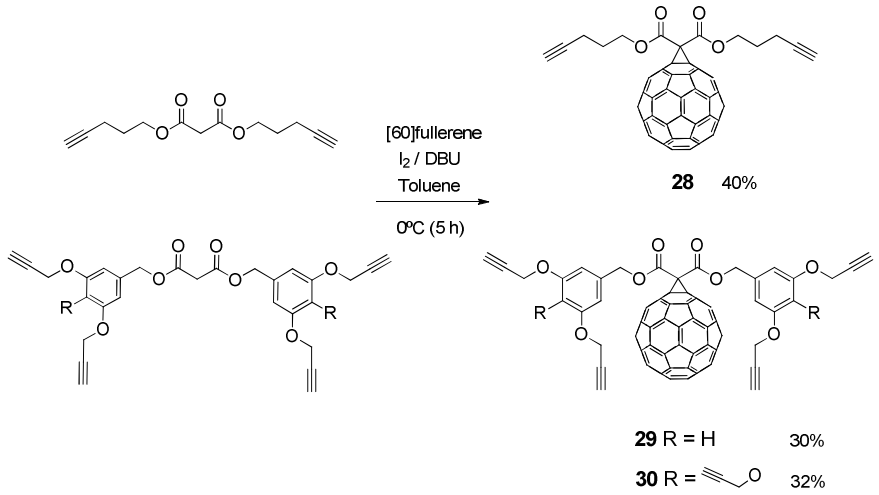

Scheme 38. Synthesis of [60]fullerene monoadducts via Bingel cyclopropanation.

It has to be pointed out that the singlet signal corresponding to the methylene group in α position with respect to the carbonyl carbon disappeared in the ^{1}H-NMR spectrum of [60]fullerene monoadducts **28**, **29** and **30**. Regarding ^{13}C-NMR, all these symmetric monoadducts belong to the C_{2v} symmetry group, so a total number of 15 signals for [60]fullerene sp^2 carbons should be detected between 146 and 138 ppm. Figure 70 shows a representative example of the ^{13}C-NMR spectrum of this kind of monoadducts (that of **28** was selected). In addition, the quaternary carbons coming from the malonate moiety appeared at ~52 ppm, while the sp^3 carbons from the [60]fullerene appeared at ~70 ppm.

[156] A. Muñoz, B. M. Illescas, M. Sánchez-Navarro, J. Rojo, N. Martín. *J. Am. Chem. Soc.*, **2011**, *133*, 16758.

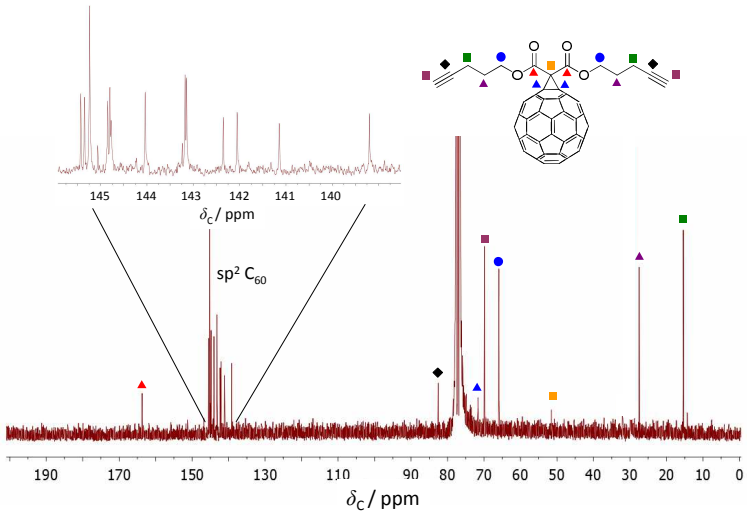

Figure 70. ^{13}C-NMR (75 MHz) spectrum of **28**, selected as a representative example of [60]fullerene monoadducts ^{13}C-NMR spectrum.

9.1.3. Synthesis of [60]fullerene monoadducts functionalized with glycodendrons

In order to get the [60]fullerene monoadducts decorated with glycodendrimers, the last step was the convergent CuAAC reaction between compound **22** bearing the fucose units and the azide group, and the Bingel monoadducts **28**, **29** and **30** (Scheme 39), functionalized with the terminal alkynes. Several modifications were necessarily made on the reaction protocol with respect to previous CuAAC conditions in order to achieve the desired products. First of all, despite the typical good solubility of [60]fullerene monoadducts in organic solvents such as dichloromethane, chloroform, toluene, dioxane or DMSO, the synthetic precursors previously described were not soluble in H_2O:THF mixture. For this reason, DMSO was used as solvent, and CuI as Cu(I) source. DIPEA was added as organic ligand in order to stabilize Cu(I) in the reaction crude. Moreover, the reaction times were extended to 48 h, trying to assure the complete functionalization of the alkyne groups from [60]fullerene monoadducts. On the other hand, for the purification of these compounds, Quadrasil Mercaptopropyl™ was used to remove the remaining copper, and exclusion size chromatography with Sephadex LH-20 as the stationary phase was employed in order to isolate them from those derivatives with lower degree of

functionalization that could be also present in the reaction crude. As a result, a series of [60]fullerene monoadducts decorated with 6, 12 and 18 fucose units were obtained (compounds **31**, **32** and **33**, respectively).

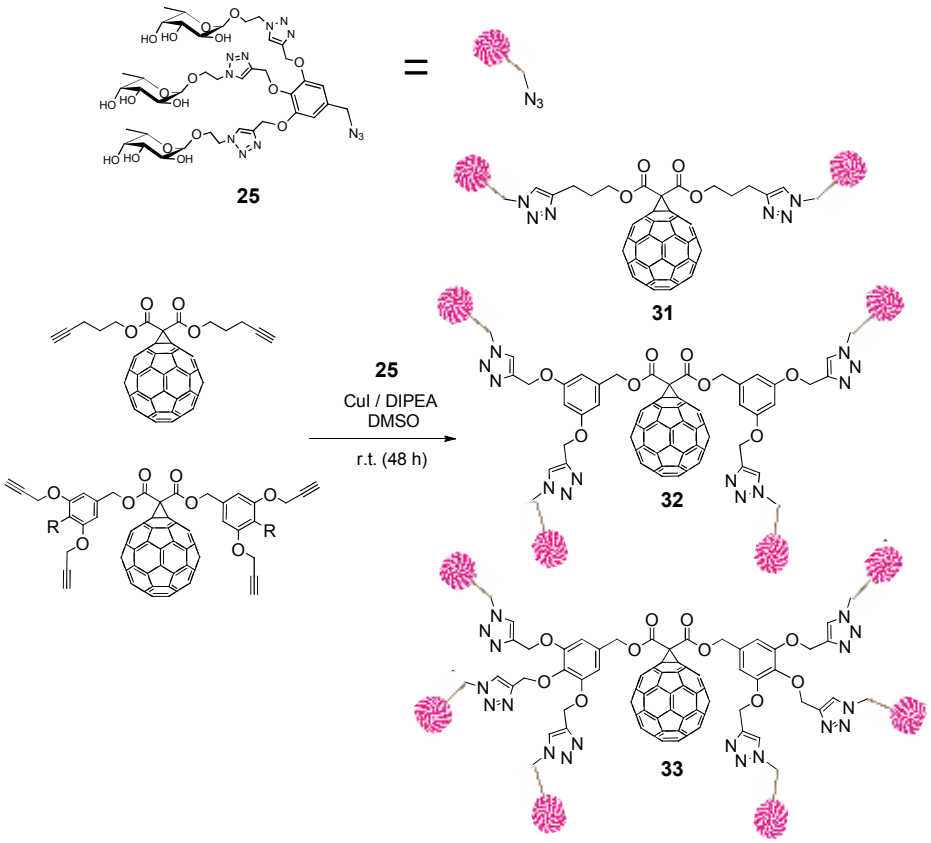

Scheme 39. Synthesis of glycofullerenes **31**, **32** and **33** via CuAAC, bearing 6, 12 and 18 fucose units, respectively.

Although these compounds showed an enhanced solubility in water, self-aggregation was a significant problem for their characterization. Figure 71 shows a comparison between the spectra for glycodendron **22** and glycofullerene **33** in the aromatic and methyl regions, respectively. Signals were significantly widened and some multiplicities were lost. In spite of these drawbacks, integral values were in good agreement with the expected values. In the FTIR spectrum, the bands corresponding to the azide and alkyne groups were not present.

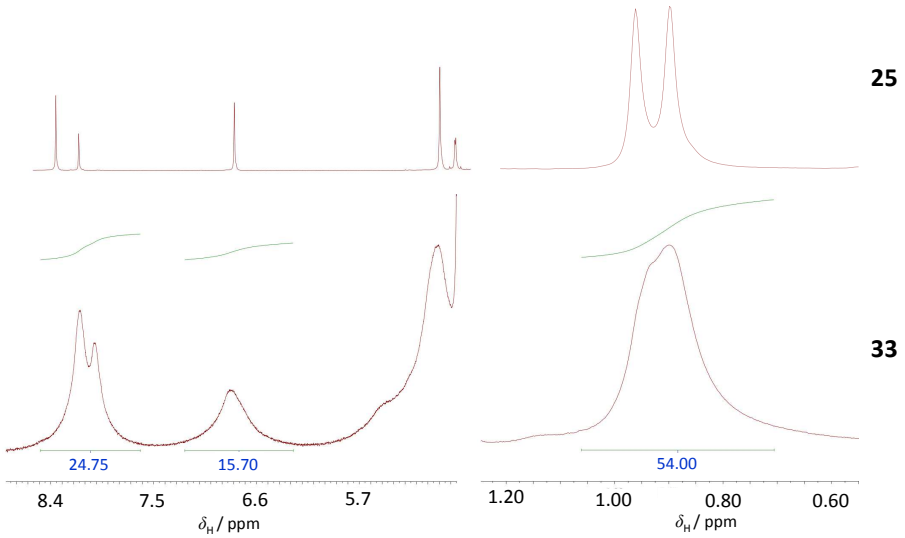

Figure 71. Comparison between ^{1}H-NMR (300 MHz) spectra for **33** and **25**.

9.1.4. Synthesis of fluorescein derivatives decorated with glycodendrons or terminal positive charges

Due to the versatility shown by CuAAC reactions, other organic substrates different from [60]fullerene monoadducts were functionalized with glycodendrimer **22**. In order to get fluorescent probes for interaction assays with *H. pylori*, a series of fluorescein derivatives with peripheral and functionalizable terminal alkynes were obtained (Scheme 40).

Treatment of fluorescein with potassium carbonate to deprotonate phenolic and carboxylic acid groups in the presence of propargyl bromide afforded the fluorescein bispropargylated derivative **34**.[157] The presence of two different propargyl residues was clearly seen by ^{1}H-NMR (triplets at 3.70 and 3.41 ppm with ^{3}J = 2.4 Hz corresponding to the terminal alkyne protons) and the absence of any residual broad singlet due to the carboxylic acid proton.

[157] L. Chen, T.- S. Hu, J. Zhu, H. Wu, Z.-J Yao. *Synlett.*, **2006**, *8*, 1225.

On the other hand, methyl fluorescein ester **35** was synthesized with the aim of obtaining the monopropargylated derivative **36**.[158] It is interesting to highlight that the structure shown in Scheme 40 for **35** is only one of the two possible tautomers arising from the proton exchange between the keto and the phenol groups of the dye, what explained the differences and equivalences observed in the ^{1}H- and ^{13}C-NMR spectra for **35** and **36** (see Experimental Section).

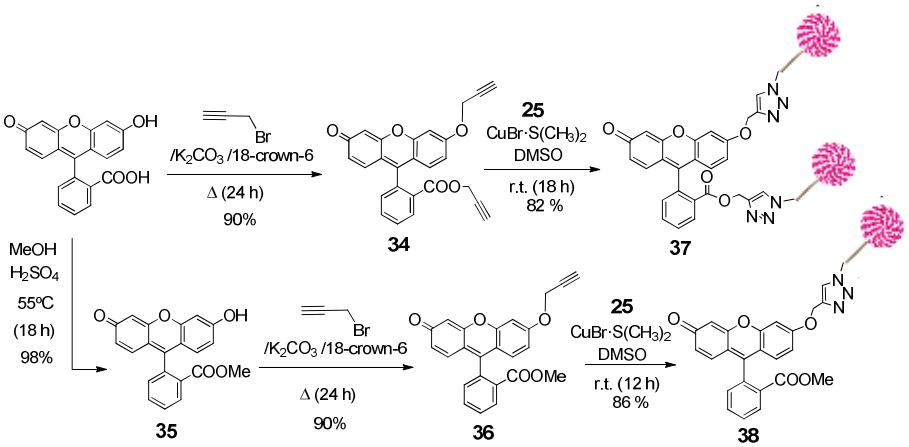

Scheme 40. Synthesis of fluorescent probes based on propargylated fluorescein substrates and glycodendrimer **22**.

Finally, the functionalization of the terminal alkynes via CuAAC afforded the glycofluoresceins **37** and **38** decorated with 6 and 3 fucose units, respectively. Figure 72 is a good example to illustrate the changes observed after modification via click chemistry. For example, the IR spectrum for **37** preserves the main diagnostic signals from glycodendrimer **22** (mainly, the **O–H** and **C–H** stretching bands around 3400 cm^{-1} and 2926 cm^{-1}, respectively) and propargylated fluorescein **34** (**C=O** stretching around 1720 cm^{-1} for the ester group and C=O stretching for the keto group at 1640 cm^{-1}), but not those signals corresponding to the azide and alkyne groups (2103 cm^{-1} for **22**, and 2122, 3276 and 3183 cm^{-1} for **34**, respectively).

[158] Y. Xiang, B. He, X. Li, Q. Zhu. *RSC Adv*. **2013**, *3*, 4876.

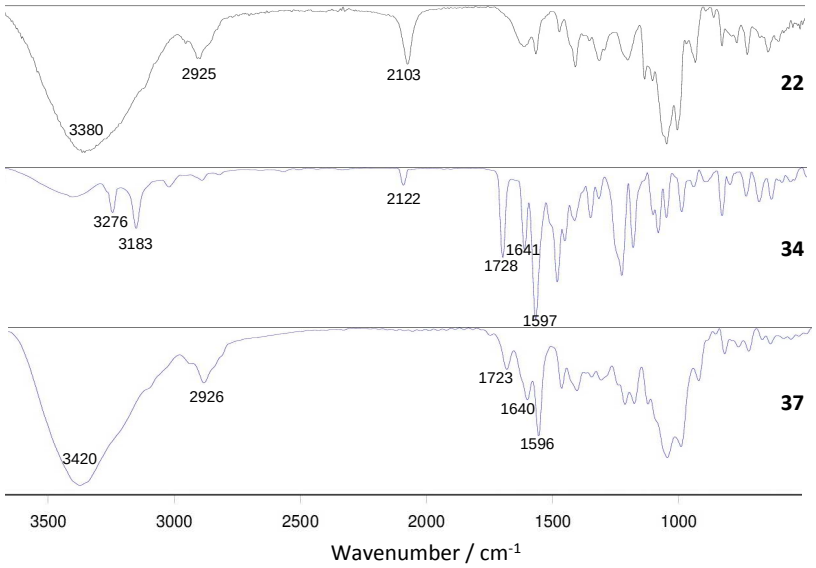

Figure 72. Comparison between the FTIR spectra of glycodendrimer **22**, propargylated fluorescein **34** and the fluorescent glycoprobe **37**.

In addition, similar fluorescein derivatives with terminal positive charges were obtained. The synthetic approach followed is depicted in Scheme 41.

Commercial aminoethanol was firstly transformed in the corresponding haloderivative hydrochloride **39**.[159] Thereafter, the amino group was protected using di-*tert*-butyl dicarbonate to get **40**,[160] which was subsequently treated with an excess of sodium azide to yield the azido derivative **41**, confirmed by the azide stretching band at 2099 cm^{-1}. This compound was used to functionalize, via CuAAC, fluorescein derivatives **34** and **36**, to afford the corresponding bis and monofunctionalized derivatives **43** and **42**, respectively. Both compounds share the appearance of a singlet around 7.6-7.7 ppm, which can be attributed to the triazole ring formed in the chain arising from the phenoxy group after click reaction. In addition, **43** showed a second singlet at 8.16 ppm corresponding to the second triazole ring linked to the oxycarbonyl substituent of the dye.

[159] C. Xiao, Y. Cheng, Y. Zhang, J. Ding, C. He, X. Zhuang, X. Chen. *J. Polym. Sci., Part A: Polym. Chem.*, **2014**, *52*, 671.

[160] L. I. Manasieva, B. U. Maria, A. Prandi, L. Brasili, S. Franchini. *Synthesis*, 2015; 47, 3767.

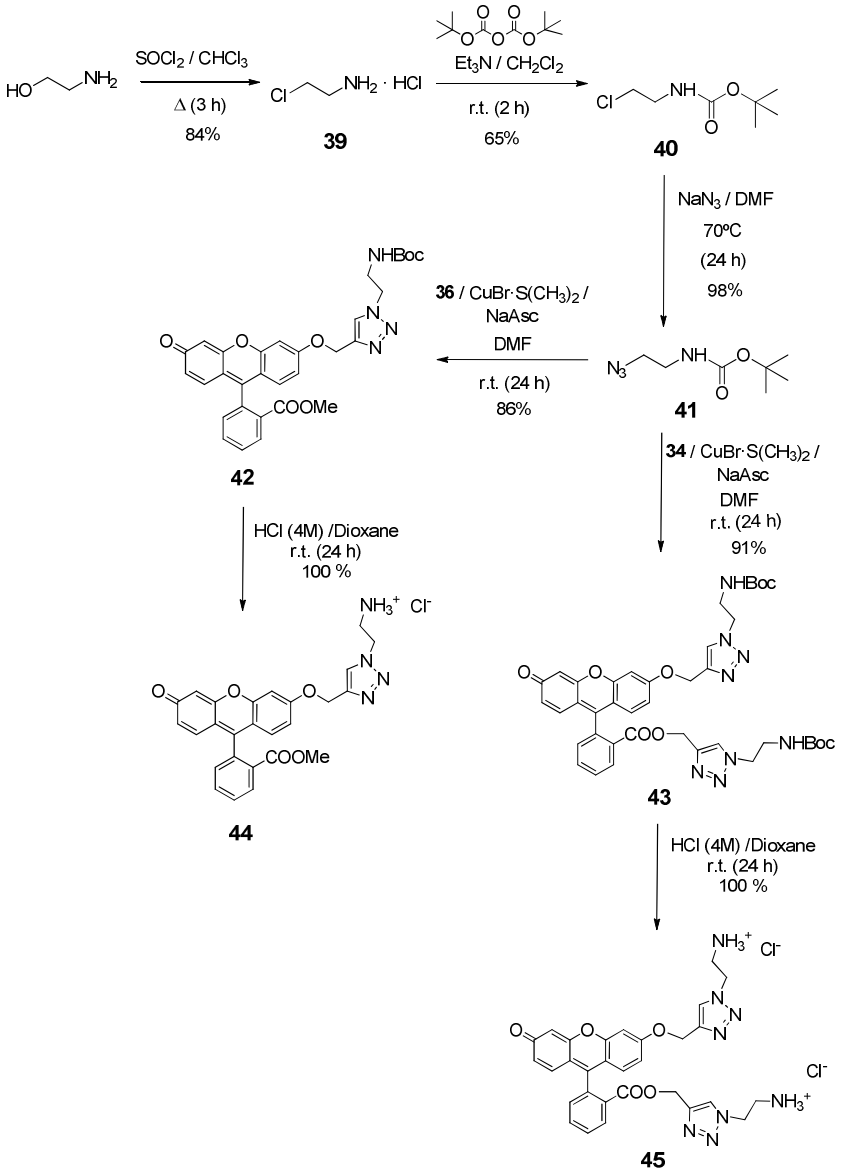

Scheme 41. Synthesis of cationic fluorescent probes based on fluorescein structure.

However, the structural characterization of **43** evidenced an interesting pattern in the ^{1}H-NMR spectrum. As it can be seen in Figure 73, the protons of the methylene group between the triazole ring and the ester group displayed the typical pattern of an AB spin system, instead of the expected singlet. Besides, an incipient splitting showing the same arrangement can be reported for the other

methylene group between the triazole ring and the phenoxy group. The HMQC spectrum confirmed that these split protons were attached to the same carbon (Figure 73 inset).

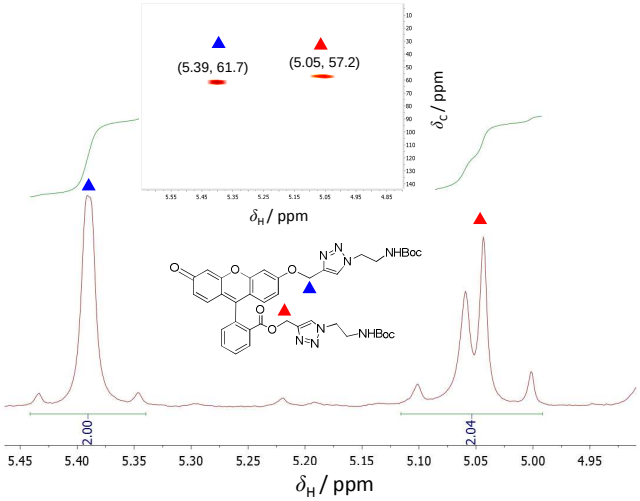

Figure 73. ^{1}H-NMR (300 MHz) and HMQC (inset) spectra for **43**, showing the AB spin system observed for methylene groups attached to the triazole rings.

This behaviour could be explained due to the presence of a bulky aromatic substituent linked to the ester group, which prevents the rotation of the single bond connecting the xanthene moiety and the aromatic ring bearing the ester group. As it has been demonstrated by computational modelization of these structures (B3LYP/def2-SVP), this triazole ring lies on the π-electron cloud of the xanthene moiety (Figure 74) and, since the molecule is not symmetric due to these π-π interactions, both methylene protons sense different magnetic environments, which explains the ^{1}H-NMR pattern observed for these protons.

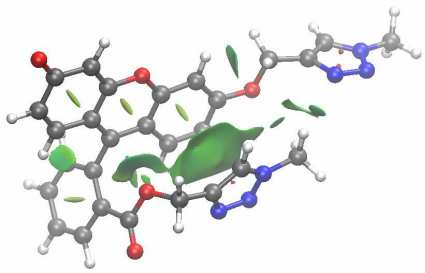

Figure 74. Computational modelization for **43**, showing the π-π interactions in green.

In addition, this geometry could explain why the triazole proton bound to the ester group is so deshielded in the ^{1}H-NMR spectrum of **43** (8.16 ppm) in comparison to the equivalent proton of the other triazole ring connected to the xanthene moiety (7.59 ppm).

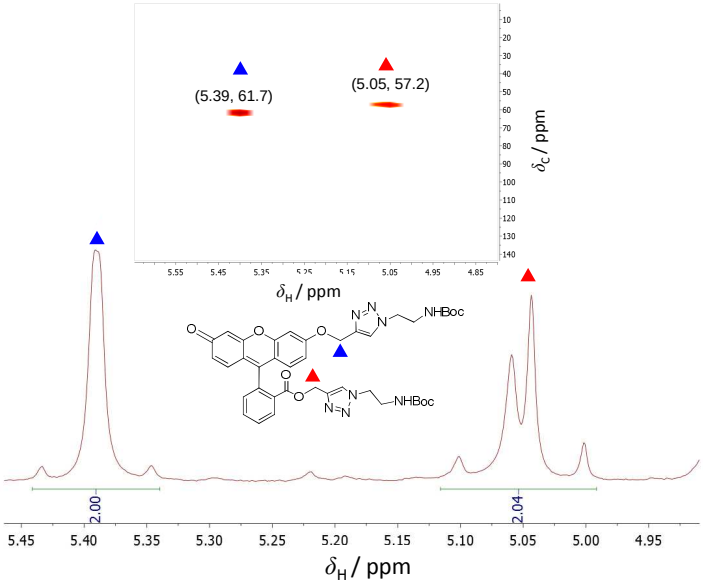

Figure 73. ^{1}H-NMR (300 MHz) spectra for **43** (MeOD-d_4) and **45** (D_2O) showing the AB spin system observed for methylene groups attached to the triazole rings.

Finally, fluorescein derivatives **42** and **43** were deprotected to get the correspondent ammonium hydrochlorides **44** and **45**, respectively, confirmed by the appearance of a broad intense band in the FTIR spectrum between 3500 and 2500 cm^{-1}. Interestingly, as it is shown in Figure 73, the AB spin system previously described was also observed in compound **45**, even though in this case two AB spin systems were clearly present for both methylene groups.

9.1.5. New [60]fullerene monoadducts soluble in highly polar organic solvents

[60]Fullerene monoadducts such as those presented in Scheme 42 showed an improved solubility in organic solvents like chloroform, dichloromethane, toluene, dioxane or DMSO, by comparison to pristine [60]fullerene. However,

they were completely insoluble in more (protic) polar solvents like methanol or acetonitrile. Taking into account that both solvents were used in the mechanistic study commented in Chapter 1, it was considered interesting to synthesize [60]fullerene monoadducts soluble in all the previous solvents, as candidates for $^1O_2$ photosensitized oxidation reactions for synthetic applications in organic chemistry.

For this aim, a branched structure based on short chains of ethylene glycol was synthesized.[161] Again (Scheme 42), gallic acid methyl ester was used as the starting material. Potassium carbonate deprotonated the phenol groups in order to favour the nucleophilic substitution reaction with **46**. However, since the Cl group is a worse leaving group than Br in propargyl bromide (see **12** and **13**), NaI was added to previously achieve the Cl-I substitution (Finkelstein reaction). The following steps were similar to those described in the precedent synthesis of [60]fullerene monoadducts decorated with peripheral terminal alkynes: reduction of the methyl ester group with $LiAlH_4$ to get the benzyl alcohol **48**, subsequent treatment with malonyl chloride to yield the correspondent symmetric malonate **49** and, finally, the Bingel cyclopropanation over the [60]fullerene core to afford the corresponding monoadduct **50**. This compound was soluble in methanol and acetonitrile.

Other topic explored was the synthesis of asymmetric [60]fullerene monoadducts bearing two different groups which could subsequently be functionalized via CuAAC reactions. As it is depicted in Scheme 43, treatment of Meldrum's acid with 4-pentyn-1-ol afforded the corresponding monoester **51**.[162] The appearance of a broad singlet signal in the ^{1}H-NMR spectrum at 9.88 ppm, as well as a broad and intense band in FTIR spectrum around 3100 cm^{-1} proved the presence of the carboxylic acid group.

[161] W. Yang, P. F. Xia, M. S. Wong. *Org. Lett*., **2010**, *12*, 4018.
[162] A. J. Hilmer, K. Tvrdy, J. Zhang, M. S. Strano. *J. Am. Chem. Soc*., **2013**, *135*, 11901.

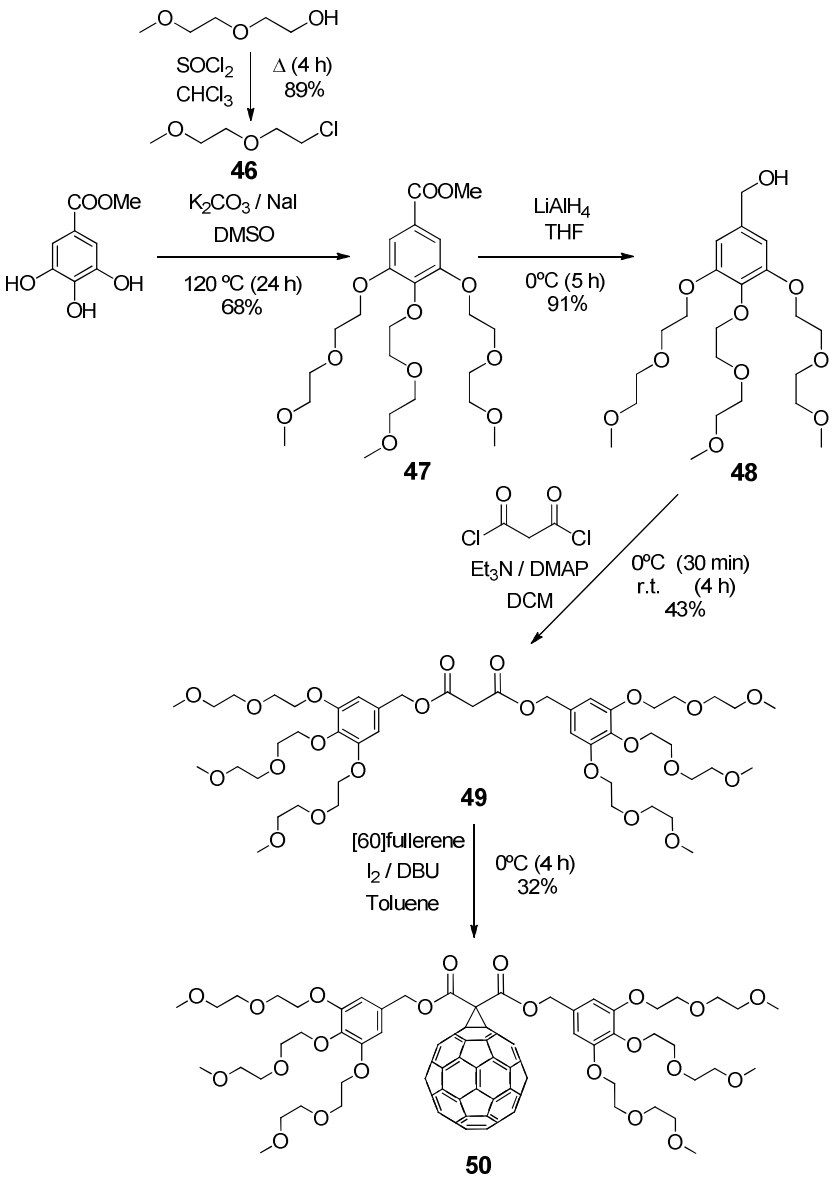

Scheme 42. Synthesis of branched ethylenglycol [60]fullerene monoadduct.

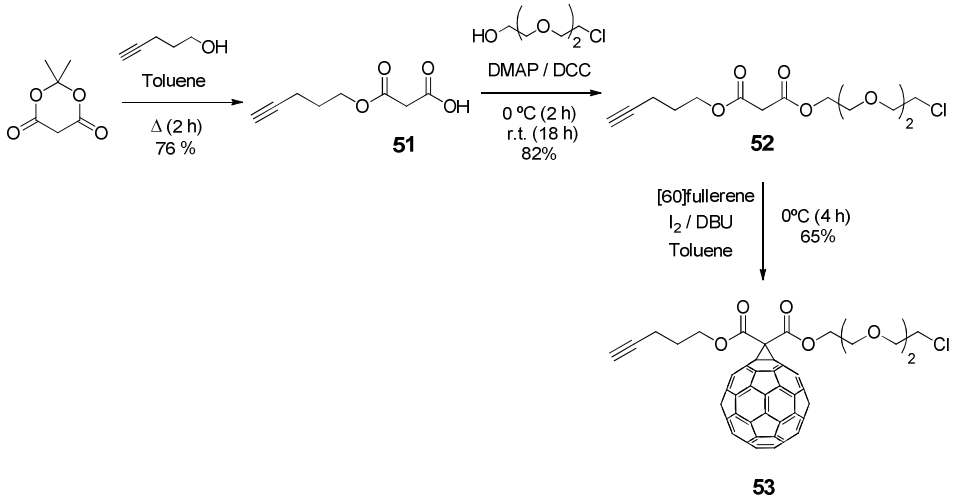

Scheme 43. Synthesis of asymmetric bis-clickable [60]fullerene monoadduct.

Thereafter, the carboxylic acid was esterified with good yield using 2-[2-(2-chloroethoxy)ethoxy]ethanol in the presence of dicyclohexylcarbodiimide (Steglich esterification). Finally, the Bingel reaction between **52** and [60]fullerene led to the monoadduct **53**. This compound could be functionalized with an azide group via CuAAC. Thereafter, the Cl atom could be substituted by treatment with sodium azide and, finally, functionalized in a second CuAAC process with a compound bearing a terminal alkyne.

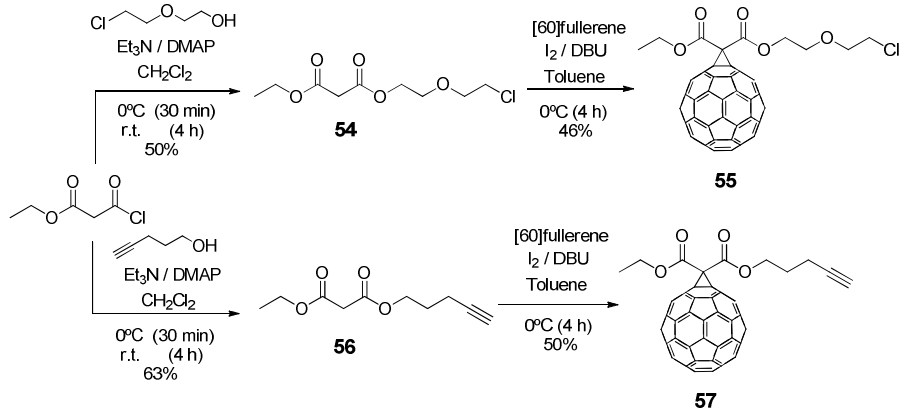

Scheme 44. Synthesis of asymmetric mono-clickable [60]fullerene monoadducts.

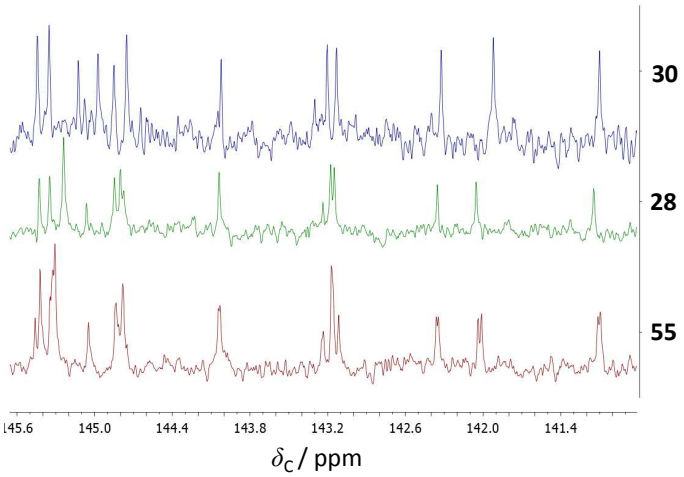

Figure 76. Comparison between ^{13}C-NMR spectra for symmetric (**28** and **30**) and asymmetric [60]fullerene monoadducts.

On the other hand, as it is shown in Scheme 44, asymmetric [60]fullerene monoadducts bearing only a single clickable position were also obtained. In this case, instead of malonyl chloride, ethyl malonyl chloride was used as the starting material to achieve the asymmetric malonate.

It is interesting to comment how the loss of symmetry in these derivatives, by comparison to other symmetric [60]fullerene monoadducts such as **28** or **30** had an influence in their ^{13}C-NMR spectrum. Considering **55** as a representative example and comparing part of the [60]fullerene Csp^2 region with that of **28** and **30,** it was possible to see a slight splitting of some ^{13}C signals (Figure 76). In the case of **55**, this compound does not belong to the C_{2v} symmetry group but to the C_s group and, for this reason, there are more non-magnetically equivalent carbons in this [60]fullerene structure.

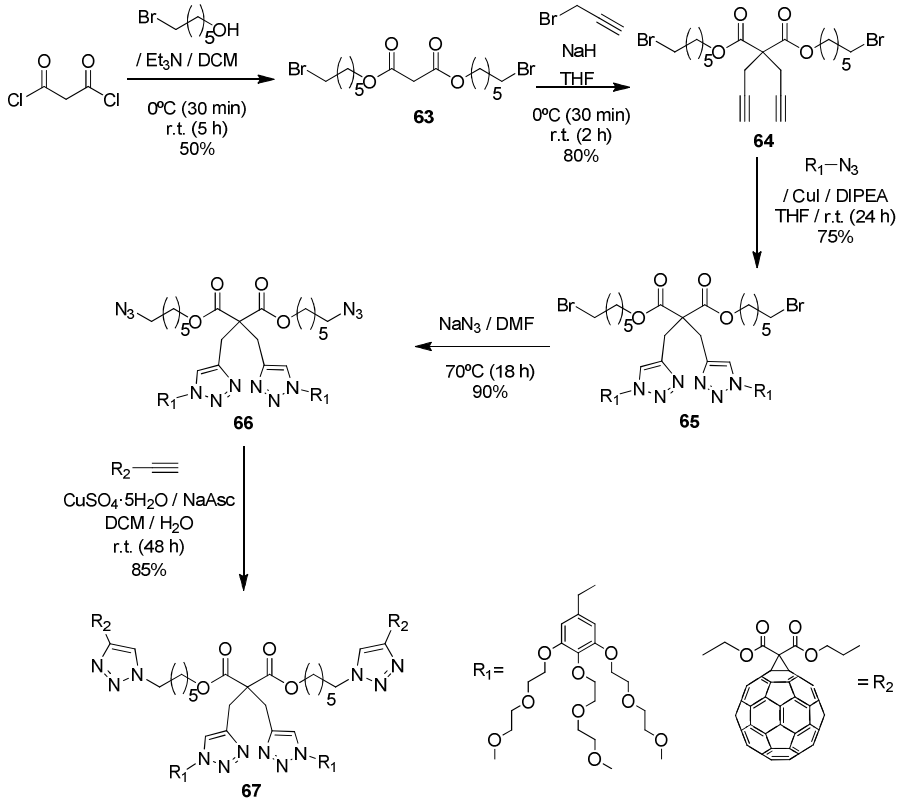

Scheme 45. Synthesis of difullerene **67** starting from bis-clickable malonate **64**.

Moreover, the synthesis of compounds having two [60]fullerene monoadducts in the same structure was also explored (Scheme 45). For this purpose, a bis-clickable symmetric malonate such as **64** was prepared.[163] The key step was the treatment of malonate **63** with NaH base to deprotonate the methylene protons in α position to both carbonyl carbons, yielding the carbanions for the substitution of Br in propargyl bromide.[164] It has to be pointed out the risk assumed by carrying out this approach, since an intramolecular Br substitution could have taken place, but **64** was obtained with good yield and several diagnostic signals were observed which confirmed its structure. In this sense, the evolution of the ^{1}H-NMR spectra shown in Figure 77 illustrates the structural changes performed in the structures of compounds shown in Scheme 45.

[163] S. F. Völker, M. Vallés−Pelarda, J. Pascual, S. Collavini, F. Ruipérez, E. Zuccatti, L. E. Hueso, R. Tena-Zaera, I. Mora-Seró, J. L. Delgado. *Chem. Eur. J.*, **2018**, *24*, 8524.
[164] E.-H. kang, I. S. Lee, T.-L. Choi. *J. Am. Chem. Soc*., **2011**, *133*, 11904.

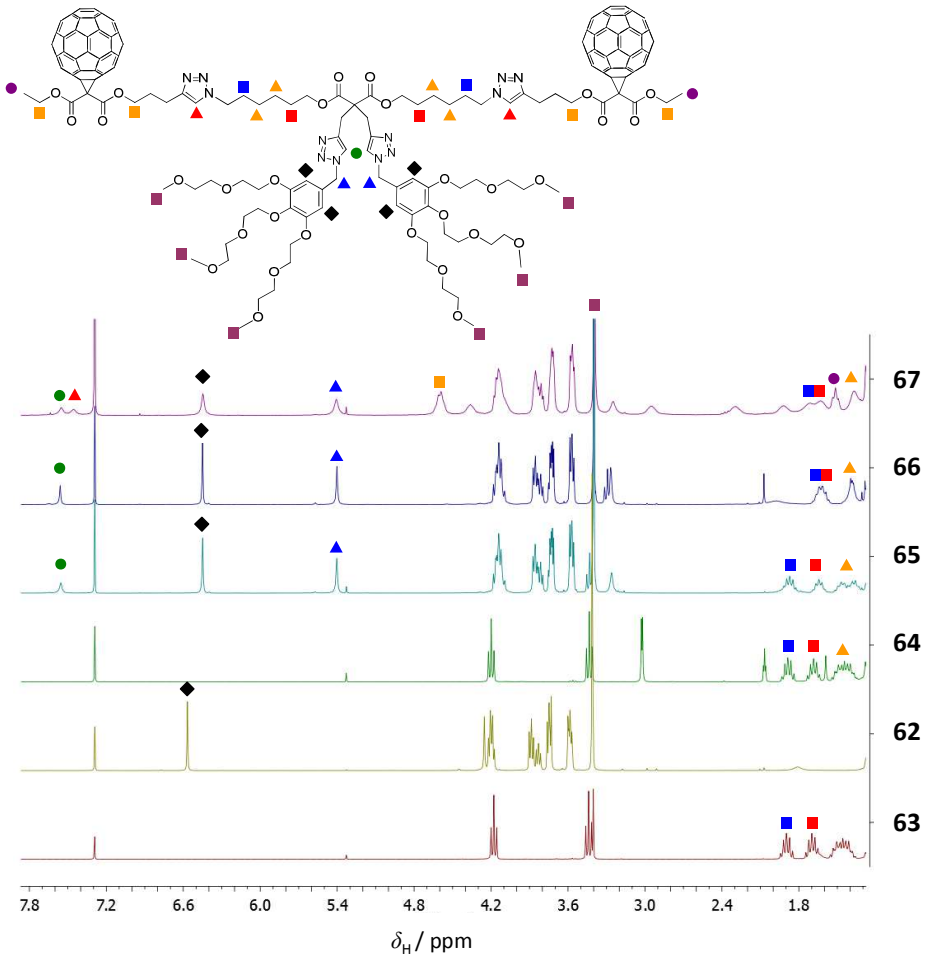

Figure 77. ^{1}H-NMR spectral evolution for the compounds found in Scheme 15.

Regarding the bispropargylic malonate **64**, the modification of the singlet signal in **63**, corresponding to the protons in α position with respect to the carbonyl carbons, by the typical propargyl doublet (3.02 ppm) and triplet (2.07 ppm) was the most relevant evidence. Thereafter, the alkynes were functionalized via CuAAC with the benzyl azide **62** to get **65**. Due to the similarity in polarity between **62** and **65**, the separation of both compounds in the reaction crude was done using a size-exclusion chromatography (Sephadex LH-20). It is interesting to see in Figure 11 how the spectrum of **65** is almost the sum of those of **62** and

64. Two main differences may be noticed: the appearance of the triazole protons at 7.57 ppm, and the disappearance of the terminal alkyne triplets at 2.07 ppm.

Thereafter, the terminal Br atoms were substituted by N_3, what, for example, was observed in the ^{1}H-NMR spectrum in terms of a shielding of the methylene protons attached to this group, from 3.43 in **65** to 3.29 ppm in **66**, as well as the typical azide stretching band at 2095 cm^{-1} in the FTIR spectrum. Finally, a second CuAAC reaction was performed between bis-azide **66** and the asymmetric [60]fullerene monoadduct **57**. In this reaction, an excess of **57** was used in order to ensure the complete functionalization of **66**. The purification was easy to carry out by silica column chromatography, since elution of the excess of **57** was rapidly achieved by using CH_2Cl_2 as the eluent and **67** was obtained afterwards by increasing the polarity to CH_2Cl_2:MeOH (95:5, v/v). According to Figure 77, a new singlet signal was observed at 7.46 ppm belonging to the new triazole rings, as well as those protons arising from the side chains of the [60]fullerene monoadduct (in the 3.6 - 4.1 ppm range).

Finally, cationic [60]fullerene monoadducts were also synthesized as photosensitizer analogues of the fluorescent cationic probes prepared for the interaction assays with *H. pylori*. According to Scheme 46, malonate **26** and its corresponding [60]fullerene monoadduct **30** were used as central scaffolds for their functionalization via CuAAC using the azide **41**. Subsequently, deprotection using HCl 4 M in dioxane afforded the hydrochlorides **70** and **71**, respectively.

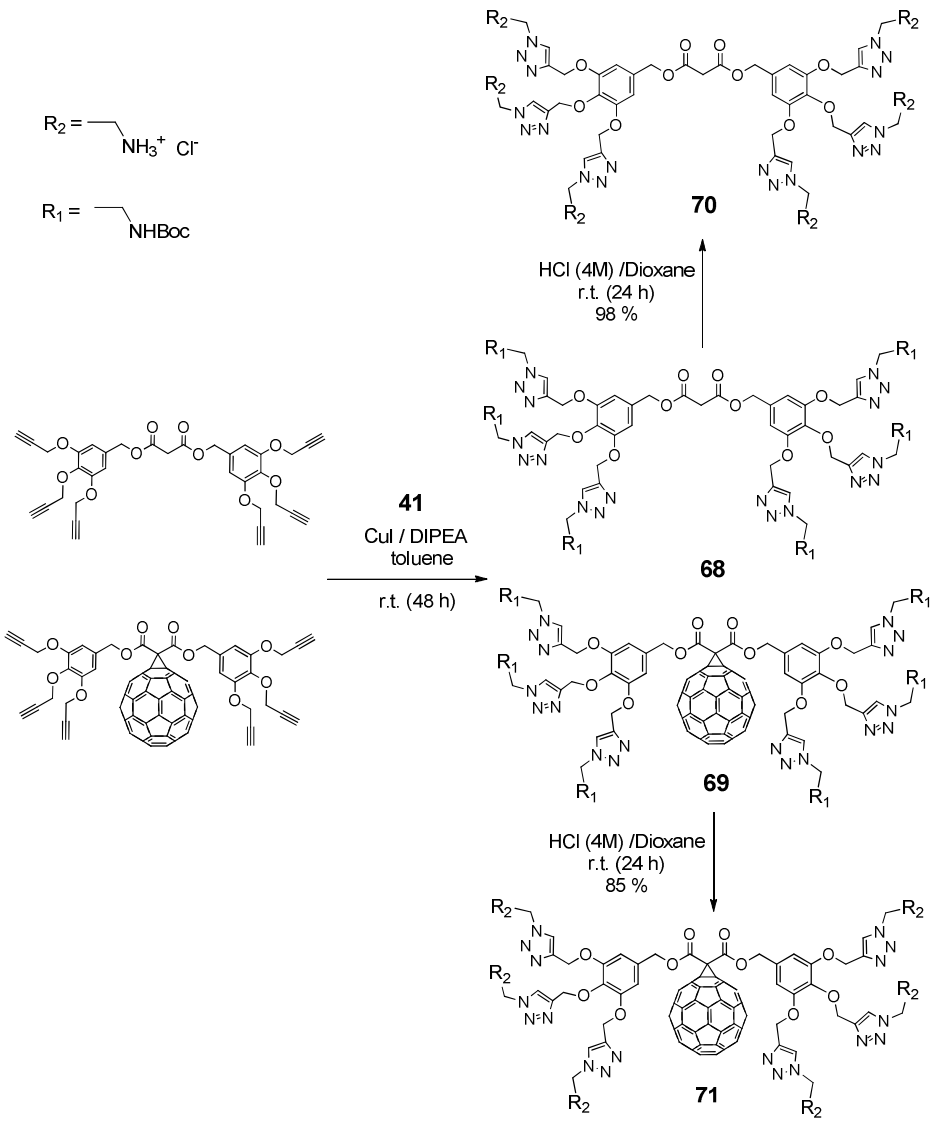

Scheme 46. Synthesis of hexacationic malonate and its corresponding [60]fullerene monoadduct.

9.1.6. Synthesis of mesoporous/magnetic silica nanoparticles and functionalization with [60]fullerene monoadducts

All the previous synthetic approaches have been focused on compounds which could be used in homogeneous solution. However, the functionalization of solid nanomaterials with [60]fullerene to get nanoheterogeneous photosensitizers, even with magnetic properties, has also been explored.

For this aim, clickable mesoporous silica nanoparticles were obtained according to the steps shown in Scheme 47.[165] In the first step, a mixture of (3-azidopropyl)triethoxysilane and tetraethylortosilicate (TEOS) was added to a basic aqueous solution of hexadecyltrimethylammonium bromide (CTAB) surfactant, where [CTAB] > cmc (0.92 to 1.0 mM in water, Sigma-Aldrich product information sheet). In contact with basic aqueous media, the hydrolysis of ethoxysilane groups led to the polymerization of Si–O bonds, including the 3-azidopropyl chain. In this process, the CTAB aggregates are occluded from the particle's surface to their bulk. The same nanoparticle synthesis was done without introducing the azide moiety as a control. In both cases, the mesoporous structure arised after surfactant removal.This procedure can be typically accomplished by calcination, but the presence of the 3-azidopropyl chains prevented this approach. However, this goal was achieved by refluxing the pore occluded nanoparticles in a mixture of methanol and HCl 12 M for 6 hours.

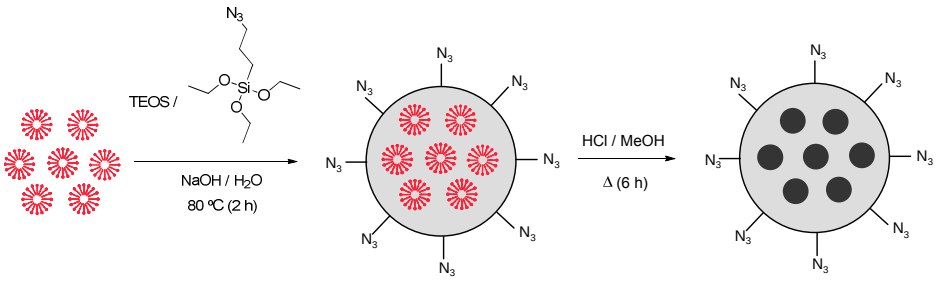

Scheme 47. Synthesis of clickable mesoporous silica nanoparticles.

Figure 78 depicts the FTIR spectra recorded for these nanoparticles. Spectrum **a** corresponds to the pore-occluded nanoparticles without the presence of azide groups. The C–H stretching bands due to the surfactant were present, but they

[165] A. Noureddine, M. Gary-Bobo, L. Lichon, M. Garcia, J. I. Zink, M. W. C. Man, X. Catto. *Chem. Eur. J.*, **2016**, *22*, 9624.

disappeared after the treatment with HCl in methanol, proving the surfactant removal. In the case of the azide functionalized nanoparticles (spectrum **c**. Figure 76), this disappearance was not observed as the alkyl chains bearing the azide groups could contribute to these signals too. However, it is important to point out the appearance of a band at 2102 cm^{-1}, showing the presence of azido groups in the nanoparticles.

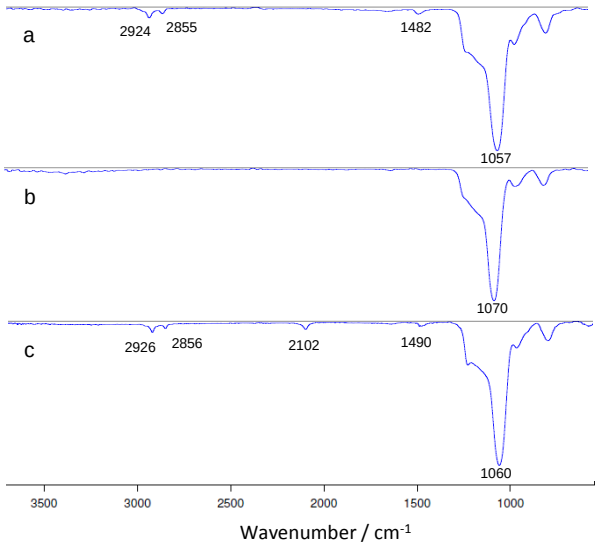

Figure 78. FTIR spectra for pore occluded mesoporous silica nanoparticles (a), after surfactant removal (b) and the nanoparticles functionalized with azido groups (c).

The TEM images (Figure 79) for these functionalized nanoparticles showed spherical particles with diameters in the order of 100 nm, as well as an inner porous structure due to the CTAB assisted synthesis.

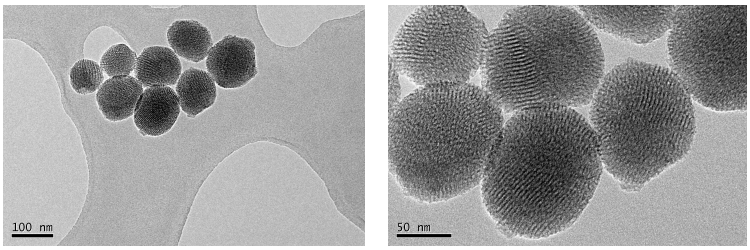

Figure 79. TEM images of the synthesized mesoporous silica nanoparticles.

Moreover, clickable nanoparticles showing magnetic properties were also prepared, as their removal and / or induced mobility using external magnetic fields is also of interest. As it is possible to see in Figure 80, Fe_3O_4-magnetite nanoparticles using $FeCl_2 \cdot 4H_2O$ and $FeCl_3$ in basic and deoxygenated water (co-precipitation method) were obtained in the first step.[166] The inert atmosphere prevented the oxidation of Fe(II) to Fe(III). Thereafter, these nanoparticles were stabilized with sodium citrate.[167] Finally, the magnetic core was coated with TEOS, and 3-azidopropyl chains. Figure 81 shows a suspension of these magnetic silica nanoparticles and how they can be removed from an aqueous solution by using an external magnet.

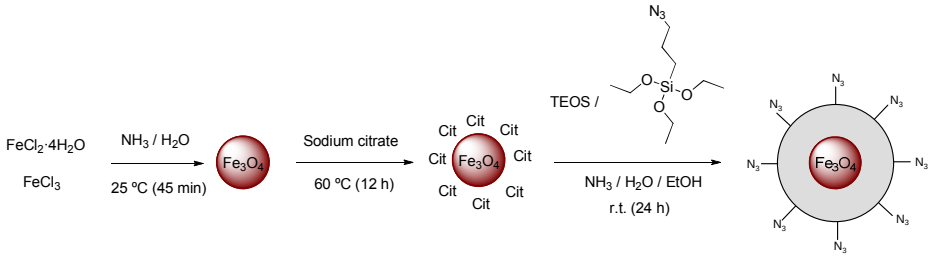

Figure 80. Synthesis of clickable magnetic silica nanoparticles ($Fe_3O_4@SiO_2–N_3$).

Figure 81. Aqueous suspension of $Fe_3O_4@SiO_2–N_3$ nanoparticles (left) and their removal from the aqueous phase by the use of a magnetic field (right).

Figure 82 shows the X-Ray diffractograms collected for Fe_3O_4 nanoparticles synthesized using the co-precipitation method (chart **a**), the Fe_3O_4 nanoparticles stabilized with sodium citrate (chart **b**) and the $Fe_3O_4@SiO_2–N_3$ nanoparticles (chart **c**). These diffractograms confirmed the synthesis of magnetite phase, exhibiting a diffraction pattern in agreement with that for standard Fe_3O_4 particles, indexed as Miller index (h k l): (2 2 0), (3 1 1), (4 0 0), (4 2 2), (5 1 1)

[166] K. Petcharoen, A. Sirivat. *Mat. Sci. Eng. B*, **2012**, *177*, 421.
[167] C. Hui, C. Shen, J. Tian, L. Bao, H. Ding, C. Li, Y. Tian, X. Shi, H.-J. Gao. *Nanoscale*, **2011**, *3*, 701.

and (4 4 0). Regarding diffractograms **a** and **b**, they were nearly the same, indicating that the sodium citrate modification had little effect on the XRD intensity of Fe_3O_4 nanoparticles. However, the intensity in diffractogram **c** was weaker than that for **a** and **b** (especially for (4 2 2), (5 1 1) and (4 4 0) peaks), which could be explained taking into account the shielding effect of amorphous silica shell, as well as the broad band found between 2 theta = 20º and 25º. On the other hand, from the broadening of the peaks in XRD spectra, it was possible to calculate the size of the magnetite core using the Scherrer equation [39], where τ is the mean size, K, a dimensionless shape factor (0.89 for spheres), λ, the X-ray wavelength (0.154 nm for Cu-alpha), β, the line broadening at half the maximum intensity (FWHM) in radians and θ, the Bragg angle.

$$\tau = (K \cdot \lambda) / (\beta \cdot \text{Cos}\,\theta) \text{ [39]}$$

The calculated particle size using [1] and considering (3 1 1) peak was 13 nm.

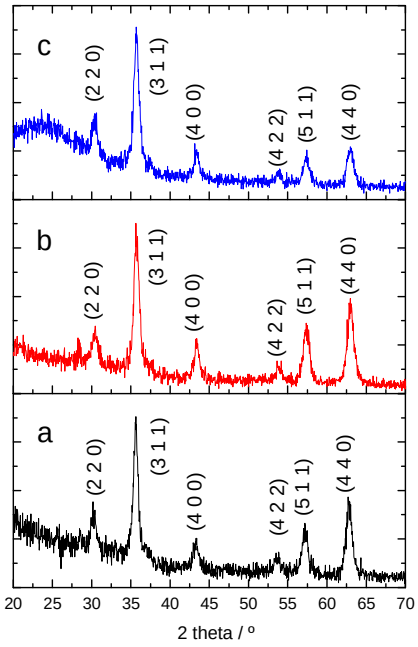

Figure 82. X-ray diffractograms for synthesized Fe_3O_4 nanoparticles (a), Fe_3O_4 nanoparticles stabilized with sodium citrate (b) and Fe_3O_4@SiO_2–N_3 nanoparticles (c).

Finally, these nanoparticles were functionalized via CuAAC with the asymmetric [60]fullerene monoadduct **57**, using CuI and DIPEA. Figures 83a and 83b show the FTIR spectra for **57** and Fe_3O_4@SiO_2 $–N_3$ nanoparticles respectively. After the reaction, some remaining azide band was still observed. However, it is interesting to remark the appearance of the C=O stretching band due to the malonate attached to the [60]fullerene (Figure 83c).

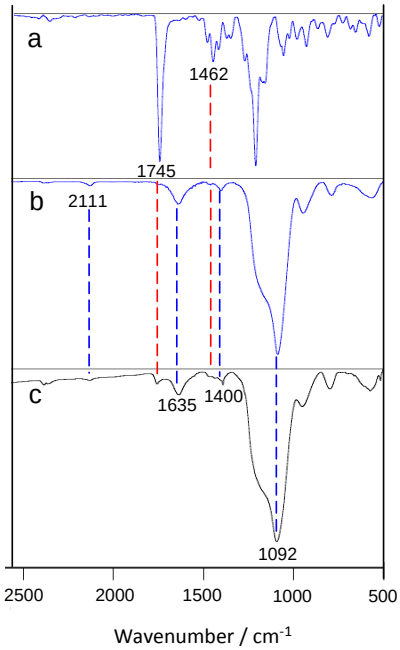

Figure 83. FTIR spectra for **57** (a), Fe_3O_4@SiO_2 $–N_3$ nanoparticles (b) and functionalized nanoparticles after CuAAC (c).

In the same manner, the mesoporous silica nanoparticles decorated with azide groups were functionalized with **57** via CuAAC. Two different batches were obtained depending on whether the reaction was carried out under reflux or not. In order to compare the influence on the photophysical properties when [60]fullerene monoadduct is covalently bound to the silica surface, a control sample was prepared where pristine [60]fullerene was immobilized on the particles without the azide groups.

9.2. Photophysical characterization

9.2.1. Absorption properties and $^1O_2$ production of the [60]fullerene derivatives

Table 15 summarizes the UV-vis absorption properties for a series of [60]fullerene monoadducts soluble in toluene. A similar behaviour was found in all the derivatives: a strong absorption band located around 330 nm with absorption coefficients as high as 40 000 M^{-1} cm^{-1}, a weak sharp peak at 428 nm and a broad band with a maximum located near 490 nm.

Table 15. Absorption properties for [60]fullerene monoadducts in toluene. Experimental uncertainty in λ_{abs}^{max} ± 1 nm and in ε ± 5%.

Compound	λ_{abs}^{max} / nm	ε / $M^{-1} \cdot cm^{-1}$
28	331 428 491	41146 2270 1400
29	331 428 491	39357 2430 1560
30	331 428 491	42068 2690 1850
50	329 428	35109 4460
53	331 428 491	38715 2670 1730
55	331 428 489	40002 2620 1700
57	330 428 487	38430 3800 2700
60	331 428 491	41078 3170 2040

The only compound which showed a different absorption spectrum was **50**, since its bands were wider than those of the other compounds, and it was not possible to distinguish a maximum for the band in the visible region near 490 nm. In this

sense, Figure 84 shows an illustrative comparison between the absorption spectra of **28** and **50.** These changes could be attributed to the self-aggregation of **50**, decorated with peripheral ethylene glycol chains, in an apolar solvent such as toluene.

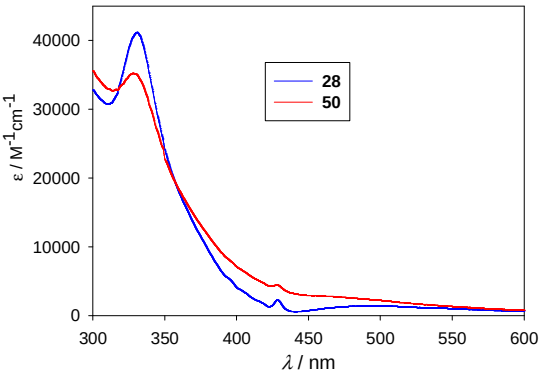

Figure 84. Comparison of UV-vis spectra between [60]fullerene monoadducts **28** and **50** in toluene.

$^1O_2$ phosphorescence decay traces recorded at 1270 nm, like those shown for **28** and **50** in Figure 85, were fitted to equation [40]. This equation is based on the same principles which were explained for [15] (2.3.1 section), although two modifications must be considered: Y_0 represents the baseline and 0.08 is an instrumental parameter which corresponds to the temporal delay related to the laser pulse triggering.

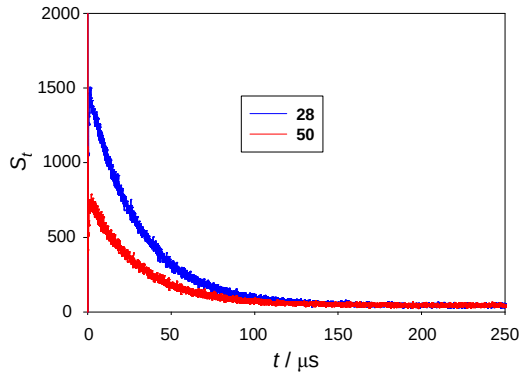

Figure 85. Comparison of $^1O_2$ decay traces between toluene solutions of [60]fullerene monoadducts **28** and **50**.

$$S_t = \left(S_0 \cdot \frac{\tau_\Delta}{\tau_\Delta - \tau_T} \cdot \left[e^{-\frac{t-0.08}{\tau_\Delta}} - e^{-\frac{t-0.08}{\tau_T}} \right] \right) + Y_0 \quad [40]$$

Table 16 summarizes τ_Δ, τ_T, S_0 and Y_0 values ranging from the experimental fittings. The measured τ_Δ values were slightly lower than $\tau_{\Delta 0}$ (31.9 μs in toluene [168]) due to some $^1O_2$ quenching by each derivative. Knowing the concentration for the [60]fullerene monoadducts, k_q^Δ values were calculated using the Stern-Volmer equation (similar to [17])

Table 16. Obtained parameters for [60]fullerene monoadducts in toluene from the fittings of the experimental $^1O_2$ decay traces to equation [40] and the corresponding Φ_Δ values. Experimental error: ± 5%. PH represents phenalenone, which was used as the reference compound.

Cpd	[Conc] / M	S_0	τ_Δ / μs	τ_T / μs	Y_0	k_q^Δ / $M^{-1}\cdot s^{-1}$	Φ_Δ [16]	Φ_Δ [41]
28	$5.95\cdot10^{-6}$	1443	30.04	0.321	43	$2.6\cdot10^{8}$	0.94	0.93
29	$4.81\cdot10^{-6}$	989	30.00	0.315	44	$4.1\cdot10^{8}$	0.86	0.92
30	$4.02\cdot10^{-6}$	1271	29.90	0.310	43	$5.2\cdot10^{8}$	0.85	0.80
50	$5.61\cdot10^{-6}$	720	29.77	0.382	45	$4.0\cdot10^{8}$	0.50	0.55
53	$5.54\cdot10^{-6}$	1136	30.02	0.298	44	$3.5\cdot10^{8}$	0.84	0.88
55	$5.27\cdot10^{-6}$	1102	30.06	0.335	44	$3.6\cdot10^{8}$	0.80	0.92
57	$5.47\cdot10^{-6}$	1052	29.96	0.349	44	$3.7\cdot10^{8}$	0.83	0.76
60	$4.67\cdot10^{-6}$	928	29.96	0.307	45	$4.3\cdot10^{8}$	0.75	0.83
PH 1	$2.26\cdot10^{-5}$	2225	29.81	0.289	44	-	0.94	
PH 2	$1.50\cdot10^{-5}$	1535	29.81	0.281	43			
PH 3	$4.4\cdot10^{-6}$	547	29.63	0.285	43			

In order to determine Φ_Δ values for these compounds, a calibration plot using phenalenone as the reference photosensitizer was built, corelating the portion of photons absorbed at 355 nm ($1\text{-}10^{-A(355nm)}$) with S_0 values. It is interesting to see in Figure 86 how, as the absorbance of phenalenone becomes lower, the intensity of $^1O_2$ phosphorescence traces decrease, due to the fact that fewer excited states are generated. Figure 87 (left) depicts the calibration plot ((S_0 = (8

[168] O. Shimizu, J. Watanabe, K. Imakubo, S. Naito. *Chem. Lett.*, **1999**, *28*, 67.

± 28) + (5600 ± 100)·(1-10$^{-A(355)}$), with r = 1.0) and Figure 87 (right), the interpolation of [60]fullerene derivatives in this plot.

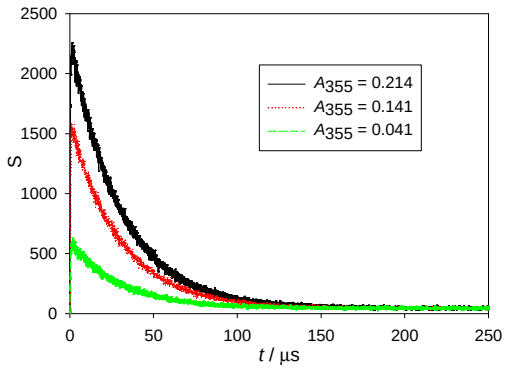

Figure 86. $^1O_2$ decay traces from phenalenone reference solutions in toluene.

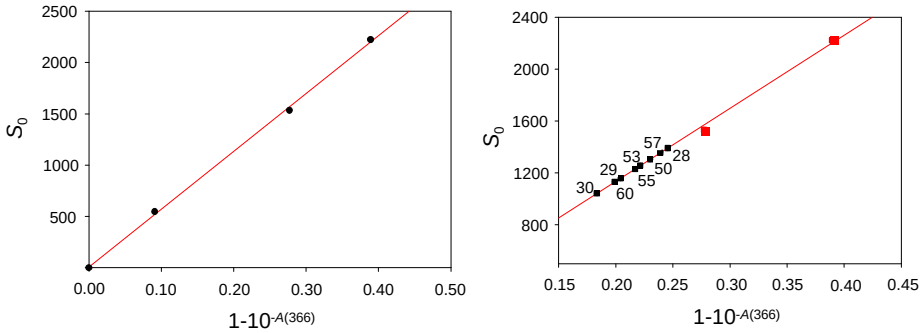

Figure 87. Experimental calibration plot using phenalenone in toluene (left) and interpolation of [60]fullerene monoadducts in this plot (right).

Considering this calibration plot and taking into account the absorbance values at 355 nm, the corresponding $S_{0,Ref}$ were calculated to be applied in equation [16] (2.3.1 section). For this equation, the value $\Phi_{\Delta,Ref}$ = 0.94 ± 0.04 was considered in order to calculate Φ_Δ reported in Table 16. Φ_Δ can be also calculated using equation [41], without considering a calibration plot but a single point and correcting by the absorbance at 355 nm for the phenalenone solution (A_{ref}).

$$\Phi_\Delta = \Phi_{\Delta,Ref} \cdot \frac{S_0}{S_{0,Ref}} \cdot \frac{A_{Ref}}{A} \quad [41]$$

The singlet oxygen quantum yields obtained in toluene for the [60]fullerene monoadducts agree well with what could be expected, and with typical values mentioned in the general background section. However, compound **50** is an exception, as the quantum yield drops to 0.55. It is interesting to compare together the changes aforementioned in UV-vis absorption spectra (Figure 84) and the decrease in the intensity for $^1O_2$ phosphorescence decay trace (Figure 85). As it was thought that the photosensitizer self-aggregation could be playing a key role in its ability for $^1O_2$ generation, Φ_Δ was determined increasing the concentration in toluene and considering other solvent with different polarity such as methanol. Due to the increment of concentration in comparison to the values shown in Table 16, the excitation wavelength was changed to 532 nm. As a consequence, the reference photosensitizers chosen were Rose Bengal (RB, for measurements in methanol) and tetraphenylporphyrin (TPP, for measurements in toluene). Experimental data arising from the fittings for $^1O_2$ phosphorescence decay traces are summarized in Table 17.

Table 17. Obtained parameters for **50** in toluene and methanol from the fittings of the experimental $^1O_2$ decay traces to equation [40] and the corresponding Φ_Δ values. Experimental error: ± 5%.

[50] / M	**Solvent**	S_0	τ_Δ / µs	τ_T / µs	Y_0	Φ_Δ
$2.21\cdot10^{-4}$	Toluene	20023	29.95	0.416	156	0.47
$1.33\cdot10^{-5}$	Methanol	23000	10.11	0.360	486	0.49
$5.14\cdot10^{-5}$	Methanol	99647	9.94	0.385	476	0.58
Reference TPP $8.8\cdot10^{-6}$	Toluene	33281	30.08	0.381	159	0.78[21b]
Reference RB $1.9\cdot10^{-6}$	Methanol	37266	9.96	0.481	496	0.80[40b]

From these results it is not possible to conclude that changes in concentration and type of solvent, at least in the concentration range explored, have an influence in Φ_Δ, and a basal value around 0.5 is characteristic for this compound.

In the same manner, the ability for $^1O_2$ generation was studied for the glycofullerenes **31**, **32** and **33** in D_2O (taking advantage of longer $^1O_2$ lifetimes

in D_2O, τ_Δ = 64.4 μs, than in H_2O, where τ_Δ = 4.4 μs[21b]). Figure 88 shows the UV-vis spectra for these compounds in D_2O, where it is possible to see that the trends pointed out for compound **50** are even more evident: the band broadening led to the disappearance of those bands located at 330 nm and also the weak and narrow one at 428 nm (compare with Figure 84). The self-aggregation commented in the structural characterization (Figure 71) could explain this behaviour.

In this case, sulfonated phenalenone was used as reference photosensitizer to calculate Φ_Δ values. Due to the practical restrictions imposed by the use of D_2O, a calibration plot with this reference was not built, but a single point with similar absorbance at 355 nm was used for the calculations (A_{355} = 0.126, concentration = $1.32 \cdot 10^{-5}$ M)

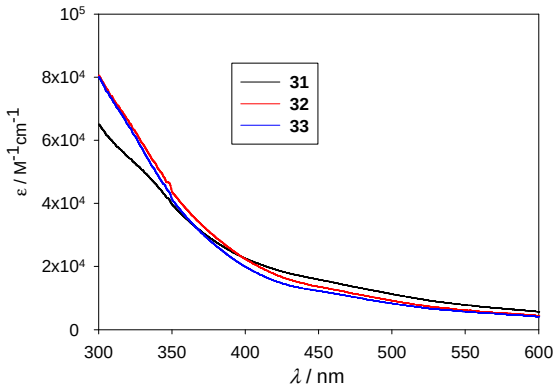

Figure 88. Comparison of UV-vis spectra between glycofullerenes **31**, **32** and **33** in D_2O.

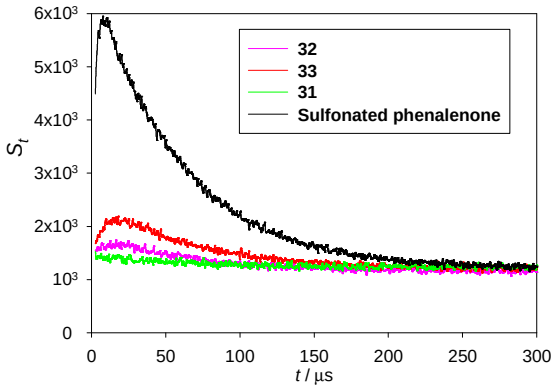

Figure 89. $^1O_2$ decay traces at 1270 nm of D_2O solutions of glycofullerenes **31**, **32** and **33**, and sulfonated phenalenone used as the reference.

Figure 89 depicts the $^1O_2$ phosphorescence decay traces of sulfonated phenalenone used as the reference compound and those of **31**, **32** and **33**. The characterization was also performed for the cationic derivative **71**. The experimental data obtained from the fittings to equation [41] are summarized in Table 18. Quantum yields for singlet oxygen production were determined using equation [16]

Table 18. Experimental conditions and photophysical parameters for glycofullerenes in D_2O from the fittings of the experimental $^1O_2$ decay traces to equation [40], in the presence and absence of NaN_3, and the corresponding Φ_Δ values. Experimental uncertainty: ± 5%.

Cpd	[Conc] / M	A_{355}	S_0	τ_Δ µs	τ_T µs	Y_0	k_q^Δ $M^{-1}\cdot s^{-1}$	Φ_Δ
31	$3.50\cdot10^{-6}$	0.1677	218	63	-	1232	$9.9\cdot10^{7}$	0.039
32	$2.94\cdot10^{-6}$	0.1618	643	64	4.4	1156	$3.3\cdot10^{7}$	0.13
33	$2.82\cdot10^{-6}$	0.1488	1203	61.4	6.4	1202	$2.7\cdot10^{8}$	0.26
71	$3.50\cdot10^{-6}$	-	-	65	-	-	-	0.035
32 + NaN_3	-	-	330	7.8	-	1212	-	-
33 + NaN_3	-	-	400	8.6	-	1211	-	-

It is interesting to compare the shape of the traces obtained for these compounds and those shown, for example, in Figure 86. The rising time observed in D_2O was slower than that in toluene and this fact resulted in longer τ_T values (τ_T(**32**) = 4.4 µs while τ_T(**29**) = 0.315 µs and τ_T(**33**) = 6.4 µs while τ_T(**30**) = 0.310 µs) although it was not possible to determine it for **31** and **71** (for this reason both traces were fitted to a monoexponential decay). Regarding Φ_Δ, a significant decrease can be observed in comparison to the parent [60]fullerene monoadducts not functionalized with the glycodendrimeric structure. From the wide variety of functionalizations explored in Table 16 and the previous knowledge commented in the background section, [60]fullerene monoadducts showed similar Φ_Δ values close to ~0.8. That is the reason why the observed decrease of Φ_Δ for **50** in toluene, and **31**, **32**, **33** and **71** in D_2O could be attributed to the photosensitizer self-aggregation. However, in this case, it is relevant to highlight that, the greater the number of sugar units, the longer τ_T and, interestingly, Φ_Δ. Finally, when

NaN_3 (1mM) was added, $^1O_2$ emission was efficiently quenched and τ_Δ decreased drastically (Figure 90), confirming that this component in the biexponential equation [40] represents the $^1O_2$ lifetime.

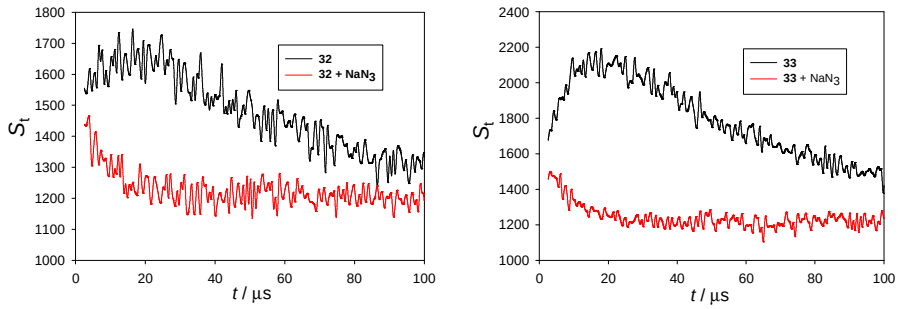

Figure 90. $^1O_2$ decay traces in D_2O solution of glycofullerenes **32** and **33** in the presence (red) and absence (black) of NaN_3.

In the same manner, the $P(T_1)$ quenching rate constant by molecular oxygen was determined by measuring the $^1O_2$ emission traces in O_2-saturated D_2O solutions. Figure 91 represents these traces for compounds **32** and **33** in air equilibrated and oxygen saturated solutions. It is possible to see that in oxygen saturated solutions, the rising times of the traces were faster for both compounds and the maxima were reached at shorter times, due to a more efficient $P(T_1)$ quenching by molecular oxygen. As a consequence, triplet excited state lifetimes obtained from the experimental fittings were shorter in oxygen saturated D_2O solutions (Table 19).

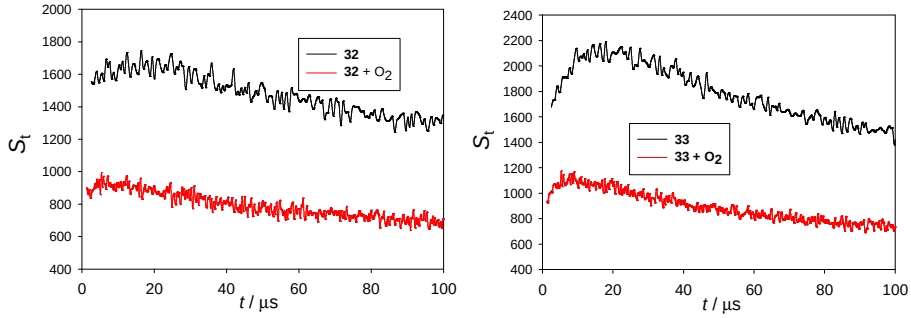

Figure 91. Comparison of $^1O_2$ decay traces for glycofullerenes **32** and **33** in air equilibrated (black) and oxygen saturated (red) D_2O solutions.

In order to calculate the bimolecular quenching rate constants in water using the Stern-Volmer equation (eq [17]), it was assumed a value of $[O_2]$ = 0.27 mM in

air equilibrated solutions and $[O_2]$ = 1.27 mM in oxygen saturated solutions.[169] From eq [17] and the experimental data it was possible to calculate, as well, the triplet state lifetime under O_2-free conditions (τ_{T0}, in the absence of quencher).

Table 19. Photophysical parameters of glycofullerenes **32** and **33** from the fittings of the experimental $^1O_2$ decay traces to equation [40], in O_2-saturated D_2O solutions. Experimental error: ± 5%.

Compound	S_0	τ_Δ / µs	τ_T / µs	Y_0	τ_{T0} / µs	k_q / $M^{-1}\cdot s^{-1}$
32 + O_2	343	61	1.4	622	16.9	$3.6\cdot10^8$
33 + O_2	549	60	1.94	625	10.5	$4.9\cdot10^8$

Table 20. τ_Δ values for silica nanoparticles (dispersed in ethanol and in solid state). [1]: λ_{exc} = 355 nm. [2]: λ_{exc} = 532 nm.

	Dispersed in ethanol		**Solid state**	
	τ_Δ / µs	τ_T / µs	τ_Δ / µs	τ_T / µs
Immobilized pristine [60]fullerene	14.6 ± 0.1[1]	0.31 ± 0.01[1]	640 ± 40[1]	-
Mesoporous SiO_2 – **57** (CuAAC reflux)	0.54 ± 0.07[1]	-	-	-
Mesoporous SiO_2 – **57** (CuAAC r.t.)	6.8 ± 0.2[1]	-	-	-
Fe_3O_4@SiO_2 – **57** (CuAAC reflux)	9.9 ± 0.6[1]	-	260 ± 10[2]	-
Fe_3O_4@SiO_2 – **57** (CuAAC 60 ºC)	7.1 ± 0.8[1]	-	310 ± 10[2]	-

At a preliminary level, τ_Δ have been measured for the mesoporous silica nanoparticles functionalized with **57**, dispersed in ethanol and in solid state, as well as the particles bearing the immobilized pristine [60]fullerene and the magnetic Fe_3O_4@SiO_2 nanoparticles functionalized with **57** (Table 20). In all the cases, τ_Δ decreases when [60]fullerene is covalently bound to the nanoparticle

[169] M. Montalti, A. Credi, L. Prodi,M. T. Gandolfi. Handbook of Photochemistry, 3rd ed.; CRC Press: Boca Raton, FL, 2006; Chapter 9, pp. 535-559.

with **57**, in comparison with pristine [60]fullerene. However, τ_Δ are similar between mesoporous SiO_2 functionalized with **57** (CuAAC carried out at r.t.), Fe_3O_4@SiO_2 nanoparticles functionalized with **57** (CuAAC carried out at toluene reflux) and Fe_3O_4@SiO_2 nanoparticles functionalized with **57** (CuAAC carried out at 60ºC). Interestingly, measurements performed in solid state afforded τ_Δ values above 100 µs, what opens the door to consider the use of these derivatives as solid phases to perform reactions without solvents, like the photooxidation of thioketones commented in Chapter 1.

9.2.2. Absorption and emission properties of fluorescein derivatives

Regarding the synthesized fluorescent probes, photophysical characterization was focused on both absorption and emission properties. Table 21 summarizes the absorption maxima and their corresponding absorption coefficients, and their emission maxima as well.

Normalized absorption and emission spectra of each compound are plotted in Figure 92, between 400-525 nm and 475-600 nm, respectively. It must be pointed out that the spectra of **34**6, **35**, **36**, **42** and **43** were measured in methanol as the solvent, but glycofluoresceins **37** and **38**, and the cationic fluoresceins **44** and **45** were measured in water. Emission spectra shown in Figure 92 were previously smoothed using the Savitzky-Golay filter (20 points). From these spectra it is possible to observe several changes depending on the molecular structure of the probe. First of all, only the fluorescein methyl ester **35** (spectrum b. Figure 92) resembles the shape shown by fluorescein in aqueous NaOH 0.1 M (spectrum j. Figure 92). When the phenoxy group in the fluorescein core is functionalized, the absorption spectrum in the visible region consists in two bands whose maxima are located around 456 and 485 nm, with a shoulder around 435 nm. However, this shoulder is less evident in those spectra recorded in water. Moreover, the absorption coefficients at 456 and 485 nm tend to be more similar than in methanol. In general, the emission spectra showed a wider band compared with that of fluorescein, with a maximum located around 516 nm (batochromically shifted to 524 nm in the case of **35**).

Table 21. Absorption and emission properties of fluorescent probes in methanol or water. Experimental uncertainty in λ_{abs}^{max} and λ_{em}^{max} ± 1 nm, and in ε and τ_{fluo} ± 5%.

Compound	Solvent	λ_{abs}^{max}	ε / $M^{-1} \cdot cm^{-1}$	λ_{em}^{max}	τ_{fluo} / ns
34	MeOH	263 309 363 457 485	19336 10300 11837 27058 20972	516	2.3
35	MeOH	265 321 360 503	16400 8900 5800 50164	524	4.0
36	MeOH	363 456 484	6906 21474 16474	517	2.2
37	H_2O	267 378 458 483	16700 6799 22755 20044	516	3.1
38	H_2O	306 379 456 480	6931 6904 21164 18703	518	2.7
42	MeOH	267 311 363 457 485	12280 5624 6334 23581 18564	516	2.4
43	MeOH	264 311 363 458 487	17275 9525 9300 24325 19400	517	2.5
44	H_2O	232 255 307 382 455 478	42742 16300 6630 7492 25721 23228	516	2.7
45	H_2O	232 308 383 456 481	38839 5967 6620 23968 22161	516	3.3

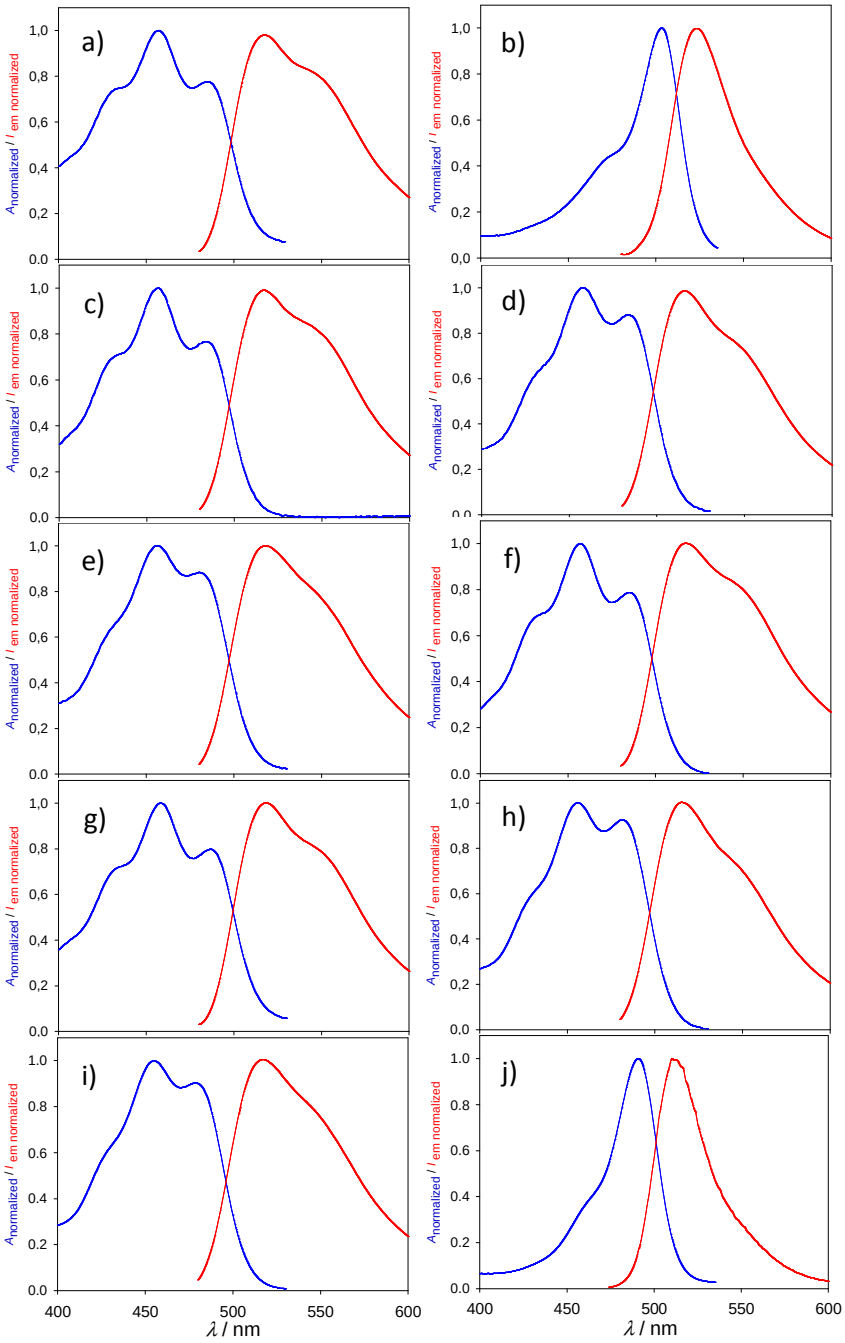

Figure 92. Normalized absorption (blue) and emission (red. λ_{exc} = 457 nm) spectra of **34** (a), **35** (b), **36** (c), **37** (d), **38** (e), **42** (f), **43** (g), **44** (h), **45** (i) and fluorescein in aqueous NaOH 0.1 M (j).

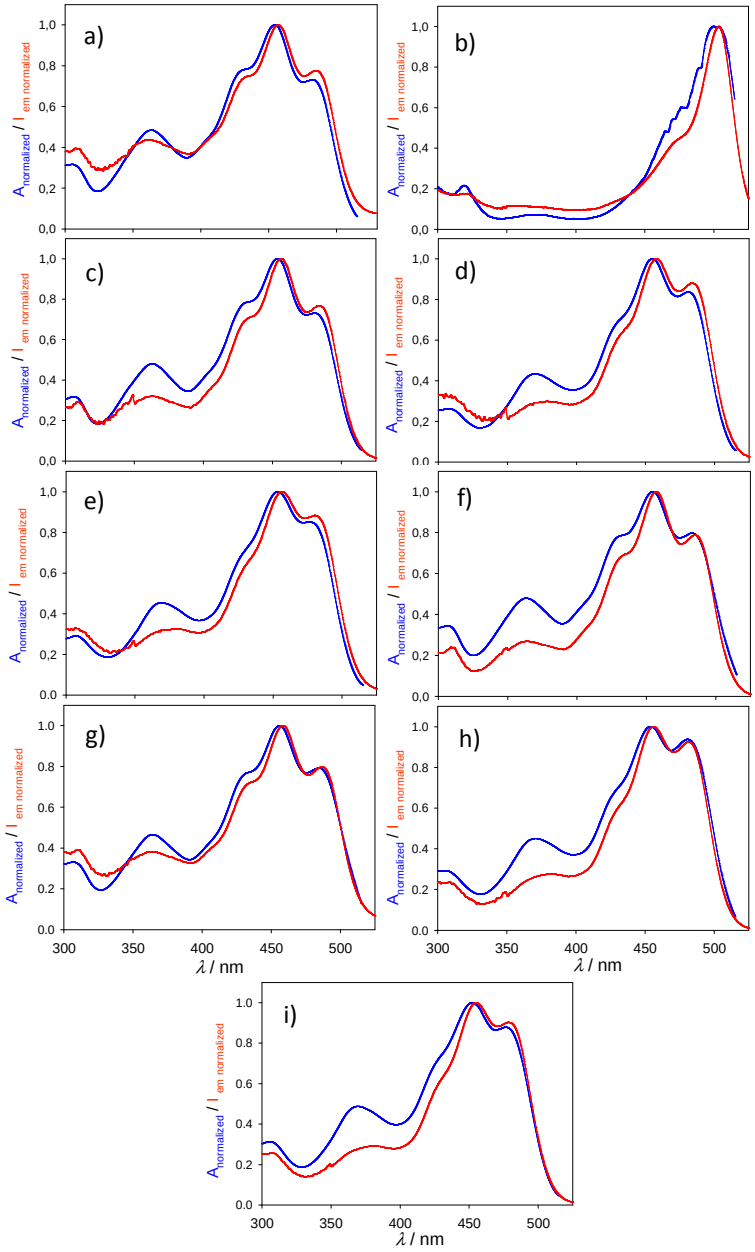

Figure 93. Absorption (blue) and excitation (red. λ_{em} = 525 nm) spectra of **34** (a), **35** (b), **36** (c), **37** (d), **38** (e), **42** (f), **43** (g), **44** (h) and **45** (i).

Time-resolved emission decay traces of each fluorescent probe were recorded at 516 nm. Fitting to a monoexponential decay function afforded the corresponding fluorescence lifetimes (τ_{fluo}) summarized in Table 21. Fluorescence lifetimes were shorter when the phenoxy group was functionalized, although the lifetime values showed a dependence on the structural peculiarities of each probe. For example, the fluorescence lifetime of glycofluorescein **37**, bearing two glycodendrimer units is remarkably longer than that of the bispropargylated fluorescein **34.** Similarly, a slight increment was observed for **43** and an even longer value for the dicationic fluorescein **45**.

Compounds **37**, **43** and **45** have in common the presence of bulky groups attached to the ester group. As previously mentioned, these groups could prevent the rotation of the single bond connecting the xanthene moiety and the aromatic ring bearing the ester group. As a result, the deactivation channel through internal conversion (rotational relaxation) could be minimized and the excited singlet, therefore, stabilized.

The excitation spectra of these probes were recorded (Figure 93) at 525 nm. The similarity between the absorption and the excitation spectra of each compound supported that only a fluorophore/excited state was present/populated in the sample (leading to the recorded monoexponential emission decays).

Fluorescence quantum yields were also determined. In this case, the calibration plot was built representing the area (F) under the emission spectra between 474 and 800 nm as a function of the portion of photons absorbed at 470 nm, $1\text{-}10^{-A(470nm)}$ (Figure 94). Fluorescein in NaOH 0.1 M was used as the reference. Since the calibration plot was not linear, a second order polynomial regression was performed ($y = A + Bx + Cx^2$, where A = -50900, B = $4.02\cdot10^8$ and C = $-2.7\cdot10^8$). Equations [42] and [43] were used in order to determine Φ_f. Both of them consider the correction by the refractive index (n) of the solvent, since some measures were carried out in methanol, while the fluorescein reference solution was dissolved in water.

$$\Phi_f = \Phi_{f,Ref} \cdot \frac{F}{F_{Ref}} \cdot \frac{n_r^2}{n^2} \quad [42] \qquad \Phi_f = \Phi_{f,Ref} \cdot \frac{F}{F_{Ref}} \cdot \frac{A_{Ref}}{A} \cdot \frac{n_r^2}{n^2} \quad [43]$$

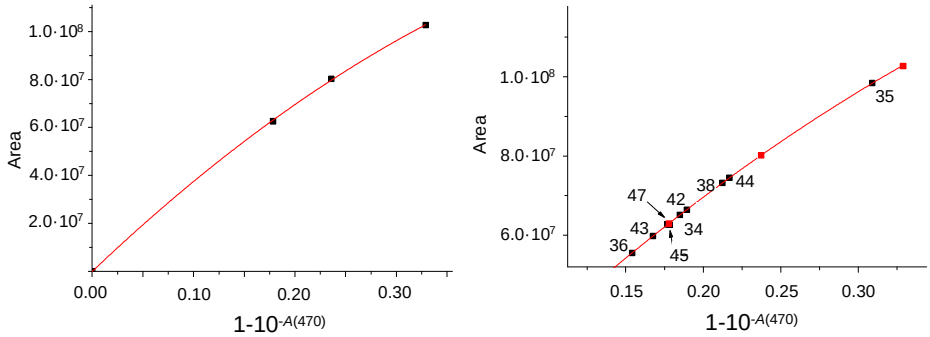

Figure 94. Calibration plots using fluorescein in aqueous NaOH 0.1 M solutions (left) and interpolation of fluorescent probes in this calibrate (right).

Equation [42] was used considering the calibration plot shown in Figure 94 and equation [43], considering only the reference point with the closest absorbance to each compound.

Table 22. Experimental parameters for determining Φ_f values according to equations [42] and [43]. Experimental error: ± 5%. Fl represents fluorescein.

Compound	A_{470}	F	Φ_f (eq [42])	Φ_f (eq [43])
34	0.0889	$1.19 \cdot 10^7$	0.17 ± 0.01	0.17 ± 0.01
35	0.1605	$7.04 \cdot 10^7$	0.66 ± 0.03	0.68 ± 0.03
36	0.0726	$9.12 \cdot 10^6$	0.15 ± 0.01	0.16 ± 0.01
37	0.0845	$1.37 \cdot 10^7$	0.20 ± 0.01	0.22 ± 0.01
38	0.1037	$1.46 \cdot 10^7$	0.18 ± 0.01	0.19 ± 0.01
42	0.0911	$1.35 \cdot 10^7$	0.19 ± 0.01	0.20 ± 0.01
43	0.0797	$1.07 \cdot 10^7$	0.16 ± 0.01	0.18 ± 0.01
44	0.0850	$1.23 \cdot 10^7$	0.18 ± 0.01	0.20 ± 0.01
45	0.1062	$2.14 \cdot 10^7$	0.27 ± 0.01	0.27 ± 0.01
Fl 1	0.1732	$1.03 \cdot 10^8$	-	-
Fl 2	0.0853	$6.26 \cdot 10^7$	-	-
Fl 3	0.1168	$8.02 \cdot 10^7$	-	-

Table 22 summarizes the quantum yields obtained for all fluorescent probes. In this case, only the dicationic fluorescein probe **45** showed an enhanced Φ_f, mainly due to the aforementioned restricted rotation (Figure 74).

According to equations [44] and [45], the radiative rate constant (k_r), and the non radiative rate constant (k_{nr}) have been determined for each fluorescent probe (Table 23)

$$k_r = \frac{1}{\tau_{fluo}} \quad [44] \qquad k_{nr} = \frac{k_r - \Phi_f k_r}{\Phi_f} \quad [45]$$

Table 23. k_r and k_{nr} values for the fluorescent probes Experimental error: ± 5%.

Compound	k_r / s^{-1}	k_{nr} / s^{-1}
34	$4.3 \cdot 10^8$	$2.1 \cdot 10^9$
35	$2.5 \cdot 10^8$	$1.3 \cdot 10^8$
36	$4.5 \cdot 10^8$	$2.6 \cdot 10^9$
37	$3.2 \cdot 10^8$	$1.3 \cdot 10^9$
38	$3.7 \cdot 10^8$	$1.7 \cdot 10^9$
42	$4.2 \cdot 10^8$	$1.8 \cdot 10^9$
43	$4.0 \cdot 10^8$	$2.1 \cdot 10^9$
44	$3.7 \cdot 10^8$	$1.7 \cdot 10^9$
45	$3.0 \cdot 10^8$	$8.1 \cdot 10^8$

From Table 23, it is interesting to point out, according to the values, that non radiative deactivation channels prevail over the radiative ones. However, this trend is no so evident in compound **45**, the derivative with the lowest k_{nr} value, which can be rationalized due to the presence of bulky substituents attached to the ester group in fluorescein and the restriction of the rotation previously pointed out.

9.3. Aggregation processes and tensioactive behaviour of glycofullerenes

As it has been previously commented in the structural and photophysical characterization sections, self-aggregation of compounds **31**, **32**, **33** and **50** in polar solvents seemed to play a key role in order to explain the decrease in Φ_Δ, in comparison with other [60]fullerene monoadducts soluble in toluene. That is the reason why the aggregation process showed by these glycofullerenes was explored. These molecules, from a structural point of view, consist of a peripheral polar shell formed by the glycodendrimers and a nonpolar carbon core constituted by the [60]fullerene unit. Therefore, a surfactant-like behaviour

could be expected to be observed, so that aggregation phenomena could be monitorized by surface tension measurements. Preliminary experiments using the Du Noüy ring method showed that the changes in surface tension were strongly dependent on time, due to the diffusion of aggregates from the bulk solution to the surface, *i.e.*, the higher amount of aggregate (surfactant) reaching the liquid-air interface, the lower was the surface tension value. In order to study this dynamical behaviour, the pendant drop method was used.

This technique is based on the analysis of the shape of a pendant drop. The forces that determine this shape are the surface tension and gravitation. Surface tension tends to minimize the surface area, leading to spherical shape. According to the Young-Laplace equation, pressure difference (Δp) between the areas inside and outside of a curved liquid interface with the principal radii of curvature (R_1 in xy plane and R_2 in zx plane, Figure 95) fulfils equation [46], where γ is the surface tension:

$$\Delta p = p_{\text{int}} - p_{\text{ext}} = \gamma\left(\frac{1}{R_1} + \frac{1}{R_2}\right) \quad [46]$$

Additionally, gravitation tends to elongate the drop along the z axis (Figure 95) and a pear-like shape results. As a result, gravitation causes a pressure difference across the z-axis according to Pascal's law. Therefore the Laplace pressure $\Delta p(z)$ at a distance z from an arbitrary reference plane with Laplace pressure Δp_0 is, according to [47]:

$$\Delta p(z) = \Delta p_0 \pm \Delta\rho \cdot g \cdot z \quad [47]$$

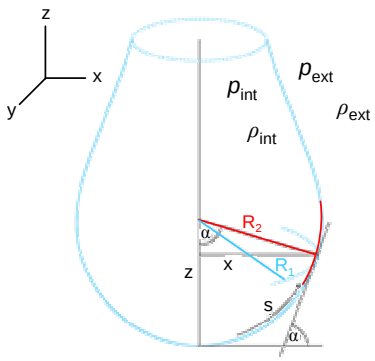

Figure 95. Schematic representation of the variables that can be defined for a pendant drop.

At the lowest point of the drop $R_1 = R_2 = R$, so it can be considered as a proper reference point with $\Delta p(z) = \Delta p_0$. As a consequence, for every point above this one it can be stated that $R_2 = x/\sin \alpha$ (Figure 95). Combining equations [46] and [47], equations [48] and [49] result.

$$\Delta p_0 = \gamma \frac{2}{R} \quad [48]$$

$$\frac{\Delta p}{\gamma} = \frac{1}{R_1} + \frac{1}{R_2} = \frac{1}{R_1} + \frac{\mathrm{Sin}(\alpha)}{\mathrm{x}} = \frac{2}{R} \pm \frac{\Delta \rho \cdot g \cdot z}{\gamma} \quad [49]$$

If the arc length *s* measured from the drop apex is considered, a series of three differential equations ([50], [51] and [52] with boundary conditions $x = 0$, $z = 0$ and $\alpha = 0$ at $s = 0$) can be defined, whose numerical solution affording the surface tension value can be obtained from fitting the drop shape.[170]

$$\frac{\mathrm{d}\alpha}{\mathrm{d}s} = -\frac{\sin(\alpha)}{x} + \frac{2}{R} \pm \frac{\Delta \rho \cdot g \cdot z}{\gamma} \quad [50] \qquad \frac{\mathrm{d}x}{\mathrm{d}s} = \cos(\alpha) \quad [51] \qquad \frac{\mathrm{d}z}{\mathrm{d}s} = \sin(\alpha) \quad [52]$$

Figure 96 shows, as representative examples, how the recorded drops change their shape depending on the surface tension, considering three solvents with different γ values at 25 ºC (a) methanol, $\gamma = 22.07$ mN·m^{-1}; (b) toluene, $\gamma = 27.93$ mN·m^{-1}and (c) water, $\gamma = 71.99$ mN·m^{-1}.[171]

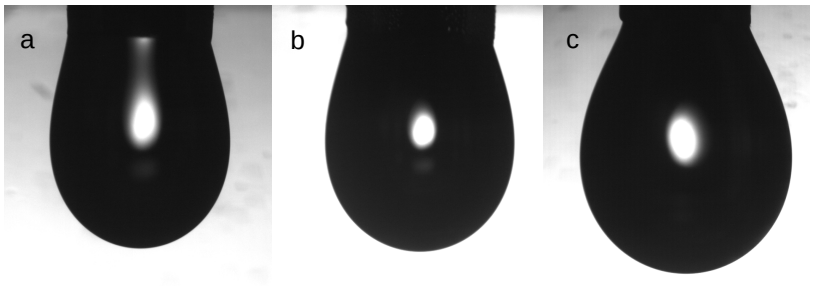

Figure 96. Recorded pendant drops for methanol (a), toluene (b) and water (c).

[170] J. D. Berry, M. J. Neeson, R. R. Dagastine, D. Y.C. Chan, R. F. Tabo. *J. Colloid Interface Sci*., **2015**, *454*, 226.

[171] D. R. Lide (ed). Handbook of Chemistry and Physics, 85th ed.; CRC Press: Boca Raton, FL, 2005; pp. 6/135-6/137.

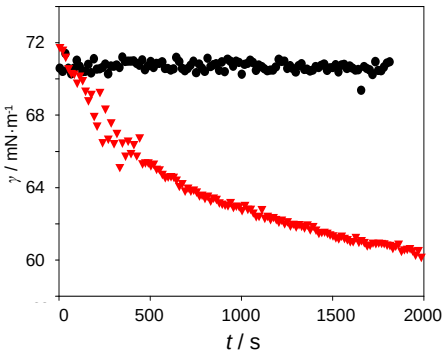

Figure 97. Dependence of surface tension on time for the adsorption of malonate **70** (black) and cationic fullerene **71** (red) to the water/air interphase at the same concentration (1 mM).

With these theoretical considerations in mind, the experimental results were the following. Firstly, compound **71** was used as an example to demonstrate that [60]fullerene monoadducts decorated with peripheral polar groups tend to self-aggregation. Figure 97 is illustrative of this idea. When the surface tension of an aqueous solution of deprotected malonate **70** (1 mM) was measured as a function of time, no changes were registered, obtaining a constant value around 71 $mN \cdot m^{-1}$. On the other hand, evident dynamics in surface tension were observed with an aqueous solution of **71** (1 mM).

Similarly, when the surface tension for aqueous solutions of glycofullerenes **31**, **32** and **33** were monitorized by this method, a series of dynamical behaviours due to the adsorption of the derivatives to the liquid-air interface was observed, although not in the same manner for all these compounds in the concentration range explored (0.003 mM – 0.3 mM). Figures 98a-c show the results for **31**, **32** and **33**, respectively.

Considering that the adsorption of each compound to the liquid-air interface followed a diffusive behaviour, it was possible to obtain information about the diffusion coefficient taking into account the Joos equation [53],[172] defined as follows:

[172] P. Joos, E. Rillaerts. *J. Colloid Interface Sci.*, **1981**, *79*, 96.

$$\gamma = \gamma_0 - 2 \cdot \mathrm{R} \cdot T \cdot c \left(\frac{D \cdot t}{\pi} \right)^{\frac{1}{2}} \quad [53]$$

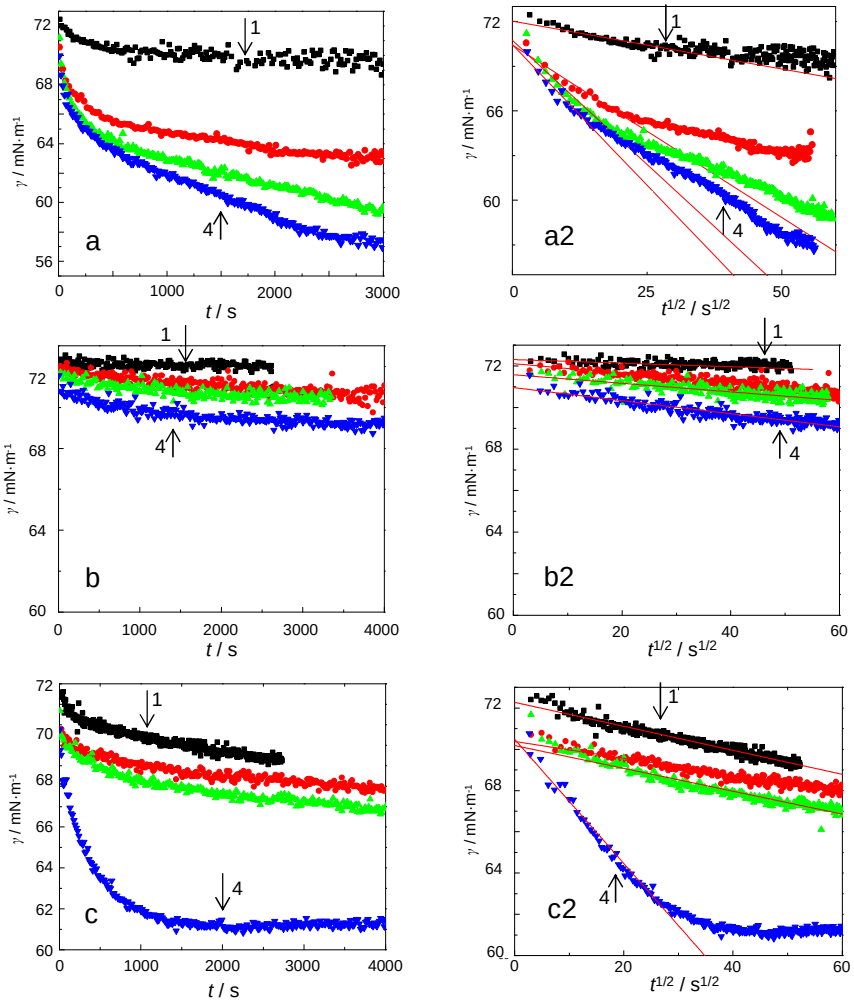

Figure 98. Dependence of surface tension on time for the adsorption of glycofullerenes **31** (a), **32** (b) and **33** (c) to the water/air interphase changing concentration. Fittings of the previous results to the equation [53] (**31**-a2, **32**-b2 and **33**-c2). **1**: 0.003 mM; **2**: 0.03 mM; **3**: 0.09 mM, and **4**: 0.3 mM.

Where γ_0 is the surface tension at time t = 0 s, R, the gas constant, T, the absolute temperature (298.15 K), c, the concentration, D, the diffusion coefficient and t, the time. Figures 98a2-98c2 show the experimental fittings for each concentration and each compound, **31**, **32**, and **33**, respectively. Table 24 summarizes D values obtained for all the solutions and glycofullerenes considered.

Table 24. Diffusion coefficient values for glycofullerenes **31**, **32** and **33** at different concentrations in water.

c / mM	D / m^2 s^{-1}		
	33	**32**	**31**
0.3	$(1.29 \pm 0.02)\cdot10^{-13}$	$(1.40 \pm 0.04)\cdot10^{-15}$	$(2.0 \pm 0.2)\cdot10^{-13}$
0.09	$(4.84 \pm 0.04)\cdot10^{-14}$	$(6.7 \pm 0.3)\cdot10^{-15}$	$(1.75 \pm 0.08)\cdot10^{-12}$
0.03	$(2.37 \pm 0.04)\cdot10^{-13}$	$(8.1 \pm 0.3)\cdot10^{-14}$	$(7.6 \pm 0.4)\cdot10^{-12}$
0.003	$(4.81 \pm 0.06)\cdot10^{-11}$	$(1.0 \pm 0.\ 4)\cdot10^{-12}$	$(5.8 \pm 0.5)\cdot10^{-11}$

From Figures 98a-c it is possible to conclude that glycofullerene **32** showed a less evident surfactant behaviour than **31** and **33**. Moreover, surface tension dynamics for compound **31** changed drastically from 0.003 mM to 0.03 mM, while this change for compound **33** was observed at higher concentrations, between 0.09 mM and 0.3 mM, reaching a plateau after 2000 s for this last concentration.

Regarding the diffusion coefficients, a gradual decrease can be observed from the most diluted solution to the most concentrated one (Figure 99). Only for compound **33** this trend is not fulfilled at 0.3 mM. This could be explained considering a stepwise aggregation mechanism, where the size of the aggregates grows continuously leading to less diffusive ones as the glycofullerene concentration is increased. It has to be pointed out that the linear fitting to equation [53] for compound **31** was performed only at short times, as a secondary non diffusive process can be observed at long times when concentration was increased (Figure 98-a2).

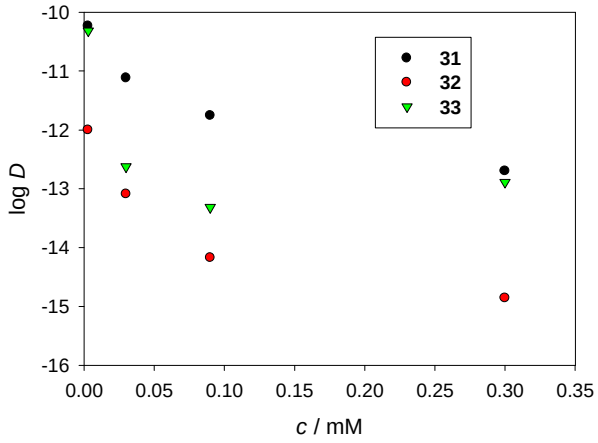

Figure 99. Dependence of diffusion coefficients on concentration for glycofullerenes **31**, **32** and **33** in water.

Due to lower and similar diffusion coefficients obtained for **32** and **33**, it is possible to conclude that these compounds tend to form bigger aggregates than **31**, what could be explained, from a structural point of view, by taking into account that these compounds decorated with 12 and 18 fucose units, respectively, are more sterically demanding than the glycofullerene bearing only 6 fucose units. Moreover, they are based on a similar dendrimer structure extending from the [60]fullerene monoadduct. Qualitatively, these results could explain the previous differences observed for $^1O_2$ photosensitized generation by these compounds in comparison to their parent non functionalized [60]fullerene monoadducts.

9.4. Interaction assays between fluorescent probes and *H. pylori*

Once the synthesis and photophysical characterization of the fluorescent probes have been discussed, the interaction assays carried out between them and *H. pylori* will be presented. The first technique explored for this aim was fluorescence microscopy. However, it demonstrated to be not a suitable option as the bacteria itself showed significant background fluorescence. Figure 100a shows a sample of *H. pylori* in bright field mode (transmission light), while Figure 100b shows the same sample when it was excited at 488 nm and the emission was collected between 500-550 nm. Some regions have been highlighted in order to show the same areas of the two images.

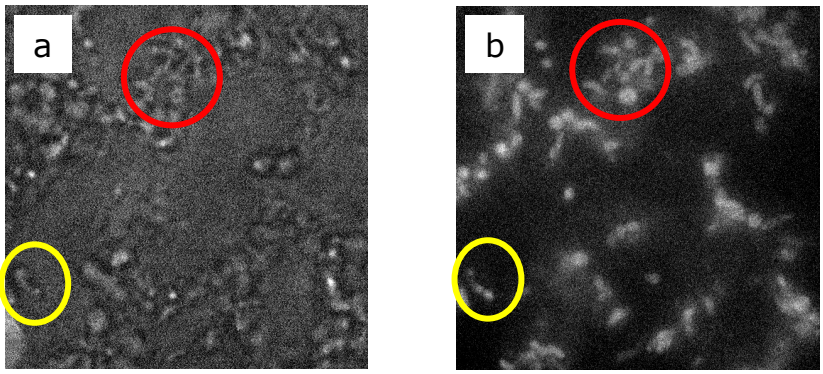

Figure 100. *H. pylori* sample in bright field mode (a) and collecting its auto-fluorescence after excitation at 488 nm (b).

As a result, flow cytometry was considered as the best solution to overcome these limitations. Flow cytometry is a technique whose main advantage lies on its ability for analyse multiple individual cell parameters in heterogeneous populations. The key point is that the analysed sample needs to be a set of individual cells which ensure that each cell is treated independently. Figure 101 represents a schematic cartoon showing the most typical configuration in a flow cytometer. It is possible to differentiate three main parts: the fluidic system for sample focusing, an optical part for sample excitation and subsequent emitted light recording, and the software for signal processing. In order to achieve the individual analysis when cells cross one by one the laser beam, they are hydrodynamically focused using a coaxial laminar flow, based on the theory developed by Reynolds, where the pressure of the fluid against the suspended

cells aligns them in a single row. Thereafter, cells reach the sensing area, a quartz cell where they are excited using a laser beam. Scattered light (forward and side scattering) as well as fluorescence emerging from this interaction between light and cells can be recorded using a series of detectors. However, it is important to comment that side scattering and fluorescent lights are filtered using dichroic mirrors and a series of emission filters (band pass, short pass or long pass). The role of the dichroic mirrors is fundamental because they select, reflect and transmit the light signals towards specific detectors collecting specific fluorescence.

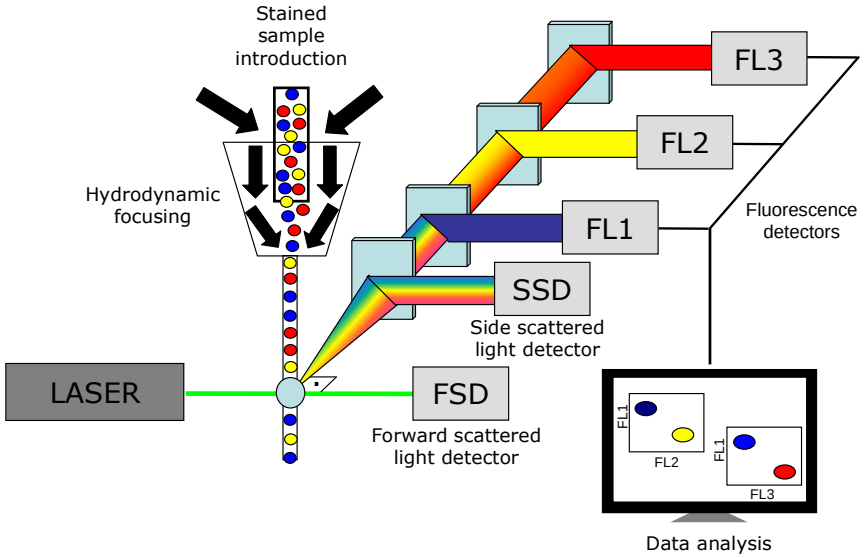

Figure 101. Most typical experimental setup for flow cytometers.

Forward and side scattered light allow identification of various cell types based on their size and morphological properties (granularity and/or topography, mainly). On the other hand, cell staining using fluorescent probes yields biochemical, biophysical, and molecular information about the cellular constituents to which the probe is attached.[173]

In this case, flow cytometry allowed the quantification and separation of fluorescence coming from *H. pylori* itself and that due to the fluorescent probes attached to the bacteria. Figure 102 shows the histograms where the normalized

[173] a) J. Picot, C. L. Guerin, C. Le Van Kim, C. M. Boulanger. *Cytotechnology*, **2012**, *64*, 109. b) M. J. Jaroszeski, G. Radcfiff. *Mol. Biotech*., **1999**, *11*, 37.

frequency is represented as a function of the fluorescence intensity recorded between 515-545 nm (fluorescein channel) after excitation with a laser centred at 488 nm. The intensity of the distribution for each compound was quantified as the median fluorescence, obtaining a series of values summarized in Table 25.

H. pylori in the presence of glycodendrimer **22** afforded similar fluorescence values to those of *H. pylori* itself, as expected. When bacteria were incubated in the presence of the fluorescent glycoprobe **37**, a slight increment was recorded, although not especially significant. However, this increment was higher for **38**. It is interesting to remark that, in spite of having less fucose units, the interaction between **38** and *H. pylori* seems to be more efficient than that for **37**. However, this fact could be explained considering the aforementioned steric hindrance and restricted rotation found in **37**. The selective interaction between the fucose units and the adhesins found on the bacteria wall are not especially strong, since these are based on weak multivalent interactions and, additionally, can be affected by the structural design and spatial distribution of the groups responsible for the interaction. On the contrary, this consideration does not seem to rule for the non-selective and stronger electrostatic interactions between *H. pylori* and probes **44** and **45**. In this case, the greater the number of positive charges, the higher emission intensity was recorded.

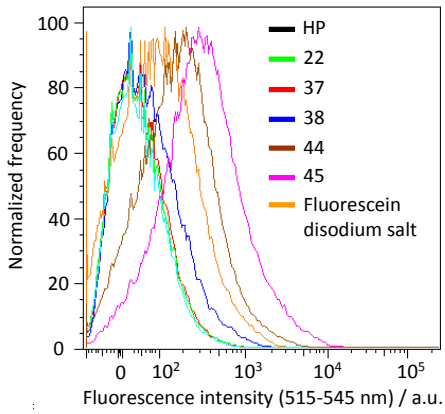

Figure 102. Recorded fluorescence histograms using flow cytometry for *H. pylori* incubated in the presence of fluorescent probes.

Table 25. Median fluorescence values obtained after the analysis of *H. pylori* suspensions incubated in the presence of fluorescent probes.

Cpd	Median fluorescence
HP	28.2 ± 0.1
22	29.8 ± 0.6
37	33.5 ± 0.8
38	57 ± 4
44	162 ± 6
45	316 ± 2
$FluorNa_2$	89 ± 3

However, it has to be kept in mind that the observed fluorescence depends not only on the amount of probe attached to the bacteria wall, but also on the relative fluorescence quantum yields. In this sense, as was shown in Table 22, the Φ_f value for dicationic probe **45** was 0.27, while this quantum yield for **44** was 0.18. This is too relevant for the disodium fluorescein probe, whose Φ_f = 0.92. As a result, the recorded fluorescence for the disodium fluorescein was greater than that for **37** or **38**, but it could be possible that less probe was attached to the bacteria. It is also important to remark that these statements can be affected by the fact that the photophysical properties can be modified from homogeneous solutions to heterogeneous media such as the bacterial wall. In any case, it can be said that, as expected, electrostatic interactions cause stronger increments in the recorded fluorescence compared to glycoprobes, although for the latter it can be concluded that fluoroprobe-bacterium interactions are taking place. It is also interesting to point out that the fluorescence was recorded at different emission channels in order to guarantee that the increments in fluorescence were due to the probes studied. Figure 103 shows the changes observed for the different compounds and channels considered. These results make sense since, taking into account the emission spectra depicted in Figure 92 for the series of probes, their emission intensity decrease from the maxima around 517 nm to longer wavelengths.

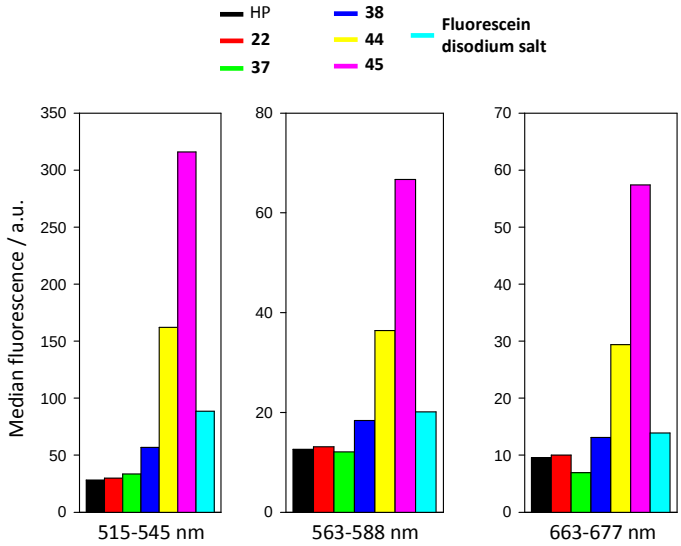

Figure 103. Median fluorescence values obtained at different emission channels after the analysis of *H. pylori* suspensions incubated in the presence of fluorescent probes.

9.5. Antimicrobial photodynamic assays against *H. pylori*

As compounds bearing the glycodendrimer **22** seemed to interact with *H. pylori*, the photodynamic activity of glycofullerenes **31**, **32**, and **33** was tested. In this sense, the ability of flow cytometry to study bacterial viability was exploited in order to analyse, using a fast and easy to carry out method, the combined effect of these photosensitizers and light on *H. pylori*. Although there are several opinions on the criteria to consider a bacterium as dead or alive, membrane integrity is assumed to be the most relevant criterion. In viable bacteria, membranes are intact and they cannot be penetrated by staining compounds. On the contrary, dead bacteria present disrupted and/or broken membranes that allow diffusion of staining dyes to their inner volume. It must be said that, sometimes, integrity of the membrane can be perfect, but the bacterium is metabolically inactive (viable but not culturable). In any case, there are several commercially available dual staining kits based on the detection of the membrane integrity. In this work, BacLight™ was used, composed by a mixture of two fluorophores: SYTO9 and propidium iodide (PI). PI is a red fluorescent nucleic acid stain that intercalates into DNA, enhancing its fluorescence 20 to 30 times. This dye is used to identify dead cells due to its ability to penetrate only cells with disrupted membranes, but it is excluded from viable cells. On the other hand, green fluorescent nucleic acid stain SYTO9 penetrates both dead and alive cells. However, propidium iodide shows stronger affinity for nucleic acids than SYTO9, so SYTO9 is displaced in the presence of PI. Collecting the fluorescence for both dyes and representing the values for each analysed event (bacterium) using the flow cytometry technique it was possible to define two regions for dead and alive bacteria.[174]

For example, starting from 100% alive and 100% dead by heat bacterial suspensions, it was possible to differentiate both regions by staining *H. pylori* with this mixture of dyes. Figure 104 shows a series of graphs for different % of living bacteria. Each point in the clouds represents an analysed event, *i.e*. a single bacterium which can lie on the dead or alive region depending on the relative staining ratio by both dyes. Figure 105, represents the calibration plot

[174] a) P. Stiefel, S. Schmidt-Emrich, K. Maniura-Weber, Q. Ren. *BMC Microbiology*, **2015**, *15*, 36. b) M. Berney, F. Hammes, F. Bosshard, H.-U. Weilenmann, T. Egli. *Appl. Environ. Microbiol*., **2007**, *73*, 3283. c) S. M. Stocks. *Cytometry A*, **2004**, *61A*, 189.

obtained from the population analysis using this approach, showing an excellent correlation between the theoretical % of living bacteria and the experimental one.

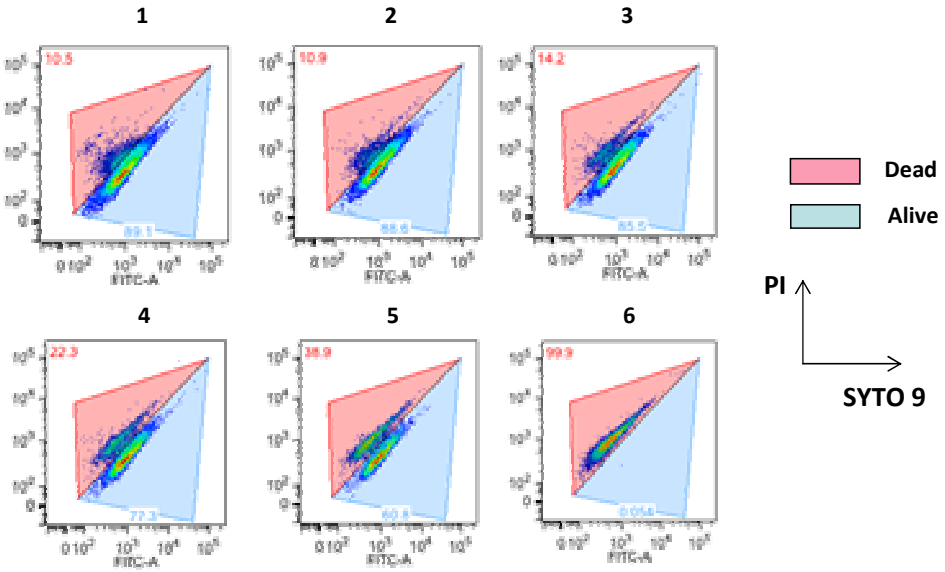

Figure 104. Dead and alive *H. pylori* population analysis using PI and SYTO9 staining, and flow cytometry analysis.

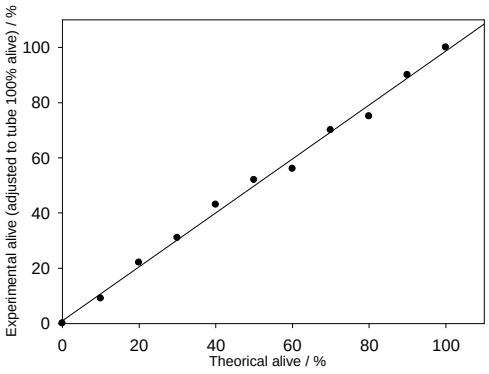

Figure 105. Calibration plot for the theoretical and experimental % alive *H. pylori* obtained after PI and SYTO9 staining, and flow cytometry analysis.

Once the protocol to differentiate between dead and alive *H. pylori* cells was optimized, this procedure was applied to evaluate the death induction after *in vitro* photodynamic treatments of *H. pylori* in the presence of glycofullerenes **31**,

32 and **33**. In addition, as was demonstrated in section 9.4 that cationic chains allowed stronger interactions, cationic [60]fullerene monoadduct **71** was also tested. The monoadducts concentration tested was 10^{-4} M, and allowed the absorption of more than 75% of the incident photons. Samples were analysed after 1 minute and 30 minutes of irradiation using a blue LED. Results are presented in Figure 106. Samples in the dark, as well as *H. pylori* suspensions alone and in presence of glycodendrimer **22** were used as controls to evaluate the photodynamic effect of irradiation in the presence of the different photosensitizers.

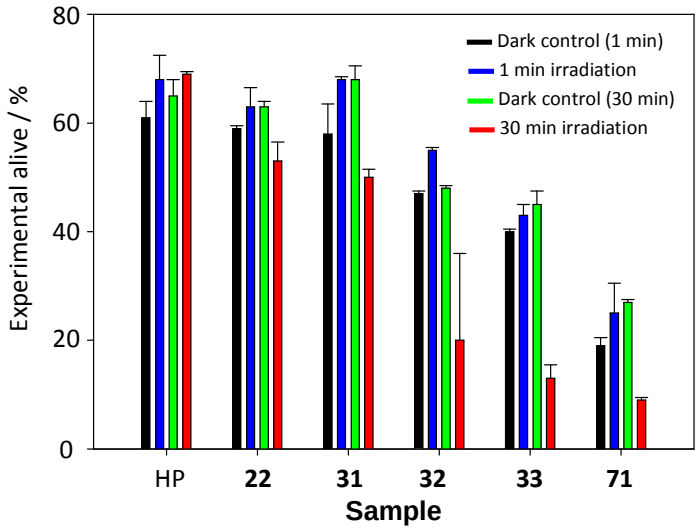

Figure 106. Experimental alive *H. pylori* populations measured by flow cytometry analysis for dark controls and samples irradiated 1 minute and 30 minutes in the presence of glycodendrimer **22**, glycofullerenes **31**, **32** and **33**, and cationic fullerene **71**.

Starting from the results obtained from *H. pylori* alone, it is interesting to comment that after all the procedure, only around 60% of the total bacteria could be considered viable. This fact is not unusual due to the susceptibility of *H. pylori* to *in vitro* environments. However, in any case, alive populations in dark controls and irradiated samples were compatible and no modifications were detected between them due to irradiation with blue light. Glycodendrimer **22**, as expected, did not show photodynamic activity against *H. pylori*. Regarding the glycofullerenes, some trends can be highlighted. None of them showed detectable effects after 1 minute of irradiation. As well, the photoactivity of **31**,

decorated with 6 fucoses, was low and, if the dark control corresponding to the sample irradiated 30 minutes is used as reference, only 26% of the initial alive population was killed (Figure 107). On the contrary, the photoinactivation achieved with **32** and **33** was quite remarkable, as 58% and 71% of the initial alive population were killed, respectively, as determined by flow cytometry. Again, in Figure 107, the relative killing efficiencies are compared to those obtained with **31**. The error bar found in **32** is due to divergent values in the duplicates, although it was interesting to consider both results. Dark controls showed a decrease in alive populations in comparison to *H. pylori* alone, more evident for **33**. However, it must be remarked that dark internal controls for each compound did not show significant fluctuations. If these compounds were toxic themselves, it could be expected a gradual decrease in the population of alive bacteria depending on time, but this was not observed.

Regarding the cationic monoadduct **71**, evident dark toxicity was observed, although with the same pattern just mentioned concerning the internal controls after 1 minute and 30 minutes.

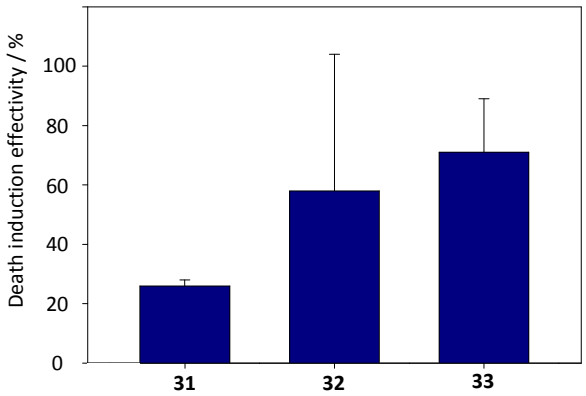

Figure 107. Photodynamic death induction effectivity performed by glycofullerenes **31**, **32** and **33** against *H. pylori*.

In order to support these conclusions, the samples affording the previous results after 30 minutes of irradiation were analysed in parallel, growing sample aliquots in culture plates. Alive populations are represented in Figure 108 for dark controls and irradiated samples. From a qualitative point of view, some of the previous conclusions are confirmed: glycodendrimer **22** had no effect, as well as glycofullerene **31**. This last evidence is slight different from flow cytometry results, where a small effect was detected, but, in any case, confirms

the low effectivity of this compound. Surprisingly, glycofullerene **32** decreased four orders of magnitude the population of alive bacteria, reaching the detection limit of the technique. This could confirm that, in flow cytometry analysis, the correct value in the duplicate was that where the experimental alive population was lower.

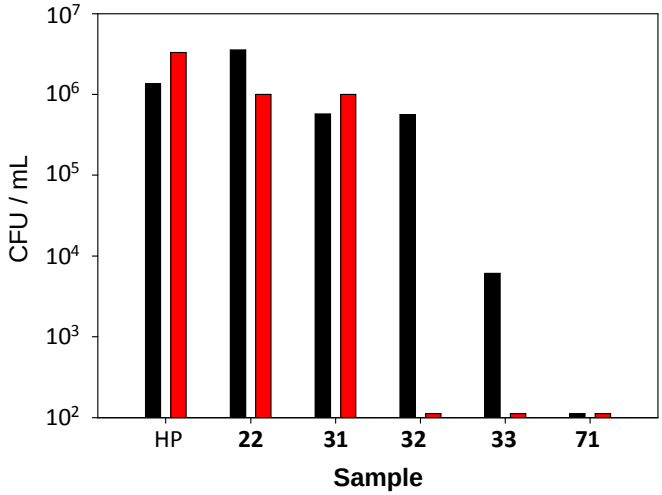

Figure 108. Experimental alive *H. pylori* populations measured by growing in plate analysis for dark controls (black) and samples irradiated 30 minutes (red) in presence of glycodendrimer **22**, glycofullerenes **31**, **32** and **33**, and cationic fullerene **71**. CFU: Colony-forming unit.

More interestingly, the aforementioned dark toxicity observed in flow cytometry results for **32** was not observed by this analysis, as the dark control population was very similar to that obtained for *H. pylori* alone. However, a decrease in the dark control was observed for **33**, which also decreased the alive population after 30 minutes of irradiation bellow the detection limit. Regarding the cationic [60]fullerene monoadduct, **71**, total death was induced in the dark.

Overall consideration of these results, taking into account the structural, photophysical, aggregation and photodynamic studies, allow to conclude that, as it was demonstrated, self-aggregation of glycofullerenes played a key role in the observed $^1O_2$ production quantum yields. In this sense, it is interesting to see how **32**, with Φ_Δ = 0.13 and decorated with 12 fucoses, showed the same photodynamic activity after 30 minutes of irradiation as **33**, with Φ_Δ = 0.26 and decorated with 18 fucoses. However, this could be partially explained considering the interaction between *H. pylori* and the photosensitizers. As the

glycofullerenes aggregate, the number of sugar units exposed to the interaction with the bacterial wall would not be the individual number for each [60]fullerene monoadduct unit, but the number of external sugar units in the aggregate. Taking into account the diffusion coefficients measured by surface tension dynamics, both compounds seemed to form aggregates with similar sizes, so the interaction could be, as well, similar. On the contrary, both photophysical properties and interaction ability for **31** were not suitable to perform a good photodynamical activity. Its Φ_{Δ} could be too small to be effective (the same could be said for **71**), and the smaller aggregates (considering the diffusion coefficients) could be interacting less with the bacterial wall.

CHAPTER 2

EXPERIMENTAL SECTION

10. CHAPTER 2 EXPERIMENTAL SECTION

10.1. General Methods

-***Thin layer chromatography****:* Reactions were monitored by thin-layer chromatography carried out on 0.2 mm TLC-aluminium sheets of silica gel (Merck, TLC Silica gel 60 F_{254}).

-***Purification of Reaction Mixtures****:* Flash column chromatographies were performed using silica gel (Merck, 230-400 mesh).

-***Nuclear Magnetic Resonance Spectroscopy****:* ^{1}H NMR and ^{13}C NMR spectra were recorded on a BRUKER DPV-300MHz, BRUKER AV-500MHz or BRUKER AVIII-700MHz using the signals of the deuterated solvents as the reference. Coupling constants (J) are reported in Hz and the chemical shifts (δ) in ppm relative to tetramethylsilane as the internal standard at room temperature (δ = 0). Spin multiplicities are reported as a singlet (s), broad singlet (br s), doublet (d), triplet (t) quartet (q) and multiplet (m).

-***Mass Spectrometry:*** Matrix-assisted laser desorption ionization-Time of Flight (MALDI-TOF) mass spectrometry (MS) was performed on a BRUKER-REFLEX spectrometer using dithranol as the matrix, or on a HP1100EMD electrospray ionization (ESI) apparatus.

-***Solvents***: All the solvents used were purified and dried following the usual methods.[83]

-***Reagents***: Reagents for synthesis were mostly purchased from Sigma-Aldrich and Acros.

10.2. Synthetic procedures

1,2,3,4-Tetra-*O*-acetyl-α-L-fucopyranoside (7)

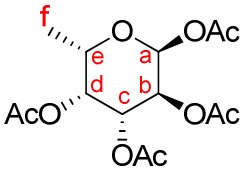

7

To a solution of 500 mg (3.0 mmol) of L-(–)-fucose and 18 mg (0.15 mmol) of 4-dimethylaminopyridine in 5 mL (62.0 mmol) of dry pyridine at 0 ºC under Ar atmosphere, 2.5 mL (26.4 mmol) of acetic anhydride were added dropwise. After 10 minutes of stirring, the reaction mixture was allowed to reach room temperature and stirred for 24 h overnight. Pyridine was removed at low pressure and the residue was suspended in 15 mL of CH_2Cl_2. The organic phase was washed with HCl 1M (3 × 15 mL), saturated aqueous $NaHCO_3$ (3 × 15 mL) and brine (3 × 15 mL). The organic layer was dried over anhydrous $MgSO_4$ and filtered. The solvent was removed at low pressure and **7** was obtained as a white solid (85 % yield).

^{1}H-NMR ($CDCl_3$, 300 MHz) δ / ppm: 6.34 (d, J = 2.4 Hz, 1H, H_a), 5.34 (m, 3H, H_b, H_c, H_d), 4.27 (c, J = 6.0 Hz, 1H, H_e), 2.18, 2.14, 2.01, 2.00 (4s, 4 × $C\underline{H}_3COO$, 12H), 1.15 (d, J = 6.0 Hz, 3H, H_f).

^{13}C-NMR ($CDCl_3$, 75 MHz) δ / ppm: 170.6, 170.2, 170.0, 167.2 (4 × $CH_3\underline{C}OO$); 90.0 (C_a); 70.6, 67.9, 67.3, 66.5 (C_b, C_c, C_d, C_e); 21.0, 20.7, 20.6, 20.6 (4 × $\underline{C}H_3COO$); 16.0 (C_f).

FTIR (KBr) (cm^{-1}): 2988, 2939 (ν **C–H**); 1748 (ν **C=O**), 1436, 1373, 1227 (ν **C–O**).

1-(2-Bromoeth-1-yl)-2,3,4-tri-*O*-acetyl-α-L-fucopyranoside (8)

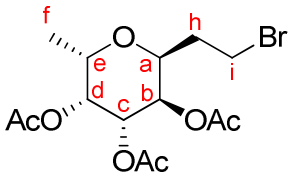

8

To a solution of 600 mg (1.8 mmol) of **7** and 0.16 mL (2.2 mmol) of 2-bromoethanol in 4 mL of dry CH_2Cl_2 at 0 ºC under Ar atmosphere, 1.1 mL (8.9 mmol) of boron trifluoride diethyletherate were added dropwise. After 2 h, the reaction mixture was allowed to reach room temperature and was stirred for 24 h. Reaction was finished by adding 20 mL of ice/water, and the aqueous phase was extracted with CH_2Cl_2 (3 × 20 mL). Combined organic layers were washed with 25 mL of water, 25 mL of saturated aqueous $NaHCO_3$ and 25 mL of brine. The final organic phase was dried over anhydrous $MgSO_4$ and filtered. The solvent was removed at low pressure and the reaction crude was purified by column chromatography using hexane:AcOEt (2:1, v/v) as eluent. Compound **8** was obtained as a pale yellow oil (50 % yield).

^{1}H-NMR ($CDCl_3$, 300 MHz) δ / ppm: 5.37 (dd, J = 10.5 Hz, J = 3.3 Hz, 1H), 5.31 (dd, J = 3.3 Hz, J = 1.2 Hz, 1H), 5.15–5.07 (m, 2H), 4.26 (c, J = 6.0 Hz, 1H, H_e), 3.99 (m, 1H, H_h), 3.89 (m, 1H, H_h), 3.49 (t, J = 6.0 Hz, 2H, H_i), 2.16, 2.08, 2.09 (3s, 3 × $C\underline{H}_3COO$, 9H), 1.14 (d, J = 6.0 Hz, 3H, H_f).

^{13}C-NMR ($CDCl_3$, 75 MHz) δ / ppm: 170.7, 170.2 (3 × $CH_3\underline{C}OO$); 96.5 (C_a); 71.2, 68.6, 68.3, 68.1 (C_b, C_c, C_d, C_e); 65.0 (C_h), 30.3 (C_i); 21.0, 20.9, 20.8 (3 × $\underline{C}H_3COO$); 16.0 (C_f).

FTIR (KBr) (cm^{-1}): 2984, 2938 (v **C–H**); 1740 (v **C=O**), 1431, 1369, 1219 (v **C–O**).

1-(2-Azidoeth-1-yl)-2,3,4-tri-*O*-acetyl-α-L-fucopyranoside (9)

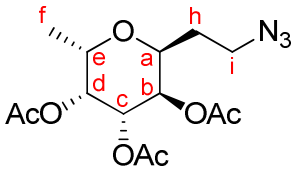

9

A mixture of 600 mg (1.5 mmol) of **8** and 790 mg (12.2 mmol) of sodium azide in 16 mL of dry DMF at 55 ºC was stirred for 24 h under Ar atmosphere. Thereafter, the reaction crude was suspended in 100 mL of AcOEt and the organic phase was washed with water (3 × 100 mL). The organic layer was dried over anhydrous $MgSO_4$ and filtered. The solvent was removed at low pressure and **9** was obtained as a pale yellow oil (93 % yield).

^{1}H-NMR ($CDCl_3$, 300 MHz) δ / ppm: 5.37 (dd, J = 10.5 Hz, J = 3.3 Hz, 1H), 5.31 (dd, J = 3.3 Hz, J = 1.2 Hz, 1H), 5.15–5.07 (m, 2H), 4.18 (c, J = 6.0 Hz, 1H, H_e), 3.85 (m, 1H, H_h), 3.62 (m, 1H, H_h), 3.42 (m, 2H, H_i), 2.16, 2.08, 1.98 (3s, 3 × $C\underline{H}_3COO$, 9H), 1.15 (d, J = 6.0 Hz, 3H, H_f).

^{13}C-NMR ($CDCl_3$, 75 MHz) δ / ppm: 170.8, 170.9, 170.2 (3 × $CH_3\underline{C}OO$); 96.6 (C_a); 71.2, 68.1, 68.0, 67.3 (C_b, C_c, C_d, C_e); 64.9 (C_h), 50.6 (C_i); 20.9, 20.8, 20.7 (3 × $\underline{C}H_3COO$); 16.0 (C_f).

FTIR (**CH_2Cl_2**) (cm^{-1}): 2924, 2854 (ν **C–H**); 2106 (ν **-N=N=N**), 1741 (ν **C=O**), 1438, 1370, 1219 (ν **C–O**).

1-(2-Azidoeth-1-yl)-α-L-fucopyranoside (10)

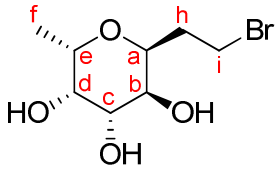

10

A mixture of 1.54 g of Amberlite IR-120 and 12 mL of 2-bromoethanol was stirred at 90 ºC under Ar atmosphere during 30 minutes. Afterwards, 1.42 g (8.64 mmol) of L-(–)-fucose were added and the reaction mixture was stirred at 90 ºC for 2.5 hours. After reaction completion, the resin was removed by filtration and the solvent evaporated at low pressure (toluene (15 mL) was used as co-solvent). Reaction crude was purified by column chromatography using AcOEt:MeOH (95:5, v/v) as eluent. Compound **10** was obtained as a white solid (40 % yield).

^{1}H-NMR (MeOD-d$_4$, 300 MHz) δ / ppm: 4.8 (d, J = 3.0 Hz, 1H), 4.10 (c, J = 6.0 Hz, 1H, H_e), 3.97–3.80 (m, 2H, H_h), 3.74 (m, 2H, H_i), 3.67 (m, 1H), 3.61–3.56 (m, 2H), 1.21 (d, J = 6.0 Hz, 3H, H_f).

^{13}C-NMR (MeOD-d$_4$, 75 MHz) δ / ppm: 100.8 (C_a); 73.7, 71.6, 70.0, 69.8 (C_b, C_c, C_d, C_e); 68.0 (C_h), 30.8 (C_i), 16.6 (C_f).

FTIR (KBr) (cm^{-1}): 3317 (ν **O–H**), 2993, 2902 (ν **C–H**); 1454, 1384, 1162, 1133, 1099, 1026.

1-(2-Azidoethyl)-α-L-fucopyranoside (11)

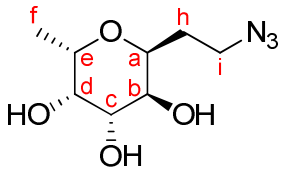

11

A mixture of 310 mg (1.2 mmol) of **10**, 150 mg (2.3 mmol) of sodium azide and 15 mg of sodium iodide was dissolved in 18 mL of 2-methoxyethanol under Ar atmosphere. Reaction mixture was stirred at 90 ºC during 72 h. Thereafter, solvent was removed at low pressure and the reaction crude was purified by column chromatography using AcOEt:MeOH (95:5, v/v) as eluent. Compound **11** was obtained as a white solid (89 % yield).

^{1}H-NMR (MeOD-d$_4$, 300 MHz) δ / ppm: 4.74 (d, J = 2.7 Hz, 1H), 3.96 (c, J = 6.6 Hz, 1H, H_e), 3.85–3.30 (m, 7H), 1.17 (d, J = 6.6 Hz, 3H, H_f).

^{13}C-NMR ($CDCl_3$, 75 MHz) δ / ppm: 100.7 (C_a); 73.6, 71.5, 69.8, 68.1, 67.8 (C_b, C_c, C_d, C_e, C_h), 51.8 (C_i), 16.7 (C_f).

FTIR (KBr) (cm^{-1}): 3320 (ν **O–H**), 2985,2938 (ν **C–H**); 2094 (ν **–N=N=N**), 1454, 1384, 1164, 1134, 1097, 1042.

Methyl 3,5-bis(propargyloxy)benzoate (12)

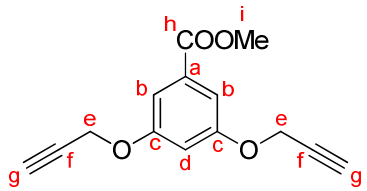

12

To a solution of 5.6 g (33 mmol) of methyl 3,5-dihydroxybenzoate and 9.1 g (76 mmol) of propargyl bromide (80 % wt in toluene) in 100 mL of acetone under Ar atmosphere, 110 mg (0.38 mmol) of 18-crown-6 and 10.1 g (72 mmol) of K_2CO_3, were added. The reaction mixture was heated under reflux for 19 h. Thereafter, the resulting suspension was filtered and the solvent was removed at low pressure. The remaining yellowish solid was purified by recrystallization in MeOH, affording compound **12** as a white solid (67 % yield).

^{1}H-NMR ($CDCl_3$, 300 MHz) δ / ppm: 7.30 (d, J = 2.4 Hz, 2H, H_b), 6.81 (t, J = 2.4 Hz, 1H, H_d), 4.71 (d, J = 2.4 Hz, 4H, H_e), 3.91 (s, 3H, H_i), 2.54 (t, J = 2.4 Hz, 2H, H_g).

^{13}C-NMR ($CDCl_3$, 75 MHz) δ / ppm: 166.6 (C_h), 158.6 (C_c), 132.3 (C_a), 109.0 (C_d), 107.7 (C_b), 78.1 (C_f), 76.1 (C_g), 56.3 (C_e), 52.5 (C_i).

FTIR (KBr) (cm^{-1}): 3271 (ν C≡**C–H**), 2130 (ν **C≡C**), 1717 (ν **C=O**), 1301, 1177 (ν **C–O)**.

Methyl 3,4,5-tris(propargyloxy)benzoate (13)

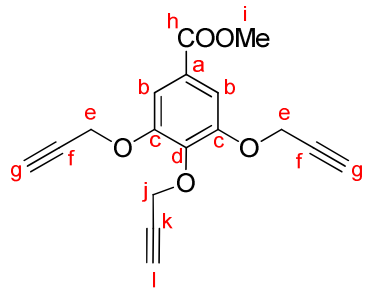

13

To a solution of 4.0 g (21.3 mmol) of methyl 3,4,5-trihydroxybenzoate and 10.6 g (77.3 mmol) of propargyl bromide (80% wt in toluene) in 100 mL of acetone under Ar atmosphere, 110 mg (0.38 mmol) of 18-crown-6 and 8.9 g (64.8 mmol) of K_2CO_3 were added. Reaction mixture was heated under reflux for 19 h overnight. The resulting suspension was filtered and the solvent removed at low pressure. The remaining yellowish solid was purified by recrystallization in MeOH, affording compound **13** as a white solid (72 % yield).

^{1}H-NMR ($CDCl_3$, 300 MHz) δ / ppm: 7.47 (s, 2H, H_b), 4.83 (d, J = 2.4 Hz, 4H, H_e), 4.80 (d, J = 2.4 Hz, 2H, H_j), 3.91 (s, 3H, H_i), 2.53 (t, J = 2.4 Hz, 2H, H_g), 2.46 (t, J = 2.4 Hz, 1H, H_l).

^{13}C-NMR ($CDCl_3$, 75 MHz) δ / ppm: 166.4 (C_h), 151.4 (C_c), 125.9 (C_d), 110.0 (C_b), 78.8 (C_k), 78.1 (C_f), 76.3 (C_g), 75.7 (C_l), 60.5 (C_j), 57.2 (C_e), 52.5 (C_i).

FTIR (KBr) (cm^{-1}): 3269 (ν C≡**C**–**H**); 2996, 2950 (ν **C**–**H**); 2122 (ν **C≡C**), 1724 (ν **C=O**), 1590 (ν **C=C Ar**) 1215, 1263, 1118 (ν **C**–**O**), 1019.

3,5-Bis(propargyloxy)benzyl alcohol (14)

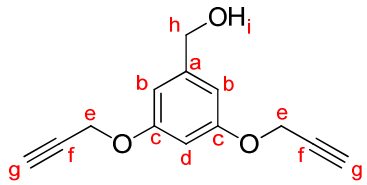

14

To a suspension of 1.14 g (30 mmol) of lithium aluminium hydride in 50 mL of dry THF at 0 ^{o}C and under Ar atmosphere, 3.80 g (15 mmol) of **12** in 20 mL of dry THF were added dropwise. After 30 minutes, the mixture was allowed to reach room temperature. Reaction was finished after 5 hours of stirring by adding, very slowly, 40 mL of aqueous NH_4Cl (5% wt) at 0 ºC. The remaining suspension was filtered and the filtrate extracted with CH_2Cl_2 (5 × 30 mL). Combined organic phases were washed with brine (2 × 30 mL). The organic layer was dried over anhydrous $MgSO_4$ and filtered. The solvent was removed at low pressure and **14** was obtained as a white solid (73 % yield).

^{1}H-NMR ($CDCl_3$, 300 MHz) δ / ppm: 6.62 (d, J = 2.4 Hz, 2H, H_b), 6.54 (t, J = 2.4 Hz, 1H, H_d), 4.67 (d, J = 2.4 Hz, 4H, H_e), 4.64 (s, 2H, H_h), 2.53 (t, J = 2.4 Hz, 2H, H_g), 1.75 (br s, 1H, H_i).

^{13}C-NMR ($CDCl_3$, 75 MHz) δ / ppm: 159.0 (C_c), 143.7 (C_a), 106.4 (C_b), 101.6 (C_d), 78.5 (C_f), 75.8 (C_g), 65.3 (C_h), 56.0 (C_e).

FTIR (KBr) (cm^{-1}): 3286 (ν **O–H**), 2121 (ν **C≡C**), 1595 (ν **C=C Ar**), 1146 (ν **C–O**).

3,4,5-Tris(propargyloxy)benzyl alcohol (15)

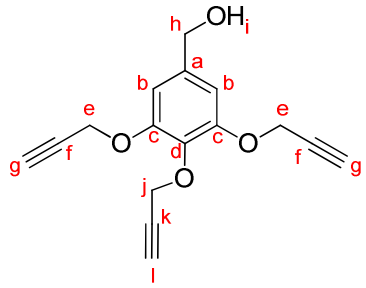

15

To a suspension of 340 mg (8.4 mmol) of lithium aluminium hydride in 20 mL of dry THF at 0 ^{o}C and under Ar atmosphere, 2.0 g (6.9 mmol) of **13** in 20 mL of dry THF were added dropwise. After 30 minutes, the mixture was allowed to reach room temperature and the reaction was finished after 5 hours by adding very slowly 40 mL of aqueous NH_4Cl (5% wt) at 0 ^{o}C. The resulting suspension was filtered and the solution extracted with CH_2Cl_2 (5 × 30 mL). Combined organic phases were washed with brine (2 × 30 mL). The organic layer was dried over anhydrous $MgSO_4$ and filtered. The solvent was removed at low pressure and **15** was obtained as a white solid (75 % yield).

^{1}H-NMR ($CDCl_3$, 300 MHz) δ / ppm: 6.78 (s, 2H, H_b), 4.77 (d, J = 2.4 Hz, 4H, H_e), 4.73 (d, J = 2.4 Hz, 2H, H_j), 4.65 (s, 2H, H_h), 2.51 (t, J = 2.4 Hz, 2H, H_g), 2.46 (t, J = 2.4 Hz, 1H, H_l), 1.77 (br s, 1H, H_i).

^{13}C-NMR ($CDCl_3$, 75 MHz) δ / ppm: 151.9 (C_c), 137.3 (C_a), 136.5 (C_d), 107.1 (C_b), 79.3 (C_k), 78.6 (C_f), 76.0 (C_g), 75.3 (C_l), 65.3 (C_h), 60.4 (C_j), 57.1 (C_e).

FTIR (KBr) (cm^{-1}): 3538 (ν **–O–H**); 3294, 3280, 3264 (ν -C≡**C–H**); 2926, 2869 (ν **C–H**); 2120 (ν **C≡C**), 1594 (ν **C=C Ar**), 1503, 1114 (ν **C–O**), 1034.

3,4,5-Tris(propargyloxy)benzyl alcohol (16)

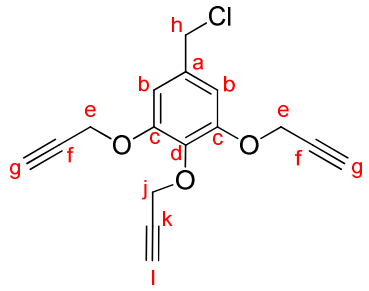

16

To a solution of 360 mg (1.3 mmol) of **15** in 60 mL of dry CH_2Cl_2 at 0 ºC and under Ar atmosphere, 660 mg (5.5 mmol) of thionyl chloride were added dropwise. Thereafter, reaction mixture was allowed to reach room temperature and stirred for 24 hours. Solvent was removed at low pressure and the reaction crude was purified by column chromatography using hexane:AcOEt (1:3, v/v). Compound **16** was obtained as a white solid (95 % yield).

^{1}H-NMR ($CDCl_3$, 300 MHz) δ / ppm: 6.76 (s, 2H, H_b), 4.77 (d, J = 2.4 Hz, 4H, H_e), 4.73 (d, J = 2.4 Hz, 2H, H_j), 4.54 (s, 2H, H_h) 2.52 (t, J = 2.4 Hz, 2H, H_g), 2.47 (t, J = 2.4 Hz, 1H, H_l).

^{13}C-NMR ($CDCl_3$, 75 MHz) δ / ppm: 151.8 (C_c); 133.6, 133.5 (C_a, C_d); 109.1 (C_b), 79.2 (C_k), 78.4 (C_f), 76.2 (C_g), 75.5 (C_l), 60.5 (C_j), 57.2 (C_e), 46.2 (C_h).

FTIR (KBr) (cm^{-1}): 3290 (ν C≡**C–H**); 2926, 2858 (ν **C–H**); 2124 (ν **C≡C**); 1590 (ν **C=C Ar**), 1449, 1099 (ν **C–O**).

tert-Butyl-*N*-(tris(hydroxymethyl)methane)carbamate (17)

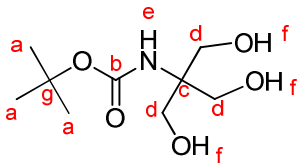

17

To a solution of 6.1 g (50.2 mmol) of tris(hydroxymethyl)aminomethane in 90 mL of MeOH/*t*-BuOH (1:1, v/v), 14.4 g (65.5 mmol) of di-*tert*-butyldicarbonate in 60 mL of *t*-BuOH were added slowly. The reaction mixture was stirred for 18 hours. Thereafter, the solvent was removed at low pressure and the compound was precipitated in cold AcOEt. Compound **17** was obtained as a white solid (91 % yield).

^{1}H-NMR ($CDCl_3$, 300 MHz) δ / ppm: 5.79 (br s, 1H, H_e), 4.52 (t, J = 5.7 Hz, 3H, H_f), 3.54 (d, J = 5.7 Hz, 6H, H_d), 1.39 (s, 9H, H_a).

^{13}C-NMR ($CDCl_3$, 75 MHz) δ / ppm: 155.0 (C_b), 77.8 (C_g), 60.3, 60.2 (C_d, C_c), 28.2 (C_a).

FTIR (KBr) (cm^{-1}): 3422 (ν –**N**–**H**), 3315 (ν –**O**–**H**); 2923, 2852 (ν **C**–**H**); 1679 (ν **C=O**), 1548 (δ_{ip} **N**–**H**), 1363.

tert-Butyl-*N*-(tris(propargyloxy)methane)carbamate (18)

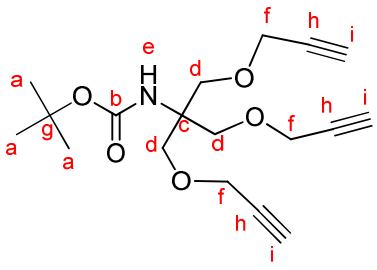

18

To a solution of 1.00 g (4.5 mmol) of **17** in 6 mL of dry DMF, under Ar atmosphere at 0 ºC, 3 mL (27.8 mmol) of propargyl bromide (80% wt in toluene) and 1.90 g (33.9 mmol) of KOH were added. The reaction mixture was stirred at 35 ºC for 24 h. Thereafter, the reaction crude was suspended in 50 mL of AcOEt and washed with water (4 × 30 mL). The organic layer was dried over anhydrous $MgSO_4$ and filtered. The solvent was removed at low pressure and the reaction crude was purified by column chromatography using hexane:AcOEt (95:5, v/v) as eluent. Compound **18** was obtained as a yellowish oil (60 % yield).

^{1}H-NMR ($CDCl_3$, 300 MHz) δ / ppm: 4.93 (s, 1H, H_e), 4.14 (d, J = 2.4 Hz, 6H, H_f), 3.78 (s, 6H, H_d), 2.43 (t, J = 2.4 Hz, 3H, H_i), 1.42 (s, 9H, H_a).

^{13}C-NMR ($CDCl_3$, 75 MHz) δ / ppm: 154.7 (C_b), 79.6 (C_h), 74.6 (C_i), 68.9 (C_c), 58.7, 58.1 (C_d, C_f), 28.4 (C_a).

FTIR (KBr) (cm^{-1}): 3428 (ν –**N**–**H**), 3292 (ν -C≡**C**–**H**), 2977, 2886, 2117 (ν **C**≡**C**), 1502 (δ_{ip} **N**–**H**), 1473, 1391, 1095 (ν **C**–**O**).

Bromomethyl-*N*-[tris(propargyloxy)methane]carbamate (19)

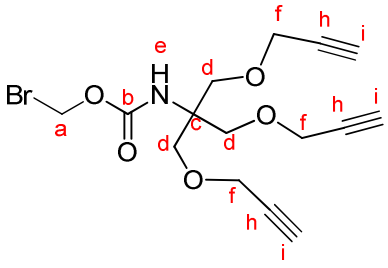

19

To a solution of 0.87 g (2.5 mmol) of **18** in 8 mL of dry CH_2Cl_2 under Ar atmosphere at 0 ºC, 4.1 mL of CF_3COOH were added dropwise during 40 minutes. The reaction mixture was stirred at 0 ºC for 2 hours. The solvent was removed at low pressure using toluene (3 × 4 mL) as a co-solvent. The remaining oil was suspended in 2 mL of dry CH_2Cl_2 under Ar atmosphere at 0 ºC. Then, 1.1 mL (6.6 mmol) of DIPEA and 490 mg (2.9 mmol) of bromoacetyl chloride in 7 mL of dry CH_2Cl_2 were added. The reaction mixture was stirred at room temperature for 15 hours. Thereafter, the reaction crude was washed with 30 mL of HCl 0.5 M and water (3 × 30 mL). The organic layer was dried over anhydrous $MgSO_4$ and filtered. The solvent was removed at low pressure and the reaction crude was purified by column chromatography using hexane:AcOEt (90:10 to 80:20, v/v). Compound **19** was obtained as a yellowish oil (30 % yield).

^{1}H-NMR (CDCl$_3$, 300 MHz) δ / ppm: 6.83 and 6.69 (s and s, 1H, H_e), 4.16 (d, J = 2.4 Hz, 6H, H_f), 3.97 and 3.80 (s and s, 2H, H_a), 3.86 and 3.85 (s and s, 6H, H_d), 2.44 (t, J = 2.4 Hz, 3H, H_i).

^{13}C-NMR (CDCl$_3$, 75 MHz) δ / ppm: 165.5 (C_b), 79.5 (C_f), 74.9 (C_i), 68.2 (C_c), 58.8, 43.0 (C_d, C_f), 29.6 (C_a).

FTIR (KBr) (cm^{-1}): 3389 (ν –**N–H**), 3289 (ν C≡**C–H**); 2945, 2854 (ν **C–H**); 2116 (ν **C≡C**), 1669 (ν **C=O**), 1526 (δ_{ip} **N–H**), 1472, 1090 (ν **C–O**).

3,4,5-Tris[(1-(2-(2,3,4-tri-*O*-acetyl-α-L-fucopyranosyl)ethyl)-1*H*-1,2,3-triazol-4-yl)methoxy]benzyl chloride (20)

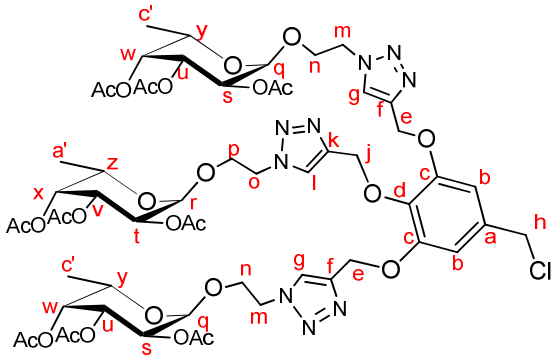

20

A mixture of 200 mg (0.56 mmol) of **9**, 44 mg (0.15 mmol) of **16**, 27 mg (0.14 mmol) of sodium ascorbate and 36 mg (0.14 mmol) of $CuSO_4 \cdot 5H_2O$ was dissolved in 2 mL of deoxygenated THF/water (1:1, v/v), and a piece of copper wire was added. After stirring for 18 h, the reaction crude was resuspended in 20 mL of AcOEt and washed with aqueous saturated NH_4Cl (2 × 10 mL), 15 mL of water and 15 mL of brine. The organic layer was dried over anhydrous $MgSO_4$ and filtered. The solvent was removed at low pressure and the reaction crude was purified by column chromatography using AcOEt eluent to remove the excess of **9**, followed by AcOEt:MeOH (95:5, v/v). Compound **20** was obtained as a white foam (91 % yield).

^{1}H-NMR ($CDCl_3$, 300 MHz) δ / ppm: 7.99 (s, 1H, H_l), 7.96 (s, 2H, H_g), 6.78 (s, 2H, H_b), 5.30-4.95 (m, 18H), 4.61 (m, 6H, H_e, H_j), 4.51 (s, 2H, H_h), 4.17-4.05 (m, 4H), 3.99 (c, *J* = 6.6 Hz, 1H, H_z), 3.95–3.80 (m, 4H), 2.14, 1.99, 1.96, 1.93 (4s, 27H, 9 × C$\underline{H}_3$COO), 1.09 (d, *J* = 6.6 Hz, 6H, $H_{c'}$), 1.08 (d, *J* = 6.6 Hz, 3H, $H_{a'}$).

^{13}C-NMR ($CDCl_3$, 75 MHz) δ / ppm: 170.7, 170.6, 170.5 170.4 170.2, 170.1 ($CH_3\underline{C}OO$), 152.4 (C_c), 144.6 (C_k), 143.7 (C_f), 137.8 (C_d), 133.7 (C_a), 124.9 (C_l), 124.4 (C_g), 108.6 (C_b), 96.4 (C_q), 96.3 (C_r); 71.1, 71.0, 68.0, 67.9, 67.9, 66.4, 66.2, 65.0, 64.9 (C_s, C_t, C_u, C_v, C_w, C_x, C_y, C_z, C_n, C_p); 63.1 (C_j), 60.5 (C_e), 50.0 (C_m), 49.7 (C_o), 46.4 (C_h); 20.9, 20.8, 20.8, 20.7 ($\underline{C}H_3COO$); 15.9 ($C_{c'}$, $C_{a'}$).

FTIR (CH_2Cl_2)(cm^{-1}): 2926, 2855 (*ν* **C**–**H**); 1744 (*ν* **C=O**), 1594 (*ν* **C=C Ar**), 1437, 1370, 1224, 1047 (*ν* **C**–**O**).

MALDI-TOF: *m/z* 1365.41 calculated for $[M]^+$ $C_{58}H_{76}ClN_9O_{27}$, found: 1365.98.

3,4,5-Tris[(1-(2-(2,3,4-tri-*O*-acetyl-*α*-L-fucopyranosyl)ethyl)-1*H*-1,2,3-triazol-4-yl)methoxy]benzyl azide (21)

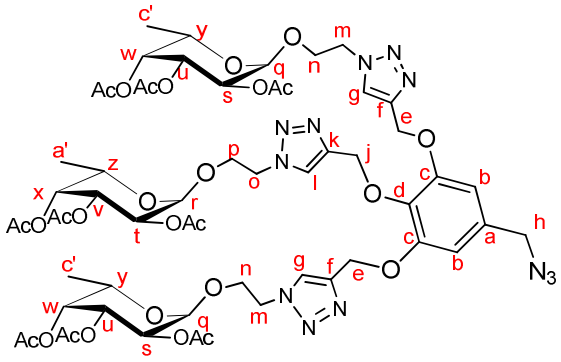

21

A mixture of 375 mg (0.27 mmol) of **20** and 144 mg (2.2 mmol) of sodium azide was dissolved, under Ar atmosphere, in 6 mL of dry DMF. The reaction mixture was stirred at 55 ºC for 24 h. Thereafter, the reaction crude was suspended in 100 mL of AcOEt and the organic phase was washed with water (3 × 100 mL).

The organic layer was dried over anhydrous $MgSO_4$ and filtered. The solvent was removed at low pressure and **21** was obtained as a white foam (90 % yield).

^{1}H-NMR ($CDCl_3$, 300 MHz) δ / ppm: 7.98 (s, 1H, H_l), 7.95 (s, 2H, H_g), 6.69 (s, 2H, H_b), 5.30–5.00 (m, 18H), 4.61 (m, 6H, H_e, H_j), 4.26 (s, 2H, H_h), 4.17–4.05 (m, 4H), 3.98 (c, J = 6.6 Hz, 1H, H_z), 3.95–3.80 (m, 4H), 2.14, 1.99, 1.95, 1.94 (4s, 27H, 9 × CH_3COO), 1.09 (d, J = 6.6 Hz, 6H, $H_{c'}$), 1.08 (d, J = 6.6 Hz, 3H, $H_{a'}$).

^{13}C-NMR ($CDCl_3$, 75 MHz) δ / ppm: 170.7, 170.6, 170.5 170.4 170.2, 170.1 (CH_3COO), 152.5 (C_c), 144.5 (C_k), 143.8 (C_f), 137.6 (C_d), 131.7 (C_a), 124.9 (C_l), 124.4 (C_g), 108.1 (C_b), 96.4 (C_q), 96.3 (C_r); 71.1, 71.0, 68.0, 67.9, 67.9, 66.4, 66.2, 65.0, 64.9 (C_s, C_t, C_u, C_v, C_w, C_x, C_y, C_z); 63.1 (C_j), 60.5 (C_e), 54.9 (C_h), 50.0 (C_m), 49.7 (C_o); 20.8, 20.8, 20.7 (CH_3COO); 15.9 ($C_{c'}$, $C_{a'}$).

FTIR (CH_2Cl_2) (cm^{-1}): 2925, 2854 (ν **C–H**); 2102 (ν **-N=N=N**), 1742 (ν **C=O**), 1593 (ν **C=C Ar**), 1438, 1371, 1223, 1046 (ν **C–O**).

MALDI-TOF: *m/z* 1372.49 calculated for $[M]^+$ $C_{58}H_{76}N_{12}O_{27}$, found: 1373.02.

3,4,5-Tris[(1-(2-(α-L-fucopiranosyl)ethyl)-1*H*-1,2,3-triazol-4-yl) methoxy]benzyl azide (22)

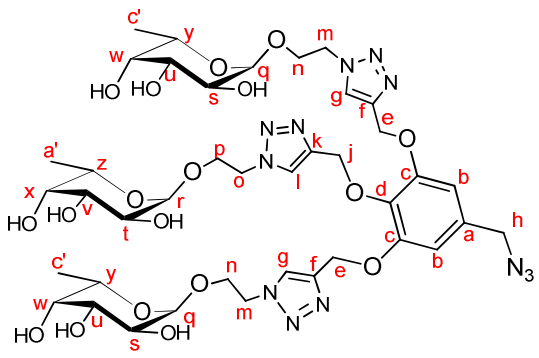

22

To a solution of 150 mg (0.11 mmol) of **21** in 6 mL of dry MeOH under Ar atmosphere at 0 ºC, a 1 M solution of sodium methoxide in methanol was added

dropwise until pH 9 was obtained. The reaction mixture was allowed for 15 minutes to reach room temperature, and it was stirred for 18 hours. Thereafter, Amberlite IR-120 was added until pH 5 was obtained. The resin was removed by filtration and the solvent was evaporated at low pressure, affording **22** as a white foam (99 % yield).

^{1}H-NMR (MeOD-d$_4$, 300 MHz) δ / ppm: 8.27 (s, 2H, H_g), 8.09 (s, 1H, H_l), 6.85 (s, 2H, H_b), 5.22 (s, 4H), 5.09 (d, J = 1.8 Hz, 2H), 4.75 (m, 3H), 4.70–4.61 (m, 6H), 4.33 (s, 2H, H_h), 4.09–3.98 (m, 3H), 3.87–3.79 (m, 3H), 3.74–3.50 (m, 9H), 3.77 (c, J = 6.6 Hz, 3H, H_y, H_z), 1.05 (d, J = 6.6 Hz, 9H, $H_{c'}$, $H_{a'}$).

^{13}C-NMR (MeOD-d$_4$, 75 MHz) δ / ppm: 153.7 (C_c), 145.5 (C_k), 144.7 (C_f), 138.6 (C_d), 133.5 (C_a), 127.0 (C_l), 126.9 (C_g), 109.3 (C_b), 100.5 (C_q), 100.4 (C_r); 73.4, 73.3, 71.5, 71.4, 69.9, 69.8, 67.7, 67.2, 67.1, 66.9 (C_s, C_t, C_u, C_v, C_w, C_x, C_y, C_z, C_n, C_p); 63.5 (C_j), 61.5 (C_e), 55.5 (C_h), 51.4 (C_m), 51.3 (C_o), 16.6 ($C_{c'}$, $C_{a'}$).

FTIR (KBr) (cm^{-1}): 3380 (*v* **O–H**), 2925 (*v* **C–H**), 2103 (*v* **–N=N=N**), 1595 (*v* **C=C Ar**),

MALDI-TOF: *m/z* 995.40 calculated for $[M+H]^+$ $C_{40}H_{58}N_{12}O_{18}$, found: 995.36.

Attempt to prepare compound 23:

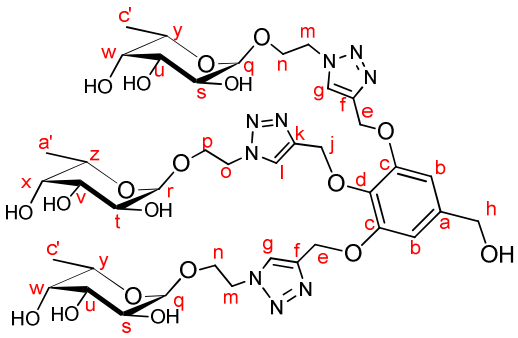

23

A mixture of 104 mg (0.44 mmol) of **5**, 35 mg (0.12 mmol) of **11,** 22 mg (0.11 mmol) of sodium ascorbate and 28 mg (0.11 mmol) of $CuSO_4 \cdot 5H_2O$ was

dissolved in 2 mL of deoxygenated THF/water (1:1, v/v), and a piece of copper wire was added. After stirring for 18 h at room temperature, 200 mg of Quadrasil Mercaptopropil™ were added to the reaction crude in order to remove copper species. The solvent was removed at low pressure and the reaction crude was purified by column chromatography using AcOEt:MeOH (1:1, v/v) as eluent. A white foam was obtained with a *m/z* peak in MALDI-TOF at 992.23 ($[M+Na]^+$ $C_{40}H_{58}O_{18}N_9Cl$ = 987.35). It corresponds to ($[M+Na]^+$ $C_{40}H_{59}O_{19}N_9$, the derivative where the Cl group at the benzylic position has been replaced by an OH group.

Bromomethyl *N*-(tris[(1-(2-(α-L-fucopiranosyl)ethyl)-1*H*-1,2,3-triazol-4-yl)methoxy])methane)carbamate (24)

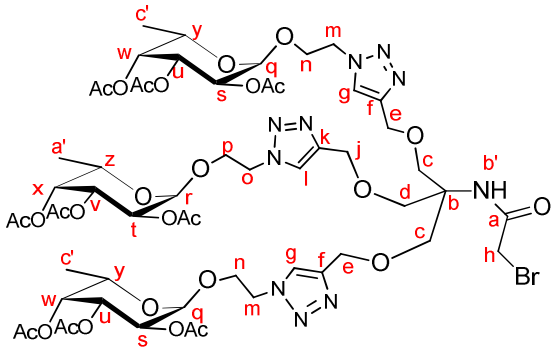

24

A mixture of 100 mg (0.28 mmol) of **9**, 29 mg (0.08 mmol) of **22**, 16 mg (0.08 mmol) of sodium ascorbate and 13 mg (0.05 mmol) of $CuSO_4 \cdot 5H_2O$ were dissolved in 1 mL of deoxygenated THF/water (1:1, v/v), and a piece of copper wire was added. After stirring for 18 h, the reaction crude was resuspended in 20 mL of AcOEt and washed with aqueous saturated NH_4Cl (2 × 10 mL), 15 mL of water and 15 mL of brine. The organic layer was dried over anhydrous $MgSO_4$ and filtered. The solvent was removed at low pressure and the reaction crude was purified by column chromatography using AcOEt in order to remove excess of **3**, followed by AcOEt:MeOH (95:5, v/v). Compound **24** was obtained as a white foam (85 % yield).

^{1}H-NMR ($CDCl_3$, 300 MHz) δ / ppm: 7.75 (s, 2H, H_g), 7.74 (s, 1H, H_l), 6.94 (s, 1H, $H_{b'}$), 5.32–5.24 (m, 7H), 5.14–5.06 (m, 7H), 4.62 (m, 8H), 4.17–4.10 (m, 3H, H_z and H_y), 3.97–3.81 (m, 16H), 2.17, 2.03, 2.00 (3s, 27H, 9 × $C\underline{H}_3COO$), 1.11 (d, J = 6.6 Hz, 9H, $H_{c'}$ and $H_{a'}$).

^{13}C-NMR ($CDCl_3$, 75 MHz) δ / ppm: 170.6, 170.4, 170.2, 170.1 ($CH_3\underline{C}OO$); 165.8 (C_a), 144.9 (C_f), 144.8 (C_k), 123.8 (C_g, C_l), 96.4 (C_q, C_r), 71.0, 68.7 (C_b); 68.0, 67.9, 66.4, 65.0, 64.9, 60.5, 60.3; 49.9 (C_o), 29.8 (C_h); 20.8, 20.7 ($\underline{C}H_3COO$); 16.0 ($C_{c'}$, $C_{a'}$).

FTIR (CH_2Cl_2) (cm^{-1}): 2927 (*v* **C–H**), 1744 (*v* **C=O**, **ester**), 1681 (*v* **C=O**, **amide**), 1371, 1225, 1053 (*v* **C–O**).

MALDI-TOF: *m/z* 1433.44 calculated for $[M+H]^+$ $C_{57}H_{81}N_{10}O_{28}$,Br, found: 1433.53.

1,3-Bis[3,5-bis(propargyloxy)benzyl]malonate (25)

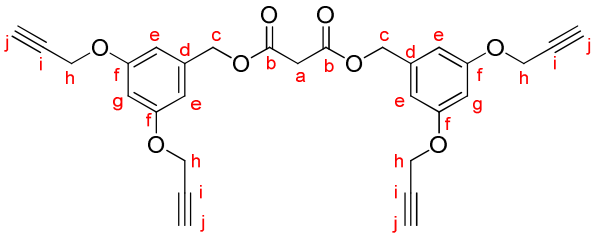

25

To a solution of 2.33 g (11 mmol) of **14**, 4 mL (29 mmol) of triethylamine and 80 mg (0.75 mmol) of 4-dimethylaminopyridine in 75 mL of dry CH_2Cl_2 at 0 ºC and under Ar atmosphere, 780 mg (5.5 mmol) of malonyl chloride in 15 mL of dry CH_2Cl_2 were added dropwise. After 30 minutes, the reaction mixture was allowed to reach room temperature and after 4 hours of stirring, the reaction crude was washed with HCl 1 M (2 × 20 mL), saturated aqueous $NaHCO_3$ (20 mL) and brine (2 × 30 mL). The organic layer was dried over anhydrous $MgSO_4$ and filtered. Solvent was removed at low pressure and the resulting oil was purified by column chromatography using CH_2Cl_2 as eluent. Compound **25** was obtained as a white solid (50 % yield).

^{1}H-NMR ($CDCl_3$, 300 MHz) δ / ppm: 6.58 (m, 6H, H_e, H_g), 5.13 (s, 4H, H_c), 4.65 (d, J = 2.4 Hz, 8H, H_h), 3.50 (s, 2H, H_a), 2.53 (t, J = 2.4 Hz, 4H, H_j).

^{13}C-NMR ($CDCl_3$, 75 MHz) δ / ppm: 166.2 (C_b), 158.9 (C_f), 137.8 (C_d), 107.6 (C_e), 102.3 (C_g), 78.4 (C_i), 75.9 (C_j), 67.0 (C_c), 56.1 (C_h), 41.6 (C_a).

FTIR (KBr) (cm^{-1}): 3259 (ν C≡**C**–**H**), 2123 (ν **C≡C**), 1726 (ν **C=O**), 1600 (ν **C=C Ar**), 1159 (ν **C–O**).

1,3-Bis[3,4,5-tris(propargyloxy)benzyl]malonate (26)

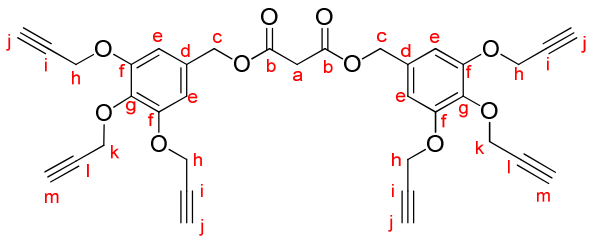

26

To a solution of 830 mg (3.08 mmol) of **15**, 1 mL (7.2 mmol) of triethylamine and 18 mg (0.17 mmol) of 4-dimethylaminopyridine in 15 mL of dry CH_2Cl_2 at 0 ºC and under Ar atmosphere, 190 mg (1.4 mmol) of malonyl chloride in 15 mL of dry CH_2Cl_2 were added dropwise. After 30 minutes, the reaction was allowed to reach room temperature and after 4 hours, the reaction crude was washed with HCl 1 M (2 × 20 mL), saturated aqueous $NaHCO_3$ (1 × 20 mL) and brine (2 × 30 mL). The organic layer was dried over anhydrous $MgSO_4$ and filtered. Solvent was removed at low pressure and the remaining oil was purified by column chromatography using CH_2Cl_2:MeOH (95:5, v/v) as eluent. Compound **26** was obtained as a white solid (52 % yield).

^{1}H-NMR ($CDCl_3$, 300 MHz) δ / ppm: 6.75 (s, 4H, H_e), 5.14 (s, 4H, H_c), 4.75 (d, J = 2.4 Hz, 8H, H_h), 4.73 (d, J = 2.4 Hz, 4H, H_k), 3.51 (s, 2H, H_a), 2.51 (t, J = 2.4 Hz, 4H, H_j), 2.46 (t, J = 2.4 Hz, 2H, H_n).

^{13}C-NMR ($CDCl_3$, 75 MHz) δ / ppm: 166.3 (C_b), 151.8 (C_f), 137.3 (C_d), 131.5 (C_g), 108.6 (C_e), 79.2 (C_l), 78.4 (C_i), 76.2 (C_j), 75.5 (C_m), 67.2 (C_c), 64.5 (C_k), 57.2 (C_h), 41.6 (C_a).

FTIR (CH_2Cl_2) (cm^{-1}): 3285 (*v* C≡**C–H**); 2931, 2890 (*v* **C–H**); 2123 (*v* **C≡C**), 1730 (*v* **C=O**), 1594 (*v* **C=C Ar**), 1500, 1214 (*v* **C–O**).

1,3-Bis(4-pentyn-1-yl)malonate (27)

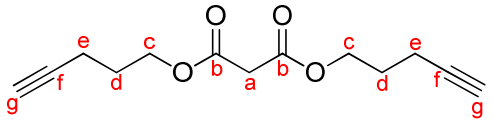

27

To a solution of 2.44 g (30.8 mmol) of 4-pentyn-1-ol, 4 mL (29 mmol) of triethylamine and 79 mg (0.75 mmol) of 4-dimethylaminopyridine in 15 mL of dry CH_2Cl_2 at 0 ºC and under Ar atmosphere, 2.0 g (14 mmol) of malonyl chloride in 15 mL of dry CH_2Cl_2 were added dropwise. After 30 minutes, the reaction was allowed to reach room temperature and after 4 hours of stirring, the reaction crude was washed with HCl 1 M (2 × 20 mL), saturated aqueous $NaHCO_3$ (1 × 20 mL) and brine (2 × 30 mL). The organic layer was dried over anhydrous $MgSO_4$ and filtered. Solvent was removed at low pressure and the remaining oil was purified by column chromatography using hexane:CH_2Cl_2 (1:4, v/v) as eluent. Compound **27** was obtained as a yellowish oil (61 % yield).

^{1}H-NMR ($CDCl_3$, 300 MHz) δ / ppm: 4.26 (t, J = 6.3 Hz, 4H, H_c), 3.38 (s, 2H, H_a), 2.29 (td, J = 6.3 Hz, J = 2.7 Hz, 4H, H_e), 1.97 (t, J = 2.7 Hz, 2H, H_g), 1.87 (q, J = 6.3 Hz, 4H, H_d).

^{13}C-NMR ($CDCl_3$, 75 MHz) δ / ppm: 166.5 (C_b), 82.9 (C_f), 69.3 (C_g), 64.1 (C_c), 41.6 (C_a), 27.5 (C_d), 15.2 (C_e).

FTIR (CH_2Cl_2) (cm^{-1}): 3290 (*v* C≡**C–H**); 2922, 2852 (*v* **C–H**); 2118 (*v* **C≡C**), 1728 (*v* **C=O**), 1147 (*v* **C–O**).

[60]Fullerene monoadduct of 1,3-bis(4-pentyn-1-yl)malonate (28)

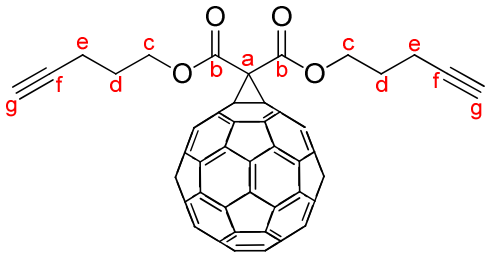

28

To a sonicated solution of 100 mg (0.48 mmol) of **27**, 460 mg (0.63 mmol) of [60]fullerene and 174 mg (0.68 mmol) of I_2, in 180 mL of dry toluene at 0 ºC and under Ar atmosphere, 222 mg (1.46 mmol) of 1,8-diazabicycloundec-7-ene in 20 mL of dry toluene were added dropwise. The reaction mixture was stirred at 0 ºC for 5 hours. Thereafter, 30 mL of saturated aqueous sodium thiosulfate were added in order to finish the reaction. The organic phase was washed with saturated aqueous sodium thiosulfate (2 × 30 mL), HCl 0.5 M (2 × 20 mL) and brine (2 x 20 mL). The organic layer was dried over anhydrous $MgSO_4$ and filtered. The solvent was removed at low pressure and the reaction crude was purified by column chromatography, firstly using CS_2 as eluent in order to remove the unreacted [60]fullerene, and followed by toluene. Compound **28** was obtained as a dark brown solid (40 % yield).

^{1}H-NMR ($CDCl_3$, 300 MHz) δ / ppm: 4.63 (t, J = 6.0 Hz, 4H, H_c), 2.43 (td, J = 6.0 Hz, J = 2.4 Hz, 4H, H_e), 2.08 (q, J = 6.0 Hz, 4H, H_d), 2.04 (t, J = 2.4 Hz, 2H, H_g).

^{13}C-NMR ($CDCl_3$, 75 MHz) δ / ppm: 163.7 (C_b); 145.4, 145.3, 145.2, 145.1, 144.9, 144.8, 144.8, 144.0, 143.2, 143.2, 143.1, 142.3, 142.1, 141.2, 139.2 (sp^2 – C_{60}); 82.6 (C_f), 71.5 (sp^3 – C_{60}), 69.9 (C_g), 65.9 (C_c), 52.0 (C_a), 27.5 (C_d), 15.4 (C_e).

FTIR (CH_2Cl_2) (cm^{-1}): 3292 (ν C≡**C**–**H**); 2922, 2851 (ν **C**–**H**); 1738 (ν **C=O**), 1460, 1233.

[60]Fullerene monoadduct of 1,3-bis(3,5 bis(propargyloxy)benzyl)malonate (29)

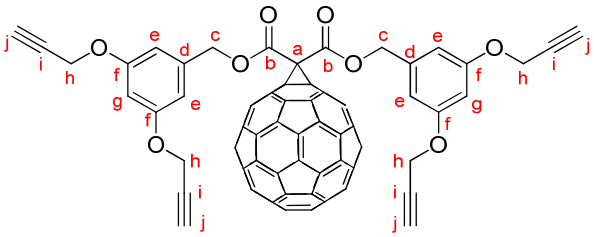

29

To a sonicated solution of 100 mg (0.20 mmol) of **25**, 270 mg (0.38 mmol) of [60]fullerene and 96 mg (0.38 mmol) of I_2, in 180 mL of dry toluene at 0 ºC and under Ar atmosphere, 148 mg (0.96 mmol) of 1,8-diazabicycloundec-7-ene in 20 mL of dry toluene were added dropwise. Reaction mixture was stirred at 0 ºC for 5 hours. Thereafter 30 mL of saturated aqueous sodium thiosulfate were added in order to finish the reaction. The organic phase was washed with saturated aqueous sodium thiosulfate (2 × 30 mL), HCl 0.5 M (2 × 20 mL) and brine (2 × 20 mL). The organic layer was dried over anhydrous $MgSO_4$ and filtered. The solvent was removed at low pressure and the reaction crude was purified by column chromatography using CS_2 as eluent to remove unreacted [60]fullerene, followed by toluene. Compound **29** was obtained as a dark brown solid (30 % yield).

^{1}H-NMR ($CDCl_3$, 300 MHz) δ / ppm: 6.70 (d, J = 2.1 Hz, 4H, H_e), 6.60 (t, J = 2.1 Hz, 2H, H_g), 5.44 (s, 4H, H_c), 4.65 (d, J = 2.4 Hz, 8H, H_h), 2.55 (t, J = 2.4 Hz, 4H, H_j).

^{13}C-NMR ($CDCl_3$, 75 MHz) δ / ppm: 163.4 (C_b), 159.0 (C_f); 145.4, 145.3, 145.2, 145.0, 145.0, 144.8, 144.7, 144.0, 143.2, 143.1, 143.1, 142.3, 142.0, 141.1, 139.2 (sp^2 – C_{60}); 137.1 (C_d), 108.2 (C_e), 102.6 (C_g), 78.3 (C_i), 76.2 (C_j), 71.5 (sp^3 – C_{60}), 68.7 (C_c), 56.1 (C_h), 51.8 (C_a).

FTIR (CH_2Cl_2) (cm^{-1}): 3292 (ν **C≡C–H**); 2956, 2854 (ν **C–H**); 2122 (ν **C≡C**), 1742 (ν **C=O**), 1596 (ν **C=C Ar**), 1453, 1368, 1150 (ν **C–O**).

[60]Fullerene monoadduct of 1,3-bis[3,4,5 tris(propargyloxy)benzyl]malonate (30)

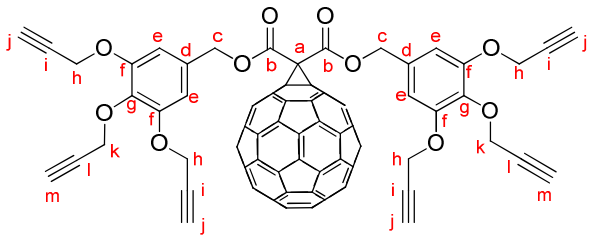

30

To a sonicated solution of 145 mg (0.24 mmol) of **26**, 307 mg (0.38 mmol) of [60]fullerene and 108 mg (0.43 mmol) of I_2, in 180 mL of dry toluene at 0 ºC and under Ar atmosphere, 145 mg (0.95 mmol) of 1,8-diazabicycloundec-7-ene in 20 mL of dry toluene were added dropwise. The reaction mixture was stirred at 0 ºC for 5 hours. Thereafter 30 mL of saturated aqueous sodium thiosulfate were added in order to finish the reaction. The organic phase was washed with saturated aqueous sodium thiosulfate (2 × 30 mL), HCl 0.5 M (2 × 20 mL) and brine (2 × 20 mL). The organic layer was dried over anhydrous $MgSO_4$ and filtered. The solvent was evaporated at low pressure and the reaction crude was purified by column chromatography using CS_2 as eluent to remove the unreacted [60]fullerene, followed by toluene:AcOEt (95:5, v/v). Compound **30** was obtained as a dark brown solid (32 % yield).

^{1}H-NMR ($CDCl_3$, 300 MHz) δ / ppm: 6.87 (s, 4H, H_e), 5.44 (s, 4H, H_c), 4.74 (m, 12H, H_h, H_k), 2.53 (t, J = 2.4 Hz, 4H, H_j), 2.47 (t, J = 2.4 Hz, 2H, H_m).

^{13}C-NMR ($CDCl_3$, 75 MHz) δ / ppm: 163.5 (C_b), 151.9 (C_f); 145.4, 145.3, 145.2, 145.0, 145.0, 144.8, 144.7, 144.0, 143.2, 143.1, 143.1, 142.3, 142.0, 141.1, 139.1 (sp^2 – C_{60}); 130.8 (C_g), 109.2 (C_e), 79.2 (C_l), 78.4 (C_i), 76.4 (C_j), 75.6 (C_m), 71.5 (sp^3 – C_{60}) 68.9 (C_c), 60.5 (C_k), 57.3 (C_h), 52.2 (C_a).

FTIR (CH_2Cl_2) (cm^{-1}): 3293 (ν C≡**C**–**H**); 2925, 2855 (ν **C**–**H**); 2123 (ν **C**≡**C**), 1744 (ν **C**=**O**), 1590 (ν **C**=**C Ar**), 1503, 1449, 1266, 1203, 1109 (ν **C**–**O**).

[60]Glycofullerene from monoadduct of bis(4-pentyn-1-yl)malonate and 3,4,5-tris[(1-(2-(α-L-fucopyranosyl)ethyl)-1*H*-1,2,3-triazol-4-yl) methoxy]benzyl azide (31)

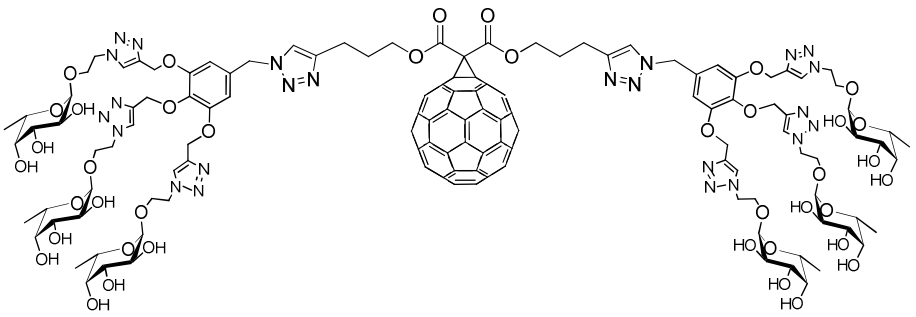

31

A mixture of 32 mg (0.03 mmol) of **28**, 97 mg (0.10 mmol) of **22**, 10 mg ($5.3 \cdot 10^{-2}$ mmol) of CuI and 30 μL ($1.7 \cdot 10^{-4}$ mmol) of DIPEA under Ar atmosphere was dissolved in 2.0 mL of deoxygenated DMSO, and a piece of copper wire was added. After stirring for 48 hours, Quadrasil Mercaptopropil™ was added to the reaction crude and stirred for 30 minutes. Thereafter, the suspension was filtered and acetonitrile was added to the solution until a solid precipitate appeared. After centrifugation (10 minutes, 6000 rpm), the solid was suspended in AcOEt and sonicated for 2 minutes. Finally, the solid was isolated by centrifugation (15 minutes, 6000 rpm). Compound **31** was obtained as a dark brown solid (63 % yield).

^{1}H-NMR (D_2O, 700 MHz) δ / ppm: 8.02 (s, 8H), 6.80 (s, 4H), 5.50 - 4.88 (m, ~12H), 4.63 (s, ~22H), 3.91 (~12H), 3.80-3.40 (m, ~24H), 0.91 (s, 18H).

^{13}C-NMR (D_2O, 175 MHz) δ / ppm: 152.0, 143.4, 143.1, 136.0, 131.4, 125.8, 107.1, 97.9, 71.8, 69.2, 67.6, 66.4, 66.2, 65.4, 61.7, 61.8, 53.8, 50.2, 15.2.

FTIR (KBr) (cm^{-1}): 3380 (*ν* **O–H**), 2925 (*ν* **C–H**), 1739 (*ν* **C=O**), 1595 (*ν* **C=C Ar**),

MALDI-TOF: *m/z* 5195.73 calculated for $[M]^+$ $C_{249}H_{254}N_{48}O_{80}$, found: 5195.43.

[60]Glycofullerene from monoadduct of bis(3,5 bis(propargyloxy)benzyl)malonate and 3,4,5-tris[(1-(2-(α-L-fucopyranosyl)ethyl)-1*H*-1,2,3-triazol-4-yl)methoxy]benzyl azide (32)

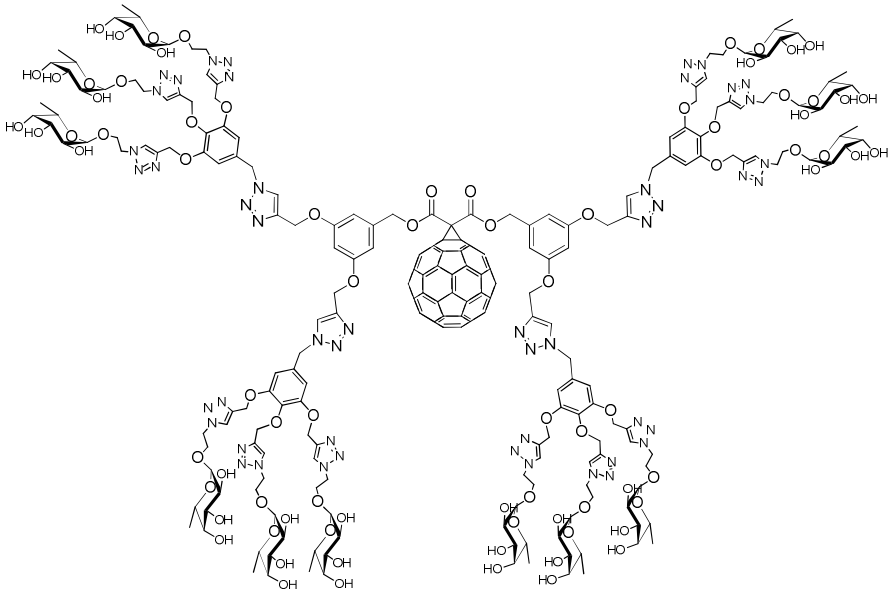

32

A mixture of 22 mg (0.02 mmol) of **29**, 98 mg (0.10 mmol) of **22**, 10 mg ($5.3 \cdot 10^{-2}$ mmol) of CuI and 30 μL ($1.7 \cdot 10^{-4}$ mmol) of DIPEA under Ar atmosphere was dissolved in 2.0 mL of deoxygenated DMSO, and a piece of copper wire was added. After stirring for 48 hours, Quadrasil Mercaptopropil™ was added to the reaction crude and stirred for 30 minutes. Thereafter, the suspension was filtered and acetonitrile was added to the solution until a precipitate appeared. After centrifugation (10 minutes, 6000 rpm), the solid was suspended in AcOEt and sonicated for 2 minutes. Finally, the solid was isolated by centrifugation (15 minutes, 6000 rpm). Compound **32** was obtained as a dark brown solid (65 % yield).

^{1}H-NMR (D_2O, 700 MHz) δ / ppm: 8.16 - 8.05 (2s, 16H), 6.80 (s, 14H), 5.63 - 4.88 (m, ~28H), 4.63 (s, ~36H), 3.93 (~24H), 3.79-3.40 (m, ~48H), 0.91 (s, 54H).

^{13}C-NMR (D_2O, 175 MHz) δ / ppm: 152.1, 143.5, 143.0, 136.0, 131.2, 125.7, 107.1, 98.1, 71.6, 69.2, 67.6, 66.4, 66.0, 65.4, 61.7, 61.6, 53.8, 50.2, 15.1.

FTIR (KBr) (cm^{-1}): 3382 (*v* **O–H**), 2921 (*v* **C–H**), 1738 (*v* **C=O**), 1592 (*v* **C=C Ar**).

MALDI-TOF: *m/z* 5195.73 calculated for $[M]^+$ $C_{249}H_{254}N_{48}O_{80}$, found: 5195.43.

[60]Glycofullerene from monoadduct of bis(3,4,5 tris(propargyloxy)benzyl)malonate and 3,4,5-tris[(1-(2-(α-L-fucopyranosyl)ethyl)-1*H*-1,2,3-triazol-4-yl)methoxy]benzyl azide (33)

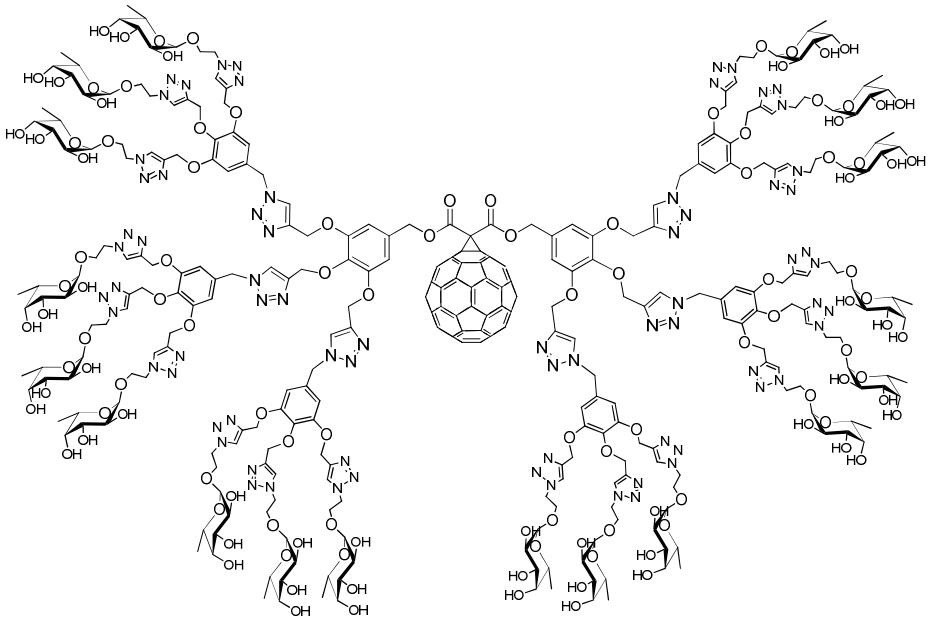

33

A mixture of 19 mg (0.02 mmol) of **30**, 98 mg (0.10 mmol) of **22**, 10 mg ($5.3\cdot10^{-2}$ mmol) of CuI and 30 µL ($1.7\cdot10^{-4}$ mmol) of DIPEA under Ar atmosphere was dissolved in 2.0 mL of deoxygenated DMSO, and a piece of copper wire was added. After stirring for 48 hours, Quadrasil Mercaptopropil™ was added to the reaction crude and stirred for 30 minutes. Thereafter, the

suspension was filtered and acetonitrile was added to the solution until a solid precipitate appeared. After centrifugation (10 minutes, 6000 rpm), the solid was suspended in AcOEt and sonicated for 2 minutes. Finally, the solid was isolated by centrifugation (15 minutes, 6000 rpm). Compound **33** was obtained as a dark brown solid (65 % yield).

^{1}H-NMR (D_2O, 700 MHz) δ / ppm: 8.14 - 8.01 (2s, 24H), 6.83 (s, 16H), 5.63 - 4.88 (m, 40H), 4.55 (s, ~54H), 3.93 (~36H), 3.81-3.35 (m, ~72H), 0.90 (s, 54H).

^{13}C-NMR (D_2O, 175 MHz) δ / ppm: 151.8, 143.6, 142.8, 136.2, 131.5, 125.7, 107.2, 98.1, 71.5, 69.4, 67.8, 66.3, 65.9, 65.4, 61.7, 61.5, 53.6, 50.1, 15.3.

FTIR (KBr) (cm^{-1}): 3393 (*v* **O–H**), 2932 (*v* **C–H**), 1740 (*v* **C=O**), 1593 (*v* **C=C Ar**).

MALDI-TOF: *m/z* 7318.56 calculated for $[M]^+$ $C_{337}H_{376}N_{72}O_{118}$, found: 7318.13.

3-(Propargyloxy)fluorescein propargyl ester (34)

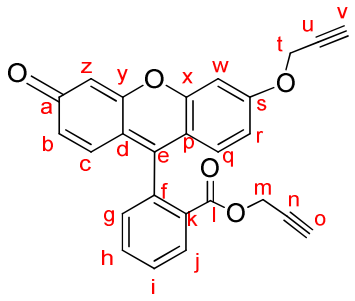

34

To a solution of 1.00 g (3.04 mmol) of fluorescein and 0.93 g (6.7 mmol) of K_2CO_3 in 15 mL of dry DMF under Ar atmosphere, 1.03 g (6.92 mmol) of propargyl bromide (80% wt in toluene) in 5 mL of dry DMF were added. The reaction mixture was stirred at 65 ºC for 4 hours. The reaction crude was resuspended in 100 mL of AcOEt and the organic phase was washed with water (3 × 100 mL). The organic layer was dried over $MgSO_4$ and filtered. The solvent was removed at low pressure and the reaction crude was purified by column

chromatography using CH_2Cl_2 as eluent. Compound **34** was obtained as an orange solid (90 % yield).

^{1}H-NMR (DMSO-d_6, 300 MHz) δ / ppm: 8.21 (dd, *J* = 7.5 Hz, *J* = 0.9 Hz, 1H, H_j), 7.90 (td, *J* = 7.5 Hz, *J* = 0.9 Hz, 1H, H_h or H_i), 7.81 (td, *J* = 7.5 Hz, *J* = 0.9 Hz, 1H, H_h or H_i), 7.53 (dd, *J* = 7.5 Hz, *J* = 0.9 Hz, 1H, H_g), 7.26 (d, *J* = 2.4 Hz, 1H, H_w), 6.92 (dd, *J* = 9.0 Hz, *J* = 2.4 Hz, 1H, H_r), 6.85 (d, *J* = 9.0 Hz, 1H, H_q), 6.78 (d, *J* = 9.6 Hz, 1H, H_c), 6.39 (dd, *J* = 9.6 Hz, *J* = 1.8 Hz, 1H, H_b), 6.25 (d, *J* = 1.8 Hz, H_z), 5.01 (d, *J* = 2.4 Hz, 2H, H_t), 4.66 (d, *J* = 2.4 Hz, 2H, H_m), 3.70 (t, *J* = 2.4 Hz, 1H, H_v), 3.41 (t, *J* = 2.4 Hz, 1H, H_o).

^{13}C-NMR (DMSO-d_6, 75 MHz) δ / ppm: 184.0, 164.0, 161.6, 158.3, 153.2, 149.4, 133.8, 133.5, 130.8, 130.8, 130.3, 130.1, 129.5, 129.0, 128.9, 117.1, 114.9, 113.9, 104.7, 101.5; 79.1, 78.3 (C_u, C_n); 77.9, 77.3 (C_v, C_o); 56.4, 52.7 (C_t, C_m).

FTIR (KBr) (cm^{-1}): 3276, 3183 (*v* C≡**C**–**H**); 2122 (*v* **C≡C**), 1727 (*v* **C=O, ester**), 1642 (*v* **C=O, keto**), 1597 (*v* **C=C Ar**), 1512.

Fluorescein methyl ester (35)

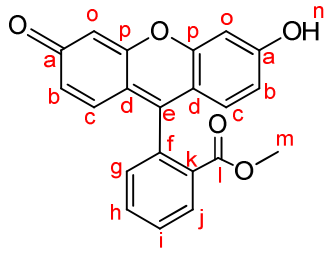

35

To a solution of 4.03 g (12.1 mmol) of fluorescein in 25 mL of MeOH, 3 mL of concentrated H_2SO_4 were added dropwise. The reaction mixture was stirred at 85 ºC during 18 hours and the reaction was finished by adding 10 mL of ice/water. $NaHCO_3$ was added slowly until neutral pH was reached. The remaining precipitate was isolated by filtration, washed with cold water and with hexane. The compound was dried at 65 ºC, obtaining **35** as a dark red solid (98 % yield).

^{1}H-NMR (DMSO-d_6, 300 MHz) δ / ppm: 11.08 (br s, 1H, H_n), 8.20 (dd, *J* = 7.5 Hz, *J* = 0.9 Hz, 1H, H_j), 7.86 (td, *J* = 7.5 Hz, *J* = 0.9 Hz, 1H), 7.77 (td, *J* = 7.5 Hz, *J* = 0.9 Hz, 1H), 7.48 (dd, *J* = 7.5 Hz, *J* = 0.9 Hz, 1H, H_g), 6.77 (d, *J* = 9.3 Hz, 2H, H_c), 6.54 (m, 4H, H_b, H_o), 3.58 (s, 3H, H_m).

^{13}C-NMR (DMSO-d_6, 75 MHz) δ / ppm: 165.2 (C_l), 150.5, 134.1, 133.2, 130.7, 130.0, 129.9, 129.5, 103.3, 52.3 (C_m).

FTIR (KBr) (cm^{-1}): 3407 (*v* **O–H**), 2949 (*v* **C–H**), 1715 (*v* **C=O, ester**), 1640 (*v* **C=O, keto**), 1597 (*v* **C=C Ar**), 1565.

3-(Propargyloxy)fluorescein methyl ester (36)

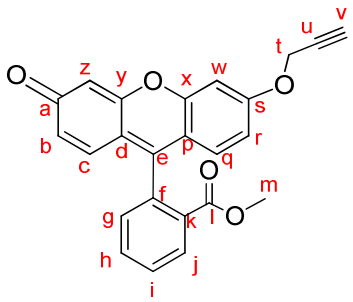

36

To a solution of 1.06 g (3.07 mmol) of **35** and 0.65 g (4.7 mmol) of K_2CO_3 in 25 mL of dry DMF under Ar atmosphere, 0.55 g (3.68 mmol) of propargyl bromide in 5 mL of dry DMF were added. The reaction mixture was stirred at room temperature during 18 hours. The reaction crude was resuspended in 100 mL of CH_2Cl_2 and the organic phase was washed with water (3 × 100 mL). The organic layer was dried over anhydrous $MgSO_4$ and filtered. The solvent was removed at low pressure and compound **36** was obtained as an orange solid (90 % yield).

^{1}H-NMR (DMSO-d_6, 300 MHz) δ / ppm: 8.22 (dd, *J* = 7.5 Hz, *J* = 0.9 Hz, 1H, H_j), 7.87 (td, *J* = 7.5 Hz, *J* = 0.9 Hz, 1H, H_h or H_i), 7.78 (td, *J* = 7.5 Hz, *J* = 0.9 Hz, 1H, H_h or H_i), 7.50 (dd, *J* = 7.5 Hz, *J* = 0.9 Hz, 1H, H_g), 7.27 (d, *J* = 2.4 Hz, 1H, H_u), 6.93 (dd, *J* = 9.0 Hz, *J* = 2.4 Hz, 1H, H_r), 6.86 (d, *J* = 9.0 Hz, 1H, H_q),

6.79 (d, *J* = 9.6 Hz, 1H, H_c), 6.39 (dd, *J* = 9.6 Hz, *J* = 1.8 Hz, 1H, H_b), 6.25 (d, *J* = 1,8 Hz, H_z), 5.00 (d, *J* = 2.4 Hz, 2H, H_t), 3.70 (t, *J* = 2.4 Hz, 1H, H_v), 3.59 (s, 3H, H_m).

^{13}C-NMR (DMSO-d$_6$, 75 MHz) δ / ppm: 185.4 (C_a), 165.7 (C_l), 161.2, 158.9, 154.0, 150.2, 134.7, 132.5, 131.1, 130.6, 130.4, 130.2, 130.1, 129.7, 128.8, 118.0, 115.3, 113.6, 106.0, 101.5, 77.4 (C_u), 76.5 (C_v), 56.4 (C_t), 52.3 (C_m).

FTIR (KBr) (cm^{-1}): 3183 (*v* C≡**C**–**H**), 2940 (*v* **C**–**H**), 2115 (*v* **C≡C**), 1720 (*v* **C=O, ester**), 1643 (*v* **C=O, keto**), 1594 (*v* **C=C Ar**).

Fluorescein glycoprobe from 3-(propargyloxy)fluorescein propargyl ester and 3,4,5-tris[(1-(2-(α-L-fucopyranosyl)ethyl)-1*H*-1,2,3-triazol-4-yl)methoxy]benzyl azide (37)

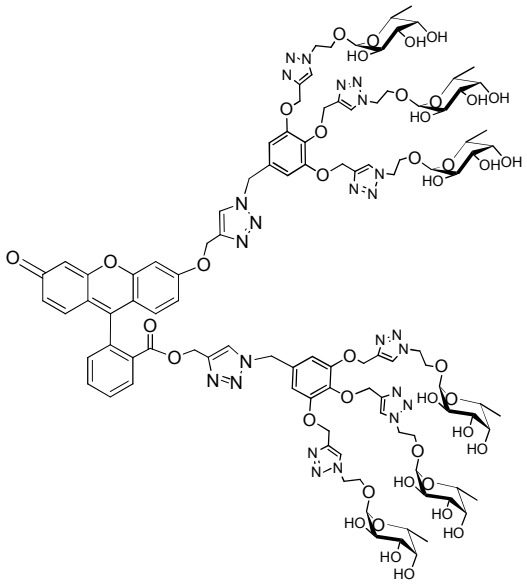

37

A mixture of 12 mg (0.03 mmol) of **34**, 70 mg (0.07 mmol) of **22**, 28 mg (0.14 mmol) of sodium ascorbate and 18 mg (0.09 mmol) of CuBr·S(CH$_3$)$_2$ was dissolved in 1.5 mL of deoxygenated DMSO under Ar atmosphere, and a piece

of copper wire was added. After stirring for 24 hours, Quadrasil Mercaptopropil™ was added to the reaction crude and stirred for 30 minutes. Thereafter, the suspension was filtered and acetonitrile was added to the solution until a precipitate appeared. After centrifugation (15 minutes, 6000 rpm), the solid was suspended in AcOEt and sonicated for 2 minutes. Finally, the solid was isolated by centrifugation (15 minutes, 6000 rpm). Compound **37** was obtained as an orange solid (82 % yield).

^{1}H-NMR (DMSO-d$_6$, 500 MHz) δ / ppm: 8.31 (s, 1H), 8.03 (2s, 8H), 7.54 (s, 3H), 7.10 (s, 1H), 6.71 (m, 7H), 6.36 (s, 1H), 6.12 (s, 1H), 5.48 (s, 2H), 5.26 (m, 4H), 4.92 (s, ~12H), 4.58 (m, ~20H), 3.87 (m, ~16H), 3.70-3.32 (m, ~32H), 2.96 (s, 6H), 0.88 (s, 6H), 0.82 (s, 12H).

^{13}C-NMR (DMSO-d$_6$, 125 MHz) δ / ppm: 184.2, 164.4, 161.7, 157.6, 154.1, 153.9, 152.1, 148.8, 143.5, 143.0, 136.0, 133.1, 131.2, 130.7, 130.2, 129.4, 129.1, 120.0, 124.7, 124.2, 116.5, 115.3, 113.7, 107.4, 105.2, 101.3, 98.7, 71.3, 69.7, 67.4, 66.6, 66.1, 65.1, 61.9, 61.8, 53.8, 50.1, 15.4.

FTIR (KBr) (cm^{-1}): 3375 (*ν* **O–H**), 2915 (*ν* **C–H**), 1731 (*ν* **C=O, ester**), 1640 (*ν* **C=O, keto**), 1595 (*ν* **C=C Ar**).

MALDI-TOF: *m/z* 2397.90 calculated for $[M+H]^+$ $C_{106}H_{132}N_{24}O_{41}$, found: 2397.90

Fluorescein glycoprobe from 3-(propargyloxy)fluorescein methyl ester and 3,4,5-tris[(1-(2-(α-L-fucopyranosyl)ethyl)-1*H*-1,2,3-triazol-4-yl)methoxy]benzyl azide (38)

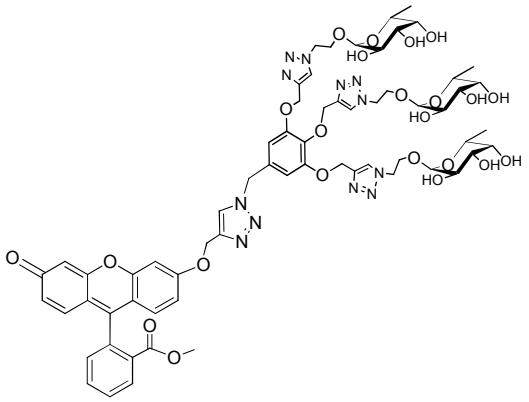

38

A mixture of 23 mg (0.06 mmol) of **36**, 70 mg (0.07 mmol) of **22**, 14 mg (0.07 mmol) of sodium ascorbate and 10 mg (0.05 mmol) of $CuBr \cdot S(CH_3)_2$ was dissolved in 1.5 mL of deoxygenated DMSO under Ar atmosphere, and a piece of copper wire was added. After stirring for 12 hours, Quadrasil Mercaptopropil™ was added to the reaction crude and stirred for 30 minutes. Thereafter, the suspension was filtered and acetonitrile was added to the solution until a precipitate appeared. After centrifugation (15 minutes, 6000 rpm), the solid was suspended in AcOEt and sonicated for 2 minutes. Finally, the solid was isolated by centrifugation (15 minutes, 6000 rpm). Compound **38** was obtained as an orange solid (82 % yield).

^{1}H-NMR (DMSO-d$_6$, 500 MHz) δ / ppm: 8.32 (s, 1H), 8.01 (2s, 5H), 7.56 (s, 2H), 7.10 (s, 1H), 6.71 (m, 5H), 6.35 (s, 1H), 6.13 (s, 1H), 5.48 (s, 2H), 5.26 (s, 2H), 4.92 (s, ~6H), 4.58 (m, ~10H), 3.87 (m, ~8H), 3.70-3.32 (m, ~20H), 2.96 (s, 3H), 0.87 (s, 9H).

^{13}C-NMR (DMSO-d$_6$, 125 MHz) δ / ppm: 185.7, 165.1, 161.6, 157.7, 154.0, 153.9, 152.1, 148.7, 143.5, 143.0, 136.0, 133.1, 131.2, 130.5, 130.2, 129.4, 129.0, 120.0, 124.7, 124.2, 116.5, 115.3, 113.7, 107.4, 105.2, 101.3, 98.9, 71.3, 69.5, 67.6, 66.3, 66.1, 65.1, 61.9, 61.8, 53.8, 52.7, 50.1, 15.6.

FTIR (KBr) (cm^{-1}): 3383 (*ν* **O–H**), 2930 (*ν* **C–H**), 1742 (*ν* **C=O, ester**), 1635 (*ν* **C=O, keto**), 1592 (*ν* **C=C Ar**).

MALDI-TOF: *m/z* 1378.50 calculated for $[M]^+$ $C_{64}H_{74}N_{12}O_{23}$, found: 1378.98.

2-Chloroethylamine hydrochloride (39)

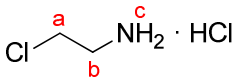

39

To a solution of 3.61 g (59.1 mmol) of aminoethanol in 20 mL of $CHCl_3$ at 0 ºC, 8.80 g (74.3 mmol) of $SOCl_2$ in 10 mL of $CHCl_3$ were added dropwise. Afterwards, the reaction mixture was refluxed for 3 h. The precipitate was isolated by filtration, washing the solid with $CHCl_3$. **39** was obtained as a dark-brown solid (84% yield)

^{1}H-NMR (D_2O, 300 MHz) *δ* / ppm: 3.87 (m, 2H, H_a), 3.41 (m, 2H, H_b).

^{13}C-NMR (D_2O, 75 MHz) *δ* / ppm: 41.2 (C_a), 40.6 (C_b).

N-Boc-2-chloroethylamine (40)

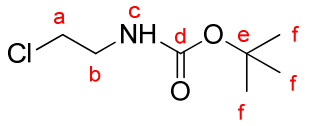

40

To a solution of 2.33 g (20 mmol) of **39** and 3 mL of Et_3N in 20 mL of CH_2Cl_2 was cooled at 0 ºC. 4.51 g (20 mmol) of di-*tert*-butyl dicarbonate in 15 mL of CH_2Cl_2 were added dropwise. After 2 h of stirring at room temperature, the reaction mixture was washed with HCl 0.1 M (20 mL), water (20 mL) and brine

(20 mL). The organic layer was dried over anhydrous $MgSO_4$ and filtered. The solvent was removed at low pressure and the reaction crude was purified by column chromatography using hexane:AcOEt (9:1, v/v) as eluent. Compound **40** was obtained as a pale yellow oil (65 % yield).

^{1}H-NMR ($CDCl_3$, 300 MHz) δ / ppm: 4.94 (br s, 1H, H_c), 3.59 (t, J = 5.7 Hz, 2H, H_a), 3.46 (c, J = 5.7 Hz, 2H, H_b), 1.45 (s, 9H, H_f).

^{13}C-NMR ($CDCl_3$, 75 MHz) δ / ppm: 155.8 (C_d), 85.3 (C_e), 44.5 (C_a), 42.6 (C_b), 28.5 (C_f).

FTIR (CH_2Cl_2) (cm^{-1}): 3344 (ν **N–H**); 2979, 2933 (ν **C–H**); 1690 (ν **C=O**), 1514, 1249, 1166.

N-Boc-2-azidoethylamine (41)

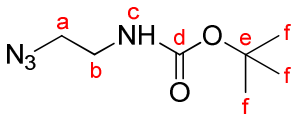

41

A mixture of 524 mg (2.9 mmol) of **16** and 1.47 g (22.6 mmol) of sodium azide in 16 mL of dry DMF at 70 ºC was stirred for 24 h under Ar atmosphere. Thereafter, the reaction crude was suspended in 100 mL of AcOEt and the organic phase was washed with water (3 × 100 mL). The organic layer was dried over anhydrous $MgSO_4$ and filtered. The solvent was removed at low pressure and **41** was obtained as a pale yellow oil (98 % yield).

^{1}H-NMR ($CDCl_3$, 300 MHz) δ / ppm: 4.85 (br s, 1H, H_c), 3.44 (t, J = 5.7 Hz, 2H, H_a), 3.32 (c, J = 5.7 Hz, 2H, H_b), 1.48 (s, 9H, H_f).

^{13}C-NMR ($CDCl_3$, 75 MHz) δ / ppm: 155.9 (C_d), 80.0 (C_e), 51.4 (C_a), 40.2 (C_b), 28.5 (C_f).

FTIR (CH_2Cl_2) (cm^{-1}): 3346 (ν **N–H**); 2979, 2934 (ν **C–H**); 2099 (ν **–N=N=N**), 1691 (ν **C=O**), 1519, 1251, 1168.

3-[(2-(*N*-Boc)aminoeth-1-yl)-1*H*-1,2,3-triazol-4-yl)methoxy]fluorescein methyl ester (42)

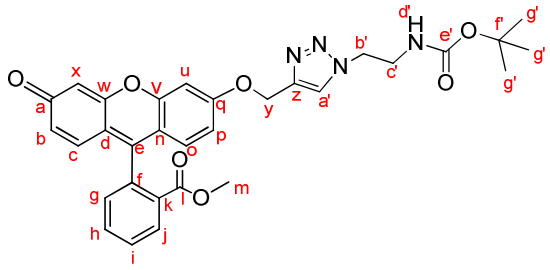

42

A mixture of 124 mg (0.32 mmol) of **36**, 69 mg (0.37 mmol) of **41**, 16 mg (0.08 mmol) of sodium ascorbate and 9 mg (0.04 mmol) of $CuBr \cdot S(CH_3)_2$ was dissolved in 2 mL of deoxygenated DMF, and a piece of copper wire was added. After stirring for 24 h, the reaction crude was suspended in 25 mL of AcOEt and washed with water (3 × 30 mL). The organic layer was dried over anhydrous $MgSO_4$ and filtered. The solvent was removed at low pressure and the reaction crude was purified by column chromatography using CH_2Cl_2 as eluent to remove the excess of **41** followed by CH_2Cl_2:MeOH (90:10, v/v). Compound **42** was obtained as an orange solid (86 % yield).

^{1}H-NMR ($CDCl_3$, 300 MHz) δ / ppm: 8.24 (dd, J = 7.5 Hz, J = 0.9 Hz, 1H, H_j), 7.74 (td, J = 7.5 Hz, J = 0.9 Hz, 1H, H_h or H_i), 7.71 (s, 1H, $H_{a'}$), 7.67 (td, J = 7.5 Hz, J = 0.9 Hz, 1H, H_h or H_i), 7.30 (dd, J = 7.5 Hz, J = 0.9 Hz, 1H, H_g), 7.12 (d, J = 2.4 Hz, 1H, H_u), 6.89 (dd, J = 9.0 Hz, J = 2.4 Hz, 1H, H_p), 6.81 (d, J = 9.0 Hz, 1H, H_o), 6.80 (d, J = 9.6 Hz, 1H, H_c), 6.57 (d, J = 9.6 Hz, 1H, H_b), 6.25 (s, 1H, H_x), 5.30 (s, 2H, H_y), 4.96 (br s, 1H, $H_{d'}$), 4.51 (t, J = 5.4 Hz, 2H, $H_{b'}$), 3.65 (c, J = 5.4 Hz, 2H, $H_{c'}$), 3.64 (s, 3H, H_m), 1.42 (s, 9H, $H_{g'}$).

^{13}C-NMR ($CDCl_3$, 75 MHz) δ / ppm: 165.7, 162.9, 159.1, 154.4 (C_z), 134.6, 132.9, 131.3, 130.7, 130,4, 130,4, 129.9, 124.1 ($C_{a'}$), 117.9, 115.5, 114.0, 101.6, 80.2 ($C_{f'}$), 62.5, 52.6, 50.3, 40.6 ($C_{c'}$), 28.4 ($C_{g'}$).

FTIR (CH_2Cl_2) (cm^{-1}): 3303 (*v* **N–H**), 2975 (*v* **C–H**), 1718 (*v* **C=O ester**), 1642 (*v* **C=O Boc**), 1597 (*v* **C=C Ar**).

MS (ESI): *m/z* 570.21 calculated for $[M]^+$ $C_{31}H_{30}N_4O_7$, found: 570.1.

3-[(1-(2-(*N*-Boc)aminoethyl)-1*H*-1,2,3-triazol-4-yl)methoxy]fluorescein [(1-(2-(*N*-Boc)aminoethyl)-1*H*-1,2,3-triazol-4-yl)methyl] ester (43)

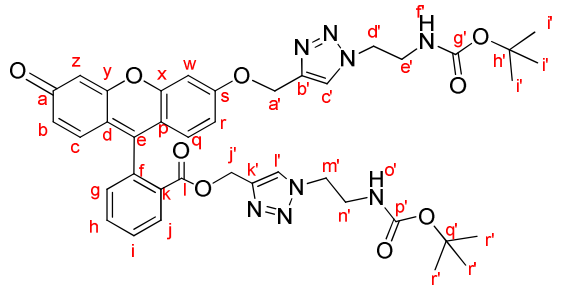

43

A mixture of 100 mg (0.24 mmol) of **34**, 97 mg (0.52 mmol) of **41,** 25 mg (0.12 mmol) of sodium ascorbate and 16 mg (0.08 mmol) of $CuBr{\cdot}S(CH_3)_2$ was dissolved in 2 mL of deoxygenated DMF, and a piece of copper wire was added. After stirring for 24 h, the reaction crude was suspended in 25 mL of AcOEt and washed with water (3 × 30 mL). The organic layer was dried over anhydrous $MgSO_4$ and filtered. The solvent was removed at low pressure and the reaction crude was purified by column chromatography using CH_2Cl_2 as eluent to remove the excess of **41** followed by CH_2Cl_2:MeOH (90:10, v/v). Compound **43** was obtained as an orange solid (91 % yield).

^{1}H-NMR (MeOD-d$_4$, 300 MHz) δ / ppm: 8.29 (dd, J = 7.5 Hz, J = 0.9 Hz, 1H, H_j), 8.16 (s, 1H, $H_{l'}$), 7.85 (td, J = 7.5 Hz, J = 0.9 Hz, 1H), 7.78 (td, J = 7.5 Hz, J = 0.9 Hz, 1H), 7.59 (s, 1H, $H_{c'}$), 7.41 (dd, J = 7.5 Hz, J = 0.9 Hz, 1H, H_g), 7.34 (d, J = 2.4 Hz, 1H, H_w), 7.00 (s, 1H), 6.97 (s, 1H), 6.92 (dd, J = 9.0 Hz, J = 2.4 Hz, 1H, H_r), 6.78 (d, J = 9.6 Hz, 1H, H_c), 6.53 (dd, J = 9.6 Hz, J = 1.8 Hz, 1H, H_b), 6.43 (d, J = 1.8 Hz, H_z), 5.04 (d, J = 12.6 Hz, 2H, $H_{j'}$), 4.52 (t, J = 5.7 Hz, 2H, $H_{d'}$), 4.41 (c, J = 5.7 Hz, 2H), 3.54 (t, J = 5.7 Hz, 2H), 3.47 (t, J = 5.7 Hz, 2H), 1.38 and 1.37 (2s, 9H and 9H, $H_{i'}$ and $H_{r'}$).

^{13}C-NMR (MeOD-d$_4$, 75 MHz) δ / ppm: 165.4, 162.6, 159.2 154.3, 153.1, 134.6, 132.6, 131.1, 130.2, 130.0, 129.3, 128.2, 125.5 ($C_{l'}$), 124.7 ($C_{c'}$), 114.5, 104.2, 100.8, 81.2, 61.7 ($C_{a'}$), 57.2 ($C_{j'}$), 49.7, 49.3, 39.9, 39.8; 28.5, 28.4 ($C_{i'}$, $C_{r'}$).

FTIR (CH_2Cl_2) (cm^{-1}): 3330 (*v* **N–H**), 2970 (*v* **C–H**), 1725 (*v* **C=O ester**), 1635 (*v* **C=O Boc**), 1594 (*v* **C=C Ar**).

MS (ESI): *m/z* 780.32 calculated for $[M]^+$ $C_{40}H_{44}N_8O_9$, found: 780.3

3-[(1-(2-Aminoethyl hydrochloride)-1*H*-1,2,3-triazol-4-yl)methoxy]fluorescein methyl ester (44)

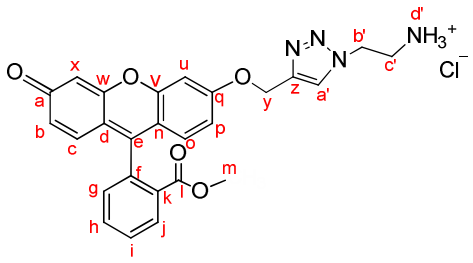

44

To a solution of 180 mg (0.32 mmol) of **42** in 2 mL of dioxane under Ar atmosphere, 0.32 mL of HCl 4 M (1.3 mmol) in dioxane were added. The mixture was stirred at room temperature and, after 30 minutes, an orange solid appeared. After 18 hours, solvent was removed at low pressure. The solid was washed with CH_2Cl_2 and dried, affording **44** as a dark orange solid (93% yield).

^{1}H-NMR (D_2O, 300 MHz) δ / ppm: 8.36 (m, 1H, H_j), 8.27 (s, 1H, $H_{a'}$), 7.88 (m, 2H, H_h, H_i), 7.50 (d, *J* = 2.4 Hz, 1H, H_u), 7.46 (m, 2H, H_b, H_c), 7.40 (m, 1H, H_g), 7.15 (dd, *J* = 9.0 Hz, *J* = 2.4 Hz, 1H, H_p), 7.07 (d, *J* = 2.4 Hz, $1H_x$), 6.99 (dd, *J* = 9.0 Hz, *J* = 2.4 Hz, $1H_o$), 5.47 (s, 2H, H_y), 4.83 (t, *J* = 6.0 Hz, 2H, $H_{b'}$), 3.62 (t, *J* = 6.0 Hz, 2H, $H_{c'}$), 3.55 (s, 3H, H_m).

^{13}C-NMR (D_2O, 75 MHz) δ / ppm: 175.6, 174.0, 167.3, 167.1, 159.9, 157.6, 142.3 (C_z), 133.3, 132.8, 131.5, 131.3, 131.0, 130.1, 129.2, 126.0 ($C_{a'}$), 122.7, 118.2, 117.2, 116.7, 103.0, 101.0, 62.3, 52.7, 47.4, 38.9

FTIR (KBr) (cm^{-1}): 3350 (*v* **N–H**), 2974 (*v* **C–H**), 1721 (*v* **C=O ester**), 1592 (*v* **C=C Ar**).

3-[(1-(2-Aminoethyl hydrochloride)-1*H*-1,2,3-triazol-4-yl)methoxy]fluorescein [(1-(2-aminoethyl hydrochloride)-1*H*-1,2,3-triazol-4-yl)methyl] ester (45)

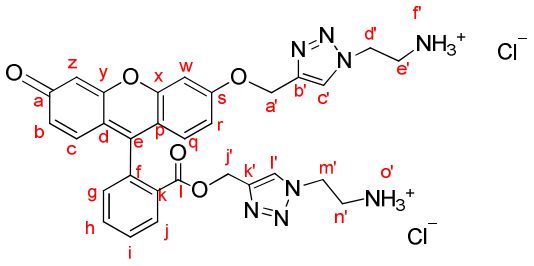

45

To a solution of 160 mg (0.20 mmol) of **43** in 2 mL of dioxane under Ar atmosphere, 0.4 mL of HCl 4 M (1.6 mmol) in dioxane were added. The mixture was stirred at room temperature and, after 30 minutes, an orange solid appeared. After 18 hours, solvent was removed at low pressure. The solid was washed with CH_2Cl_2 and dried, affording **45** as a dark orange solid (85% yield).

^{1}H-NMR (D_2O, 300 MHz) δ / ppm: 8.35 (m, 1H, H_j), 8.32 (s, 1H, $H_{c'}$), 7.89 (m, 2H, H_h, H_i), 7.71 (s, 1H, $H_{l'}$), 7.52 (d, J = 2.4 Hz, 1H, H_w), 7.45 (d, J = 9.3 Hz, 1H, H_r or H_q), 7.39 (d, J = 9.3 Hz, 1H, H_r or H_q), 7.37 (m, 1H, H_g), 7.18 (dd, J = 9.3 Hz, J = 2.4 Hz, 1H, H_b), 7.04 (d, J = 2.4 Hz, 1H, H_z), 6.96 (dd, J = 9.3 Hz, J = 2.4 Hz, 1H, H_c), 5.54 (d, J = 12 Hz, $H_{a'}$), 5.03 (d, J = 13 Hz, 1H, $H_{j'}$), 4.85 (d, J = 13 Hz, 1H, $H_{j'}$), 4.84 (t, J = 6.0 Hz, 2H, $H_{d'}$ or $H_{m'}$), 4.74 (t, J = 6.0 Hz, 2H, $H_{d'}$ or $H_{m'}$), 3.64 (t, J = 6.0 Hz, 2H, $H_{n'}$), 3.55 (t, J = 6.0 Hz, 2H, $H_{e'}$).

^{13}C-NMR (D_2O, 75 MHz) δ / ppm: 175.3, 167.4, 166.3, 164.4, 159.5, 157.5, 142.1 ($C_{b'}$), 141.1 ($C_{k'}$), 133.4, 132.9, 132.0, 131.8, 131.3, 131.1, 130.0, 129.0, 126.2 ($C_{c'}$), 125.7 ($C_{l'}$), 122.5, 118.3, 117.1, 116.7, 102.7, 101.0, 62.5, 57.4, 47.4, 47.1, 38.9, 38.8,

FTIR (KBr) (cm^{-1}): 3337 (ν **N–H**), 2968 (ν **C–H**), 1722 (ν **C=O ester**), 1594 (ν **C=C Ar**).

1-(2-Chloroethoxy)-2-methoxy-ethane (46)

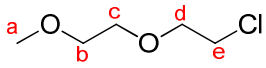

46

To a mixture of 8.66 g (72 mmol) of diethylenglycol methyl ether and 5.73 g (92 mmol) of pyridine in 60 mL of $CHCl_3$ under Ar atmosphere, 11.00 g of thionyl chloride in 15 mL of $CHCl_3$ were added dropwise. The reaction mixture was refluxed for 4 hours and, thereafter, the reaction crude was washed with water (2 × 150 mL). The organic layer was dried over anhydrous $MgSO_4$ and filtered. The solvent was removed at low pressure. Compound **46** was obtained as a yellowish oil (89 % yield).

^{1}H-NMR ($CDCl_3$, 300 MHz) δ / ppm: 3.80–3.76 (m, 2H), 3.71–3.64 (m, 4H), 3.60–3.57 (m, 2H), 3.41 (s, 3H, H_a).

^{13}C-NMR ($CDCl_3$, 75 MHz) δ / ppm: 72.0 (C_b), 71.5 (C_d), 70.7 (C_c), 59.2 (C_a), 42.7 (C_e).

FTIR (CH_2Cl_2) (cm^{-1}): 2879 (*ν* **C–H**), 1456, 1359, 1299, 1108 (*ν* **C–O**), 1057, 665.

Methyl 3,4,5-tris[2-(2-methoxyethoxy)ethoxy]benzoate (47)

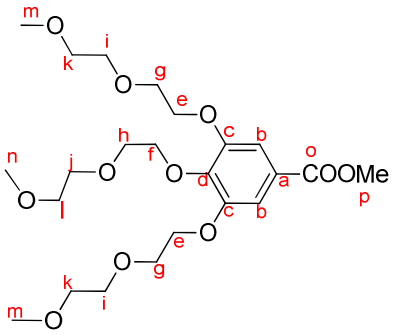

47

A solution of 580 mg (3.1 mmol) of methyl 3,4,5-trihydroxybenzoate, 1.56 g (11.2 mmol) of **46**, 1.53 g (11.2 mmol) of K_2CO_3 and 200 mg de NaI in 150 mL of DMSO, under Ar atmosphere, was stirred at 120 ºC for 18 hours. The reaction crude was extracted with AcOEt (4 × 100 mL). The combined organic layers were washed with 100 mL of brine. The organic phase was dried over anhydrous $MgSO_4$ and filtered. The solvent was removed at low pressure and the remaining oil was purified by column chromatography using AcOEt as eluent. Compound **47** was obtained as a yellowish oil (68 % yield).

^{1}H-NMR ($CDCl_3$, 300 MHz) δ / ppm: 7.31 (s, 2H, H_b), 4.28–4.21 (m, 6H), 3.91–3.82 (m, 6H), 3.76–3.72 (m, 6H), 3.60–3.55 (m, 6H), 3.40 (s, 6H, H_m), 3.39 (s, 3H, H_n).

^{13}C-NMR ($CDCl_3$, 75 MHz) δ / ppm: 166.7 (C_o), 152.4 (C_c), 142.6 (C_a), 125.1 (C_d), 109.1 (C_b); 72.6, 72.2, 72.1, 70.9, 70.7, 70.6, 69.7, 69.0 (C_e, C_f, C_g, C_h, C_i, C_j, C_k, C_l); 59.2 (C_m), 59.1 (C_n), 52.3 (C_p).

FTIR (CH_2Cl_2) (cm^{-1}): 2877 (*ν* **C–H**), 1716 (*ν* **C=O**), 1586 (*ν* **C=C Ar**), 1501, 1429, 1103 (*ν* **C–O**), 765.

3,4,5-Tris[2-(2-methoxyethoxy)ethoxy]benzyl alcohol (48)

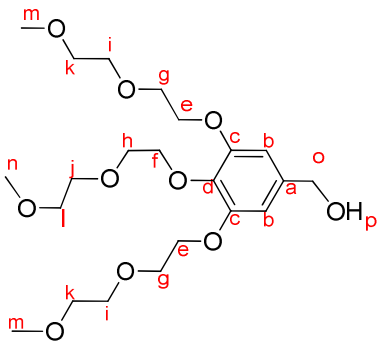

48

To a suspension of 125 mg (3.3 mmol) of lithium aluminium hydride in 10 mL of dry THF at 0 ºC and under Ar atmosphere, 1.0 g (2.9 mmol) of **47** in 20 mL of dry THF were added dropwise. After 30 minutes, the reaction was allowed to

reach room temperature. Reaction was finished after 5 hours of stirring by adding, at 0 ºC and dropwise, 40 mL of aqueous NH_4Cl (5% wt). The resulting suspension was filtered and extracted with CH_2Cl_2 (5 × 30 mL). Combined organic phases were washed with brine (2 × 30 mL). The organic layer was dried over anhydrous $MgSO_4$ and filtered. The solvent was removed at low pressure and **48** was obtained as a white solid (91 % yield).

^{1}H-NMR ($CDCl_3$, 300 MHz) δ / ppm: 6.63 (s, 2H, H_b), 4.59 (s, 2H, H_o) 4.21–4.15 (m, 6H), 3.84 (t, J = 5.1 Hz, 4H), 3.79 (t, J = 5.1 Hz, 2H), 3.76–3.72 (m, 6H), 3.59–3.56 (m, 6H), 3.40 (s, 9H, H_m, H_n).

^{13}C-NMR ($CDCl_3$, 75 MHz) δ / ppm: 152.7 (C_c), 137.7 (C_a), 136.6 (C_d), 106.4 (C_b); 72.4, 72.1, 72.0, 70.7, 70.6, 70.4, 69.9, 68.9 (C_e, C_f, C_g, C_h, C_i, C_j, C_k, C_l); 65.3 (C_o), 59.1 (C_m, C_n).

FTIR (CH_2Cl_2) (cm^{-1}): 3450 (*v* **O–H**), 2925, 2877, 1590 (*v* **C=C** Ar), 1501, 1436, 1101 (*v* **C–O**).

1,3-Bis(3,4,5-tris[2-(2-methoxyethoxy)ethoxy]benzyl)malonate (49)

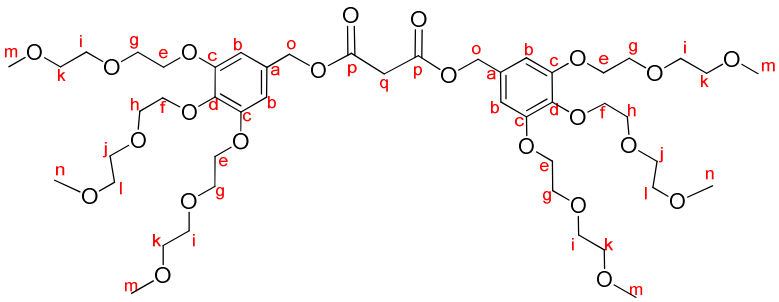

49

To a solution of 1.18 g (2.6 mmol) of **48**, 0.8 mL (5.8 mmol) of triethylamine and 35 mg (0.28 mmol) of 4-dimethylaminopyridine in 15 mL of dry CH_2Cl_2 at 0 ºC and under Ar atmosphere, 156 mg (1.1 mmol) of malonyl chloride in 8 mL of dry CH_2Cl_2 were added dropwise. After 30 minutes, the reaction was allowed to reach room temperature and after 4 hours the reaction crude was washed with

HCl 1 M (2 × 20 mL), saturated aqueous $NaHCO_3$ (20 mL) and brine (2 × 30 mL). The organic layer was dried over anhydrous $MgSO_4$ and filtered. Solvent was removed at low pressure and the remaining oil purified by column chromatography using AcOEt:MeOH (95:5, v/v) as eluent until a mixture of **48** and **49** was obtained. Thereafter, this mixture was subsequently purified by exclusion-size chromatography (Sephadex LH-20) and CH_2Cl_2:MeOH (1:1, v/v) as eluent. Compound **49** was obtained as a colourless oil (43 % yield).

^{1}H-NMR ($CDCl_3$, 300 MHz) δ / ppm: 6.58 (s, 4H, H_b), 5.05 (s, 4H, H_o) 4.17–4.13 (m, 12H), 3.84 (t, J = 5.1 Hz, 8H), 3.79 (t, J = 5.1 Hz, 4H), 3.72–3.69 (m, 12H), 3.56–3.53 (m, 12H), 3.46 (s, 2H, H_q), 3.37 (s, 18H, H_m, H_n).

^{13}C-NMR ($CDCl_3$, 75 MHz) δ / ppm: 166.4 (C_p), 152.8 (C_c), 138.6 (C_a), 130.7 (C_d), 108.1 (C_b); 72.5, 72.2, 72.1, 70.9, 70.7, 70.6, 69.9, 69.0 (C_e, C_f, C_g, C_h, C_i, C_j, C_k, C_l); 67.4 (C_o), 59.2 (C_m), 59.1 (C_n), 41.5 (C_q).

FTIR (CH_2Cl_2) (cm^{-1}): 2877 (*v* **C–H**), 1733 (*v* **C=O**), 1591 (*v* **C=C** Ar), 1506, 1438, 1107 (*v* **C–O**), 849.

MALDI-TOF: *m/z* 993.48 calculated for $[M+H]^+$ $C_{47}H_{76}O_{22}$, found: 993.51.

[60]Fullerene monoadduct of 1,3-bis(3,4,5-tris[2-(2-methoxyethoxy) ethoxy]benzyl)malonate (50)

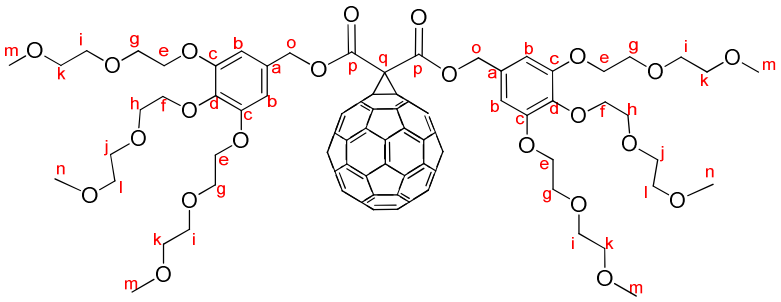

50

To a sonicated solution of 115 mg (0.11 mmol) of **49**, 160 mg (0.22 mmol) of [60]fullerene and 55 mg (0.22 mmol) of I_2, in 90 mL of dry toluene at 0 ºC and under Ar atmosphere, 70 mg (0.48 mmol) of 1,8-diazabicycloundec-7-ene in 10 mL of dry toluene were added dropwise. The reaction mixture was stirred at 0 ºC for 5 h and thereafter 30 mL of saturated aqueous sodium thiosulfate were added in order to finish the reaction. The organic phase was washed with saturated aqueous sodium thiosulfate (2 × 30 mL), HCl 0.5 M (2 × 20 mL) and brine (2 × 20 mL). The organic layer was dried over anhydrous $MgSO_4$ and filtered. The solvent was removed at low pressure and the reaction crude was purified by column chromatography using CS_2 as eluent to remove unreacted [60]fullerene, followed by AcOEt:MeOH (85:15, v/v). Compound **50** was obtained as a dark brown solid (32 % yield).

^{1}H-NMR ($CDCl_3$, 300 MHz) δ / ppm: 6.68 (s, 4H, H_b), 5.38 (s, 4H, H_o) 4.15–4.11 (m, 12H), 3.83 (t, J = 5.1 Hz, 8H), 3.78 (t, J = 5.1 Hz, 4H), 3.72–3.68 (m, 12H), 3.56–3.53 (m, 12H), 3.37 (s, 6H, H_n), 3.36 (s, 12H, H_m).

^{13}C-NMR ($CDCl_3$, 75 MHz) δ / ppm: 166.5 (C_p), 152.9 (C_c); 145.4, 145.3, 145.2, 145.1, 145.0, 144.8, 144.7, 144.6, 144.0, 143.2, 143.1, 143.0, 142.3, 141.8, 141.0, 139.0 (sp^2 – C_{60}); 138.8 (C_a), 130.1 (C_d), 108.5 (C_b), 71.5 (sp3 – C60); 72.5, 72.2, 72.1, 70.9, 70.7, 70.6, 69.8, 69.0 (C_e, C_f, C_g, C_h, C_i, C_j, C_k, C_l); 71.5 (C_{60}), 69.1 (C_o), 59.2 (C_m), 59.1 (C_n), 52.3 (C_q).

FTIR (CH_2Cl_2) (cm^{-1}): 2923, 2877 (*v* **C–H**); 1746 (*v* **C=O**), 1591 (*v* **C=C Ar**), 1504, 1441, 1111 (*v* **C–O**).

MALDI-TOF: *m/z* 1711.47 calculated for $[M+H]^+$ $C_{107}H_{74}O_{22}$, found: 1711.45.

1-(4-Pentyn-1-yl)propanedioic acid ester (51)

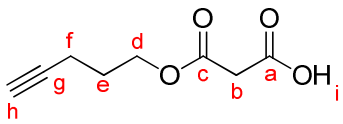

51

To a solution of 2.32 g (15.8 mmol) of Meldrum's acid in 50 mL of dry toluene under Ar atmosphere, 1.35 g (16 mmol) of 4-petyn-1-ol in 10 mL of dry toluene were added. The reaction was refluxed for 2 hours. Thereafter, the reaction solvent was removed at low pressure and the reaction crude was purified by column chromatography using CH_2Cl_2:MeOH (98:2, v/v) as eluent. Compound **51** was obtained as a pale yellow solid (76 % yield).

^{1}H-NMR ($CDCl_3$, 300 MHz) δ / ppm: 9.88 (br s, 1H, H_i), 4.30 (t, J = 6.3 Hz, 2H, H_d), 3.45 (s, 2H, H_b), 2.30 (td, J = 6.3 Hz, J = 2.7 Hz, 2H, H_f), 1.98 (t, J = 2.7 Hz, 1H, H_h), 1.89 (q, J = 6.3 Hz, 2H, H_e).

^{13}C-NMR ($CDCl_3$, 75 MHz) δ / ppm: 171.4 (C_a), 167.0 (C_c), 82.8 (C_g), 69.4 (C_h), 64.6 (C_d), 40.8 (C_b), 27.4 (C_e), 15.2 (C_f).

FTIR (CH_2Cl_2) (cm^{-1}): 3290 (ν C≡**C**–**H**), 3100 (ν **O**–**H**), 2963 (ν **C**–**H**), 2118 (ν **C≡C**), 1725 (ν **C=O**), 1400, 1323, 1158, 1028.

1-[2-(2-(2-Chloroethoxy)ethoxy)-eth-1-yl] 3-[1-(4-pentyn-1-yl)]malonate (52)

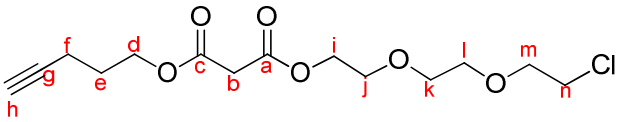

52

To a solution of 330 mg (1.91 mmol) of **51**, 384 mg (2.27 mmol) of 2-(2-(2-chloroethoxy)ethoxy)ethanol and 50 mg (0.39 mmol) of 4-dimethylaminopyridine in 8 mL of dry CH_2Cl_2 at 0 ºC under Ar atmosphere, 408 mg (1.98 mmol) of *N*,*N*'-dicyclohexylcarbodiimide in 4 mL of dry CH_2Cl_2 were added dropwise. After 2 h, the reaction mixture was allowed to reach room temperature and stirred for 18 hours. Thereafter, the white precipitate due to dicyclohexylurea was removed by filtration and the reaction solvent was evaporated at low pressure. The reaction crude was purified by column chromatography using CH_2Cl_2:MeOH (98:2, v/v) as eluent. Compound **52** was obtained as a colourless oil (82 % yield).

^{1}H-NMR ($CDCl_3$, 300 MHz) δ / ppm: 4.31 (m, 2H, H_i), 4.26 (t, J = 6.3 Hz, 2H, H_d), 3.77-3.72 (m, 4H, H_j, H_k), 3,69-3.61 (m, 6H, H_l, H_m, H_n), 3.42 (s, 2H, H_b), 2.29 (td, J = 6.3 Hz, J = 2.7 Hz, 2H, H_f), 1.97 (t, J = 2.7 Hz, 1H, H_h), 1.87 (q, J = 6.3 Hz, 2H, H_e).

^{13}C-NMR ($CDCl_3$, 75 MHz) δ / ppm: 166.7, 166.5 (C_a, C_c); 82.9 (C_g), 71.4 (C_k); 70.8, 70.7 (C_l, C_m); 69.3 (C_h), 69.1 (C_j), 64.7 (C_d), 64.1 (C_i), 42.9 (C_n), 41.5 (C_b), 27.5 (C_e), 15.2 (C_f).

FTIR (CH_2Cl_2) (cm^{-1}): 3289 (ν C≡**C**–**H**), 2922 (ν **C**–**H**), 2118 (ν **C≡C**), 1731 (ν **C=O**), 1576, 1131 (ν **C**–**O**), 1035.

[60]Fullerene monoadduct of 1-[2-(2-(2-chloroethoxy)ethoxy)eth-1-yl]-3-[1-(4-pentyn-1-yl)]malonate (53)

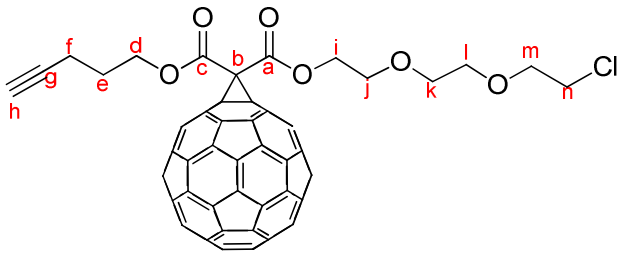

53

To a sonicated solution of 45 mg (0.14 mmol) of **52**, 196 mg (0.27 mmol) of [60]fullerene and 71 mg (0.28 mmol) of I_2, in 100 mL of dry toluene at 0 ºC and under Ar atmosphere, 88 mg (0.56 mmol) of 1,8-diazabicycloundec-7-ene in 10 mL of dry toluene were added dropwise. The reaction mixture was stirred at 0 ºC for 4.5 h and, thereafter, 30 mL of saturated aqueous sodium thiosulfate were added in order to finish the reaction. The organic phase was washed with saturated aqueous sodium thiosulfate (2 × 30 mL), HCl 0.5 M (2 × 20 mL) and brine (2 × 20 mL). The organic layer was dried over anhydrous $MgSO_4$ and filtered. The solvent was removed at low pressure and the reaction crude was purified by column chromatography using CS_2 as eluent to remove the unreacted

[60]fullerene, followed by toluene:AcOEt (95:5, v/v). Compound **53** was obtained as a dark brown solid (65 % yield).

^{1}H-NMR ($CDCl_3$, 300 MHz) δ / ppm: 4.66 (m, 2H, H_i), 4.62 (t, J = 6.3 Hz, 2H, H_d), 3.90 (m, 2H), 3,77 (t, J = 5.7 Hz, 2H, H_m), 3.70 (m, 4H), 3.64 (t, J = 5.7 Hz, 2H, H_n), 2.42 (td, J = 6.3 Hz, J = 2.7 Hz, 2H, H_f), 2.08 (q, J = 6.3 Hz, 2H, H_e), 2.04 (t, J = 2.7 Hz, 1H, H_h).

^{13}C-NMR ($CDCl_3$, 75 MHz) δ / ppm: 163.8, 163.6 (C_a, C_c); 145.4, 145.3, 145.3, 145.2, 145.1, 144.9, 144.8, 144.8, 144.7, 144.0, 143.2, 143.2, 143.1, 143.1, 142.4, 142.3, 142.1, 142.0, 141.2, 141.1, 139.2, 139.2 (sp^2 – C_{60}); 82.7 (C_g), 71.6 (C_k); 70.9, 70.8 (C_l, C_m); 69.8 (C_h), 69.0 (C_j), 66.4 (C_d), 65.9 (C_i), 43.0 (C_n), 27.5 (C_e), 15.4 (C_f).

FTIR (CH_2Cl_2) (cm^{-1}): 3296 (ν C≡**C**–**H**), 2925 (ν **C**–**H**), 1745 (ν **C=O**), 1460, 1433, 1236.

MALDI-TOF: *m/z* 1038.09 calculated for $[M]^+$ $C_{74}H_{19}O_6Cl$, found: 1038.14.

1-[2-(2-Chloroethoxy)ethyl]-3-(ethyl)malonate (54)

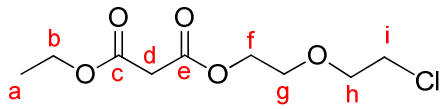

54

To a solution of 2.05 g (16.4 mmol) of 2-(2-chloroethoxy)ethanol and 47 mg (0.37 mmol) of 4-dimethylaminopyridine in 40 mL of dry CH_2Cl_2 at 0 ºC and under Ar atmosphere, 2.04 g (13.6 mmol) of ethyl malonyl chloride in 10 mL of dry CH_2Cl_2 were added dropwise. After 30 min, the reaction mixture was allowed to reach room temperature and after 5 hours the reaction crude was washed with HCl 1 M (2 × 20 mL), saturated aqueous $NaHCO_3$ (20 mL) and brine (2 × 30 mL). The organic layer was dried over anhydrous $MgSO_4$ and filtered. Solvent was removed at low pressure and the remaining oil was purified

by column chromatography using CH_2Cl_2:MeOH (98:2, v/v) as eluent. Compound **54** was obtained as a colourless oil (50 % yield).

^{1}H-NMR ($CDCl_3$, 300 MHz) δ / ppm: 4.32 (m, 2H, H_f), 4.20 (t, J = 7.2 Hz, 2H, H_b), 3.77–3.72 (m, 4H, H_g, H_h), 3.63 (t, J = 5.7 Hz, 2H, H_i), 3.41 (s, 2H, H_d), 1.28 (t, J = 7.2 Hz, 3H, H_a).

^{13}C-NMR ($CDCl_3$, 75 MHz) δ / ppm: 166.7, 166.6 (C_c, C_e); 71.4 (C_h), 69.0 (C_g), 64.5 (C_b), 61.7 (C_f), 42.8 (C_i), 41.6 (C_d), 14.2 (C_a).

FTIR (CH_2Cl_2) (cm^{-1}): 2983 (ν **C–H**), 1731 (ν **C=O**), 1448, 1413, 1370, 1133, 1036.

[60]Fullerene monoadduct of 1-[2-(2-chloroethoxy)ethyl]-3-(ethyl)malonate (55)

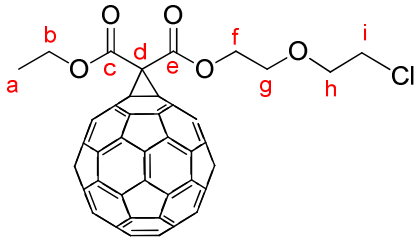

55

To a sonicated solution of 37 mg (0.16 mmol) of **54**, 199 mg (0.28 mmol) of [60]fullerene and 71 mg (0.28 mmol) of I_2, in 100 mL of dry toluene at 0 ºC and under Ar atmosphere, 89 mg (0.57 mmol) of 1,8-diazabicycloundec-7-ene in 10 mL of dry toluene were added dropwise. The reaction mixture was stirred at 0 ºC for 4.5 h and, thereafter, 30 mL of saturated aqueous sodium thiosulfate were added in order to finish the reaction. The organic phase was washed with saturated aqueous sodium thiosulfate (2 × 30 mL), HCl 0.5 M (2 × 20 mL) and brine (2 × 20 mL). The organic layer is dried over $MgSO_4$ and filtered. The solvent was removed at low pressure and the reaction crude was purified by column chromatography using CS_2 as eluent to remove the unreacted [60]fullerene, followed by toluene:AcOEt (98:2, v/v). Compound **55** was obtained as a dark brown solid (65 % yield).

^{1}H-NMR ($CDCl_3$, 300 MHz) δ / ppm: 4.67 (m, 2H, H_f), 4.57 (t, J = 7.2 Hz, 2H, H_b), 3.91 (m, 2H, H_g), 3.80 (t, J = 5.7 Hz, 2H, H_h), 3.63 (t, J = 5.7 Hz, 2H, H_i), 1.50 (t, J = 7.2 Hz, 3H, H_a).

^{13}C-NMR ($CDCl_3$, 75 MHz) δ / ppm: 166.7, 166.6 (C_c, C_e); 145.4, 145.3, 145.3, 145.2, 145.1, 144.9, 144.8, 144.8, 144.7, 144.0, 143.2, 143.2, 143.1, 143.1, 142.4, 142.3, 142.1, 142.0, 141.2, 141.1, 139.2, 139.2 (sp^2 – C_{60}); 71.6 (sp^3 – C_{60}), 71.5 (C_h), 69.0 (C_g), 66.2 (C_b), 63.6 (C_f), 42.9 (C_i), 14.4 (C_a).

FTIR (CH_2Cl_2) (cm^{-1}): 2959 (ν **C–H**), 1745 (ν **C=O**), 1430, 1234.

1-(Ethyl)-3-[1-(4-pentyn-1-yl)]malonate (56)

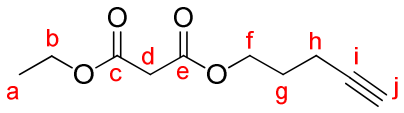

56

To a solution of 1.84 g (21.8 mmol) of 4-pentyn-1-ol, 3 g (22 mmol) of triethylamine and 62 mg (0.52 mmol) of 4-dimethylaminopyridine in 40 mL of dry CH_2Cl_2, at 0 ºC and under Ar atmosphere, 2.0 g (14 mmol) of ethyl malonyl chloride in 10 mL of dry CH_2Cl_2 were added dropwise. After 30 minutes, the reaction was allowed to reach room temperature and stirred for 4 hours. The reaction crude was washed with HCl 1 M (2 × 20 mL), saturated aqueous $NaHCO_3$ (20 mL) and brine (2 × 30 mL). The organic layer was dried over anhydrous $MgSO_4$ and filtered. Solvent was removed at low pressure and the remaining oil was purified by column chromatography using hexane:AcOEt (8:2, v/v) as eluent. Compound **56** was obtained as a colourless oil (63 % yield).

^{1}H-NMR ($CDCl_3$, 300 MHz) δ / ppm: 4.26 (t, J = 6.6 Hz, 2H, H_f), 4.20 (c, J = 7.2 Hz, 2H, H_b), 3,37 (s, 2H, H_d), 2.30 (td, J = 6.6 Hz, J = 2.7 Hz, 2H, H_h), 1.97 (t, J = 2.7 Hz, 1H, H_j), 1.87 (q, J = 6.6 Hz, 2H, H_g), 1.28 (t, J = 7.2 Hz, 3H, H_a).

^{13}C-NMR ($CDCl_3$, 75 MHz) δ / ppm: 166.7, 166.8 (C_c, C_e); 82.9 (C_i), 69.3 (C_j), 64.1 (C_f), 61.7 (C_b), 41.7 (C_d), 27.5 (C_g); 15.2, 14.2 (C_a, C_h).

FTIR (CH_2Cl_2) (cm^{-1}): 3287 (ν C≡**C**–**H**), 2983 (ν **C**–**H**), 2120 (ν **C**≡**C**), 1731 (ν **C**=**O**), 1332, 1270, 1151, 1033.

[60]Fullerene monoadduct of 1-(ethyl)-3-[1-(4-pentyn-1-yl)]malonate (57)

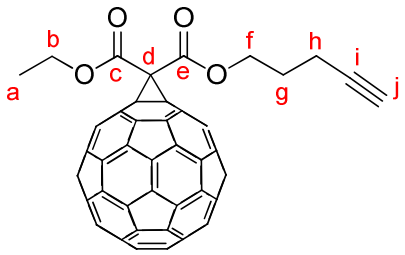

57

To a sonicated solution of 28 mg (0.14 mmol) of **56**, 200 mg (0.28 mmol) of [60]fullerene and 66 mg (0.26 mmol) of I_2, in 90 mL of dry toluene at 0 ºC and under Ar atmosphere, 88 mg (0.60 mmol) of 1,8-diazabicycloundec-7-ene in 10 mL of dry toluene were added dropwise. The reaction mixture was stirred at 0 ºC for 5 hours and, thereafter, 30 mL of saturated aqueous sodium thiosulfate were added in order to finish the reaction. The organic phase was washed with saturated aqueous sodium thiosulfate (2 × 30 mL), HCl 0.5 M (2 × 20 mL) and brine (2 × 20 mL). The organic layer was dried over anhydrous $MgSO_4$ and filtered. The solvent was removed at low pressure and the reaction crude was purified by column chromatography using CS_2 as eluent to remove unreacted C_{60}, followed by toluene. Compound **57** was obtained as a dark brown solid (50 % yield).

^{1}H-NMR ($CDCl_3$, 300 MHz) δ / ppm: 4.65 (t, J = 6.6 Hz, 2H, H_f), 4.60 (c, J = 7.2 Hz, 2H, H_b), 2.46 (td, J = 6.6 Hz, J = 2,7 Hz, 2H, H_h), 2.11 (qu, J = 6.6 Hz, 2H, H_g), 2.07 (t, J = 2.7 Hz, 1H, H_j), 1.53 (t, J = 7.2 Hz, 3H, H_a).

^{13}C-NMR ($CDCl_3$, 75 MHz) δ / ppm: 163.4, 163.3 (C_c, C_e); 145.4, 145.3, 145.3, 145.3, 145.1, 144.9, 144.8, 144.1, 143.3, 143.2, 143.1, 142.4, 142.1, 142.0, 141.1, 141.1, 139.4, 139.1 (sp^2 – C_{60}); 82.6 (C_i), 71.6 (sp^3 – C_{60}), 69.8 (C_j), 65.8 (C_f), 63.7 (C_b), 27.6 (C_g), 15.3 (C_h), 14.4 (C_a).

FTIR (CH_2Cl_2) (cm^{-1}): 3287 (*v* C≡**C**–**H**), 2983 (*v* **C**–**H**), 2120 (*v* **C**≡**C**), 1731 (*v* **C**=**O**), 1332, 1270, 1151, 1033.

3-(Boc-amino)-1-propanol (58)

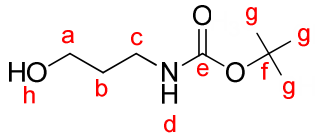

58

To a solution of 1.51 g (19.9 mmol) of 3-amino-1-propanol and 2.22 g (16 mmol) of triethylamine in 50 mL of $CHCl_3$, 4.81 g (21.6 mmol) of di-*tert*-butyldicarbonate in 20 mL of $CHCl_3$ were added dropwise over 1 hour. The reaction was stirred at room temperature for 4 hours. The solvent was removed at low pressure and the reaction crude was purified by column chromatography using hexane:AcOEt (1:1, v/v) as eluent. Compound **58** was obtained as a colourless oil (87 % yield).

^{1}H-NMR ($CDCl_3$, 300 MHz) δ / ppm: 4.80 (br s, 1H, H_d), 3.65 (t, J = 5.7 Hz, 2H, H_a), 3.27 (t, J = 5.7 Hz, 2H, H_c), 2.74 (br s, 1H, H_h), 1.65 (q, J = 5.7 Hz, 2H, H_b), 1.43 (s, 9H, H_g).

^{13}C-NMR ($CDCl_3$, 75 MHz) δ / ppm: 157.3 (C_e), 79.8 (C_f), 59.4 (C_a), 37.1 (C_c), 33.0 (C_b), 28.5 (C_g).

FTIR (CH_2Cl_2) (cm^{-1}): 3341 (*v* **O**–**H**); 2975, 2937, 2879 (*v* **C**–**H**); 1685 (*v* **C**=**O**), 1522, 1169.

Bis-(3-(Boc-amino)-1-propyl)malonate (59)

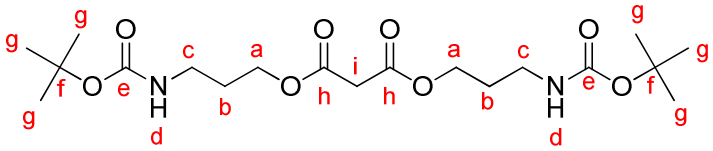

59

To a solution of 1.00 g (6.30 mmol) of **58**, 1 mL (7.3 mmol) of triethylamine and 37 mg (0.35 mmol) of 4-dimethylaminopyridine in 15 mL of dry CH_2Cl_2 at 0 ºC and under Ar atmosphere, 0.41 g (2.8 mmol) of malonyl chloride in 15 mL of dry CH_2Cl_2 were added dropwise. After 30 minutes, the reaction was allowed to reach room temperature and after 4 hours of stirring, the reaction crude was washed with HCl 1 M (2 × 20 mL), saturated aqueous $NaHCO_3$ (20 mL) and brine (2 × 30 mL). The organic layer was dried over anhydrous $MgSO_4$ and filtered. Solvent was removed at low pressure and the remaining oil was purified by column chromatography using hexane:AcOEt (1:1, v/v) as eluent. Compound **59** was obtained as a transparent oil (52 % yield).

^{1}H-NMR ($CDCl_3$, 300 MHz) δ / ppm: 4.82 (br s, 2H, H_d), 4.25 (t, J = 6.0 Hz, 4H, H_a), 3.42 (s, 2H, H_i), 3.22 (c, J = 6.0 Hz, 4H, H_c), 1.87 (q, J = 6.3 Hz, 4H, H_b), 1.46 (s, 18H, H_g).

^{13}C-NMR ($CDCl_3$, 75 MHz) δ / ppm: 166.8 (C_h), 156.1 (C_e), 79.5 (C_f), 63.3 (C_a), 41.6 (C_i), 37.4 (C_c) 29.1 (C_b), 28.5 (C_g).

FTIR (CH_2Cl_2) (cm^{-1}): 3360 (ν **N–H**), 2975 (ν **C–H**), 1668 (ν **C=O**), 1522, 1169.

[60]Fullerene monoadduct of bis(3-(Boc-amino)-1-propyl)malonate (60)

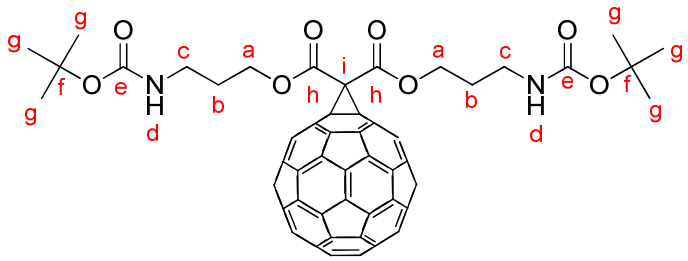

60

To a sonicated solution of 51 mg (0.12 mmol) of **59**, 200 mg (0.28 mmol) of [60]fullerene and 72 mg (0.28 mmol) of I_2, in 90 mL of dry toluene under Ar atmosphere and at 0 ^{o}C, 91 mg (0.62 mmol) of 1,8-diazabicycloundec-7-ene in 10 mL of dry toluene were added dropwise. The reaction mixture was stirred at 0 ^{o}C for 5 h and, thereafter, 30 mL of saturated aqueous sodium thiosulfate were added in order to finish the reaction. The organic phase was washed with saturated aqueous sodium thiosulfate (2 × 30 mL), HCl 0.5 M (2 × 20 mL) and brine (2 × 20 mL). The organic layer was dried over anhydrous $MgSO_4$ and filtered. The solvent was removed at low pressure and the reaction crude was purified by column chromatography using CS_2 as eluent to remove unreacted [60]fullerene, followed by toluene. Compound **60** was obtained as a dark brown solid (46 % yield).

^{1}H-NMR ($CDCl_3$, 300 MHz) δ / ppm: 4.94 (br s, 2H, H_d), 4.60 (t, J = 6.3 Hz, 4H, H_a), 3.35 (c, J = 6.3 Hz, 4H, H_c), 2.09 (q, J = 6.3 Hz, 4H, H_b), 1.49 (s, 18H, H_g).

^{13}C-NMR ($CDCl_3$, 75 MHz) δ / ppm: 166.8 (C_h), 157.3 (C_e); 145.4, 145.3, 145.2, 145.1, 144.9, 144.8, 144.8, 144.0, 143.2, 143.2, 143.1, 142.3, 142.1, 141.2, 139.2 ($sp^2 - C_{60}$); 79.8 (C_f), 71.5 ($sp^3 - C_{60}$), 59.4 (C_a), 52.1 (C_i), 37.1 (C_c), 33.0 (C_b), 28.5 (C_g).

FTIR (CH_2Cl_2) (cm^{-1}): 3348 (ν **N–H**), 2970 (ν **C–H**), 1670 (ν **C=O**), 1520.

3,4,5-Tris[2-(2-methoxyethoxy)ethoxy]benzyl chloride (61)

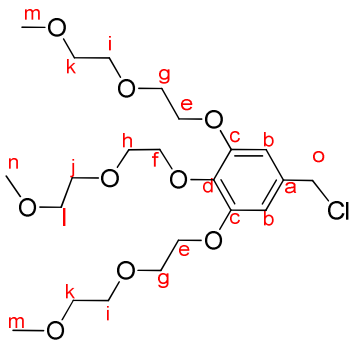

61

To a solution of 630 mg (1.4 mmol) of **48** in 60 mL of dry CH_2Cl_2, at 0 ºC and under Ar atmosphere, 660 mg (5.5 mmol) of thionyl chloride were added dropwise. Thereafter, reaction mixture was allowed to reach room temperature and stirred for 24 hours. Solvent was removed at low pressure and the reaction crude was purified by column chromatography using AcOEt:MeOH (95:%, v/v). Compound **61** was obtained as a yellowish oil (90 % yield).

^{1}H-NMR ($CDCl_3$, 300 MHz) δ / ppm: 6.62 (s, 2H, H_b), 4.56 (s, 2H, H_o) 4.23–4.15 (m, 6H), 3.83 (t, J = 5.1 Hz, 4H), 3.79 (t, J = 5.1 Hz, 2H), 3.76–3.70 (m, 6H), 3.59–3.56 (m, 6H), 3.41 (s, 9H).

^{13}C-NMR ($CDCl_3$, 75 MHz) δ / ppm: 152.8 (C_c), 137.7 (C_a), 136.6 (C_d), 106.2 (C_b); 72.5, 72.1, 72.0, 70.7, 70.6, 70.3, 69.9, 68.9 (C_e, C_f, C_g, C_h, C_i, C_j, C_k, C_l); 59.1 (C_m, C_n), 46.1 (C_o).

FTIR (CH_2Cl_2) (cm^{-1}): 2925, 2877 (*v* **C–H**); 1590 (*v* **C=C Ar**), 1501, 1436, 1101 (*v* **C–O**).

3,4,5-Tris[2-(2-methoxyethoxy)ethoxy]benzyl azide (62)

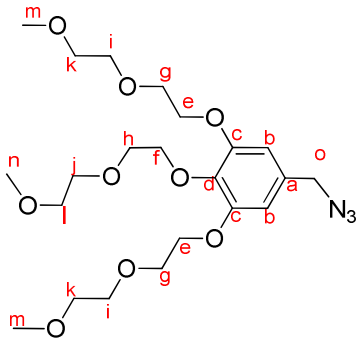

62

A mixture of 375 mg (0.27 mmol) of **23** and 144 mg (2.2 mmol) of sodium azide was dissolved, under Ar atmosphere, in 6 mL of dry DMF. The reaction mixture was stirred at 55 ºC for 24 h. Thereafter, the reaction crude was suspended in 30 mL of AcOEt and the organic phase was washed with water (3 × 30 mL). The organic layer was dried over anhydrous $MgSO_4$ and filtered. The solvent was removed at low pressure and **24** was obtained as a white foam (90 % yield).

^{1}H-NMR ($CDCl_3$, 300 MHz) δ / ppm: 6.57 (s, 2H, H_b), 4.25 (s, 2H, H_o) 4.20 (c, J = 5.1 Hz, 6H), 3.88 (t, J = 5.1 Hz, 4H), 3.83 (t, J = 5.1 Hz, 2H), 3.76–3.70 (m, 6H), 3.59–3.56 (m, 6H), 3.41 (s, 9H, H_m, H_n).

^{13}C-NMR ($CDCl_3$, 75 MHz) δ / ppm: 152.6 (C_c), 137.9 (C_a), 136.6 (C_d), 106.4 (C_b); 72.5, 72.1, 71.9, 70.7, 70.6, 70.3, 69.9, 68.9 (C_e, C_f, C_g, C_h, C_i, C_j, C_k, C_l); 59.1 (C_m, C_n), 55.3 (C_o).

FTIR (CH_2Cl_2) (cm^{-1}): 2930 (ν **C–H**), 2103 (ν **–N=N=N)**, 1590 (ν **C=C Ar**), 1501, 1436, 1101 (ν **C–O**).

1,3-Bis(6-bromohex-1-yl)malonate (63)

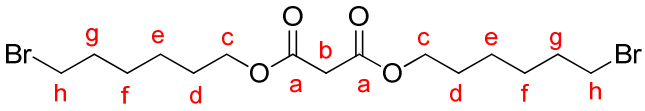

63

To a solution of 2.00 g (11 mmol) of 6-bromohexan-1-ol, 2.4 mL (13.2 mmol) of triethylamine and 89 mg (0.84 mmol) of 4-dimethylaminopyridine in 30 mL of dry CH_2Cl_2 at 0 ºC and under Ar atmosphere, 0.72 g (4.9 mmol) of malonyl chloride in 15 mL of dry CH_2Cl_2 were added dropwise. After 30 minutes, the reaction was allowed to reach room temperature and after 4 hours of stirring, the reaction crude was washed with HCl 1 M (2 × 20 mL), saturated aqueous $NaHCO_3$ (1 × 20 mL) and brine (2 × 30 mL). The organic layer was dried over anhydrous $MgSO_4$ and filtered. Solvent was removed at low pressure and the remaining oil was purified by column chromatography using hexane:CH_2Cl_2 (3:7, v/v) as eluent. Compound **63** was obtained as a yellowish oil (50 % yield).

^{1}H-NMR ($CDCl_3$, 300 MHz) δ / ppm: 4.08 (t, J = 6.3 Hz, 4H, H_c), 3.34 (t, J = 6.6 Hz, 4H, H_h) 3.31 (s, 2H, H_b), 1.81 (q, J = 6.9 Hz, 4H, H_g), 1.61 (q, J = 6.9 Hz, 4H, H_d), 1.46 – 1.29 (m, 8H, H_e, H_f).

^{13}C-NMR ($CDCl_3$, 75 MHz) δ / ppm: 166.8 (C_a), 65.5 (C_c), 41.8 (C_b); 33.8, 32.7, 28.4, 27.9, 25.2 (C_d, C_e, C_f, C_g, C_h).

FTIR (CH_2Cl_2) (cm^{-1}): 2935, 2861 (*ν* **C–H**); 1734 (*ν* **C=O)**, 1147.

1,3-Bis(6-bromohex-1-yl)-2,2-dipropargyl malonate (64)

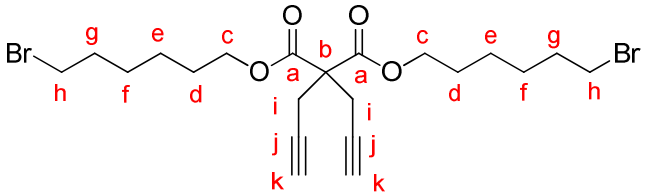

64

To a suspension of 90 mg (2.3 mmol) of sodium hydride (60%, dispersion in mineral oil) in 6 mL of dry THF at 0 ºC and Ar atmosphere, 420 mg (0.97 mmol) of **63** in 2 mL of dry THF were added dropwise. Thereafter, the reaction was allowed to reach room temperature. After 30 minutes, 0.23 mL (2.1 mmol) of propargyl bromide (80 % wt in toluene) were added and stirred for 2 hours. The reaction was finished by adding saturated aqueous NH_4Cl solution and extracted with ethyl acetate (2 × 10 mL). The organic layer was washed with brine (2 × 20 mL) and dried over anhydrous $MgSO_4$. Solvent was removed at low pressure and the remaining oil was purified by column chromatography using hexane:AcOEt (95:5, v/v) as eluent to give **64** as a colourless oil (80 % yield).

^{1}H-NMR ($CDCl_3$, 300 MHz) δ / ppm: 4.20 (t, J = 6.3 Hz, 4H, H_c), 3.43 (t, J = 6.6 Hz, 4H, H_h), 3.02 (d, J = 2.7 Hz, 4H, H_i), 2.07 (d, J = 2.7 Hz, 2H, H_k), 1.89 (q, J = 6.9 Hz, 4H, H_g), 1.68 (q, J = 6.9 Hz, 4H, H_d), 1.54 – 1.37 (m, 8H, H_e, H_f).

^{13}C-NMR ($CDCl_3$, 75 MHz) δ / ppm: 168.8 (C_a), 78.7 (C_j), 71.9 (C_k), 66.1 (C_c), 56.4 (C_b); 33.9, 32.6, 28.4, 27.7, 25.2 (C_d, C_e, C_f, C_g, C_h); 22.7 (C_i)

FTIR (CH_2Cl_2) (cm^{-1}): 3296 (ν C≡**C**–**H**); 2930, 2855 (ν **C**–**H**); 2117 (ν **C≡C**), 1737 (ν **C=O**).

MS (ESI): *m/z* 504.05 calculated for $[M]^+$ $C_{21}H_{30}Br_2O_4$, found: 504.0.

1,3-Bis(6-bromohex-1-yl)-2,2-bis[(3,4,5-tris[2-(2-methoxyethoxy) ethoxy]benzyl)-1*H*-1,2,3-triazol-4-yl)methyl]malonate (65)

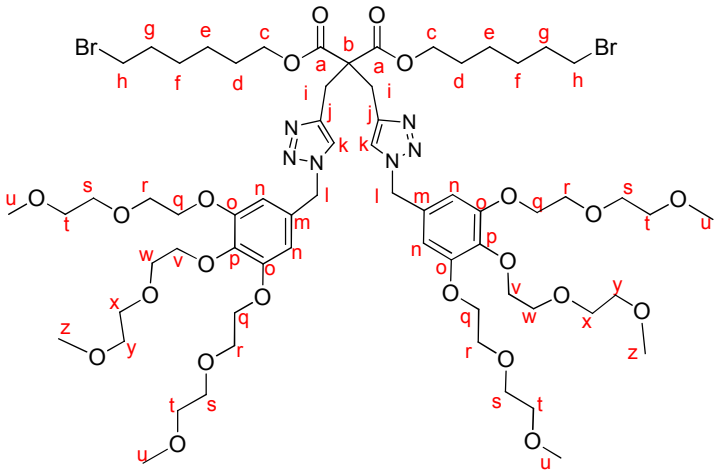

65

A mixture of 100 mg (0.2 mmol) of **62**, 47 mg (0.09 mmol) of **64,** 10 mg ($5.3 \cdot 10^{-2}$ mmol) of CuI and 30 µL ($1.7 \cdot 10^{-4}$ mmol) of DIPEA under Ar atmosphere was dissolved in 2 mL of deoxygenated THF, and a piece of copper wire was added. After stirring for 24 h at room temperature, the reaction crude was suspended in 20 mL of AcOEt and washed with aqueous saturated NH_4Cl solution (2 × 10 mL), 15 mL of water and 15 mL of brine. The organic layer was dried over anhydrous $MgSO_4$ and filtered. The solvent was removed at low pressure and the reaction crude was purified by column chromatography using AcOEt:MeOH (95:5, v/v) as eluent until a mixture of **62** and **65** was obtained. Thereafter, this mixture was purified by exclusion-size chromatography (Sephadex LH-20) and CH_2Cl_2:MeOH (1:1, v/v) as eluent. Compound **65** was obtained as a colourless oil (75 % yield).

^{1}H-NMR ($CDCl_3$, 300 MHz) δ / ppm: 7.57 (s, 2H, H_k), 6.45 (s, 4H, H_n), 5.41 (s, 4H, H_l), 4.14 (m, 20H), 3.86 (t, J = 5.1 Hz, 8H), 3.81 (t, J = 5.1 Hz, 4H), 3.75–3.71 (m, 12H), 3.58–3.56 (m, 12H), 3.43 (t, J = 6.6 Hz, 4H, H_h), 3.40 (s, 18H, H_u, H_z), 1.87 (q, J = 6.9 Hz, 4H, H_g), 1.64 (q, J = 6.9 Hz, 4H, H_d), 1.52 – 1.30 (m, 8H, H_e, H_f).

^{13}C-NMR ($CDCl_3$, 75 MHz) δ / ppm: 168.6 (C_a), 153.1 (C_o), 148.3 (C_j) 138.5 (C_m), 130.1 (C_p), 128.1 (C_k), 107.2 (C_n); 72.4, 72.1, 72.0, 70.7, 70.5, 70.4, 69.7,

69.0 (C_e, C_f, C_g, C_h, C_i, C_j, C_k, C_l); 65.7 (C_c), 59.2 (C_m), 59.1 (C_n), 56.3 (C_l), 33.8, 32.6, 28.2, 27.7, 25.1 (C_d, C_e, C_f, C_g, C_h), 23.5 (C_i)

FTIR (CH_2Cl_2) (cm^{-1}): 2933, 2878 (*v* **C–H**); 1732 (*v* **C=O**), 1590 (*v* **C=C Ar**), 1109.

MALDI-TOF: *m/z* 1479.56 calculated for $[M+H]^+$ $C_{65}H_{104}Br_2N_6O_{22}$, found: 1479.63.

1,3-Bis(6-azidohex-1-yl)-2,2-bis[(3,4,5-tris[2-(2-methoxyethoxy) ethoxy]benzyl)-1*H*-1,2,3-triazol-4-yl)methyl]malonate (65)

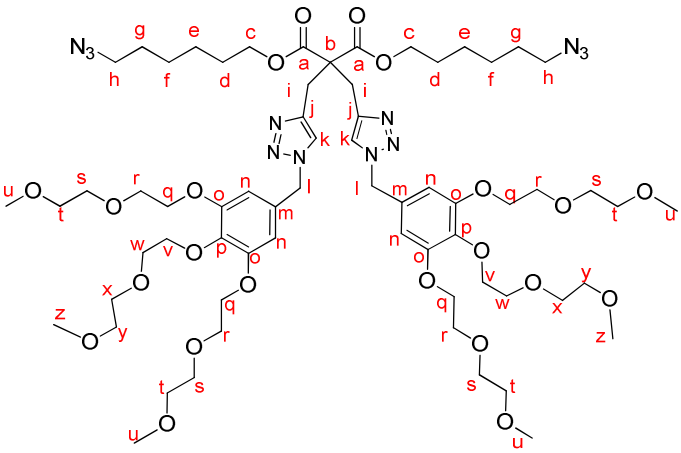

66

A mixture of 200 mg (0.13 mmol) of **65** and 70 mg (1.04 mmol) of sodium azide in 8 mL of dry DMF at 70ºC was stirred for 18 h under Ar atmosphere. Thereafter, the reaction crude was resuspended in 40 mL of AcOEt and the organic phase was washed with water (3 × 40 mL). The organic layer was dried over anhydrous $MgSO_4$ and filtered. The solvent was removed at low pressure and **66** was obtained as a pale yellow oil (90 % yield).

^{1}H-NMR ($CDCl_3$, 300 MHz) δ / ppm: 7.56 (s, 2H, H_k), 6.45 (s, 4H, H_n), 5.40 (s, 4H, H_l), 4.14 (m, 20H), 3.86 (t, J = 5.1 Hz, 8H), 3.81 (t, J = 5.1 Hz, 4H), 3.75–

3.71 (m, 12H), 3.58–3.55 (m, 12H), 3.40 (s, 18H, H_u, H_z), 3.29 (t, J = 6.6 Hz, 4H, H_h), 1.69 – 1.57 (m, 8H, H_d, H_g), 1.45 – 1.30 (m, 8H, H_e, H_f).

^{13}C-NMR ($CDCl_3$, 75 MHz) δ / ppm: 168.6 (C_a), 153.1 (C_o), 148.3 (C_j) 138.5 (C_m), 130.1 (C_p), 128.1 (C_k), 107.2 (C_n), 78.1 (C_h); 72.4, 72.1, 72.4, 70.9, 70.4, 69.9, 69.0 (C_e, C_f, C_g C_i, C_j, C_k, C_l); 65.7 (C_c), 59.2 (C_m), 59.1 (C_n), 56.3 (C_l), 33.8, 32.6, 28.2, 27.7, 25.1 (C_d, C_e, C_f, C_g, C_h), 23.5 (C_i)

FTIR (CH_2Cl_2) (cm^{-1}): 2929, 2876 (ν **C–H**); 2095 (ν **N=N=N**), 1732 (ν **C=O**), 1591 (ν **C=C Ar**), 1108 (ν **C–O**).

Difullerene from [60]fullerene monoadduct of 1-(ethyl) 3-[1-(4-pentyn-1-yl)]malonate and 1,3-bis(6-azidohex-1-yl)-2,2-bis[(3,4,5-tris[2-(2-methoxyethoxy)ethoxy]benzyl)-1*H*-1,2,3-triazol-4-yl)methyl]malonate (67)

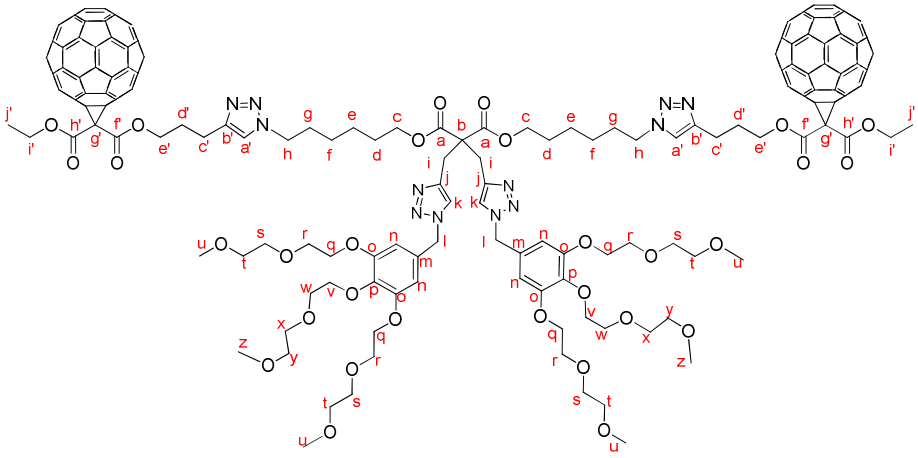

67

A mixture of 150 mg (0.11 mmol) of **66**, 230 mg (0.25 mmol) of **57**, 27 mg (0.14 mmol) of sodium ascorbate and 36 mg (0.14 mmol) of $CuSO_4 \cdot 5H_2O$ was dissolved in 2 mL of deoxygenated CH_2Cl_2/water (1:1, v/v) under Ar atmosphere. After stirring for 48 h at room temperature, the reaction crude was suspended in 20 mL of CH_2Cl_2 and washed with aqueous saturated NH_4Cl solution (2 × 10

mL), 15 mL of water and 15 mL of brine. The organic layer was dried over anhydrous $MgSO_4$ and filtered. The solvent was removed at low pressure and the reaction crude was purified by column chromatography using CH_2Cl_2 as eluent to remove excess of **57** and a mixture of CH_2Cl_2:MeOH (95:5, v/v) to get compound **67** as a dark brown solid (85 % yield).

^{1}H-NMR ($CDCl_3$, 500 MHz) δ / ppm: 7.55 (s, 2H, H_k), 7.46 (s, 2H, $H_{a'}$), 6.45 (s, 4H, H_n), 5.41 (s, 4H, H_l), 4.59 (m, 8H, $H_{e'}$, $H_{i'}$), 4.36 (s, 4H), 4.14 (m, 16H), 3.85 (m, 8H), 3.81 (t, J = 4.8 Hz, 4H), 3.72 (m, 12H), 3.57 (m, 12H), 3.39 (s, 18H, H_u, H_z), 2.95 (s, 4H, H_h), 2.29 (s, 4H, $H_{c'}$), 1.92 (s, 4H, $H_{d'}$), 1.66 (br s, 8H, H_d, H_g), 1.52 (t, J = 6.6 Hz, 6H, $H_{j'}$), 1.37 (br s, 8H, H_e, H_f).

^{13}C-NMR ($CDCl_3$, 125 MHz) δ / ppm: 168.6 (C_a), 163.1 ($C_{h'}$, $C_{f'}$), 153.1 (C_o), 148.3 (C_j), 145.4, 145.3, 145.3, 145.3, 145.1, 144.9, 144.8, 144.1, 143.3, 143.2, 143.1, 142.4, 142.1, 142.0, 141.1, 141.1, 139.4, 139.1 (sp^2 – C_{60}); 138.5 (C_m), 130.1 (C_p), 128.1 (C_k), 107.2 (C_n), 78.1 (C_h); 72.4, 72.1, 72.4, 70.9, 70.4, 69.9, 69.0 (C_e, C_f, C_g C_i, C_j, C_k, C_l); 65.9 ($C_{e'}$), 65.7 (C_c), 63.2 ($C_{i'}$) 59.2 (C_m), 59.1 (C_n), 56.3 (C_l), 33.8, 32.6, 28.2, 27.7, 27,6, 25.1 (C_d, C_e, C_f, C_g, C_h, $C_{d'}$), 23.5 (C_i), 17.1 ($C_{c'}$), 14.6 ($C_{j'}$).

FTIR (CH_2Cl_2) (cm^{-1}): 2927, 2875 (*v* **C**–**H**); 1742 (*v* **C=O**), 1592 (*v* **C=C Ar**), 1238, 1110 (*v* **C**–**O**).

Bis[3,4,5-tris(1-(2-(*N*-Boc)aminoethyl)-1*H*-1,2,3-triazol-4-yl)methoxy]benzyl malonate (68)

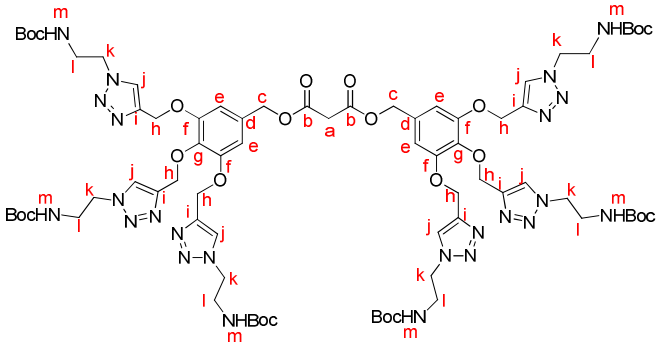

68

A mixture of 50 mg (0.082 mmol) of **21**, 100 mg (0.54 mmol) of **41,** 10 mg ($5.3 \cdot 10^{-2}$ mmol) of CuI and 30 µL ($1.7 \cdot 10^{-4}$ mmol) of DIPEA under Ar atmosphere was dissolved in 2 mL of deoxygenated toluene, and a piece of copper wire was added. After stirring for 48 h at room temperature, the reaction crude was suspended in 20 mL of AcOEt and washed with aqueous saturated NH_4Cl (2 × 10 mL), 15 mL of water and 15 mL of brine. The organic layer was dried over anhydrous $MgSO_4$ and filtered. The solvent was removed at low pressure and the reaction crude was purified by column chromatography using CH_2Cl_2:MeOH (95:5, v/v). Compound **68** was obtained as a colourless oil (88 % yield).

^{1}H-NMR ($CDCl_3$, 300 MHz) δ / ppm: 7.93 (s, 6H, H_j), 6.84 (s, 4H, H_e), 5.70 (br s, 6H, H_m), 5.44 (s, 4H, H_c), 5.11 (s, 12H, H_h), 4.54 (m, 12H, H_k), 3.65 (br s, 14H, H_l and H_a), 1.42 (s, 54H, 6×(($C\underline{H}_3$)$_3$C).

^{13}C-NMR ($CDCl_3$, 75 MHz) δ / ppm: 166.9 (C_b), 156.4, 152.4, 149.1, 137.1 (C_d), 132.1 (C_g), 128.5, 108.9 (C_e), 81.2, 67.6 (C_c), 63.5 (C_k), 47.8, 41.3, 40.8, 28.1 (CH_3).

FTIR (CH_2Cl_2) (cm^{-1}): 3370 (*v* **N–H**); 2985, 2932 (*v* **C–H**); 1720 (**C=O ester**), 1684 (*v* **C=O amide**), 1596 (*v* **C–C Ar**).

[60]Fullerene monoadduct from bis[3,4,5-tris(1-(2-(*N*-Boc)aminoethyl)-1*H*-1,2,3-triazol-4-yl)methoxy]benzyl malonate (69)

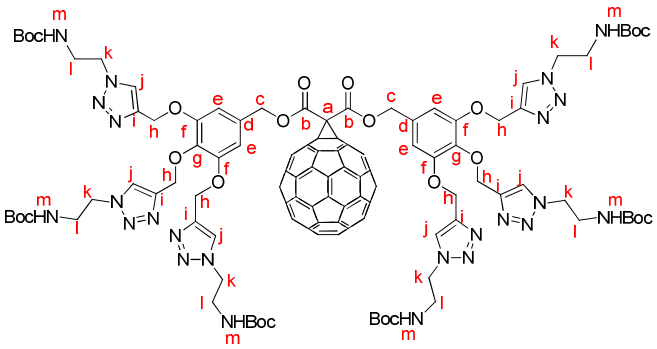

69

A mixture of 110 mg (0.082 mmol) of **30**, 100 mg (0.54 mmol) of **41,** 10 mg ($5.3 \cdot 10^{-2}$ mmol) of CuI and 30 μL ($1.7 \cdot 10^{-4}$ mmol) of DIPEA under Ar atmosphere was dissolved in 2 mL of deoxygenated toluene, and a piece of copper wire was added. After stirring for 48 h at room temperature, the reaction crude was suspended in 20 mL of AcOEt and washed with aqueous saturated NH_4Cl (2 × 10 mL), 15 mL of water and 15 mL of brine. The organic layer was dried over anhydrous $MgSO_4$ and filtered. The solvent was removed at low pressure and the reaction crude was purified by column chromatography using CH_2Cl_2:MeOH (95:5, v/v). Compound **69** was obtained as a brown solid (82 % yield).

^{1}H-NMR ($CDCl_3$, 300 MHz) δ / ppm: 7.91 (s, 6H, H_j), 6.86 (s, 4H, H_e), 5.75 (br s, 6H, H_m), 5.24 (s, 4H, H_c), 5.15 (s, 12H, H_h), 4.55 (m, 12H, H_k), 3.70 (br s, 12H, H_l), 1.41 (s, 54H, $(C\underline{H}_3)_3C$)

^{13}C-NMR ($CDCl_3$, 75 MHz) δ / ppm: 163.1 (C_b), 156.1, 152.3, 150.4; 145.4, 145.3, 145.2, 145.0, 145.0, 144.8, 144.7, 144.0, 143.2, 143.1, 143.1, 142.3, 142.0, 141.1, 139.1 (C_{60}); 137.5 (C_d), 132.1 (C_g), 127.8, 109.2 (C_e), 81.1, 71.5, 68.2 (C_c), 63.1 (C_k), 47.8, 41.0, 28.0 (CH_3).

FTIR (CH_2Cl_2) (cm^{-1}): 3365 (*ν* **N–H**); 2980, 2930 (*ν* **C–H**); 1725 (**C=O ester**), 1690 (*ν* **C=O amide**), 1594 (*ν* **C–C Ar**)

Bis[3,4,5-tris(1-(2-aminoethyl hydrochloride)-1*H*-1,2,3-triazol-4-yl)methoxy]benzyl malonate (70)

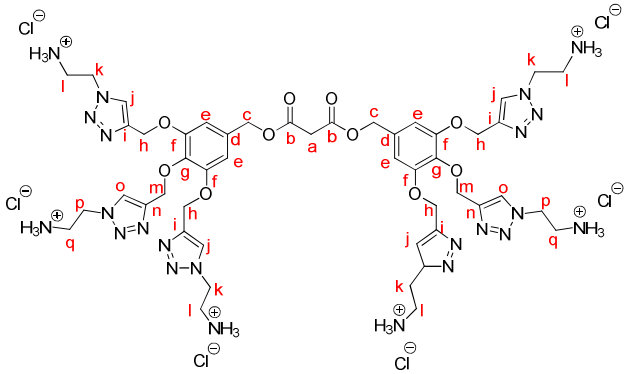

70

To a solution of 50 mg ($2.9 \cdot 10^{-2}$ mmol) of **68** in 2 mL dioxane under Ar atmosphere, 0.35 mL of HCl 4 M (1.39 mmol) in dioxane were added. The mixture was stirred at room temperature and, after 30 minutes, a white solid appeared. After 18 hours, solvent was removed at low pressure. The solid was washed with CH_2Cl_2 and dried, affording **70** as a white solid (98 % yield).

^{1}H-NMR (D_2O, 300 MHz) δ / ppm: 8.16 (s, 4H, H_j), 7.95 (s, 2H, H_o), 6.82 (s, 4H, H_e), 5.23 (s, 4H, H_c), 5.07 (s, 8H, H_h), 5.05 (s, 4H, H_m), 4.84 (t , J = Hz, 8H, H_k), 4.82 (t , J = 6.0 Hz, 4H, H_p), 3.54 (t , J = 6.0 Hz, 8H, H_l), 3.52 (t , J = 6.0 Hz, 4H, H_q).

^{13}C-NMR (D_2O, 75 MHz) δ / ppm: 168.1 (C_b), 151.8 (C_f), 142.6, 136.4 (C_d), 132.3 (C_g), 126.5, 108.1 (C_e), 67.3, 66.4, 66.2, 58.1, 57.9, 42.3 (C_a).

FTIR (KBr) (cm^{-1}): 3290 (ν **N–H**), 2927 (ν **C–H**), 1722 (**C=O ester**), 1594 (ν **C–C Ar**).

[60]Fullerene monoadduct from bis[3,4,5-tris(1-(2-aminoethyl hydrochloride)-1*H*-1,2,3-triazol-4-yl)methoxy]benzyl malonate (71)

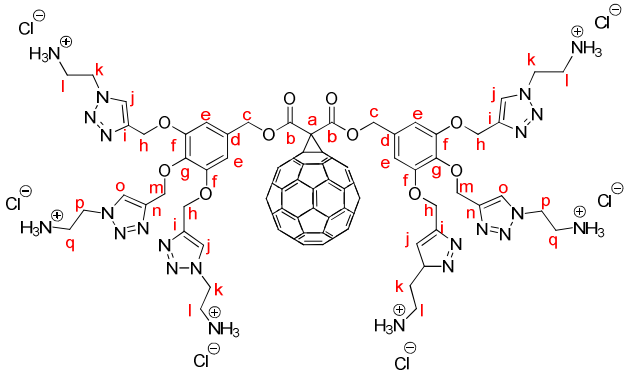

71

To a solution of 50 mg ($2.0 \cdot 10^{-2}$ mmol) of **69** in 2 mL dioxane under Ar atmosphere, 0.24 mL of HCl 4 M (0.96 mmol) in dioxane were added. The mixture was stirred at room temperature and, after 30 minutes, a brown solid appeared. After 18 hours, solvent was removed at low pressure. The solid was washed with CH_2Cl_2 and dried, affording **71** as a dark brown solid (85 % yield).

^{1}H-NMR ($CDCl_3$, 300 MHz) δ / ppm: 8.25 (s, 4H, H_j), 8.04 (s, 2H, H_o), 6.89 (s, 4H, H_e), 5.55 (s, 4H, H_c), 4.95 (s, 12H, H_h, H_m), 4.74 (m, 12H, H_k, H_p), 3.61 (m, 12H, H_l, H_q).

^{13}C-NMR ($CDCl_3$, 75 MHz) δ / ppm: 164.6 (C_b), 151.8 (C_f); 145.4, 145.3, 145.2, 145.0, 145.0, 144.8, 144.7, 144.0, 143.2, 143.1, 143.1, 142.3, 142.0, 141.1, 139.1 (C_{60}); 136.4 (C_d), 132.3 (C_g), 125.1, 124.9, 107.1 (C_e), 67.3, 63.4, 63.2, 55.8, 55.3.

FTIR (KBr) (cm^{-1}): 3290 (*v* **N–H**), 2930 (*v* **C–H**), 1717 (**C=O ester**), 1592 (*v* **C–C Ar**).

(3-Azidopropyl)triethoxysilane (72)

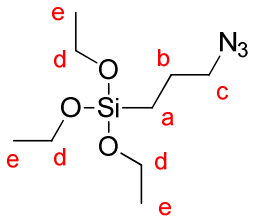

72

To a solution of 1.12 g (17.2 mmol) of sodium azide and 0.66 g (2 mmol) of tetrabutylammonium bromide in 20 mL of dry acetonitrile under Ar atmosphere, 2.00 g (8.3 mmol) of (3-chloropropyl)triethoxysilane in 50 mL of dry acetonitrile were added dropwise. The reaction mixture was refluxed for 22 hours. Thereafter, the solvent was removed at low pressure and the product was resuspended in 50 mL of hexane. The solution was filtered through celite and the solvent was removed at low pressure, yielding **72** as a colourless oil (98% yield)

^{1}H-NMR ($CDCl_3$, 300 MHz) δ / ppm: 3.75 (q, J = 6.9 Hz, 6H, H_d), 3.20 (t, J = 7.2 Hz, 2H, H_c), 1.65 (m, 2H, H_b), 1.16 (t, J = 6.9 Hz, 9H, H_e), 0.61 (m, 2H, H_a).

^{13}C-NMR ($CDCl_3$, 75 MHz) δ / ppm: 58.6 (C_d), 54.0 (C_c), 22.8 (C_b), 18.4 (C_e), 7.8 (C_a).

FTIR (CH_2Cl_2) (cm^{-1}): 2975, 2928, 2886, 2096 (ν **N=N=N**), 1102, 1079, 786.

Synthesis of mesoporous silica nanoparticles

- **Non-functionalized mesoporous silica nanoparticles**

  To 80 mL of distilled and deionized water, 1 mL of sodium hydroxide 0.2 M (2 mmol) and 0.3 g (0.8 mmol) of hexadecyltrimethylammonium bromide were added. The solution was heated to 80 ºC and stirred vigorously. Thereafter, 1.92 g (9.2 mmol) of tetraethylortosilicate were added dropwise over 2 min. A white precipitate appeared and the reaction

mixture was stirred at 80 ºC for two hours. The precipitate was filtered, washed with water and methanol and dried.

- **Functionalized mesoporous silica nanoparticles with azide groups**

  To 80 mL of distilled and deionized water, 1 mL of sodium hydroxide 0.2M (2 mmol) and 0.3 g (0.8 mmol) of hexadecyltrimethylammonium bromide were added. The solution was heated to 80 ºC and stirred vigorously. Thereafter a mixture of 1.79 g (8.6 mmol) of tetraethyl ortosilicate and 0.11 g (0.44 mmol) were added dropwise over 2 min. A white precipitate appeared and the reaction mixture was stirred at 80 ºC for two hours. The precipitate was filtered, washed with water and methanol and dried.

  To remove the surfactant from the pores, 425 mg of the nanoparticles were refluxed 6 h in a mixture of 100 mL of methanol and 5 mL of concentrated HCl. The precipitate was filtered, washed with water and methanol and dried.

Synthesis of magnetite nanoparticles

To 1.50 g of $FeCl_2 \cdot 4H_2O$ and 3.00 g of $FeCl_3$ in Ar atmosphere, 100 mL of deoxygenated distilled and deionized water were added. The temperature was set to 25 ºC. Thereafter, the reaction mixture was stirred vigorously, and 10 mL of 28 % wt NH_3 were added, changing the colour of the reaction crude from orange to black. After 45 minutes. Magnetite nanoparticles were isolated using a magnet and washing them with water and ethanol.

Coating of magnetite nanoparticles with citrate

150 mg of the previously synthesized magnetite nanoparticles were resuspended in 25 mL of sodium citrate solution with a concentration of 0.5 M, under Ar Atmosphere. The mixture was sonicated for 30 min to reduce aggregation. The reaction mixture was stirred for 12 h 60 ºC. Thereafter, the solid was collected using a magnet and was washed with acetone to remove the excess of sodium citrate

Synthesis of magnetic silica nanoparticles

45 mg of citrate-stabilized nanoparticles were dispersed in 16 mL of distilled and deionized water, and sonicated for 30 minutes. Thereafter, 2 mL of 28 % wt NH_3 and 80 mL of ethanol were added, as well as a mixture of 700 mg (3.4 mmol) of tetraethylortosilicate and 45 mg (0.18 mmol) of **72**. The reaction mixture was stirred for 24 h at room temperature. The solid was collected using a magnet and washed with water.

Functionalization of nanoparticles with 57

Two different batches were obtained depending on whether the reaction was carried out under reflux or not.

Method A:

A suspension of 100 mg of nanoparticles (SiO_2–N_3 or Fe_3O_4@SiO_2 –N_3), 20 mg of **57**, 130 mg of CuI and 0.23 mL of DIPEA in 8 mL of toluene was stirred at room temperature or refluxed for 24 hours. Afterwards, the suspension was filtered and the solid was washed with toluene and acetone.

Method B:

A suspension of 100 mg of nanoparticles ((SiO_2–N_3 or Fe_3O_4@SiO_2 –N_3), 20 mg of **57**, 130 mg of CuI and 0.23 mL of DIPEA in 8 mL of toluene was stirred at 60 ºC or refluxed for 24 hours. Afterwards, the suspension was filtered and the solid was washed with toluene and acetone.

Control sample:

[60]fullerene (30 mg) was immobilized on non-functionalized mesoporous silica nanoparticles (100 mg) using toluene as solvent and removing it at low pressure.

10.3. Photophysical characterizations

-***UV-vis***: Ground-state absorption spectra were recorded using a Varian Cary 6000i UV-Vis-NIR spectrophotometer.

-***Fluorescence***: Corrected emission spectra were registered after setting the absorbance at 457 nm to 0.1 for each sample (**34**, **35**, **36**, **37**, **38**, **42**, **43**, **44** and **45**), in order to avoid the inner filter effect. Spectra were recorded using a Spex Fluoromax 4 spectrofluorimeter, by exciting the samples at 457 nm. The excitation spectra were recorded for the same samples recording the emission at 525 nm. Time-resolved measurements for the determination of the fluorescence kinetics were performed with a PicoQuant Fluotime 200 time-correlated single photon counting combined with a Picoquant's PMA 182-M single photon detector.

Fluorescence quantum yields were measured for solutions where the absorbance at 470 nm was previously set to 0.1. The emission spectrum of each sample was recorded by exciting it at 470 nm. Fluorescein in aqueous NaOH 0.1 M was used as standard ($\Phi_f = 0.92$).

-***Photosensitized generation of $^1O_2$***: Decay traces of $^1O_2$ were acquired by time resolved phosphorescence recorded after setting the absorbance at 355 nm to 0.1 for each sample (**28**, **29**, **30**, **31**, **32**, **33**, **50**, **53**, **55**, **57**, **60** and **71**). For photosensitizer excitation, a diode-pumped solid state Q-switched Nd:YAG laser (CryLas, FTQ355-QS) was used. Repetition rate was 10 kHz, producing ~1 ns FWHM laser pulses at 355 nm (5 mW, 0.5 μJ per pulse) and 532 nm (12 mW, 1.2 μJ per pulse). $^1O_2$ NIR phosphorescence was detected at 1270 nm using a Hamamatsu NIR-PMT(H10330-45) detector. Phenalenone (Φ_Δ = 0.94), sulfonated phenalenone (Φ_Δ = 1.00), Rose Bengal (Φ_Δ = 0.80) and tetraphenylporphyrin (Φ_Δ = 0.78) were used as references in toluene (λ_{exc} = 355 nm), D_2O (λ_{exc} = 355 nm), methanol (λ_{exc} = 532 nm) and toluene (λ_{exc} = 532 nm), respectively.

-***Well plate actinometry***: In order to determine the amount of photons absorbed by the specific geometries of the irradiated wells in the 96-well plates used for the photodynamic assays with *H. pylori*, a potassium ferrioxalate actinometry similar to that shown in Chapter 1 was carried out. Black 96-well microplates with flat bottom were used to contain the samples. In this case V_1 = 0.2 mL, V_2 = 0.1 mL and V_3 = 1.6 mL. Irradiation times were 7, 15, 22 and 30 s. Figure 109 shows the calibration graphs for the 16 wells considered as the most suitable for the photodynamic experiments, taking into account the relative spatial location with respect to the blue LED lamp used as light source. Table 26 summarizes the experimental calibration equations.

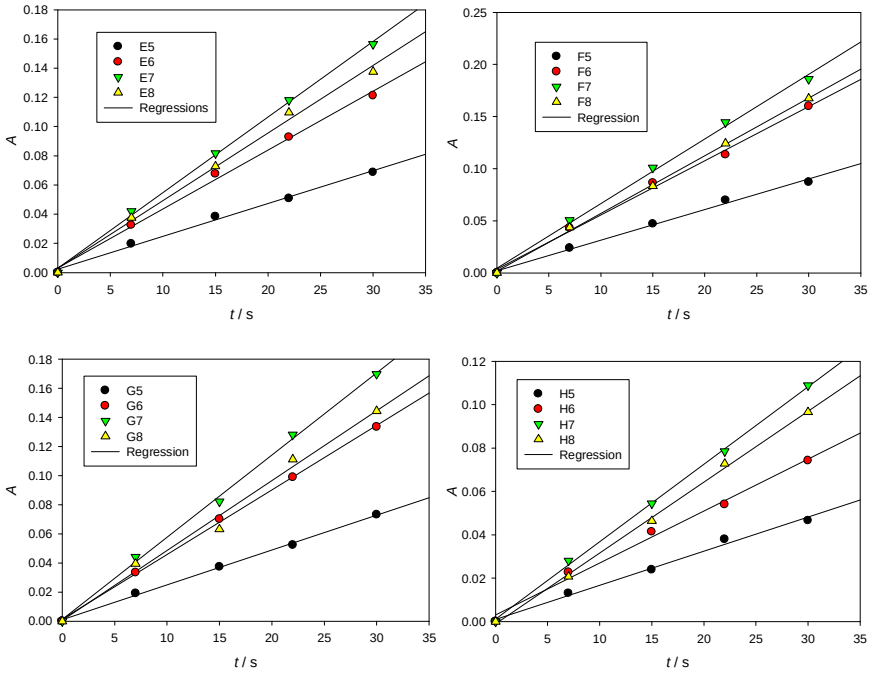

Figure 109. Calibration graphs of the chemical actinometry carried out with 96-well microplates.

Table 26. Calibration equations from chemical actinometry for each microplate.

Microplate	Regression line	r
E5	$A = (2.2 \pm 0.1)\cdot 10^{-3}\cdot t + (0.2 \pm 0.2)\cdot 10^{-2}$	0.997
E6	$A = (4.0 \pm 0.1)\cdot 10^{-3}\cdot t + (0.3 \pm 0.3)\cdot 10^{-2}$	0.998
E7	$A = (5.1 \pm 0.1)\cdot 10^{-3}\cdot t + (0.3 \pm 0.2)\cdot 10^{-2}$	0.999
E8	$A = (4.6 \pm 0.2)\cdot 10^{-3}\cdot t + (0.3 \pm 0.3)\cdot 10^{-2}$	0.998
F5	$A = (2.9 \pm 0.1)\cdot 10^{-3}\cdot t + (0.2 \pm 0.2)\cdot 10^{-2}$	0.997
F6	$A = (5.2 \pm 0.2)\cdot 10^{-3}\cdot t + (0.4 \pm 0.4)\cdot 10^{-2}$	0.998
F7	$A = (6.2 \pm 0.2)\cdot 10^{-3}\cdot t + (0.4 \pm 0.4)\cdot 10^{-2}$	0.998
F8	$A = (5.5 \pm 0.1)\cdot 10^{-3}\cdot t + (0.2 \pm 0.2)\cdot 10^{-2}$	1.000
G5	$A = (2.39 \pm 0.05)\cdot 10^{-3}\cdot t + (0.1 \pm 0.1)\cdot 10^{-2}$	0.999
G6	$A = (4.43 \pm 0.07)\cdot 10^{-3}\cdot t + (0.2 \pm 0.1)\cdot 10^{-2}$	1.000
G7	$A = (5.6 \pm 0.1)\cdot 10^{-3}\cdot t + (0.1 \pm 0.3)\cdot 10^{-2}$	0.999
G8	$A = (4.8 \pm 0.2)\cdot 10^{-3}\cdot t + (0.3 \pm 0.3)\cdot 10^{-2}$	0.995
H5	$A = (1.57 \pm 0.08)\cdot 10^{-3}\cdot t + (0.1 \pm 0.1)\cdot 10^{-2}$	0.996
H6	$A = (2.4 \pm 0.1)\cdot 10^{-3}\cdot t + (0.3 \pm 0.2)\cdot 10^{-2}$	0.996
H7	$A = (3.57 \pm 0.06)\cdot 10\text{-}3\cdot t + (0.1 \pm 0.1)\cdot 10^{-2}$	1.000
H8	$A = (3.27 \pm 0.07)\cdot 10^{-3}\cdot t\ \text{-}(0.1 \pm 0.1)\cdot 10^{-2}$	0.999

From these equations, the amount of incident photons and incident power were calculated for each microplate in the same manner as shown in Chapter 1. Tables 27 and 28 summarize the incident photons and incident power results, respectively.

Table 27. Amount of incident photons (10^8 q_p / einstein s^{-1}) on each microplate.

	E	F	G	H
8	6.8 ± 0.3	8.1 ± 0.1	7.0 ± 0.3	4.8 ± 0.1
7	7.6 ± 0.1	9.1 ± 0.3	8.3 ± 0.1	5.23 ± 0.08
6	5.9 ± 0.2	7.6 ± 0.3	6.5 ± 0,1	3.5 ± 0.1
5	3.3 ± 0.2	4.3 ± 0.1	3.50 ± 0.07	2.3 ± 0.1

Table 28. Incident light power (mW) on each microplate.

	E	F	G	H
8	16.6 ± 0.7	19.9 ± 0,4	17.2 ± 0,7	11.8 ± 0,2
7	18.6 ± 0,4	22.3 ± 0,7	20.3 ± 0,4	12.8 ± 0,2
6	14.5 ± 0,4	18.7 ± 0,7	15.9 ± 0,3	8.6 ± 0,4
5	8.1 ± 0,4	10.5 ± 0,5	8.6 ± 0,2	5.6 ± 0,3

Figure 110 shows a contour map and a tridimensional representation of the incident blue light power. It is interesting to highlight the sensitivity of potassium ferrioxalate actinometry to detect the presence of a central spotlight on microplate F7 and a radial decrease from this point away.

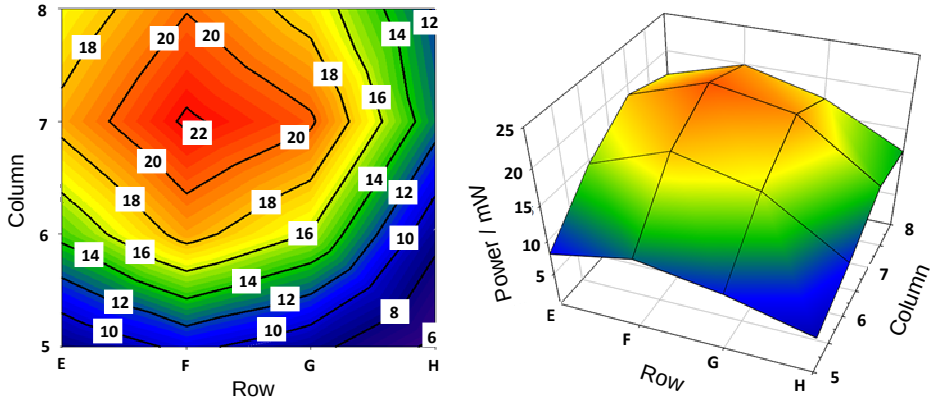

Figure 110. Incident light power distribution on contour and tridimensional maps for 16 wells in the 5–8 and E–H region.

10.4. Experimental setup for the evaluation of the aggregation of [60]fullerene glycodendrimeric derivatives

The experimental setup shown in Figure 111 was used to take the images of the pendant drops, which were formed at the tip of a needle in a transparent chamber (quartz cell). Temperature was controlled and fixed at 25 ºC. The shape of the drop was monitorized by imaging it with a CCD camera using backlighting, where a diffuse light source makes the detection of the curvature of the drop convenient since water and air are transparent media.

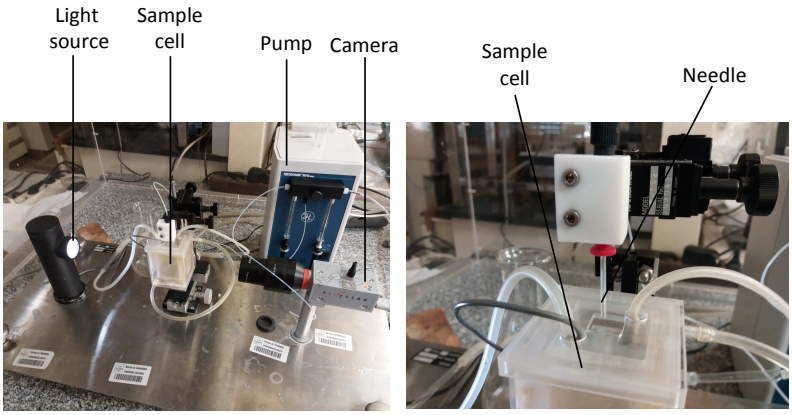

Figure 111. Experimental setup for pendant drop method.

10.5. Flow cytometry analysis

A FACSCanto II flow cytometer (BD Bioscience) equipped with blue (488-nm, air-cooled, 20-mW solid state), red (633-nm, 17-mW HeNe), and violet (405-nm, 30-mW solid state) lasers was used for the evaluation of the interaction between *H. pylori* and the fluorescent glycoprobes as well as for the quantification of *H. pylori* survival in the photodynamic experiments with the glycofullerene derivatives. Regarding *H. pylori*, strain TIGR 26695 (The Institute for Genome Research), with complete genome sequenced, cultured in Columbia Agar medium supplemented with blood (COS) was used in all the experiments.

10.5.1. Interaction assays between fluorescent probes and *H. pylori*

Incubation in 96-well plates during 45 minutes of *H. Pylori* alone (0.42 nephelometry units) or in the presence of aqueous NaCl (9 mg/mL) with **22**, **37**, **38**, **44**, **45** and fluorescein disodium salt ($1.3 \cdot 10^{-4}$ M) was followed by centrifugation (6000 rpm, 10 min.) and a subsequent washing of the resulting pellets with aqueous NaCl (saline solution, 9 mg/mL; 2 × 6000 rpm, 10 min). Finally, bacteria samples were resuspended in aqueous NaCl (saline solution, 9 mg/mL) for analysis by flow cytometry.

10.5.2. Photodynamic assays

A 48 h cultured *H. pylori* sample on COS was suspended in 8 mL of aqueous NaCl (9 mg/mL) until 0.3 units of nephelometry were achieved.

To each microplate, the following volumes were added: 160 μL of aqueous NaCl (9 mg/mL), 20 μL of **22**, **31**, **32**, **33**, or **71** stock solution (1 mM) and 20 μL of *H. pylori* stock solution. All the procedures developed after the addition of the photosensitizers were carried out under red light or in the dark,. The solutions were incubated at room temperature for 1 h with orbital shaking. Thereafter, the 96-well plate was placed in the illumination setup and irradiated for 1 minute / 30 minutes. After each irradiation time, 10 μL of each sample was stained with 1.5 μL of Syto9 and 0.2 μL of PI (Live/Dead BacLight™ Bacterial Viability and Counting Kit (Invitrogen, L34856)) using aqueous NaCl (9 mg/mL) as solvent, with an overall final volume of 990 μL. Staining was performed at room temperature for 15 minutes in the dark. Then, 10 μL of microsphere beads were added just before the samples were acquired, being that time less than 1 hour since the staining was performed.

Analysis of the photodynamic activity was performed by colony counting in culture plates as well, by growing, after 30 minutes of irradiation, 1:10, 1:100 and 1:1000 dilutions of 20 μL of each sample. 10 μL of each dilution were seeded on COS and incubated for 5-days in a CO_2 incubator.

All these procedures were performed for an illuminated well plate and for a second well plate kept in the dark as control.

For the dead/alive calibration, *H. pylori* was killed by heat (100 ºC, 15 minutes), getting a 100% dead sample. Thereafter, this solution was mixed with a 100 % alive sample, following these mixtures: 1 mL alive + 0 mL dead, 0.9 mL alive + 0.1 mL dead, 0.8 mL alive + 0.2 mL dead, 0.7 mL alive + 0.3 mL dead, 0.6 mL alive + 0.4 mL dead, 0.5 mL alive +0.5 mL dead, 0.4 mL alive + 0.6 mL dead, 0.3 mL alive +0.7 mL dead, 0.2 mL alive – 0.8 mL dead, 0.1 mL alive + 0.9 mL dead and 0 mL alive – 1 mL dead.

Table 29. Incident energy on each plate and sample after 30 minutes of irradiation.

Sample	Plates	Power / mW	Mean energy (30 min.) / J
HP	E6 / H7	8.1 / 12.8	19 ± 6
22	E8 / G6	16.6 / 15.9	29.2 ± 0.9
31	F7 / G7	22.3 / 20.3	38 ± 3
32	E7 / F6	18.6 / 18.7	33.6 ± 0.1
33	F8 / G8	19.9 / 17.2	33 ± 4
71	G5 / H6	8.6 / 6.6	13.7 ± 3

CONCLUSIONS

11. CONCLUSIONS

The main conclusions of this work are the following:

Chapter 1

- Experimental evidences have been found to support a parallel reaction mechanism for the photooxidation of thioketones mediated by $^1O_2$, considering a peroxythiocarbonyl species as a common reactive intermediate for all the photoproducts.
- Sulfine and ketone are not the only photoproducts when there are hydrogens in α position respect to the thiocarbonyl carbon, as a proton transfer can take place in the peroxythiocarbonyl intermediate.
- Sulfine formation can be explained without the need of intramolecular release of atomic oxygen, but an intermolecular oxygen transfer to another thioketone molecule from the peroxythiocarbonyl intermediate.
- Ketone/sulfine ratio can be reversed by controlling the reaction conditions: protic solvents, acidic media and high substrate concentrations improve sulfine generation as the major photoproduct.

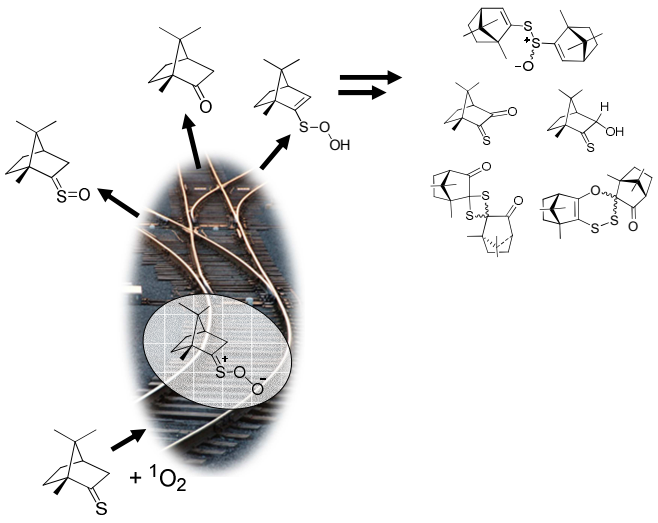

- Photooxidation of thioketones by $^1O_2$ to yield sulfine at synthetic scale under the principles of Green Chemistry has been accomplished using a heterogeneous system after the immobilization of the photosensitizer and thioketone on silica gel.
- Experimental evidences have been collected for the photooxidation of thionucleobases such as 4-thiouracyl, where the photoproduct distribution and the tentatively assigned structures do not agree with the proposals found in the bibliography.

Chapter 2

- In order to get new $^1O_2$ photosensitizers for photodynamic treatment of *H. pylori*, the synthesis of a series of glycodendrimeric structures based on fucose has been carried out, and they have been used to decorate [60]fullerene monoadducts.
- Φ_Δ values for the new glycofullerene derivatives have been found to be lower in D_2O than those of the parent [60]fullerene monoadducts in toluene, due to the self-aggregation.
- The interaction between the synthesized fucosylated glycodendrimeric structures and *H. pylori* has been demonstrated by flow cytometry analysis using fluorescent probes, although these interactions have been proved to be weaker than those mediated by electrostatic forces.
- A protocol for dead/live analysis of *H. pylori* bacterium has been optimized using flow cytometry and staining with SYTO9 and propidium iodide.
- Glycofullerenes decorated with 12 and 18 fucose units demonstrated to have a photodynamic action against *H. pylori*, decreasing four orders of magnitude the population of the bacteria after 30 minutes of irradiation, at 0.1 mM photosensitizer concentrations.

REFERENCES

12. REFERENCES

1. J. Toffelson, *Nature,* **2011**, *478*, 300.

2. P. Gerland, A. E. Raftery, H. Ševčíková, N. Li, D. Gu, T. Spoorenberg, L. Alkema, B. K. Fosdick, J. Chunn, N. Lalic, G. Bay, T. Buettner, G. K. Heilig, J. Wilmoth, *Science*, **2014**, *346*, 234.

3. Y. Wang, H. Suzuki, J. Xie, O. Tomita, D. J. Martin, M. Higashi, D. Kong, R. Abe, J. Tang. *Chem. Rev*., **2018**, *118*, 5201.

4. A. S. Mullin, J. T. Fourkas. *J. Phys. Chem. Lett*., **2015**, *6*, 3882.

5. G. Ciamician. *Science*, **1912**, *36*, 385.

6. A. Beeler. *Chem. Rev*., **2016**, *116*, 9629.

7. A. Albini, M. Fagnoni. *Green Chem*., **2004**, *6*, 1.

8. P. T. Anastas, J. C. Warner. Green Chemistry: Theory and Practice, Oxford University Press: New York, 1998, p.30.

9. C. M. Friend. *Chem. Rec*., **2014**, *14*, 944.

10. B. König. *Eur. J. Org. Chem*., **2017**, *15*, 1979.

11. T. Junkers. *Eur. Polym. J*., **2015**, *62*, 273.

12. V. Srivastava, P. P. Singh. *RSC. Adv*., **2017**, *7*, 31377.

13. P. C. Gotzsche. *J. R. Soc. Med*., **2011**, *104*, 41.

14. S. H. Yun, S. S. J. Kwok. *Nat. Biomed. Eng*., **2017**, *1*, 8.

15. B. Wardle. Principles and Applications of Photochemistry, Wiley: London, 2009, pp. 148-149.

16. P. R. Ogilby. *Chem. Soc. Rev*., **2010**, *39*, 3181.

17. C. Schweitzer, R. Schmidt. *Chem. Rev*., **2003**, *103*, 1685.

18. a) I. Rosenthal. Chemical and Physical Sources of Singlet Oxygen. In Singlet O_2. Vol. I, Physical and Chemical Aspects. A. A. Frimer ed. CRC Press: Boca Raton, FL, 1985, pp. 13-38. b) J. Bland. *J. Chem. Educ*., **1976**, *53*, 274. c) A. M. Braun, M.-T. Maurette, E. Oliveros. Photochemical Technology. Wiley: London, 1991, p. 452.

19. a) M. A. Filatov, M. O. Senge. *Mol. Syst. Des. Eng*., **2016**, *1*, 258. b) S. Benz, S. Nötzli, J. S. Siegel, D. Eberli, H. J. Jessen, *J. Med. Chem*., **2013**, *56*, 10171. c) C. Changtonga, D. W. Carneya, L. Luoa, C. A. Zotoa, J. L. Lombardi, R. E. Connors. *J. Photochem. Photobiol., A,* **2013**, *260*, 9.

20. C. M. Mano, F. M. Prado, J. Massari, G. E. Ronsein, G. E. Martínez, S. Miyamoto, J. Cadet, H. Sies, M. H. G. Medeiros, E. J. H. Bechara, P. Di Mascio. *Sci. Rep*., **2014**, *4*, 5938.

21. a) N. J. Turro, J. C. Scaiano, V. Ramamurthy. Principles of Molecular Photochemistry: An Introduction, University Science Books: Sausalito, 2009, p. 383. b) D. García-Fresnadillo, S. Lacombe. Reference Photosensitizers for the Production of Singlet Oxygen. In Singlet Oxygen: Applications in Biosciences and Nanosciences, Volume 1 (Eds.: Nonell, S.; Flors C.), The Royal Society of Chemistry, Cambridge, 2016, pp. 105-143. c) M. C. DeRosa, R. J. Crutchley. *Coord. Chem. Rev*., **2002**, *233-234*, 351.

22. S. Nonell, C. Flors. Steady-State and Time-Resolved Singlet Oxygen Phosphorescence Detection in the Near-IR. In Singlet oxygen. Applications in Biosciences and Nanosciences. Volume 2, The Royal Society of Chemistry, Cambridge, 2016, pp. 10-21.

23. a) S. Nonell, S. E. Braslavsky. *Methods in enzymology*, **2000**, *319*, 37. b) A. Jimenez-Banzo, X. Ragas, P. Kapusta, S. Nonell, *Photochem. Photobiol. Sci.*, **2008**, *7*, 1003.

24. H. Wu, Q. Song, G. Ran, X. Lu, B. Xu. *Trends Anal. Chem*., **2011**, *30*, 133.

25. S. Kim, M. Fujitsuka, T. Majima. *J. Phys. Chem. B*, **2013**, *117*, 13985.

26. S. K. Pedersen, J. Holmehave, F. H. Blaikie, A. Gollmer, T. Breitenbach, H. H. Jensen, P. R. Ogilby. *J. Org. Chem.*, **2014**, 79, 3079.

27. R. Ruiz-Gonzalez, R. Zanocco, Y. Gidi, A. L. Zanocco, S. Nonell. E. Lemp. *Photochem. Photobiol.*, **2013**, *89*, 1427.

28. B. Song, G. Wang, M. Tan, J. Yuan. *J. Am. Chem. Soc*., **2006**, *128*, 13442.

29. G. Zhang, X. Li, H. Ma, D. Zhang, J. Li, D. Zhu. *Chem. Commun.*, **2004**, 2072.

30. D. García-Fresnadillo. Solarsafewater: Tecnologías solares para la desinfección y descontaminación del agua, UNSAM editorial: Buenos Aires, 2005, pp. 231-232.

31. R. W. Redmond, J. N. Gamlin. *Photochem. Photobiol*., **1999**, *70*, 391.

32. a) A. J. Sánchez-Arroyo, E. Palao, A. R. Agarrabeitia, M. J. Ortiz, D. García-Fresnadillo. *Phys. Chem. Chem. Phys*., **2017**, *19*, 69. b) T. Yogo, Y. Urano, Y. Ishitsuka, F. Maniwa, T. Nagano. *J. Am. Chem. Soc*., **2005**, *127*, 12162. c) Y. C. Lai, S. Y. Su, C. C. Chang. *Appl. Mater. Interfaces*, **2013**, *5*, 12935.

33. a) F. Wilkinson, A. A. Abdel-Shafi, *J. Phys. Chem. Sect. A*, **1999**, *103*, 5425. b) D. J. McGarvey, P. G. Szekeres, F. Wilkinson. *Chem. Phys. Lett*., **1992**, *199*, 314.

34. a) H. G. Jeong, M. S. Choi. *Isr. J. Chem*., **2016**, *56*, 110. b) K. Ishii. *Coord. Chem. Rev*, **2012**, *256*, 1556.

35. a) D. García-Fresnadillo, Y. Georgiadou, G. Orellana, A. M. Braun, E. Oliveros. *Helv. Chem. Acta*, **1996**, *79*, 1222. b) M. E. Jiménez-Hernández, F. Manjón, D. García-Fresnadillo, G. Orellana. *Solar Energy*, **2006**, 80, 1382. c) L. Villén F. Manjón, D. García-Fresnadillo, G. Orellana. *Appl. Catal. B Environ*., **2006**, *69*, 1. d) D. García-Fresnadillo. *ChemPhotoChem*, **2018**, *2*, 512.

36. a) J. Arnbjerg, M. J. Paterson, C. B. Nielsen, M. Jørgensen, O. Christiansen, P. R. Ogilby. *J. Phys. Chem. A*, **2007**, *111*. b) T. Ishi-i, Y. Taguri, S. Kato, M. Shigeiwa, H. Gorohmaru, S. Maeda, S. Mataka. *J. Mater. Chem*., **2007**, *17*, 3341. c) N. Gandra, P. L. Chiu, W. Li, Y. R. Anderson, S. Mitra, H. He, R. Gao. *J. Phys. Chem. C*, **2009**, *113*, 5182.

37. H. W. Kroto, J. R. Heath, S. C. O'Brien, R. F. Curl, R. E. Smalley, *Nature*, **1985**, *318*, 162.

38. R. C. Haddon, *Acc. Chem. Res*., **1992**, *25*, 127.

39. a) H. Ajie, M. M. Alvarez, S. J. Anz, R. D. Beck, F. Diederich, K. Fostiropoulos, D. R. Huffman, W. Krätschmer, Y. Rubin, K. E. Shriver, D. Sensharma, R. L. Whetten, *J. Phys. Chem*., **1990**, *94*, 8630. b) Y. P. Sun. Molecular and Supramolecular Photochemisty. Organic Photochemistry. CRC Press: Boca Raton, 1997, p. 329.

40. a) J. W. Arbogast, A. P. Darmanyan, C. S. Foote, F. N. Diederich, R. L. Whetten, Y. Rubin, M. M. Alvarez, S. J. Anz. *J. Phys. Chem.* **1991**, *95*, 11. b) F. Wilkinson, W. P. Helman, A. B. Ross. *J. Phys. Chem. Ref. Data*, **1993**, *22*, 113.

41. A. Montellano-López, A. Mateo-Alonso, M. Prato. *J. Mater. Chem*., **2011**, *21*, 1305.

42. Y. Nakamura, M. Taki, S. Tobita, H. Shizuka, H. Yokoi, K. Ishiguro, Y. Sawaki, J. Nishimura. *J. Chem. Soc*. *Perkin Trans. 2*, **1999**, 127.

43. T. Hamano, K. Okuda, T. Mashino, M. Hirobe, K. Arakane, A. Ryu, S. Mashiko, T. Nagano. *Chem. Commun.*, **1997**, 21.

44. F. Prat, R. Stackow, R. Bernstein, W. Qian, Y. Rubin, C. S. Foote. *J. Phys. Chem. A*, **1999**, *103*, 7230.

45. K. K. Chin, S.-C. Chuang, B. Hernández, L. M. Campos, M. Selke, C. S. Foote, M. A. García-Garibay. *Photochem. Photobiol. Sci*. **2008**, *7*, 49.

46. a) M. Zamadar, A. Greer. Handbook of Syntehtic Photochemistry. Wiley-VCH: Weinheim, 2010, pp. 353-354. b) A. M. Braun, M.-T. Maurette, E. Oliveros. Photochemical Technology. Wiley: London, 1991, p. 452.

47. G. O. Schenck, *Naturwissenschaften*, **1948**, *35*, 28.

48. a) M. Prein, W. Adam. *Angew. Chem. Int. Ed*., **1996**, *35*, 477. b) E. L. Clennan *Tetrahedron*, **2000**, *56*, 9151. c) D. A. Singleton, C. Hang; M. J. Szymanski, M. P. Meyer, A. G. Leach, K. T. Kuwata, J. S. Chen, A. Greer, C. S. Foote, K. N. Houk. *J. Am. Chem. Soc*., **2003**, *125*, 1319.

49. H.-J. Chen, W.-B. Han, H.-D. Hao and Y. Wu, *Tetrahedron*, **2013**, *69*, 1112.

50. F. Lévesque, P. H. Seeberger. *Angew. Chem. Int. Ed*., **2012**, *51*, 1706.

51. G. Vassilikogiannakis, M. Stratakis and M. Orfanopoulos. *J. Org. Chem.*, **1998**, *63*, 6390.

52. G. Mazzone, M. E. Alberto, N. Russo, E. Sicilia. *Phys. Chem. Chem. Phys.***, 2014**, *16*, 12773.

53. N. Hananya, O. Green, R. Blau, R. Satchi-Fainaro, D. Shabat. *Angew. Chem. Int. Ed*., **2017**, *56*, 11793.

54. W. Adam, M. Prein. *Acc. Chem. Res.* **1996,** *29*, 275.

55. R. Ozen, F. Kormal, M. Balci, B. Atasoy. *Tetrahedron*, **2001**, *57*, 7529.

56. a) D. A. Butterfield, J. Kanski. *Peptides,* **2002**, *23*, 1299. b) C. Schöneich. *Arch. Biochem. Biophys.*, **2002**, *397*, 370.

57. J. J. Liang, C. L. Gu, M. L. Kacher, C. S. Foote. *J. Am. Chem. Soc*., **1983**, *105*, 4717.

58. F. Jensen, A. Greer, E. L. Clennan. *J. Am. Chem. Soc*., **1998**, *120*, 4439.

59. E. L. Clennan. *Acc. Chem. Res*., **2001**, *34*, 875.

60. E. L. Clennan, A. Greer. *J. Org. Chem*., **1996**, *61*, 4793.

61. E. L. Clennan. *Tetrahedron Lett*., **1999**, *40*, 6519.

62. S. M. Bonesi, A. Albini. *J. Org. Chem*., **2000**, *65*, 4532.

63. a) R. Rajee, V. Ramamurthy. *Tetrahedron Lett.*, **1978**, *19*, 5127. b) V. Jayathirtha Rao, V. Ramamurthy. *Indian J. Chem. Sect. B,* **1980**, *19B*, 143. c) N. Ramnath, V. Ramesh, V. Ramamurthy. *J. Chem. Soc., Chem. Commun*., **1981**, 112. d) V. J. Rao, K. Muthuramu, V. Ramamurthy. *J. Org. Chem*., **1982**, *47*, 127. e) N. Ramnath, V. Ramesh, V. Ramamurthy. *J. Org. Chem*. **1983**, *48*, 214. f) P. Arjunan, V. Ramamurthy, K. Venkatesan. *J. Org. Chem*. **1984**, *49*, 1765. g) V. P. Rao, V. Ramamurthy. *Tetrahedron* 1985, *41*, 2169.

64. a) A. Maciejewski, R. P. Steer. *Chem. Rev*., **1993**, *93*, 67. b) A. Corsaro, V. Pistarà. *Tetrahedron*, **1998**, *54*, 15027. c) A. Gilbert, J. Baggott, Essentials of Molecular Photochemistry, Blackwell Scientific Publications: Oxford, 1991, pp 518−520.

65. R. Huisgen, G. Mloston, K. Polborn. *J. Org. Chem*., **1996**, 61, 6570.

66. A. C. B. Lucassen. Sulfine-based Synthesis of Four-, Five- and Six-Membered Heterocycles. Ph.D. Thesis, Radboud University Nijmegen, Netherlands. 2003.

67. R. Bastin, H. Albadri, A. C. Gaumont, M. Gulea. *Org. Lett*., **2006**, *8*, 1033.

68. J. Carbon, H. David, M. H. Studier, *Science*, **1986**, *161*, 1146.

69. F.-Y. Wei, T. Suzuki, S. Watanabe, S. Kimura, T. Kaitsuka, A. Fujimura, H. Matsui, M. Atta, H. Michiue, M. Fontecave, K. Yamagata, T. Suzuki, K. Tomizawa. *J. Clin. Invest.*, **2011**, *121*, 3598.

70. M. Presta, M. Belleri, A. Vacca, D. Ribatti. *Leukemia*, **2002**, *16*, 1490.

71. S. Mai, M. Pollum, L. Martínez-Fernández, N. Dunn, P. Marquetand, I. Corral, C. E. Crespo-Hernández, L. González. *Nat. Commun*., **2016**, *7*, 13077.

72. A. Favre, C. Saintomé, J. L. Fourrey, P. Clivio, P. Laugâa. *J. Photochem. Photobiol. B*, **1998**, *42*, 109.

73. E. Gemenetzidis, O. Shavorskaya, Y.-Z. Xu, G. Trigiante. *J. Dermatol. Treat*., **2013**, *24*, 209.

74. a) X. Zou, X. Dai, K. Liu, H. Zhao, D. Song, H. Su. *J. Phys. Chem. B*, **2014**, *118*, 5864. b) P. Mehta, S. C. Mehta. *Asian J. Chem*., **1999**, 11, 528.

75. S. E. Braslavsky. *Pure Appl. Chem*., **2007**, *79*, 293.

76. A. E. Croce. *Can. J. Chem*., **2008**, *86*, 918.

77. B. S. Berlett, R. L. Levine, E. R. Stadtman. *Anal. Biochem*., **2000**, *287*, 329.

78. a) A. M. Álvarez-García. Síntesis estereoselectiva y aplicaciones de nuevos tioderivados con esqueleto norbornánico. Ph.D. Thesis, Complutense University of Madrid, 2008. b) R. Huisgen, G. Mloston, A. Pröbstl. *Hetereoatom Chem*., **2001**, *12*, 136.

79. F. Wilkinson, W. P. Herman, A. B. Ross. *J. Phys. Chem. Ref. Data*, **1995**, *24*, 663.

80. a) A. Toutchkine, D. Aebisher, E. L. Clennan. *J. Am. Chem. Soc*. **2001**, *123*, 4966. b) A. Toutchkine, E. L. Clennan. *J. Am. Chem. Soc*. **2000**, *122*, 1834.

81. a) T. J. Back, B. P. Dyck, M. Parvez. *J. Org. Chem*., **1995**, *60*, 703. b) I. Crossland. *Acta Chem. Scand*., **1977**, *31b*, 890. c) F. A. G. El-Essawy, S. M. Yassin, I. A. El-Sakka, A. F. Khattab, I. Sotofte, J. O. Madsen, A. Senning, *J. Org. Chem*., **1998**, *63*, 9840. d) M. I. Hegab, A. A. Abd El-Galil, F. M. E. Abdel-Megeid, *Z. Naturforsch. (B)*, **2002**, *57*, 922.

82. R. Huang, J. H. Espenson. *J. Org. Chem*., **1999**, *64*, 6935.

83. D. D. Perrin, I. F. Amarego, D. R. Perrin, *Purification of laboratory Chemicals*, Pergamon Press, Oxford, **1980**.

84. a) H. J. Kuhn, S. E. Braslavsky, R. Schmidt. *Pure Appl. Chem*., **2004**, *76*, 2105. b) M. Montalti, A. Credi, L. Prodi, M. T. Gandolfi. Handbook of Photochemistry, 3rd ed.; CRC Press: Boca Raton, FL, pp. 601−616, **2006**.

85. S. E. Braslavsky. *Pure Appl. Chem.*, **2007**, *79*, 293.

86. H. von Tappeiner, A. Jodlbauer. *Dtsch. Arch. Klin. Med.*, **1904**, *80*, 427.

87. P. Agostinis, K. Berg, K. A. Cengel,T. H. Foster, A. W. Girotti, S. O. Gollnick, S. M. Hahn, M. R. Hamblin, A. Juzeniene, D. Kessel, M. Korbelik, J. Moan, P. Mroz, D. Nowis, J. Piette, B. C. Wilson, J. Golab. *CA-Cancer J. Clin.*, **2011**, *61*, 250.

88. M. J. Davies. *Biochem. Biophys. Res. Commun*., **2003**, *305*, 761.

89. K. Suwa, T. Kimura, P. Schaap. *Photochem. Photobiol*., **1978**, *28*, 469.

90. M. Rougee, R. V. Bensasson, E. J. Land, R. Pariente. *Photochem. Photobiol*., **1988**, *47*, 485.

91. a) J. Cadet, R. Teoule. *Photochem. Photobiol*., **1978**, 28, 661. b) S. Steenken, S.V. Jovanovic. *J. Am. Chem. Soc*., **1997**, *119*, 617. c) J. L. Ravanat, G. Remaud, J. Cadet. *Arch. Biochem. Biphys*., **2000**, *374*, 118.

92. A. P. Castano, T. N. Demidova, M. R. Hamblin. *Photodiagnosis Photodyn. Ther*., **2004**, 1, 279.

93. A. C. E. Moor. *J. Photochem. Photobiol. B*, **2000**, 57, 1.

94. N. L. Oleinick, R. L. Morris, I. Belichenko. *Photochem. Photobiol. Sci.*, **2002**, *1*, 1.

95. C. Salet, G. Moreno, F. Ricchelli, P. Bernardi. *J. Biol. Chem*., **1997**, *272*, 21938.

96. a) D. J. Granville, C. M. Carthy, H. Jiang, G. C. Shore, B. M. McManus, D. W. Hunt. *FEBS Lett*., 1998, *437*, 5. b) M. E. Varnes, S. M. Chiu, L. Y. Xue, N. L. Oleinick. *Biochem. Biophys. Res. Commun*., **1999**, *255*, 673. c) D. Kessel, Y. Luo. *Cell Death Differ*., **1999**, *6*, 28.

97. a) N. A. Thornberry, Y. Lazebnik. *Science*. **1998**, *281*, 1312. b) G. Nunez, M. A. Benedict, Y. Hu, N. Inohara. *Oncogene*, **1998**, 17, 3237.

98. A. G. Porter, R. U. Janicke. *Cell Death Differ*., **1999**, *6*, 99.

99. S. Krajewski, S. Tanaka, S. Takayama, M. J. Schibler, W. Fenton, J.C. Reed. *Cancer Res.*, **1993**, *53*, 4701.

100. R. R. Alison, C. H. Sibata. *Photodiagnosis Photodyn. Ther*., **2010**, *7*, 61.

101. B. Rodríguez-Amigo, O. Planas, R. Bresolí-Obach, J. Torra, R. Ruíz-González, S. Nonell. Photodynamic Medicine. From Bench to Clinic. RSC: Cambridge. p. 27, 2016.

102. L. B. Josefsen, R. W. Boyle. *Br. J. Pharmacol*., **2008**, *154*, 1.

103. S. B. Brown, E. A. Brown, I. Walker. *Lancet Oncol.*, **2004**, *5*, 497.

104. Q. Peng, K. Berg, J. Moan, M. Konqshauq, J. M. Nesland. *Photochem. Photobiol*., **1997**, *65*, 235.

105. a) D. C. Hone, P. I. Walker, R. Evans-Gowing, S. FitzGerald, A. Beeby, I. Chambrier, M. J. Cook, D. A. Russell. *Langmuir*, **2002**, *18*, 2985. b) M. E. Wieder, D. C. Hone, M. J. Cook, M. M. Handsley, J. Gavrilovic, D. A. Russell. *Photochem. Photobiol. Sci.*, **2006**, *5*, 727.

106. a) P. Couleaud, V. Morosini, C. Frochot, S. Richeter, L. Raehm, J. O. Durand. *Nanoscale*, **2010**, *2*, 1083. b) J. Zhou, L. Zhou, C. Dong, Y. Feng, S. Wei, J. Shen, X. Wang, *Mater. Lett.*, **2008**, *62*, 2910.

107. A. Labib, V. Lenaerts, F. Chouinard, J. C. Leroux, R. Ouellet, J. E. van Lier. *Pharm. Res.*, **1991**, *8*, 1027.

108. C. S. Jin, G. Zheng. *Lasers Surg. Med*., **2011**, *43*, 734.

109. N. Nishiyama, H. R. Stapert, G. D. Zhang, D. Takasu, D. L. Jiang, T. Nagano, T. Aida, K. Kataoka. *Bioconjugate Chem.*, **2003**, *14*, 58.

110. a) T. Stuchinskaya, M. Moreno, M. J. Cook, D. R. Edwards, D. A. Russell. *Photochem. Photobiol. Sci.*, **2011**, *10*, 822. b) G. Obaid, I. Chambrier, M. J. Cook, D. A. Russell. *Angew. Chem., Int. Ed.*, **2012**, *51*, 6158. c) H. Benachour, A. Seve, T. Bastogne, C. Frochot, R. Vanderesse, J. Jasniewski, I. Miladi, C. Billotey, O. Tillement, F. Lux, M. Barberi-Heyob. *Theranostics*, **2012**, *2*, 889. d) M. Gary-Bobo, Y. Mir, C. Rouxel, D. Brevet, I. Basile, M. Maynadier, O. Vaillant, O. Mongin, M. Blanchard-Desce, A. Morere, M. Garcia, J. O. Durand, L. Raehm. *Angew. Chem., Int. Ed.*, **2011**, *50*, 11425. e) G. R. Reddy, M. S. Bhojani, P. McConville, J. Moody, B. A. Moffat, D. E. Hall, G. Kim, Y. E. Koo, M. J. Woolliscroft, J. V. Sugai, T. D. Johnson, M. A. Philbert, R. Kopelman, A. Rehemtulla, B. D. Ross. *Clin. Cancer Res.*, **2006**, *12*, 6677. f) Y. Mir, S. A. Elrington, T. Hasan. *Nanomedicine*, **2013**, *9*, 1114.

111. P. M. R. Pereira, B. Korsak, B. Sarmento, R. J. Schneider, R. Fernandes, J. P. C. Tomé. *Org. Biomol. Chem*., **2015**, *13*, 2518.

112. R. I. Aminov. *Front. Microbiol*., **2010**, *1*, 134.

113. M. R. Hamblin, T. Hasan. *Photochem. Photobiol. Sci*., **2004**, *3*, 436.

114. a) A. Tavares, C. M. B. Carvalho, M. A. Faustino, M. G. P. M. S. Neves, J. P. C. Tomé, A. C. Tomé, J. A. S. Cavaleiro, A. Cunha, N. C. M. Gomes, E. Alves, A. Almeida. *Mar. Drugs*, **2010**, *8*, 91. b) O. E. Akilov, K. O'Riordan, S. Kosaka, T. Hasan. *Med. Laser Appl*., **2006**, *21*, 251.

115. F. Javed, L. P. Samaranayake, G. E. Romanos. *Photochem. Photobiol. Sci.*, **2014**, *13*, 726.

116. a) B. Pudziuvyte, E. Bakiene, R. Bonnett, P. A. Shatunov, M. Magaraggia, G. Jori. *Photochem. Photobiol. Sci.*, **2011**, *10*, 1046. b) M. B. Spesia, D. A. Caminos, P. Pons, E. N. Durantini. *Photodiagn. Photodyn. Ther.*, **2009**, *6*, 52.

117. a) W. Du, C. Sun, Z. Liang, Y. Han, J. Yu. *World J. Microbiol. Biotechnol.*, **2012**, *28*, 3151. b) K. Sahu, H. Bansal, C. Mukherjee, M. Sharma, P. K. Gupta. *J. Photochem. Photobiol. B*, **2009**, *96*, 9.

118. a) G. Valduga, B. Breda, G. M. Giacometti, G. Jori, E. Reddi. *Biochem. Biophys. Res. Commun.*, **1999**, *256*, 84. b) K. Komagoe, H. Kato, T. Inoue, T. Katsu. *Photochem. Photobiol. Sci*., **2011**, *10*, 1181.

119. H. Kato, K. Komagoe, T. Inoue, T. Katsu. *Anal. Sci.*, **2010**, 26, 1019.

120. R. Dosselli, R. Millioni, L. Puricelli, P. Tessari, G. Arrigoni, C. Franchin, A. Segalla, E. Teardo, E. Reddi. *Proteomics*, **2012**, *77*, 329.

121. E. Alves, N. Santos, T. Melo, E. Maciel, M. L. Dória, M. A. Faustino, J. P. Tomé, M. G. Neves, J. A. Cavaleiro, A. Cunha, L. A. Helguero, P. Domingues, A. Almeida, M. R. Domingues. *Rapid Commun. Mass Spectrom.*, **2013**, *27*, 2717.

122. M. Schäfer, C. Schmitz, G. Horneck. *Int. J. Radiat. Biol*., **1998**, *74*, 249.

123. A. O'Connor, C. A. O'Morain, A. C. Ford. *Nat. Rev. Gastroenterol. Hepatol*., **2017**, *14*, 230.

124. A. P. Moran. *Carbohydr. Res*., **2008**, *343*, 1952.

125. F. Maixner, B. Krause-Kyora, D. Turaev, A. Herbig, M. R. Hoopmann, J. L. Hallows, U. Kusebauch, E. E. Vigl, P. Malfertheiner, F. Megraud, N. O'Sullivan, G. Cipollini, V. Coia, M. Samadelli, L. Engstrand, B. Linz, R. L. Moritz, R. Grimm, J. Krause, A. Nebel, Y. Moodley, T. Rattei, A. Zink. *Science*, **2016**, *351*, 162.

126. H. L. Mobley. *Aliment. Pharmacol. Ther*., **1996**, *10*, 57.

127. a) M. A. Monteiro, P.Y. Zheng, B. J. Appelmelk, M. B. Perry. *FEMS Microbiol. Lett*., **1997**, *154*, 103. b) T. O. Croinin, M. Clyne, B. Drumm. *Gastroenterology*, **1998**, *114*, 690. c) H. P. Wirth, M. Yang, E. Sanabria-Valentín, D. E. Berg, A. Dubois, M. J. Blaser. *FASEB J*., **2006**, *20*, 1534.

128. B. J. Appelmelk, M. A. Monteiro, S. L. Martin, A. P. Moran, C. M. J. E. Vandenbroucke-Grauls. *Trends Microbiol*., **2000**, *8*, 565.

129. D. Ilver, A. Arnqvist, J. Ogren, I. M. Frick, D. Kersulyte, E. T. Incecik, D. E. Berg, A. Covacci, L. Engstrand, T. Boren. *Science*, **1998**, *279*, 373.

130. J. Mahdavi, B. Sonden, M. Hurtig, F. O. Olfat, L. Forsberg, N. Roche, J. Angstrom, T. Larsson, S. Teneberg, K. A. Karlsson, S. Altraja, T. Wadström, D. Kersulyte, D. E. Berg, A. Dubois, C. Petersson, K. E.

Magnusson, T. Norberg, F. Lindh, B. B. Lundskog, A. Arnqvist, L. Hammarström, T. Borén. *Science*, **2002**, *297*, 573.

131. S. Suerbaum, C. Josenhans. *Nat. Rev. Microbiol*., **2007**, *5*, 441.

132. K. M. Ottemann, A. C. Lowenthal. *Infect Immun*. **2002**, *70*, 1984.

133. a) P. Ruggiero. *Curr. Pharm. Des*., **2010**, *16*, 4225. b) P. B. Ernst, B. D. Gold. *Annu. Rev. Microbiol*., **2000**, *54*, 615.

134. J. G. Kusters, A. H. M. van Vliet, E. J. Kuipers. *Clin. Microbiol. Rev*., **2006**, *19*, 449.

135. F. Bazzoli, R. M. Zagari, S. Fossi, P. Pozzato, A. Roda, E. Roda. *Gastroenterology*, **1993**, *104*, 40.

136. J. Y. Park, K. B. Dunbar, M. Mitui, C. A. Arnold, D. M, Lam-Himlin, M. A. Valasek, I. Thung, C. Okwara, E. Coss, B. Cryer, C. D. Doern. *Dig. Dis. Sci.*, **2016**, *61*, 2373.

137. J. Molina-Infante, J. P. Gisbert. *World J. Gastroenterol*., **2014**, *20*, 10338.

138. V, Papastergiou, S. D. Georgopoulos, S. Karatapanis. *World J. Gastrointest. Pathophysiol*., **2014**, *5*, 392.

139. J. Bedwell, J. Holton, D. Vaira, A. J. MacRobert, S. G. Bown. *Lancet*, **1990**, *335*, 1287.

140. S. S. Choi, H. K. Lee, H. S. Chae. *J. Photochem. Photobiol. B: Biology*, **2010**, *101*, 206.

141. E. Millson, M. Wilson, A. J. MacRobert, S. G. Bown. *J. Photochem. Photobiol. B: Biology*, **1996**, *32*, 59.

142. M. R. Hamblin, J. Viveiros, C. Yang, A. Ahmadi, R. A. Ganz, M. J. Tolkoff. *Antimicrobial Agents Chemother*., **2005**, *49*, 2822.

143. M. Calvino-Fernández, D. García-Fresnadillo, S. Benito-Martínez, A. McNicholl, X. Calvet, J. P. Gisbert, T. Parra-Cid. *Eur. J. Med. Chem*., **2013**, *68*, 284.

144. D. Hüttenberger, C. Simon, C. Mohrbacher, N. Betz, I. Bauer-Marschall, A. Stachon, T. Giesen, H.-J. Foth. *Photodiagn. Photodyn*., **2017**, *17*, 12.

145. R. A. Ganz, J. Viveiros, A. Ahmad, A. Ahmadi, A. Khalil, M. J. Tolkoff, N. S. Nishioka, M. R. Hamblin. *Lasers Surg. Med*., **2005**, *36*, 260.

146. A. J. Lembo, R. A. Ganz, S. Sheth, D. Cave, C. Kelly, P. Levin, P. T. Kazlas, P. C. Baldwin III, W. R. Lindmark, J. R. McGrath, M. R. Hamblin. *Lasers Surg. Med*., **2009**, *41*, 337.

147. a) Y. C. Lee, R. T. Lee. Acc. Chem. Res., **1995**, 28, 321. b) M. Mammen, S.-K. Choi, G. M. Whitesides. *Angew. Chem. Int. Ed*., **1998**, *37*, 2754. c) J.

J. Lundquist, E. J. Toone. *Chem. Rev.*, **2002**, *102*, 555. d) J. C. Sacchettini, L. G. Baum, C. F. Brewer. *Biochemistry*, **2001**, *40*, 3009.

148. a) M. Sánchez-Navarro, A. Muñoz, B. M. Illescas, J. Rojo, N. Martín. *Chem. Eur. J*., **2011**, *17*, 766. b) J. F. Nierengarten, J. Iehl, V. Oerthel, M. Holler, B. M. Illescas, A. Muñoz, N. Martín, J. Rojo, M. Sánchez-Navarro, S. Cecioni, S. Vidal K. Buffet, M. Durka, S. P. Vincent. *Chem. Commun*., **2010**, *46*, 3860.

149. a) A. Muñoz, D. Sigwalt, B. M. Illescas, J. Luczkowiak, L. Rodríguez-Pérez, I. Nierengarten, M. Holler, J. S. Remy, K. Buffet, S. P. Vincent, J. Rojo, R. Delgado, J. F. Nierengarten, N. Martín. *Nat. Chem*., **2016**, *8*, 50. b) B. M. Illescas, J. Rojo, R. Delgado, N. Martín. *J. Am. Chem. Soc*., **2017**, *139*, 6018.

150. a) X. P. He, Y. L. Zeng, Y. Zang, J. Li, R. A. Field, G. R. Chen. *Carbohydr. Res*., **2016**, *429*, 1. b) V. K. Tiwari, B. B. Mishra, K. B. Mishra, N. Mishra, A. S. Singh, X. Chen. *Chem. Rev*., **2016**, *116*, 3086.

151. E. Arce, P. M. Nieto, V. Díaz, R. García-Castro, A. Bernad, J. Rojo. *Bioconjugate Chem*. **2003**, *14*, 817.

152. D. Kushwaha, V. K. Tiwari. *J. Org. Chem*., **2013**, *78*, 8184.

153. Y. M. Chabre, D. Giguère, B. Blanchard, J. Rodrigue, S. Rocheleau, M. Neault, S. Rauthu, A. Papadopoulos, A. A. Arnold, A. Imberty, R. Roy. *Chem. Eur. J*., **2011**, *17*, 6545.

154. M. Medal, C. W. Tornøe. *Chem. Rev*., **2008**, *108*, 2952.

155. C. Bingel. *Chem. Ber*., **1993**, *126*, 1957.

156. A. Muñoz, B. M. Illescas, M. Sánchez-Navarro, J. Rojo, N. Martín. *J. Am. Chem. Soc*., **2011**, *133*, 16758.

157. L. Chen, T.- S. Hu, J. Zhu, H. Wu, Z.-J Yao. *Synlett.*, **2006**, *8*, 1225.

158. Y. Xiang, B. He, X. Li, Q. Zhu. *RSC Adv*. **2013**, *3*, 4876.

159. C. Xiao, Y. Cheng, Y. Zhang, J. Ding, C. He, X. Zhuang, X. Chen. *J. Polym. Sci., Part A: Polym. Chem.*, **2014**, *52*, 671.

160. L. I. Manasieva, B. U. Maria, A. Prandi, L. Brasili, S. Franchini. *Synthesis*, 2015; 47, 3767.

161. W. Yang, P. F. Xia, M. S. Wong. *Org. Lett*., **2010**, *12*, 4018.

162. A. J. Hilmer, K. Tvrdy, J. Zhang, M. S. Strano. *J. Am. Chem. Soc*., **2013**, *135*, 11901.

163. S. F. Völker, M. Vallés-Pelarda, J. Pascual, S. Collavini, F. Ruipérez, E. Zuccatti, L. E. Hueso, R. Tena-Zaera, I. Mora-Seró, J. L. Delgado. *Chem. Eur. J*., **2018**, *24*, 8524.

164. E.-H. kang, I. S. Lee, T.-L. Choi. *J. Am. Chem. Soc*., **2011**, *133*, 11904.

165. A. Noureddine, M. Gary-Bobo, L. Lichon, M. Garcia, J. I. Zink, M. W. C. Man, X. Catto. *Chem. Eur. J*., **2016**, *22*, 9624.

166. K. Petcharoen, A. Sirivat. *Mat. Sci. Eng. B*, **2012**, *177*, 421.

167. C. Hui, C. Shen, J. Tian, L. Bao, H. Ding, C. Li, Y. Tian, X. Shi, H.-J. Gao. *Nanoscale*, **2011**, *3*, 701.

168. O. Shimizu, J. Watanabe, K. Imakubo, S. Naito. *Chem. Lett.,* **1999**, *28*, 67.

169. M. Montalti, A. Credi, L. Prodi,M. T. Gandolfi. Handbook of Photochemistry, 3rd ed.; CRC Press: Boca Raton, FL, 2006; Chapter 9, pp. 535-559.

170. J. D. Berry, M. J. Neeson, R. R. Dagastine, D. Y.C. Chan, R. F. Tabo. *J. Colloid Interface Sci*., **2015**, *454*, 226.

171. D. R. Lide (ed). Handbook of Chemistry and Physics, 85th ed.; CRC Press: Boca Raton, FL, 2005; pp. 6/135-6/137.

172. P. Joos, E. Rillaerts. *J. Colloid Interface Sci*., **1981**, *79*, 96.

173. a) J. Picot, C. L. Guerin, C. Le Van Kim, C. M. Boulanger. *Cytotechnology*, **2012**, *64*, 109. b) M. J. Jaroszeski, G. Radcfiff. *Mol. Biotech*., **1999**, *11*, 37.

174. a) P. Stiefel, S. Schmidt-Emrich, K. Maniura-Weber, Q. Ren. *BMC Microbiology*, **2015**, *15*, 36. b) M. Berney, F. Hammes, F. Bosshard, H.-U. Weilenmann, T. Egli. *Appl. Environ. Microbiol*., **2007**, *73*, 3283. c) S. M. Stocks. *Cytometry A*, **2004**, *61A*, 189.